Intramolecular Interactions in TRP Channels, and Gate and Proton Activation of PAC Channel

by

Ruiqi Cai

A thesis submitted in partial fulfillment of the requirements for the degree of

Doctor of Philosophy

Department of Physiology
University of Alberta

ABSTRACT

The mammalian transient receptor potential (TRP) channels, composed of six subfamilies and 28 members, play crucial roles in sensory physiology and malfunctions of TRP channels cause channelopathies. High-resolution structures of TRP channels indicate conformational arrangements showing physical proximity of the TRP or TRP-like domain to the pre-S1 helix and S4-S5 linker, and between the pore-forming region S5/S6 helix. Since the structures, resolved under unnatural conditions, are representative states showing snapshots of highly dynamic conformations of TRP channels, whether these domains do physically interact with each other and their functional importance have not yet been determined in living cells. Inner membrane located phosphatidylinositol 4,5-bisphosphate (PIP2) is well known to modulate the majority of the TRP channels but the underlying mechanism is not well understood. TRPV6 channel is one of the most calcium-selective TRP channels implicated in breast cancer progression with largely undetermined mechanisms. A novel proton-activated chloride channel (PAC) was recently identified as an acid-induced outward rectified

anion channel, without sequence similarity to any known ion channels. How the PAC pore gate is composed and proton sensing remain unclear.

In Chapter 2, by two-electrode voltage clamping in *Xenopus* oocytes, immunofluorescence and patch clamping on mammalian cells, we identified interactions between a conserved aromatic residue in the **N**-terminal pre-S1 helix and a cationic residue in the **C**-terminal TRP (-like) helix of TRPP3 (Trp81:K568), -P2 (Trp201:K688), -V1 (Trp426:Arg701), -M8 (Trp682:Arg998) and -C4 (Trp314:Arg639), and found that these N/C interactions are required for the channel function. The PIP2 distinctly affected the N/C binding to regulate the channel function. This study describes a PIP2-modulated interaction between N/C domains that is functionally critical and likely shared among TRP channels.

In Chapter 3, by electrophysiology in *Xenopus* oocytes, calcium imaging in mammalian cells and biotinylation. we functionally characterized residues W593 and I597 in the **C**-terminal TRP, R470 in the S4-S5 **l**inker and W321 in the **N**-terminal pre-S1 helix of TRPV6 channel, and found that the **L**inker to **C**-terminal TRP helix (L/C) and

the **N**-terminal pre-S1 helix to **C**-terminal TRP helix (N/C) interactions are autoinhibitory for the channel function. The stimulatory effect of PIP2 on the TRPV6 function can be accounted for by its ability to disrupt the autoinhibitory L/C and N/C bindings. This study revealed PIP2-regulated autoinhibitory interactions within TRPV6, which represents a novel mechanism of regulation that may be shared by other TRP channels.

In Chapter 4, by electrophysiology, *in-vitro* pull down, disulfide bond formation assays and molecular dynamic simulations, we found that in TRPV6 a highly conserved residue R532 in the S5 helix presumably forms a salt bridge with D620 in the S6 helix, which acts as an autoinhibitory intramolecular (S5/S6 helix) interaction. Neutralized mutant R532Q is known to be gain-of-function in breast cancer cells. We found that both WT and R532Q mutant TRPV6 interact with subunit p85 of PI-3 kinase thereby promoting breast cancer progression through activating a PI3K/Akt pathway to promote epithelial-mesenchymal transition and inhibit apoptosis. However, mutant R532Q showed stronger effects than WT TRPV6. This study uncovered novel mechanistic insights into the intramolecular regulation of the TRPV6 channel function and roles of

TRPV6 in breast cancer development, which may contribute to drug discovery for TRPV6-related diseases such as breast cancer.

In Chapter 5, by means of two-electrode voltage clamp, immunofluorescence, biotinylation and flow cytometry we characterized PAC channel gate and the mechanism of proton-induced channel activation. We found that hydrophobic residue W304 acts as the closed gate while I307 as the open gate in the pore-lining S2 helix, controlling the Cl^- permeation at high (*e.g.*, pH 7.5) and low extracellular pH (*e.g.*, pH 4.5) conditions, respectively. Four protonatable residues located in the extracellular loop were found to be involved in acid-sensing. Hydrophilic substitutions of the closed gate residue W304 constitutively opened the channel at high extracellular pH for WT PAC and even when PAC was rendered proton-insensitive. This study revealed that PAC adopts a mechanism of alternate pore gates formed by hydrophobic residues W304 and I307 and identified four protonatable extracellular residues involved in proton binding or sensing.

In summary, this thesis consists of investigations on functionally important intramolecular interactions in TRP channels that are differently regulated by PIP2, and on

gates and proton activation of the PAC channel.

PREFACE

This thesis is an original work by Ruiqi Cai. The frog-related experiments have been approved by University of Alberta Animal Care Protocol AUP00000234, Project Name "Molecular Physiology of Polycystins and Fibrocystin, products of the autosomal dominant polycystic kidney disease genes".

Chapter 2 of this thesis has been published as "Direct binding between pre-S1 and TRP-like domains in TRPP channels mediates gating and functional regulation by PIP2" in ***Cell Reports***, 22, 1560-1573, 2018.

Wang Zheng, Ruiqi Cai, Laura Hofmann, Vasyl Nesin, Qiaolin Hu, Wentong Long, Mohammad Fatehi, Xiong Liu, Shaimaa Hussein, Tim Kong, Jingru Li, Peter E. Light, Jingfeng Tang, Veit Flockerzi, Leonidas Tsiokas, and Xing-Zhen Chen

Wang Zheng, I and Laura Hofmann contributed equally to this paper.

In this paper, I have conceived the part of PIP2 regulation and performed significant experiments including electrophysiology on *Xenopus* oocytes, all co-immunoprecipitation assays and PIP2 related data. I have actively participated in preparations of manuscript, figures and revisions.

Conceptualization, W.Z., R.C., and X.-Z.C.; Investigation, W.Z., R.C., L.H., V.N., Q.H., W.L., M.F., X.L., S.H., T.K., and J.L.; Supervision, P.E.L., J.T., V.F., L.T., and X.-Z.C.; Writing, W.Z., L.T., V.F., and X.-Z.C.

Chapter 3 of this thesis is accepted by ***iScience*** as "Autoinhibition of TRPV6 channel

and regulation by PIP2".

Ruiqi Cai, Xiong Liu, Rui Zhang, Laura Hofmann, Wang Zheng, Ruhul Md Amin, Lingyun Wang, Qiaolin Hu, Ji-Bin Peng, Marek Michalak, Veit Flockerzi, Declan W Ali, Jingfeng Tang, and Xing-Zhen Chen

I and Xiong Liu contributed equally to this paper.

In this paper, I conceived and designed all the experiments and have conducted majority of electrophysiology, co-immunoprecipitation, *in-vitro* pull down and all PIP2 related experiments. Besides, I wrote the first draft of the manuscript, built the figures and prepared the revisions. Of note, Rui Zhang was responsible for the zebrafish data.

Conceptualization, R.C. and X.-Z.C.; Investigation, R.C., X.L., R.Z., L.H., W.Z., M.R.A., L.W., Q.H.; Supervision, J.-B.P., D.A., V.F., J.T. and X.-Z.C. Writing, R.C. and X.-Z.C.

Chapter 4 of this thesis is a manuscript ready to be submitted as "Role of the S5/S6 helix interaction in the regulation of the TRPV6 channel function and breast cancer progression".

Ruiqi Cai, Lingyun Wang, Xiong Liu, JingFeng Tang, Ji-Bin Peng, Xing-Zhen Chen

In this paper, I conceived the concept of S5/S6 helix interaction, designed and performed all electrophysiology, co-immunoprecipitation, biomedical assays on cultured cancer cells, Western blotting on cell signaling pathways and Kaplan–Meier analysis. I wrote the first version of the manuscript and prepared for the revisions. Of note, Lingyun Wang and Ji-Bin Peng performed the MD and generated the corresponding data.

Conceptualization, R.C. and X.-Z.C.; Investigation, R.C., L.-Y.W., X.L. Supervision, J.T., J.-B.P. and X.-Z.C. Writing, R.C., L.-Y. W., J.-B.P. and X.-Z.C.

Chapter 5 of this thesis is a manuscript submitted as “Hydrophobic gates and proton binding in proton-activated chloride channel”.

Ruiqi Cai, JingFeng Tang, Xing-Zhen Chen

In this paper, I conceived the idea to determine gate(s) and proton activation in PAC. I designed and performed all the experiments. Also, I drafted the manuscript and prepared for the revisions.

Conceptualization, R.C. and X.-Z.C.; Investigation, R.C. Supervision, J.T. and X.-Z.C. Writing, R.C. and X.-Z.C.

ACKNOWLEDGMENTS

It's very lucky for me to get the chance to conduct my PhD study in Dr. Xing-Zhen Chen lab for the past years. I would like to cordially thank each of them.

At the very first, my utmost thanks go to my supervisor Dr. Chen, who is always available for valuable discussions on different projects inspiring me greatly. I have gained rich experience more than experimental skills, scientific writing and critical thinking, but also opportunities to cooperate efficiently. Importantly, Dr. Chen also provided me sufficient freedom to expand the edge of knowledge. Indeed, Dr. Chen has contributed a lot to what I achieved, which are impossible on my own.

I am highly grateful for my supervisory committee, Drs. Joanne Lemieux and Todd Alexander. They have always been very helpful throughout my PhD study, offering constructive suggestions and unique chances to facilitate my research. Additionally, I want to thank Dr. Veit Flockerzi for his kind hosting in Homburg, where I obtained precious experience beyond patch clamping.

Besides, I would like to thank my colleagues Qian Wang, Qiaolin Hu, Xiong Liu and especially Wang Zheng, who has helped me prominently. Also, I would like to thank all staff from Department of Physiology, Dr. Funk, Kim, Donna, Dancy, Linda, Debbie, Sharon, Dominique and financial supports from IRTG, Alberta Innovates and FoMD.

In particular, thanks from my deepest heart go to my parents, wife, relatives and passed-away grandfathers for their irreplaceable love and supports.

TABLE OF CONTENTS

LIST OF FIGURES

Chapter 1

Chapter 3

Chapter 4

Chapter 5

LIST OF ABBREVIATIONS

2-APB	2-aminoethoxydiphenyl borate
aa	amino acid
ADPKD	autosomal dominant polycystin kidney disease
Akt	protein kinase B
BAPTA-AM	1,2-bis(2-aminophenoxy)ethane N,N,N',N'-tetraacetic acid acetoxymethyl ester
CFTR	cystic fibrosis transmembrane conductance regulator
Co-IF	co-immunofluorescence
Co-IP	co-immunoprecipitation
COSMIC	catalogue of somatic mutations in cancer
Cryo-EM	cryo-electron microscopy
Ctrl	control
DAG	diacyl glycerol
Dpf	day(s) post-fertilization
DTT	dithiothreitol
DMSO	dimethyl sulfoxide
EMT	epithelial to mesenchymal transition
ER	estrogen receptor
ERG	electroretinogram
FBS	fetal bovine serum
FL	full-length
GOF	gain-of-function
GSK-3β	glycogen synthase kinase 3β
GST	glutathione S-transferase
HEK293	human embryonic kidney 293
HER	human epidermal growth factor 2
HR	hazard ratio
IP3	inositol 1,4,5-triphosphate
MONNA	2-[(4-methoxynaphthalen-2-yl)amino]-5-nitrobenzoic acid

MD	molecular dynamic
MCF-7	michigan cancer foundation-7
NFA	niflumic acid
NFAT	nuclear factor of activated T-cell transcription factor
NMDG	N-methyl D-glucamine
NS	not significant
PAC	proton-activated chloride channel
PCL	polycystin like
PH	pleckstrin homology
PI3K	phosphoinositide 3-kinases
PIP2	phosphatidylinositol 4,5-bisphosphate
PLC	phospholipase C
POPC	1-palmitoyl-2-oleoyl-sn-glycero-3-phosphocholine
PR	progesterone receptor
Q-PCR	quantitative polymerase chain reaction
RMSD	root mean square deviation
RMSF	root mean square fluctuation
RT	room temperature
SNAI1	snail family transcriptional repressor 1
TEV	tobacco etch virus
TNBC	triple-negative breast cancer
TRP	transient receptor potential
WT	wildtype

LIST OF MUTANTS GENERATED IN THIS THESIS

TRPP3		**TRPV6 (1)**		**TRPV6 (2)**	**PAC**	
I40A	W81Y	F468A	R589Q	R532Q	W304N	I307V
ΔT43-P50	W81F	R470A	R628Q	R532A	I307N	I307L
ΔK51-L80	W81H	F472A	R632Q	R532D	A308N	I307F
ΔW81-L95	W81D	F478A	K484Q/R589Q/R632Q	R532W	L309N	W304N/I307N
W81A	W81E	W593A	R470F	R532F	L310N	W304Q/I307Q
G82A	W81K	R594A	W593F	R532K	A313N	D91N
T83A	W81R	W321A	W593Y	D620A	F314N	E94Q
T84A	W81L	I597A	K320Q/K322Q/R323Q	D620R	L315N	H98A
L85A	K568A	W321I	R409Q	D620F	A316N	E107Q
T86A	K568R	I597W	R414Q	D620W	L317N	H130A
E87A	K568D	W321I/I597W	R584Q	D620E	F318N	H131A
N88A	K568E	W321E	R594Q	R532W/D620W	W304Q	E133Q
T89A	R594Q	W321E/I597R	K606Q	R532F/D620W	W304S	E176Q
A90G	R596Q	I597E	R607Q	R532D/D620R	W304T	E181Q
E91A	R598Q	W321R/I597E	R610Q	R532C/D620C	W304G	D195N
N92A	R599Q	Δ(-32G)-P327 (ΔN)	R615Q		W304A	E224Q
R93A	R594Q/R596Q/R598Q/R599Q	ΔN-I597E	R621Q		W304V	E257Q/E261Q
E94A	ΔR594-K599	ΔN-I597W	R636Q		W304L	D269N
L95A		ΔN-I597R	R641Q		W304I	D289N
TRPP2		W593A/I597A	R643Q		W304F	D297N
F604P	F604P/K688A	W321A/R470A	R646Q		I307Q	E322Q
F604P/W201A		W321A/W593A	R654Q		I307G	I307W
TRPM8		R470A/I597A	K661Q		I307A	AQNN/W304N
W682A	R998A	K484Q	K666Q		I307Y	
TRPV1		R588Q	Q473A		H131A/E224Q/D289N/D297N (AQNN)	
W426A	Q423A	**TRPC4**				
R701A		G503S	G503S/R639A	G503S/W314A		

CHAPTER 1

INTRODUCTION

1.1 Discovery and expansion of transient receptor potential (TRP) channels

The founder of the TRP channel superfamily is identified from a naturally occurred and behaviorally light-insensitive *Drosophila melanogaster* mutant strain, more than half a century ago (Cosens and Manning, 1969). Despite the indistinguishable retinal morphology as wildtype (WT), the mutant strain, upon prolonged illumination, exhibited a transient decline in potential by electroretinogram (ERG) and became irresponsive to light, distinct from the ability of the WT to have more steady ERG and be constantly light responsive. Thus this mutant strain was named transient receptor potential (TRP). Two decades later, the molecular identity of *trp* gene was revealed and proposed to encode an unprecedented protein as a light activated calcium permeable channel (Hardie and Minke, 1992; Montell and Rubin, 1989), mediating the phototransduction with its homologues TRP-like and TRPγ channels (Hardie, 2001). Following the characterizations of *Drosophila* trp proteins, the vertebrate homologues were gradually uncovered starting from a human homologue, thereafter called TRP canonical 1 (TRPC1), by analyzing amino acid sequence similarities. Although predominately found in nervous system, specific mammalian TRP channels have been ubiquitously detected in various cells contributing to cardiovascular, digestive, urinary system and reproductive system (De Clercq and Vriens, 2018; Holzer, 2011; Moran et al., 2004; Yue et al., 2015), through Northern blotting, RT-PCR, western blotting and immunostaining. TRP channels mainly act as sensory receptors involved in numerous physiological cascades such as thermo-,

mechano-, osomo-, chemo-, and photosensation (Minke and Cook, 2002).

Depending on the similarity in amino acid sequences, 28 members of mammalian TRP channels are further classified into 6 subfamilies, namely TRP polycystin (-P), vanilloid (-V), melastatin (-M), mucolipin (-ML), ankyrin (-A) and canonical (-C) (Fig. 1-1). Another notable TRP channel subfamily, however not found in mammalian so far, is TRP no-mechano-potential-C (-N) merely detected in zebrafish and *Caenorhabditis elegans* as the 7th subfamily (Xiao and Xu, 2009). A recent phylogenetic study proposed a novel 8th TRP channel subfamily named soromelastatin (TRPS) by analysis of a database containing more than a thousand TRPM-like sequences (Himmel et al., 2020), but in depth molecular and functional investigations are required to further verify.

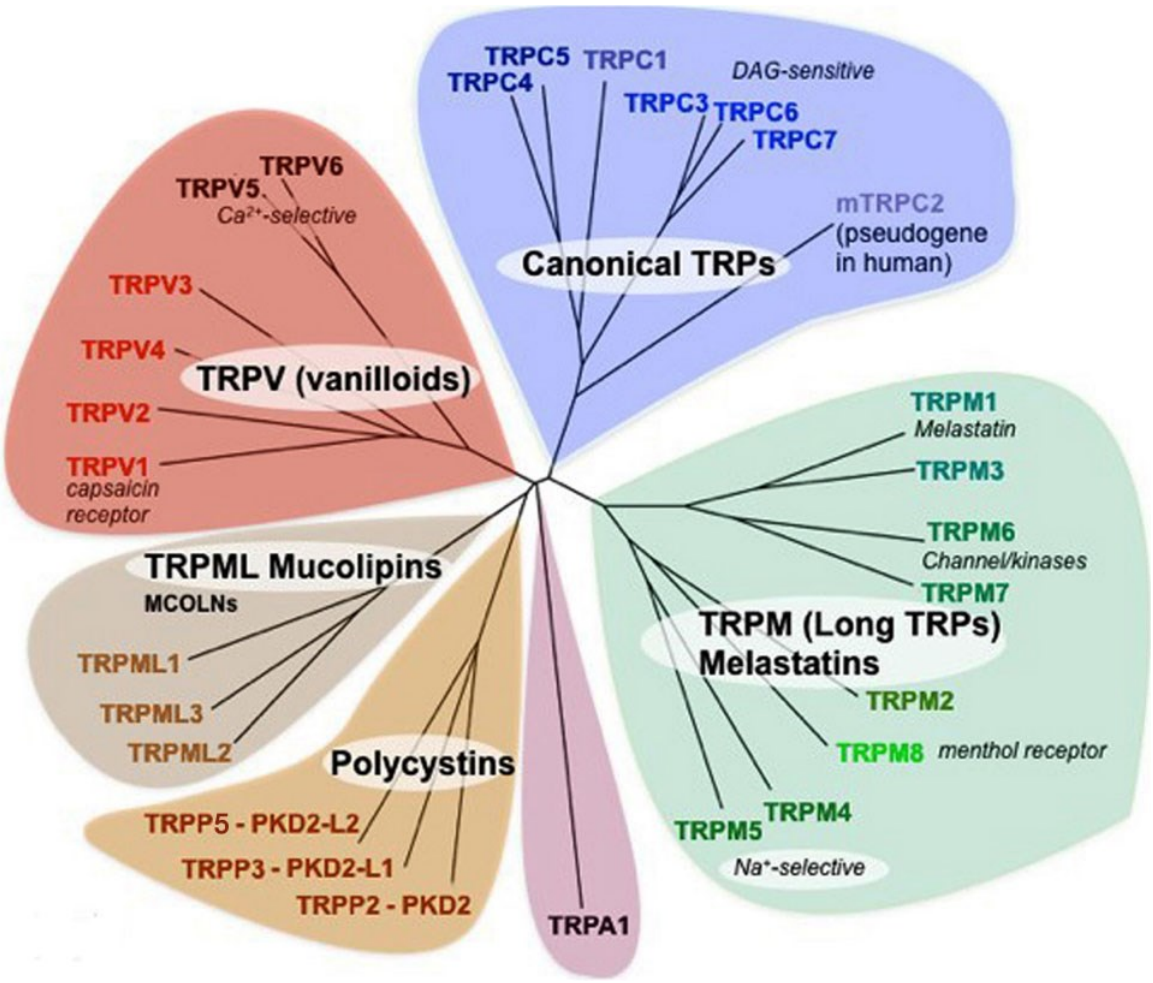

Fig. 1-1. Phylogeny of representative mammalian TRP channels. The phylogenic tree was generated by aligning the transmembrane domains of mammalian TRP channels. Adapted and permission acquired from Tsagareli et al., *Behav. Pharmacol.*, 2019 and Clapham, *Nature*, 2003 (Tsagareli and Nozadze, 2019; Clapham, 2003).

1.1.1 TRP channels and diseases

Abnormal function due to mutations or altered expressions of TRP channels could lead to multiple human diseases (Nilius, 2007), which also termed as TRP channelopathies, besides the important physiological roles of TRP channels. Among the

TRP channelopathies, members from all six TRP channel subfamilies have been reported as genetic causes of inherited diseases. For instance, there are autosomal dominant polycystin kidney disease (ADPKD, TRPP2), scapuloperoneal spinal muscular atrophy and Charcot-Marie-Tooth disease type 2C (TRPV4), autosomal-recessive congenital stationary night blindness (TRPM1), autosomal-dominant progressive familial heart block type 1 (TRPM4), autosomal dominant familial episodic pain syndrome (TRPML1), focal and segmental glomerulosclerosis (TRPC6), familial episodic pain syndrome (TRPA1) (Nilius and Owsianik, 2011). In addition to the inheritable diseases, TRP channels have also been linked to diseases including but not limited to cancer (TRPV6, -V1, -M1, -M4, -M5, -C1, -C6 etc.), transient neonatal hyperparathyroidism (TRPV6), diabetes (TRPV1, -M2, -M5), gastrointestinal and bladder disorders (TRPV1, -V4, -M8, -A1), cardiac hypertrophy (TRPC6), familial Alzheimer's disease (TRPM7), dermatological disorders (TRPV3) (Kaneko and Szallasi, 2014).

1.1.2 Properties of TRP channel structures

Functional TRP channels form a homo- or heterotetramer to mediate cation permeation on the cell surface. Subunits of TRP channels share the same topology features of six membrane-spanning helices (S1-S6) with N- and C-termini in the cytosol. Within one subunit, S1-S4 helices are recognized as a voltage sensing like domain resembling the voltage sensing domain of the voltage-gated potassium channels. While

S5, S6 helices and an extracellular loop in between constitute the channel pore region. Despite of these similarities, TRP channel subfamilies have unique functional domains located within the cytosolic N- and C-termini. Multiple ankyrin repeats are dominantly found in the N-terminus of TRPA1, whereas TRPV, -C, -M also contain certain ankyrin repeats in the N-terminus (Niemeyer, 2005). In addition, TRPM channels have a featured N-terminal TRPM homology domain conserved in all subfamily members. On the proximal region of C-terminus, a motif called TRP box conserved in TRPV, -C and -M has proposed importance in regulation of channel function. The distal of C-terminus, meanwhile, contains PDZ domains for TRPCs and -V3, kinase domains for TRPM2, M6 and -M7, EF-hand calcium binding domain for TRPPs and -Cs (Clapham, 2003). Of note, the extracellular loop between S1 and S2 helices in TRPP, -M, -ML subfamilies are much extended compared to others (Fig. 1-2).

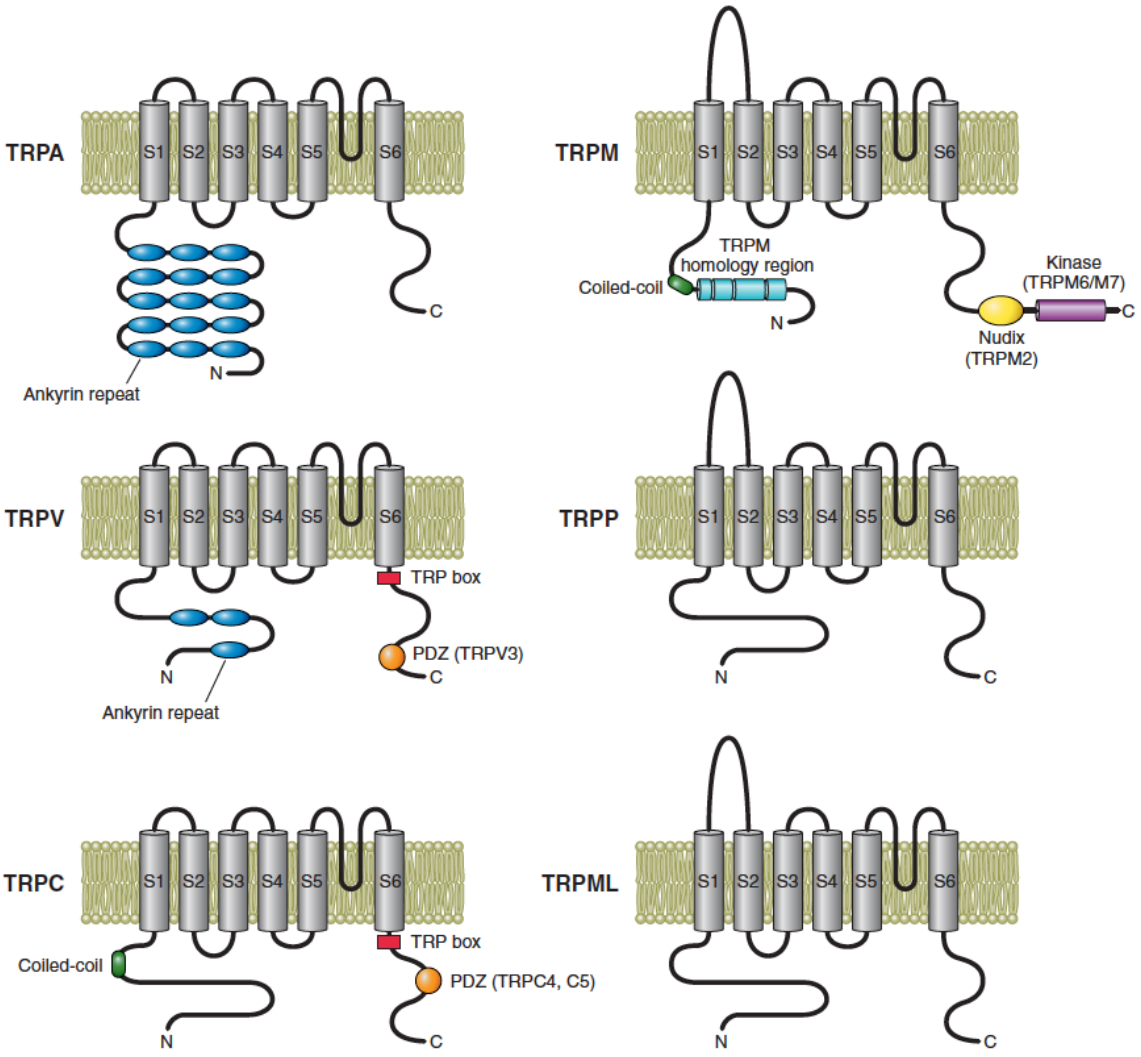

Fig. 1-2. Membrane topology and functional domains of N- and C-termini of mammalian TRP channels. Permission is not required, from Earley and Brayden, *Physiol Rev*., 2015 (Earley et al., 2015).

1.1.3 Functional regulation of TRP channels

All TRP proteins are non-selective cation permeable channels, except for two highly-calcium selective channels, TRPV5 and TRPV6 (Peng et al., 2018). TRP channels

are recognized as polymodal since various external stimuli activate TRP channels. When activated, TRP channels mediate extracellular cations to diffuse across the cell membrane leading to cell deplorization or cellular signaling cascades (Clapham, 2003). Given the crucial importance of TRP channels in maintenance of normal physiology and close links to pathology, efforts to elucidate the mechanisms of functional regulation of TRP channels have been made through decades. Although no unified mechanisms have been proved for all TRP channels, generally there are four regulatory categories, namely phospholipids, ligands, post-translational modification and membrane potential, suggested to explain the activation of TRP channels (Ramsey et al., 2006). The most abundant inner cell membrane locating phospholipid with double phosphorylation is known as phosphatidylinositol 4,5-bisphosphate (PIP2) (Suh and Hille, 2008). Majority of TRP channels function have been validated to be regulated by PIP2, but the specific effects (ie. activation or inhibition) and mechanisms (direct or indirect) differ. PIP2 activates channel function of TRPV5, -V6, -C3, -M4, -M5, -M8 while inhibits TRPV3, -C4, -P2. On the other hand, PIP2 seems to have dual roles on TRPV1, -C5, -C6, -C7, -M7 function under different experimental conditions (Nilius et al., 2008). It has been known that PIP2 regulates TRP channel function either through direct binding to clusters of cationic residues within TRP channels such as TRPV1, -C4, -C6, -M4, -M5,- M6, or indirectly through phospholipase C downstream pathways especially for TRPC channels. Forms of post-translational modifications for TRP channels reported include

phosphorylation (almost all TRPs), ubiquitination (TRPA1), SUMOylation (TRPV1, -M4), palmitoylation (TRPP3), however whether more TRP channels are post-translationally modified remained to be verified. As TRP channels are polymodal, lots of ligands and even synthetic compounds are well known to regulate specific TRP channels. Particularly, the thermo-TRP channels are activated by natural compounds like capsaicin, resiniferatoxin/Double-knot toxin (TRPV1), menthol (TRPM8), bisandrographolide (TRPV4), respectively. As for synthetic ligands, non-specific compound like 2-aminoethyl diphenylborinate activates TRPV1, -V2 and -V3, while inhibits TRPV6, as well as icilin activates both TRPM8 and -A1. Other specific ligand such as GSK1016790A and olvanil only works on TRPV4 and -V1, respectively (Nilius and Owsianik, 2011). Although no canonical voltage sensing domains, similar to the voltage gated potassium channels, have been found in TRP channels, biophysical studies have shown that positively charged lysine and arginine in S4 helix and S4-S5 linker of TRPM8 and -V1 are proposed to be sensitive to changes of membrane potential (Voets et al., 2004).

1.1.4 Advances in cryo-EM structures of TRP channels

The high-resolution structures of TRP channels remain elusive until the recent revolutionary advances in cryo-electron microscopy. The first available near-atomic cryo-EM structure of TRP channels is a rat TRPV1 truncated mutant, with similar

function as WT, resolved at 3.4 Å in a closed state (Liao et al., 2013). The overall structure of rTRPV1 is a tetramer, which resembles previously known domain-swapped structures of voltage-gated ion channels with a S1-S4 domain close to a neighbor S5-loop-S6 pore region (Liao et al., 2013). Ion permeation of rTRPV1 was also visualized by calculation of distance along pore axis, in which two narrowest parts proposed as gates are formed by side chains of G643 (upper gate or selectivity filter) and I679 (lower gate) from four subunits (Liao et al., 2013). From then on, accumulating high-resolution structures of TRP channels have been reported for the past years. Presently, 117 cryo-EM as well as 22 X-ray crystal structures are deposited in the protein data bank, which cover majority members of TRP channels (Fig. 1-3). Importantly, besides the closed TRP channels structures, a number of open, activated or inhibited TRP channels binding to various ligands, phospholipids or chemicals were resolved. These structural breakthroughs enable unprecedented chances to understand the gating mechanisms and functional regulation of TRP channels.

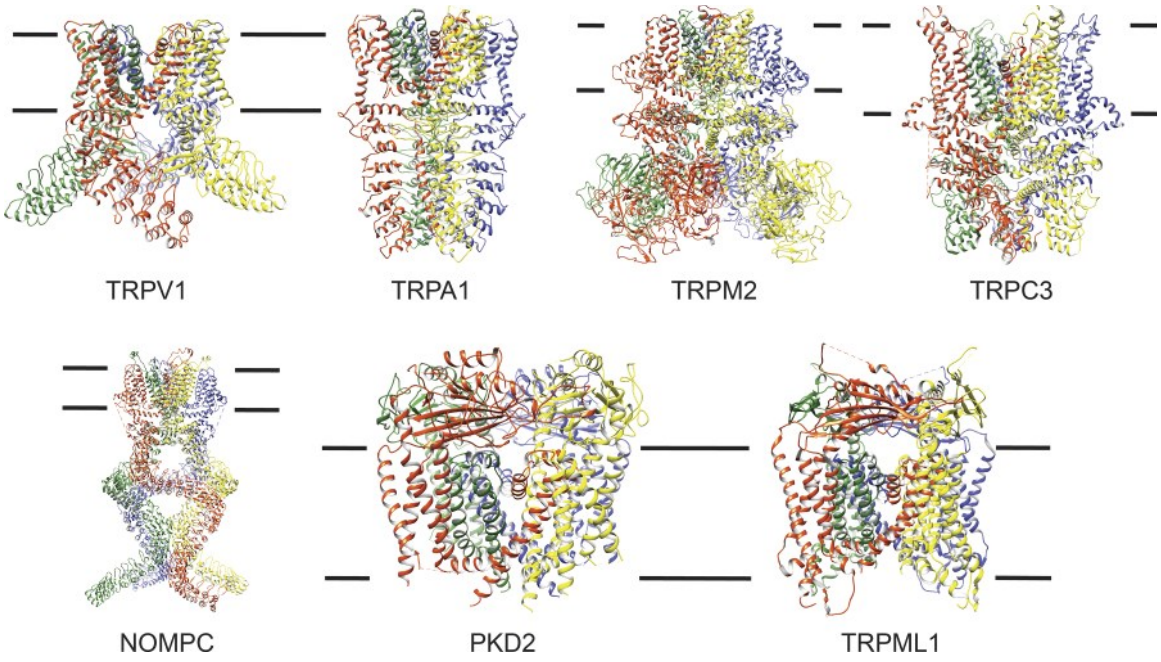

Fig. 1-3. Representative structures of TRP subfamilies. TRP channels are shown in ribbon diagrams viewed parallel to the membrane, with each subunit color-coded differently. TRP channels are decorated with unique soluble domains outside the relatively conserved transmembrane core structure embedded within the lipid bilayer delimited with two black horizontal lines. PDB accession numbers: TRPV1 (3J5P), TRPA1 (3J9P), TRPM2 (6MIX), TRPC3 (6CUD), no mechanoreceptor potential C (NOMPC; 5VKQ), PKD2 (5T4D), and TRPML1 (5WJ5). Adapted and permission acquired from Cao, *J Gen Physiol.*, 2020 (Cao, 2020).

1.1.5 Suggested intramolecular interactions in TRP channels

TRP channels are polymodal upon regulation of different kinds of endogenous or exogenous modulators. However, it is not clear whether regulations initiated by different factors induce similar conformational changes that lead to opening or closing of TRP channels. In an ion channel, two or more proximal amino acids within a subunit could

form energy favorable π-π, π-cation, salt bridge interactions, van der Waals force and hydrogen bond. Examples of intramolecular interactions in ion channels include, but are not limit to, voltage gated ion channels (Altier et al., 2012; Sharmin and Gallin, 2017), chloride channels (Dhani and Bear, 2006), Orai1 channel (Kim et al., 2018). For the TRP channels, the first suggested intramolecular interactions were reported in rTRPV1 cryo-EM structure (Liao et al., 2013), in which each of N-terminal pre-S1 helix just before the S1 helix and the S4-S5 linker exhibits close proximity to the C-terminal TRP domain. Similar patterns are also observed in later resolved TRP channel structures. But the existence and the functional importance of the proposed interactions were not yet verified.

1.1.6 Animal models for TRP channels

Given the proposed importance in physiology and pathology, channel function of mammalian TRP channels have been investigated by extensive studies using *Xenopus* oocyte, mammalian cell lines as models. However, the physiological roles of many TRP channels remain unidentified even with a specific TRP channel deficient mouse models (Desai and Clapham, 2005). It is possible that some proteins could have the redundance function or up-regulated when a TRP channel is deficient. A very good example is a recent report showing that only if TRPA1, -V1 and -M3, which are known heat sensors, are triple-knocked out at the same time, would the mice became noxious heat insensitive

(Vandewauw et al., 2018). As for the pathology, TRP channelopathies are often caused by gain-of-function or loss-of-function TRP mutant, which are verified by biophysical studies, but the mechanistic insights from mouse models are absent. In addition to mouse, zebrafish is another common and powerful model to mimic TRP-related diseases and provide mechanistic insights (Venkatachalam and Montell, 2007). It is worthwhile to generate specific knock-in mice models to better understand the detailed mechanisms involved, which would further validate the importance of TRP channel as therapeutic targets in clinical trials.

1.2 TRP polycystin channels

TRP polycystin (TRPP) subfamily was named after its founding member TRPP2, mutations in which could result in autosomal dominant polycystic kidney disease (ADPKD). Mainly targeting the endoplasmic reticulum in a cell as a calcium release channel, TRPP2 also locates on the primary cilia in the kidney, where it forms a complex with polycystin-1 (PKD1) and their roles on ADPKD have been the subject of great attention. Meanwhile, TRPP2 contributes to maintenance of vascular systems and organ morphogenesis (Busch et al., 2017; Du et al., 2016). TRPP2 shares high sequence homology to its remaining family members TRPP3 (78%) and -P5 (71%) (Samanta et al., 2018). Abnormalities of TRPP3 or -P5 cannot initiate development of ADPKD. TRPP3,

originally named polycystin like (PCL), was characterized as a non-selective cation permeable channel (Chen et al., 1999). Expressions of TRPP3 have been broadly detected in kidney, tongue, brain, testis and cardiac muscles. However, TRPP3 has been proposed as a sour sensing candidate together with PKD1-like 3 (PKD1L3) and a mechano-sensor in neuron to maintain natural formation of spinal curvature (Sternberg et al., 2018; Yu et al., 2012). But the role of TRPP3 and PKD1L3 in acid sensing became contradictory, with reports showing that the PKD1L3 and TRPP2 knockout mice, respectively, have normal and partial loss of sour tasting (Horio et al., 2011). Our lab recently proposed that TRPP3 alone exhibits acid activation as "off-response" in *Xenopus* oocytes (Hussein et al., 2015). Yet, more physiological relevance of TRPP3 and -P5 needs further investigations.

1.2.1 Structures of TRPP channels and proposed intramolecular interactions

The precise architectures of TRPP2 (3 to 4.2 Å) and -P3 (3.4 Å) have been determined in recent years by cryo-EM. So far, there are TRPP2 structures in closed and open states, and one TRPP3 structure in open state (Cao, 2020). The overall structures of TRPP2 and TRPP3 are similar to other TRP channels. The arrangements of pre-S1 and TRP-like domains in TRPP2 and TRPP3 structures are not fully available due to truncations (Su et al., 2018). Although present structures of TRPP2 and TRPP3 are both resolved from truncated mutants, they still provide tremendous details to understand the

underlying mechanism of gating process. Structurally, TRPP3 is identical to TRPP2 and both of them have a characteristic polycystin domain, composed by S1-S2 loop, recently found to contain intramolecular interactions stabilizing TRPP2 structure and facilitating its opening (Vien et al., 2020). Proposed as voltage sensitive, both TRPP2 and -P3 have cationic residues in S4 helix suggested to interact with residues in S3 helix. Later in TRPP3, S4 helix is suggested to have a transitional conformation change upon depolarization to disrupt the S3-S4 helix intramolecular interactions and open the channel (Ng et al., 2019). More interactions between pore-polycystin domain, S4-pore helix are proposed but not yet experimentally examined (Su et al., 2018).

1.2.2 Regulation of TRPP channels

TRPP2 and -P3 channels are known to be regulated through various mechanisms. For instance, TRPP2 expression is translationally controlled by endoplasmic reticulum stress and RNA binding protein far upstream element-binding protein 1 (Yang et al., 2013; Zheng et al., 2016a). Scaffolding protein filamin-a stabilizes expression, facilitates membrane targeting, and inhibits channel activity of TRPP2 (Wang et al., 2012; Wang et al., 2015). Cytosolic residues within TRPP2 and also TRPP3 proteins can be post translationally modified by phosphorylation, palmitoylation (Zheng et al., 2016b). On the other hand, TRPP2 is activated by a ligand called wnt9b through a direct ligand-receptor interaction between WNT9B and PKD1 (Kim et al., 2016), but no ligand has been

identified for TRPP3. Similar to other TRP channels, TRPP2 is regulated by endogenous levels of PIP2 (Ma et al., 2005). An epidermal growth factor induced and TRPP2 required currents observed in kidney epithelial cells are inhibited by presence of PIP2. But further mechanism of the way that PIP2 affects TRPP2 function is not tested. PIP2 regulation on TRPP3 and -P5, however, remains undetermined. There are many other ways reported to regulate TRPP3 function such as pH, voltage, cell volume changes, trimerization, receptor for activated protein kinase 1, amiloride analogs (Dai et al., 2007; Shimizu et al., 2009; Yang et al., 2012).

1.3 TRP vanilloid 6 channel

The epithelial TRP vanilloid 6 (TRPV6) channel was originally called CaT1 for calcium transport protein, identified by a functional searching for calcium-absorption channels in rat duodenum (Fig. 1-4) (Peng et al., 1999). Due to amino acid homology and structural relationship to TRPV subfamily, CaT1 is renamed to TRPV6 after the founding member TRPV1, which is the vanilloid receptor. TRPV6 shares a 75% sequence identity to its close homologue TRPV5, both of which are unique channels for their high calcium-selectivity among the non-selective TRP channel superfamily (Peng et al., 2018). The tissue distributions of TRPV6 and -V5 vary, albeit they share many similarities. Abundant in the small intestine, TRPV6 has a broad expression spectrum and is present

in testis, prostate, ovary, pancreas, placenta, exocrine glands (sweat, mammary and salivary), kidney and liver (Peng et al., 2018). Especially, TRPV6 is found to enriched in epithelia cells of duodenum and proximal colon, where the dominant trancellular calcium absorption occurs (Hoenderop et al., 2005). Compared to the ubiquitous TRPV6, TRPV5 has a predominant expression in kidney, especially in the collecting and distal convoluted tubules (Peng et al., 2018), functioning in calcium reabsorption. Correspondingly, the TRPV6 channel plays crucial roles on transcellular calcium absorption or transportation in small intestine, exocrine and reproductive processes, and possibly has other unrevealed physiological relevance warrants further studies.

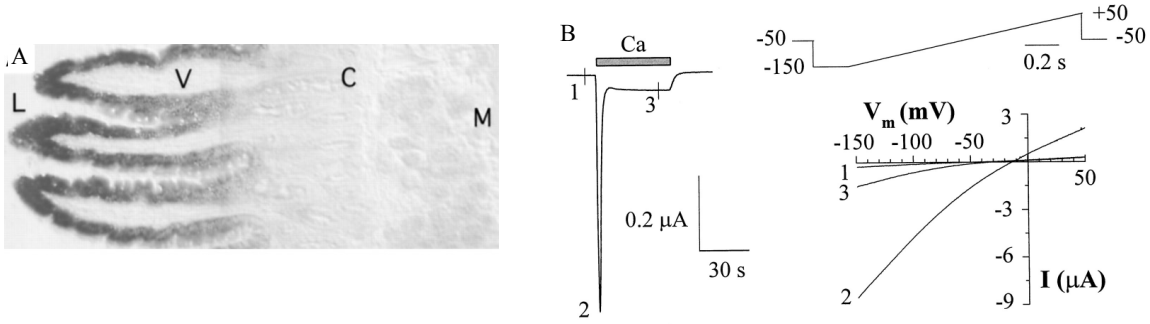

Fig. 1-4. Expression of TRPV6 in rat intestine and biophysical properties. (A) Image shows the presence of *TRPV6* in duodenum by in situ hybridization (M, muscle layer; V, villi; C, crypt;L, lumen). (B) Representative current traces from oocytes expressing TRPV6 induced by 5 mM Ca^{2+} at a holding potential of -50 mV. Adapted and permission acquired from Peng et al., *J Biol Chem.*, 1999 (Peng et al., 1999).

1.3.1 Regulation of TRPV6 channel function

TRPV6 channel is one of the most calcium selective channels among TRP channels, with calcium to sodium ions permeability ratio over 130 (Yue et al., 2001). When heterogeneously expressed in living cells, TRPV6 is constitutively open and can dramatically increase calcium uptake in oocytes (Peng et al., 1999). Two electrode voltage clamp showed that extracellular calcium induce a rapidly desensitizing spike current, which is oocyte endogenous calcium-activated chloride current inhibitable by chloride channel blockers, and followed by a plateau, regarded as the calcium induced TRPV6 channel activity (Fig. 1-4) (Peng et al., 1999). Presently, PIP2 and calmodulin are two endogenous components known to regulate TRPV6 channel function. A feedback loop was proposed that calcium influx through TRPV6 increases intracellular calcium levels and activates the phospholipase C, which hydrolyzes TRPV6-stimulatory PIP2, and results in TRPV6 inactivation reversible by application of PIP2 (Thyagarajan et al., 2008). As of now, PIP2 has been well documented as a direct activator of TRPV6 by excised patches and planar lipid bilayer (Thyagarajan et al., 2008; Zakharian et al., 2011). PIP2 depletion by a rapamycin inducible PIP2 5-phosphatase in HEK293 cells or a concentrated phosphatidylinositol 4-kinase inhibitor wortmannin inhibits TRPV6 channel function (Thyagarajan et al., 2008). The native PIP2 binding sites in TRPV6, however, are not known. Molecular dynamic simulations data suggested a glycine (G488), corresponding to an arginine (R575) suggested to bind PIP2 in human and rat TRPV1, has enhanced PIP2 affinity when substituted by arginine (Velisetty et al., 2016). On the

other hand, TRPV6 function is negatively regulated by calmodulin (Niemeyer et al., 2001). Calmodulin has been functionally characterized to bind C-terminus of TRPV6 in a 1:1 stoichiometry (Niemeyer et al., 2001). Furthermore, the threonine (T702) in calmodulin binding domain can be phosphorylated by protein kinase C, which provides a dual regulation of this domain (Niemeyer et al., 2001). Physiologically, expression of TRPV6 is regulated by the hormone 1,25-dihydroxyvitamin D3, prolactin and estrogen (Fecher-Trost et al., 2014; Hoenderop et al., 2005). A notable chemical called 2-aminoethoxydiphenyl borate (2-APB), known to activate TRPV1-3, -A1, -M6, whereas inhibits TRPV6 function in addition to TRPC3, -C6, -C7, -M2, -M7 (Singh et al., 2018b; Voets et al., 2001).

1.3.2 Structures of TRPV6 channel

High-resolution structures of TRPV6 have been resolved by X-ray crystallography as well as recently developed cryo-EM (Yelshanskaya et al., 2020). The first available TRPV6 structure was crystalized and in its closed conformation, then followed by cryo-EM or crystal structures of TRPV6 opening (Yelshanskaya et al., 2020). These near atomic structures of TRPV6 unveil previously unclear details in depth, although some mutations and truncations were introduced to promote high yield of TRPV6 channel in mammalian cell lines (Yelshanskaya et al., 2020). The overall structures of TRPV6 have the features of TRP channels with 6 transmembrane-spanning helices, cytosolic N- and

C-termini, pore region constituted by S5-P-S6 regions (Fig. 1-5). The distinguishable calcium selectivity of TRPV6 is structurally supported by observation of a narrowest physical constriction composed by four aspartate residues (D541) (Saotome et al., 2016). While the S4-S5 linker is missing in the first crystal structure, it's present in later cryo-EM structures, which exhibits a close proximity to the amphipathic TRP helix after S6 helix running paralleled to the cell surface (Fig. 1-5) (McGoldrick et al., 2018). The α helical TRP helices of TRPV6 and -V5 (motif WRxxI) are alike but not the same as a canonical TRP domain with a motif WKxxR/K. The importance of these domains and arrangements remains unknown. Later, in addition to closed and open structures of TRPV6, more structures in distinct states like inhibited by 2-APB and in complex with calmodulin were determined (Yelshanskaya et al., 2020). Although the activator PIP2 binding to TRPV6 remains elusive, structural data of its close homologue TRPV5 reveal that PIP2 analogue binds to N-terminal linker, S4-S5 linker and C-terminal TRP domain (Hughes et al., 2018). Mechanisms of TRPV6-calmodulin or TRPV5-calmodulin interaction are similar suggested by structures, through cation-π bounding mainly mediated by a tryptophan in the end of S6 helix and a lysine in C-lobe of calcium binding-calmodulin in a one to one ratio (Hughes et al., 2018; Singh et al., 2018a). Positioning of inhibitor 2-APB in the S1-S4 helices close to the cytoplasmic side induce TRPV6 closure by competing a stimulatory lipid binding to TRPV6 (Singh et al., 2018b).

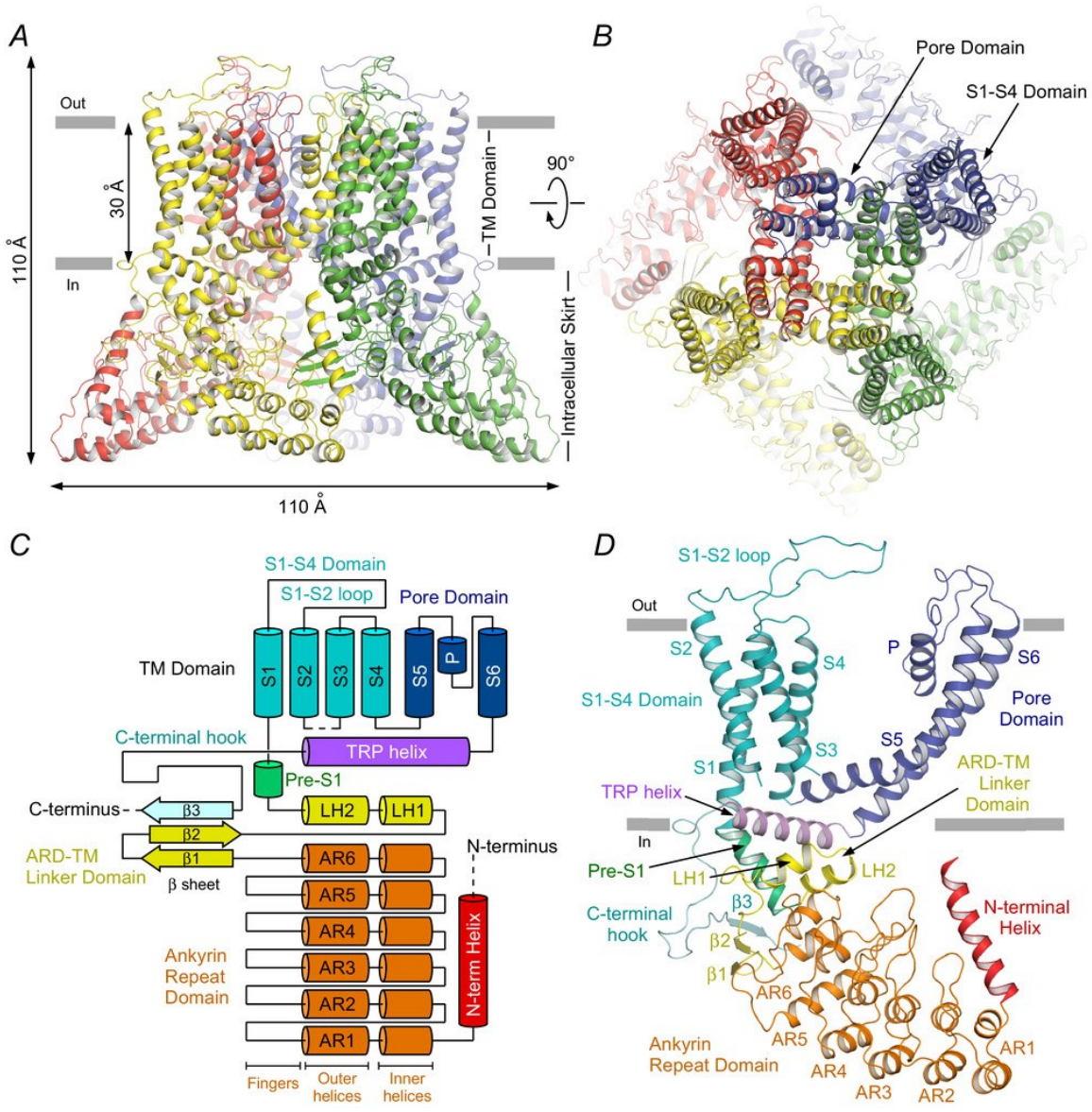

Fig. 1-5. Structural features of human TRPV6. Side (A) and top (B) views of the human TRPV6 tetramer (PDB ID: 6BO8), with each subunit shown in a different colour. C, domain organization diagram of the TRPV6 subunit. D, a single human TRPV6 subunit, with domains coloured similarly to C. Reused and permission acquired from Yelshanskaya et al., *J Physiol.*, 2020. (Yelshanskaya et al., 2020).

1.3.3 TRPV6 channel in human diseases and animal models

Expression of TRPV6 can be broadly found in various tissues indicating its diverse roles in physiology and importantly diseases, in addition to its prominent calcium absorption in the small intestine. Abnormalities in expression or function of TRPV6 have been proposed to contribute to different diseases. After the early molecular identification, TRPV6 was first found to be transcriptionally up-regulated in human prostate cancer specimen in comparison with benign prostate tissues with undetectable *TRPV6* by independent groups (Fixemer et al., 2003; Peng et al., 2001; Wissenbach et al., 2001). All of the criteria such as pathological stage, extraprostatic extension and Gleason grade correlate with higher expression of TRPV6 mRNA, which makes TRPV6 to be a promising prognostic biomarker for prostate cancer clinical assessment. Development of antibodies against TRPV6 enabled a systematic investigation on a number of cancer tissues, which demonstrated that significantly enriched TRPV6 protein, consistent to its higher mRNA level detected in prostate cancer, was detected by immunohistochemistry in breast, prostate, ovarian, thyroid and colon cancerous biopsies, while in low or negligible levels in normal tissues (Zhuang et al., 2002). More recently, pancreatic cancer is added to the list of cancers related to TRPV6 elevation (Song et al., 2018). Of note, the effects of TRPV6 on colon cancer seem contradictory since studies showed that TRPV6 up-regulation by vitamin-D3 receptor activation protects from the progression of colon cancer (Chow et al., 2007). Different from these cancers potentially promoted by TRPV6, the cervical squamous cell carcinoma patients with poorer survival rate in early stage is

reported to have lower expression of TRPV6 (Chow et al., 2007). Besides proposed as an oncochannel (Huber, 2013), TRPV6 albeit is not highly expressed in the kidney contributes to higher risk of kidney stone formation when harbouring non-synonymous polymorphisms (C157R, M378V, M681T), presumably due to TRPV6-associated hypercalciuria (Suzuki et al., 2008). Loss-of-function TRPV6 mutants caused by frame shift are suggested to impair the maternal-fetal calcium absorption, which is an emerging pathology termed as transient neonatal hyperparathyroidism (Suzuki et al., 2018). Regarding the importance of TRPV6, genetically modified animal models have been developed. The changes in calcium homeostasis of TRPV6 knockout mice include severe male infertility (Weissgerber et al., 2012), decreased calcification, calcium absorption in intestine and kidney (Benn et al., 2008), the latter three of which is opposite in the TRPV6 transgenic mice (Peng et al., 2018). A spontaneous TRPV6 mutant in zebrafish, called matt-und-schlapp, is loss-of-function caused by early termination in N-terminus and lead to defects in calcium uptake and bone formation (Vanoevelen et al., 2011). The applications of animal models would provide invaluable insights into TRPV6 channel related physiological and pathological implications.

1.4 Breast cancer

Breast cancer is one of the most severe and common cancers among women globally

(Becker, 2015). The fundamental risks for breast cancer occurrence is age, followed by family history, reproductive factors, estrogen and lastly but not the least life style (Sun et al., 2017). There are three major types of breast cancer, depending on whether estrogen receptor (ER), progesterone receptor (PR) and human epidermal growth factor 2 (HER2) exist or not (Waks and Winer, 2019), which are luminal ($ER^+/PR^+/HER2^-$), $HER2^+$ ($ER^-/PR^-/HER2^+$) and basal like ($ER^-/PR^-/HER^-$) tumours. The luminal tumours account for 70% of all breast cancer and have the feasibility to be effectively treated with presence of ER and PR by hormonal therapies. The basal like tumours or well known as triple-negative breast cancer (TNBC) constitute of about 15% cases while this subtype remain hardly treatable with absence of all three receptors (Waks and Winer, 2019). Currently, with accumulation of massive investigations on breast cancer, the therapeutic interventions against breast cancer could include a systematic combination of endocrine therapy, immunotherapy, radiotherapy, chemotherapy or surgery (Tong et al., 2018). Despite of these advances, breast cancer remains highly deadly and in 2018 alone more than 0.6 million women died (Bray et al., 2018). During the same period, around 2.1 million new cases were diagnosed with a trend to increase (Bray et al., 2018). Thus, more mechanistic researches are demanded to solve the problem of breast cancer.

1.4.1 Ion channels and breast cancer

The associations between ion channels and breast cancer have been emerging since

1980s when the multidrug resistance in human leukemia cells was examined by patch clamp techniques (Prevarskaya et al., 2018). Accumulated evidence showed that ion channels involve in the breast cancer progression through contribution to major cancer hallmarks known as uncontrolled proliferation, apoptotic resistance, invasion and metastasis, and angiogenesis. Ca^{2+} as a second messenger are well known to control a number of cellular processes such as proliferation, migration (Clapham, 2007). Calcium influx mediated by a variety of calcium channels, ranging from voltage or ligand gated calcium channels, ORAI channels and importantly TRP channels, are crucial for development of breast cancer via multiple mechanisms (Azimi et al., 2014). For example, mRNA knockdown of $Ca_V3.1$, -3.2, ORAI1, -3, P2X5, -7, TRPV4, -V6, -M7, lead to reductions of cell proliferation, migration, invasion as well as epithelial to mesenchymal transition (EMT) markers in breast cancer cell lines (Azimi et al., 2014). In the cytosol, K^+ mediated by potassium channels are the most concentrated cations modulating the cell depolarization and repolarization. Potassium channels, including voltage gated, two-pore, inwardly rectifying G-protein-coupled and calcium-activated potassium channels, found to be elevated in breast cancer tissues could promote proliferation through accelerating cell cycle by faster depolarization (Urrego et al., 2014). Chloride channels, like cystic fibrosis transmembrane conductance regulator, calcium-activated CLCA2, -A4 and chloride intracellular channel-4 (CLIC-4), are suggested suppressors to inhibit metastasis of breast cancer (Bustin et al., 2001; Peretti et al., 2015; Suh et al., 2007; Zhang et al.,

2013), while calcium-activated chloride channel ANO1, chloride channel-3 (CLC-3) when knocked down impair the progression in cell and animal models (Britschgi et al., 2013; Zhou et al., 2018).

1.4.2 TRPV6 channel and breast cancer

The aberrant elevations of both TRPV6 mRNA and protein in breast cancer samples were known for decades (Zhuang et al., 2002). This finding is later confirmed by a variety of investigations focusing on breast cancer cell lines and specimen from patients (Bolanz et al., 2008; Dhennin-Duthille et al., 2011; Peters et al., 2012). A first systematic study showed that a breast cancer cell T47D with TRPV6 knockdown by siRNA has decreased cell viability and calcium uptake, while moderately increased apoptosis (Bolanz et al., 2008). A followed study from the same group confirmed these with separate methods and additionally found that suppression of TRPV6 in T47D cell reduces the DNA synthesis (Peters et al., 2012). With the publically available breast cancer databases, analysis on TCGA and NKI-295 microarray cohorts showed that ER negative patients have higher *TRPV6* expression than ER positive patient (Peters et al., 2012). Furthermore, the overall survival is longer in breast cancer patients with lower *TRPV6* expression than those with high expression of *TRPV6* (Peters et al., 2012). siRNA knockdown of TRPV6 in other breast cancer cells MDA-MB-231 and MCF-7 had no effect on cell proliferation but impaired the migration of both cell lines and invasion of

MDA-MB-231 cells (Dhennin-Duthille et al., 2011). However, the endogenous levels of TRPV6 mRNA in MCF-7 and MDA-MB-231 are low, compared with that in T47D cells (Peters et al., 2012). Importantly, this study also demonstrated that the presence of TRPV6 mRNA and protein is significantly enriched in breast cancer invasive regions (Dhennin-Duthille et al., 2011). Thus far, the mechanistic insights in to how TRPV6 contributes to breast cancer progression are not yet understood, compared with the better-revealed roles of TRPV6 in prostate cancer and others through different cellular pathways (Stewart, 2020).

1.5 PAC channel

Chloride channels are selectively permeable to various anions, in which Cl^- is predominately abundant. Different from cation channels like TRP channels, chloride channels are very diverse without featured sequence or structure homology. Generally, chloride channels contain massive members and can be classified as certain members of the voltage-sensitive ClC subfamily, calcium-activated channels, high-conductance channels, the cystic fibrosis transmembrane conductance regulator (CFTR) and volume-regulated channels (Duran et al., 2010), which play vital roles in regulation of excitable muscle cell or neuron, trasepithelial transport, acidification of cellular organelles and cell volume. The function of a previously unknown chloride channel has

been described to be responsible for strongly outward rectifying chloride current upon depolarization induced by extracellular protons with half-maximum activation around pH 5.5 at room temperature (Auzanneau et al., 2003). This unique acid-induced chloride current, which could be blocked by chloride channel inhibitors, has been observed in firstly in sertoli cells and followed by various cultured mammalian cells (Auzanneau et al., 2003; Capurro et al., 2015). Increased temperature could shift the chloride channel to be more sensitive to higher pH (Sato-Numata et al., 2013), indicating the potential functionality in human physiology. It has a highest preference to Cl^-, followed by Br^-, I^-, and is impermeable to gluconate (Auzanneau et al., 2003). Efforts have been made to elucidate the molecular identity of the unknown chloride channel and many candidates have been tested and excluded (Auzanneau et al., 2003; Sato-Numata et al., 2017; Sato-Numata et al., 2013). A recent study using RNAi technique, in combination of a yellow fluorescence protein linked with iodine-sensitive domain, unbiasedly screened, identified and renamed a TMEM206 protein as the long-sought proton-activated chloride (PAC) channel (Yang et al., 2019), which is independently confirmed by a slightly later work (Fig. 1-6) (Ullrich et al., 2019). The presence of PAC channel is highly conserved across species from fish, frog, chicken to mammals (Ullrich et al., 2019; Yang et al., 2019). The tissue expression pattern of the PAC channel was accordingly examined with highest expression in cerebral cortex (Yang et al., 2019). Genomic studies have implicated the potential importance in evolutional hypoxia adaption in human and swine

living in high altitude (Dong et al., 2014; Yi et al., 2010). Mouse model with silenced PAC channel protects the permanent middle cerebral artery occlusion caused neuronal death (Yang et al., 2019). Meanwhile, PAC channel in cultured HEK293 and primary neurons are necessary for acid-induced cell death (Ullrich et al., 2019; Yang et al., 2019). Given no sequence similarity and structural information available for the PAC channel, the gate(s) and the proton activation are elusive.

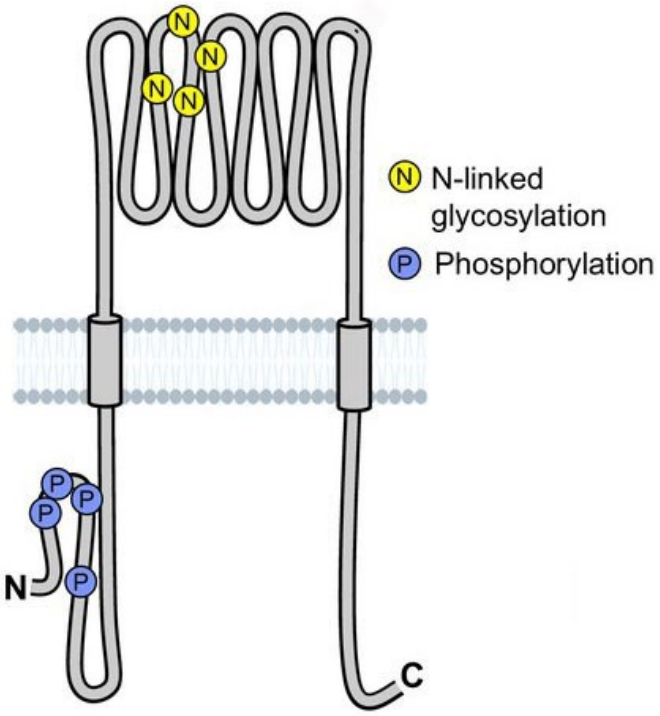

Fig. 1-6. Scheme of PAC membrane topology. Predicted N-linked glycosylation and phosphorylation sites are indicated. The permission is not acquired from Ullrich et al. *eLife*, 2019 (Ullrich et al., 2019).

1.6 Hydrophobic gate in ion channels

The concept of hydrophobic gate is originated from water behaviour observed in carbon nanotubes and model nanopores during molecular dynamic (MD) simulations (Aryal et al., 2015). Water molecule in the hydrophobic pore with a diameter smaller than 14 Å could undergo liquid-vapour oscillations, namely transitions between wet-dewet states (Hummer et al., 2001). The pore diameter controls the hydration rate, ie. the probability of pore at liquid state, inside the pore. When pore diameter is 9 Å or smaller, the pore hydration rate could be close to 0, while small changes of diameter between 9-12 Å could efficiently regulate pore hydration rate (Fig. 1-7). Besides the diameter, the hydrophobicity of the pore components also matters. With a substitution of hydrophilic pore, the pore hydration could retain at almost highest level even when pore diameter is small as 3 Å. In comparison, the semi-hydrophobic pore is able to regulate the pore hydration in between. Thus, the pore hydration could be effectively modulated by pore diameter with small changes as well as hydrophobicity. Subsequent MD simulations on model nanopores demonstrated that the hydrophobic gates at the vapour state, instead of physically blocking, form energetic barrier to occlude both water and ion permeation, which could be modulated by small diameter changes, hydrophobicity and membrane voltages, and indicates the potential application of hydrophobic gate theory on biological nanopores, ion channels.

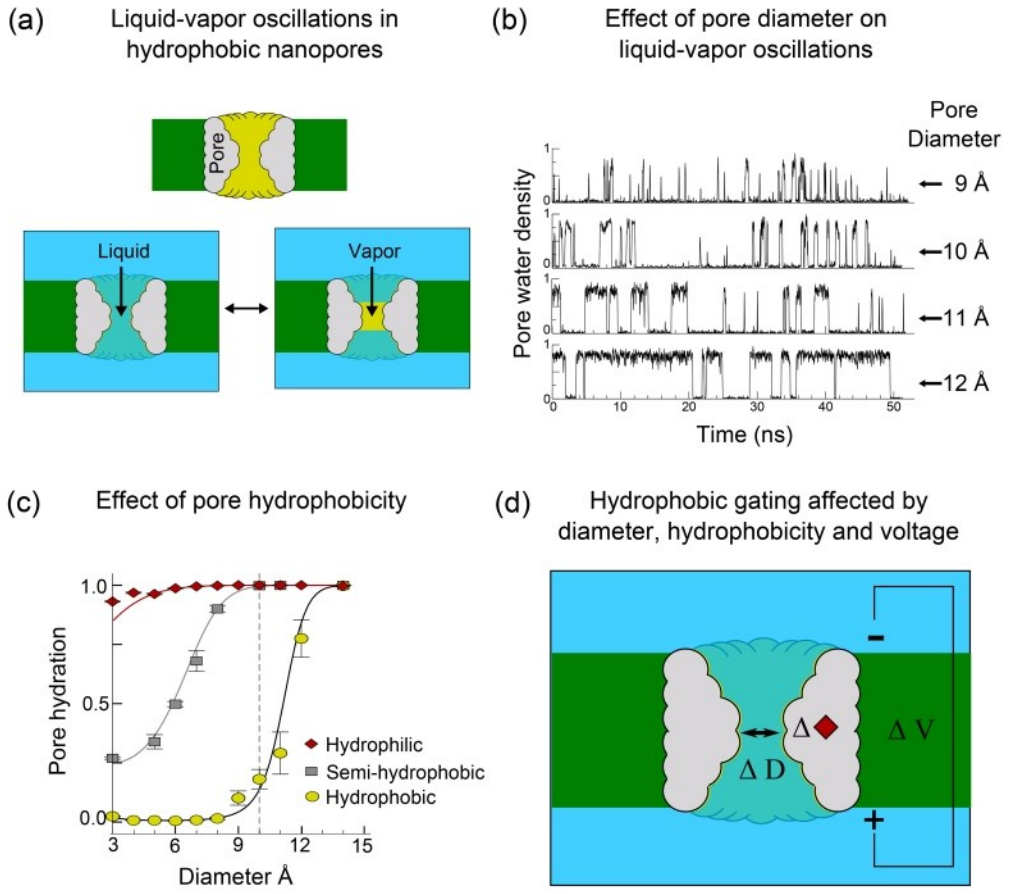

Fig. 1-7. Principles of hydrophobic gate theory. (A) Cartoon representation of a cross-section through a model hydrophobic nanopore. (B) Oscillations occur on the nanosecond timescale, and the stability of the wetted state is highly dependent upon pore diameter. (C) The probability of the pore being in the liquid or wetted state is not only dependent upon diameter, but also the hydrophobicity of atoms lining the pore. (D) Factors that affect the hydrophobic gate. No permission is required from Aryal et al., *J Mol Biol.*, 2016 (Aryal et al., 2016)

Ion channels are membrane proteins at nanoscale, with at least two membrane-spanning domains, which are selectively or non-selectively permeable to specific cations or anions when the channel is open. The very first evidence linking the hydrophobic gate theory and biological ion channel is reported in MD analysis on the

mechanosensitive channel of small conductance (MscS) cystalized structure, which has a pore with 5 Å diameter composed by highly hydrophobic leucine residues (Anishkin and Sukharev, 2004). Subsequently, the hydrophobic gate theory has further been validated in diverse ion channels, including pentameric ligand-gated ion channels and tetrameric potassium channels (Aryal et al., 2015). With the breakthroughs in cryo-EM techniques, atomic structures of ion channels in different states are available and could be compared and analyzed. The physical restrictions of a resolved ion channel could be easily located with the help of high-resolution structure. The selectivity filter is relatively immobile and often insensitive to external stimuli while the gate region could be modulated by ligands, mechano-force and voltage changes. Ligand-binding pocket or mechano- or voltage-sensing domains in the ion channels would induce conformational changes such as helical twists to open or close the gate(s) upon specific stimuli. So far, ion channels have been found to contain a pore region lined by a series of hydrophobic amino acids, but functional studies are still limited to test their importance under living cell conditions (Rao et al., 2019). Prior to the cryo-EM era, substituted-cysteine accessibility method was one way to identify the pore gate(s) (Karlin and Akabas, 1998). Nonetheless, based on hydrophobic gate theory, the gates could be characterized by unbiased scans of candidate amino acids with hydrophilic mutations, which hypothetically increase the pore hydration rate to open the channel. Our group have recently systematically identified hydrophobic residues in several TRP channels, some of which are consistent with the structural data

(Zheng et al., 2018b; Zheng et al., 2019). Another notable mechanism involves inactivation achieved by large conformational changes, like the ball-and-chain model in potassium channels (Fan et al., 2020; Zandany et al., 2015), distinct from open or closed state often with moderate changes.

1.7 Objectives, hypotheses and rationales

1.7.1 Objectives

The main thesis is to understand the importance of intramolecular interactions in TRP channels, and pore gate and regulation of PAC. The detailed objectives are 1) to explore the undetermined mechanisms of N/C binding in TRPP3, -P2, -V1, -M8 and C4 channel function, and mechanism of regulation by PIP2; 2) to characterize intramolecular L/C and N/C bindings in TRPV6 and how PIP2 stimulates the channel; 3) to investigate the physical and functional interactions between helices S5 and S6 in TRPV6 and how pathogenic mutation R532Q promotes breast cancer progression; and 4) to characterize the PAC channel pore gate and how protons activate the channel.

1.7.2 Hypotheses

We hypothesize 1) that in TRPP3, -P2, -V1, -M8 and C4 channels the N/C binding is mediated by functionally required amino acids, and that PIP2 binds to cationic residues to

modulate the N/C binding and channel function; 2) that the L/C and N/C bindings depending on critical residues are both autoinhibitory for that TRPV6 function and that PIP2 disrupts the L/C and N/C bindings through which it stimulates TRPV6; 3) that residue R532 in S5 forms a salt bridge with D620 in S6 to stabilize the S5/S6 helix interaction in TRPV6, and that mutant R532Q with abolished autoinhibition is gain-of-function, which promotes the breast cancer progression by activation of a PI3K/Akt pathway; 4) that the PAC closed and open states are controlled by two different hydrophobic gate residues, and that proton binding/sensing for channel activation involves protonatable residues located in the extracellular loop.

1.7.3 Rationales

TRP channels are ion channels that act as sensors on the membrane in response to extra- or intracellular stimuli. Dysregulated expression and mutation-caused malfunction of TRP channels have been associated with numerous human diseases. Understanding the functional mechanisms of the TRP channels is vital to developing clinical interventions for TRPs-related channelopathies. In the first high-resolution structure of rTRPV1, physical proximities between pre-S1, S4-S5 linker and TRP helices were suggested, followed by accumulated structures of TRP channels with similar structural arrangements. But the existence and functional importance of the corresponding intramolecular interactions have not been investigated in living cells. PIP2 regulates most TRP channels

while the underlying mechanisms are not well understood. Furthermore, whether there are interactions between PIP2 regulation and intramolecular interactions remains unclear. Our lab has well-established two-electrode voltage clamp electrophysiology system to examine the function of overexpressed TRP channels in *Xenopus* oocytes, which enables membrane targeting of most TRP channels and other ion channels. However, for example, TRPP3 could not target to the surface in the mammalian cells. We also have established routine techniques including, but not limited to, co-immunoprecipitation, *in-vitro* pull down, co-immunofluorescence, and Western blotting to verify the protein-peptide and protein-PIP2 interactions, whole-cell protein expression, and membrane targeting. Furthermore, we investigated the physiological relevance of TRPV6 mutants in zebrafish which exhibits bone calcification defects when its orthologous is absent.

The oncogenic role of TRPV6 has not been established but its elevated expression is proposed to contribute to breast cancer (especially triple negative breast cancer) development experimentally and clinically. Breast cancer remains as one of the most lethal cancer types. The S5 and S6 helices and the loop in between form the channel pore in TRPV6 and the other TRP channels. The importance of this arrangement has not been experimentally examined *in vivo*. Interestingly, a R532Q mutation has been linked to pathogenicity by a cancer database COSMIC. The functional effect of R532Q and its possible involvement in cancer progression warrant investigations. Thus, elucidation of TRPV6 channel regulation and effects on downstream cellular signaling pathways

implicated in breast cancer cells should be critical to evolve effective drug designs. In combination with the electrophysiology and biomedical techniques to understand the biophysical properties of TRPV6 mutants, our lab has cultured cancer cell lines to stably express TRPV6 WT and mutants to explore the molecular mechanisms involved.

The recently identified PAC channel is proton-activated and is presumably involved in acidosis induced cell death during stroke and ischemia reperfusion, but the channel pore gate composition and mechanism of proton-induced activation are unclear. Based on the hydrophobic gate theory, ion channels on the cell membrane control ion flow across the channel pore, depending on hydrophobic pore-lining residue(s) as the gate(s). Hydrophilic substitution of gate residue(s) would constitutively open the channel and thus render the channel as gain-of-function. PAC was reported to be activated by extracellular low pH with a Hill coefficient of 3.6, but the proton binding sites are unclear. The *Xenopus* oocytes expression system is well suitable for systematically examination of pore gate residues as well as putative proton sensing residue(s) in PAC using our routine two-electrode voltage clamp and associated techniques. We meanwhile have cultured HEK293 and neuronal SY-SH5Y cells as more physiological models to test the gain-of-function nature of mutant channels through determining their effect on cell death of expressing mammalian cells using flow cytometry.

CHAPTER 2

RESULTS #1

Direct preS1-TRP domain binding in TRP channels mediates gating and functional regulation by PIP2

2.1 ABSTRACT

Transient receptor potential (TRP) channels are regulated by diverse stimuli comprising thermal, chemical and mechanical modalities. Although they share significant homology in critical regions and functional regulation by phosphatidylinositol-4,5-bisphosphate (PIP2), it remains unknown whether they share a common gating mechanism. Here we revealed an intramolecular interaction of the N- and C-termini (N-C) of TRPP3, which is functionally essential. The interaction was mediated by aromatic Trp81 in pre-S1 domain and cationic Lys568 in TRP-like domain. Structure-function analyses revealed similar N-C interaction in TRPP2/-M8/-V1/-C4 via highly conserved tryptophan and lysine/arginine. PIP2 bound to cationic residues in TRPP3 including K568 thereby disrupting the N-C interaction and negatively regulating TRPP3. PIP2 had similar negative effects on TRPP2 whereas it facilitated the N-C interaction in TRPM8/-V1 resulting in channel potentiation. Thus, PIP2 suppresses or enhances TRP channels activation by modulating the N-C interaction. Our study discovered a shared mechanism of TRP channels gating.

2.2 INTRODUCTION

Transient receptor potential (TRP) channels are sensors of various physical and chemical stimuli (Montell, 2005). They form a superfamily of cation channels which is divided into eight subfamilies according to sequence similarities, TRPV (vanilloid), TRPC (canonical), TRPM (melastatin), TRPP (polycystin), TRPA (ankyrin), TRPML (mucolipin), TRPN (no mechanoreceptor potential C), and TRPY (yeast) (Venkatachalam and Montell, 2007). TRP channels function as tetramers in which each subunit contains six transmembrane segments (S1- S6) with S5-loop-S6 forming part of a central pore module, and cytosolic N- (amino) and C- (carboxy) termini (Montell, 2005). A short N-terminal α-helical domain upstream of S1, called the pre-S1 domain, was proposed to be involved in allosteric gating (Saotome et al., 2016; Paulsen et al., 2015; Liao et al., 2013; Huynh et al., 2016). TRPC, TRPV and TRPM proteins contain in their C-terminus almost immediately after S6 a TRP domain characterized by a signature motif xWKxxR (also called a TRP box) important for channel activation and PIP2 binding (Ramsey et al., 2006; Valente et al., 2011). The corresponding fragment in other TRPs is termed a TRP-like domain. The TRP or TRP-like domains in structurally resolved TRPs all adopt α-helical configuration (Saotome et al., 2016; Paulsen et al., 2015), suggesting that they may have similar functional roles. While TRP channels have long been recognized to respond to remarkably diverse stimuli ranging from pH, changes of temperature, light,

touch, pheromones, osmolarity and noxious chemicals, which is well correlated with their various functions in sensory physiology such as sensations of pain, hotness, warmth and coldness, taste, pressure and vision (Clapham et al., 2001; Montell, 2005; Ishimaru and Matsunami, 2009; Eijkelkamp et al., 2013; Venkatachalam and Montell, 2007; Clapham, 2003), it still remains largely unknown as to how these diverse stimuli induce conformational changes resulting in pore opening and channel activation.

Ion channel activation involves protein conformational changes leading to channel switch from a closed, ion non-conducting state to an open, ion conducting state. This can be induced by membrane voltage, chemical ligands, or mechanical stress which is recognized by sensor domains of the channel, resulting in pore gate opening. Signal transduction from a sensor domain to the pore gate must require complex conformational changes including various intramolecular interactions. It is generally assumed that TRP channels respond to various stimulatory inputs through their distinct sensor domains. In the present study, we investigated shared structural and functional mechanisms that transduce the action of extracellular agonists into channel activation.

Phosphatidylinositol 4,5- bisphosphate (PIP2) is predominately present in the inner leaflet of the cell surface membrane and accounts for more than 99% of the doubly phosphorylated phosphatidylinositol (McLaughlin et al., 2002). PIP2 is known to directly or indirectly regulate TRP, Kir, ENaC and KCNQ channels (Xie et al., 2007; Pochynyuk et al., 2008; Zhang et al., 2003; Qin, 2007). The direct regulation by PIP2 is through

direct binding of its negatively charged inositol head group with a pocket formed by cationic residues in a channel protein (Suh and Hille, 2008). The indirect regulation by PIP2 is mainly mediated by the phospholipase C (PLC) pathway in which PLC cleaves PIP2 into soluble inositol 1,4,5-trisphosphate (IP3) and membrane-anchored diacyl glycerol (DAG) (Kadamur and Ross, 2013). IP3 activates IP3R Ca^{2+} channel on the endoplasmic reticulum membrane to release Ca^{2+} ions which initiates various cellular responses; together with DAG the elevated cytoplasmic Ca^{2+} activates protein kinase C, thereby regulating a number of ion channels and other downstream targets (Huang, 2007; Suh and Hille, 2005). Despite their low overall sequence similarity and sensitivity to highly diverse agonists almost all mammalian TRPs are known to be modulated by PIP2 (Rohacs, 2014). Some channels, including TRPV5, TRPV6, TRPM4, TRPM5 and TRPM8 are positively modulated (Liu and Qin, 2005; Thyagarajan et al., 2008; Liu and Liman, 2003; Lee et al., 2005; Bousova et al., 2015), others such as TRPC4 and TRPP2 (Otsuguro et al., 2008; Ma et al., 2005) are negatively regulated, whereas TRPV1 channel function is stimulated or inhibited by PIP2 depending on the experimental conditions (Rohacs et al., 2008; Lukacs et al., 2007). Although PIP2 is known to bind to cationic residues in some TRPs in vitro, including TRPV1, TRPM8 and TRPM4 (Rohacs et al., 2005; Bousova et al., 2015; Poblete et al., 2015), it remains largely unclear as to the structural basis of the unified underlying mechanism.

In this study, using two-electrode voltage clamp in *Xenopus* laevis oocytes, patch

clamp in mammalian cells, surface localization and immunofluorescence, we first identified conserved aromatic residues in the pre-S1 and cationic residues in the TRP/TRP-like domains of TRPP3, TRPP2, TRPV1, TRPM8 and TRPC4 and studied their functional roles. By in vitro pull-down and co-immunoprecipitation (co-IP) we then examined the functional importance of the N- terminus to C-terminus (N-C) binding that is mediated by an aromatic-cationic residue pair. Further, we examined how PIP2 regulates the N-C binding as a shared mechanism through which different agonists regulate TRPs channel function.

2.3 METHODS

Plasmids, mutagenesis, antibodies and chemicals

Human Flag-TRPP3 cDNA (accession #: NM_016112) was cloned into vector pCHGF (Yang et al., 2012) for *Xenopus* laevis oocyte expression. HA-tagged human TRPP2 (NM_000297) plasmid for *Xenopus* oocyte expression (Arif et al., 2016) was a kind gift of Dr. Yong Yu (St. John's University, NY). Human TRPP2 was also cloned to pcDNA3 vector for mammalian cell expression. Human PKD1 (NM_001009944) for mammalian cell expression was previously described (Kim et al., 2016). Rat TRPM8 (NM_134371) plasmid was kindly provided by Dr. David Julius (University of California at San Francisco, CA). Rat TRPV1 (NM_031982) in the pGEMEM plasmid was from Dr. Sharona Gordon (University of Washington, WA). All mutations were made with QuikChange Lightning Site-Directed Mutagenesis kit (Agilent Technologies, La Jolla, CA) and confirmed by sequencing. Rabbit antibodies against Flag (D-8) and HA (Y-11), and mouse antibodies against TRPV1 (E-8), GST (B-14), β-actin (C-4) and PIP2 (PIP2 2C11) were purchased from Santa Cruz Biotechnology (Santa Cruz, CA). Mouse antibody against His (N144/14) for Western blotting was from NeuroMab (Davis, CA). Mouse antibody against His (27E8) and rabbit antibody against His (#2365) were purchased from Cell Signaling Technology (Danvers, MA) and were used in immunoprecipitation and immunofluorescence assays, respectively. Antibodies against

TRPM8 were generated in-house. Secondary antibodies were purchased from GE Healthcare (Waukesha, WI). Menthol (TRPM8 agonist), capsaicin (TRPV1 agonist) and U-73122 (PLC inhibitor) were purchased from Sigma (St. Louis, MO). Wortmannin was from InvivoGen (San Diego, CA) and diC8 was purchased from Echelon Biosciences (Salt Lake City, UT).

Xenopus oocytes expression

Capped RNAs of TRPP3, TRPP2, TRPM8 and TRPV1were in vitro transcribed with mMESSAGE mMACHINE kit (Ambion, Austin, TX) and injected (25-50 ng RNA in 50 nl water per oocyte) into *Xenopus* oocytes prepared as previously described (Zheng et al., 2015). Control oocytes were injected with equal volumes of water. Electrophysiological measurements were performed 1-3 days after injection. The present study was approved by the Ethical Committee for Animal Experiments of the University of Alberta, and was carried out in accordance with the Guidelines for Research with Experimental Animals of the University of Alberta and the Guide for the Care and Use of Laboratory Animals (NIH Guide) revised in 1996.

Two-electrode voltage clamp

Two-electrode voltage clamp experiments in *Xenopus* oocytes were performed as described (Yang et al., 2012). Briefly, the two electrodes (Capillary pipettes, Warner

Instruments, Hamden, CT) impaling an oocyte were filled with 3 M KCl to form a tip resistance of 0.3-2 MΩ. Unless otherwise indicated, whole-cell currents of oocytes were recorded at room temperature (RT) in standard extracellular solution containing 100 mM NaCl, 2 mM KCl, 1 mM $MgCl_2$ and 10 mM HEPES (pH 7.5) with or without 5 mM $CaCl_2$. Duration of application of extracellular agonist Ca^{2+}, menthol or capsaicin was indicated in time course recordings. Currents were recorded using a Geneclamp 500B amplifier and Digidata 1322A AD/DA converter (Molecular Devices, Union City, CA). The pClamp 9 software (Axon Instruments, Union City, CA) was employed for data acquisition and analysis. Currents and voltages were digitally recorded at 200 μs/sample and filtered at 2 kHz through a Bessel filter. SigmaPlot 13 (Systat Software, San Jose, CA) was used for data fitting and plotting. Wortmannin or U-73122 was introduced to oocytes through incubation for 30-60 min prior to measurements. diC8 or water (control) was on-site injected by a third electrode into the oocytes in the recording chamber.

Oocyte surface protein biotinylation

Xenopus oocytes were washed three times with ice-cold PBS solution followed by incubation with 0.5 mg/ml sulfo-NHS-SS-Biotin (Pierce, Rockford, IL) for 30 min at RT. 1 M NH4Cl was used to quench the non-reacted biotin. Oocytes were then washed with ice-cold PBS solution and harvested in ice-cold CelLytic M lysis buffer (Sigma) supplemented with proteinase inhibitor mixture (Thermo Scientific, Waltham, MA).

Lysates were incubated at 4˚C overnight with gentle shaking upon addition of 100 µl streptavidin (Pierce). The surface protein absorbed by streptavidin was resuspended in a SDS loading buffer and subjected to SDS-PAGE.

Oocytes immunofluorescence

Whole mount immunofluorescence assays using *Xenopus* oocytes were performed as described (Zheng et al., 2015). Briefly, oocytes were washed in PBS, fixed in 4% paraformaldehyde for 15 min, washed three times in PBS plus 50 mM NH4Cl, and then permeabilized with 0.1% Triton X- 100 for 4 min. Oocytes were then blocked in PBS plus 3% skim milk for 30 min, and then incubated overnight with indicated primary antibodies, followed by incubation with secondary AlexaFluor 488-conjugated donkey anti-rabbit or Cy3-conjugated goat anti-mouse antibody antibodies (Jackson ImmunoResearch Laboratories, West Grove, PA) for 30 min. Oocytes were then mounted in Vectashield (Vector Labs, Burlington, ON) and examined on an AIVI spinning disc confocal microscopy (Cell Imaging Facility, Faculty of Medicine and Dentistry, University of Alberta). The surface expression was assessed by quantifying the plasma membrane immunofluorescence using Volocity 6.2 (Perkin Elmer, Waltham, MA).

Co-IP

Co-IP experiments were performed using a modified protocol (Zheng et al., 2016a).

Briefly, a group of 30 oocytes expressing an indicated TRP channel and/or peptides were washed twice with PBS and solubilized in ice-cold CelLytic-M lysis buffer (Sigma) supplemented with proteinase inhibitor mixture. Supernatants were collected after centrifugation at 16,000 g for 15 min and precleared for 1 hr with protein G-Sepharose (GE Healthcare), and then incubated with indicated antibodies at 4 °C overnight. After the addition of 100 μl of 50% protein G-Sepharose, the mixture was incubated for 4 hr or overnight with gentle shaking at 4 °C. The immune complexes absorbed to protein G-Sepharose were washed five times with Nonidet P-40 lysis buffer (50 mM Tris, pH 7.5, 150 mM NaCl, 1% Nonidet P-40) and eluted by SDS loading buffer. Precipitated proteins were analyzed by Western blotting using indicated antibodies.

***In vitro* His pull-down**

Purified GST-tagged human TRPP3 N-terminus (M1-L95, 2 μg) from *E. coli* was incubated with the same amount of purified His-tagged human TRPP3 C-terminal fragment (I560-K660) from *E. coli* in the CelLytic-M lysis buffer (Sigma). The mixture was incubated at RT for 1 hr with gentle shaking, followed by another hour of incubation after addition of 10 μl 50% Ni-NTA agarose bead (Qiagen, Hilden, Gernamy). The beads were then washed three times with PBS buffer supplemented with 1% Nonidet P-40, and the remaining proteins were eluted using SDS loading buffer and resolved by SDS-PAGE and transferred to a nitrocellulose membrane (Bio-Rad, Hercules, CA). The membrane

was then immunoblotted with His and GST antibodies.

Ca^{2+} imaging

Ca^{2+} imaging experiments were performed at 37 °C using a Polychrome V (TILL Photonics, Martinsried, Germany) and CCD camera (PCO, Kelheim, Germany)-based imaging system at a Zeiss Axiovert S100 fluorescence microscope equipped with a Zeiss Fluar 20×/0.75 objective. Data acquisition was accomplished with the imaging software TILLvisION (TILL Photonics).

HEK293 Cells were seeded on 2.5 cm round glass coverslips and transiently co-transfected with the pcDNA3 plasmid harboring rat TRPM8 and pcAGGS-IRES-GFP vector. 48 hr after transfection, cells were incubated in media supplemented with 2 μM Ca^{2+}-sensitive fluorescent dye Fura-2-AM (TEVLabs, Austin, TX) for 30 min in the dark at 37 °C. Cells were then washed four times with Ca^{2+}-free solution (in mM: 115 NaCl, 5 KCl, 2 $MgCl_2$, 10 HEPES, pH 7.4 adjusted with NaOH) to remove excess Fura-2-AM. The coverslips with the Fura-2-loaded cells were transferred to a bath chamber containing Ca^{2+}-free solution, and Fura-2 fluorescence (>510 nm) was monitored after excitation at 340 and 380 nm for 30 ms each at a rate of 1 Hz for 600 s. Cells were marked and ratios of the background-corrected Fura-2 fluorescence at 340 and 380 nm (F340/F380) were plotted versus time. 2 mM $CaCl_2$ and 100 μM menthol were added to the bath solution as indicated.

Mammalian cell electrophysiology

Electrophysiology using mammalian HEK cells expressing PKD1 and TRPP2 was performed similarly as previously (Kim et al., 2016). Specifically, HEK cells were seeded on coverslips and transiently co-transfected with plasmids expressing PKD1 and/or TRPP2. Immediately before each experiment, a coverslip was placed into a recording chamber. The extracellular solution was normal Tyrode solution containing (in mM): 135 NaCl, 5.4 KCl, 0.33 NaH_2PO_4, 1 $MgCl_2$, 1.8 $CaCl_2$, 5 HEPES, 5.5 glucose (pH 7.4). Pipettes were made from capillary glass (plain; Fisher Scientific, Pittsburgh, PA) with a micropipette puller and polisher (PP-830 and MF-830, respectively; Narishige, Tokyo, Japan). They were back-filled with internal solution composed of (in mM): 100 K-aspartate, 30 KCl, 0.3 Mg-ATP, 10 HEPES, 10 EGTA, and 0.03 GTP (pH 7.2).

The pipette resistance varied from 3–5 MΩ when filled with the internal solution. Offset potential was corrected just before a gigaohm seal formation. Series resistance and capacitance transients were compensated when CHO-K1 cells were used with an Axon 200B amplifier (Molecular Devices) and pClamp 10.0 software (Axon Instrument, Foster City, CA). Cell capacitance was compensated by 70-80%. Currents were digitized with a Digidata 1550A converter (Molecular Devices), filtered through an internal four-pole Bessel filter at 1 kHz, and sampled at 2 kHz.

Time-course inward and outward whole-cell currents were obtained by employing a

step-pulse protocol from -100 to +100 mV every 5 s for 200 ms duration from a holding potential of -60 mV. I-V curves were taken before and 2-3 min after the addition of WNT9B in the bath solution and derived from a step protocol ranging from -100 to +100 mV with 20 mV increments for 200 ms duration from a holding potential of -60mV. Steady-state currents towards the end of the pulse (between 50 and 100 ms) were used in I-V curves. Cells with a similar diameter displaying similar in magnitude stable baseline currents among various groups were selected for recordings and used for further analysis.

Statistical analyses

Data were analyzed and plotted using Sigmaplot 13, and expressed as mean ± SEM, where SEM stands for the standard error of the mean. Student t-tests were used to compare two sets of data, whereas One-way ANOVA for multiple comparisons. A probability value (P) of less than 0.05, 0.01, or 0.001 was considered statistically significant and indicated by *, **, and ***, respectively.

2.4 RESULTS

Interaction between the N- and C-termini of TRPP3 and TRPP2 and functional importance

Among the N-terminal amino acid (aa) residues M1-T39, S41 and S42 of human TRPP3, only C38 was previously shown to be critical for the channel function (Yang et al., 2012; Zheng et al., 2016b). We here wanted to identify aa(s) within I40-L95 of the N-terminus that is (are) functionally important. Using *Xenopus* oocytes expression, the two-electrode voltage clamp electrophysiology, and Ca^{2+}-induced channel activation as a readout, we found that deleting aa W81-L95 but not deleting aa T43-P50, K51-L80 or replacing I40 by an alanine (A) abolishes the channel activation (Fig. 2-1A). Applying alanine substitution scanning to fragment W81-L95 found that only the mutation at tryptophan (W) 81 abolishes the channel activation (Fig. 2-1B), without affecting the surface membrane targeting (Fig. 2-1H). Substitution of W81 by an aromatic or anionic residue retained full or partial channel function while substitution by leucine (L) or a cationic residue resulted in loss of function (Fig. 2-1C and H). These data suggest the importance of the aromatic side chain in W81 for TRPP3 channel function. If the aromatic side chain in W81 is near the cationic side of an arginine (R) or lysine (K), an energetically favorable π-cation interaction may occur. Recently reported TRPs structures revealed physical proximity between the N-terminal pre-S1 and the C-terminal TRP (or

TRP-like) domains (Saotome et al., 2016; Huynh et al., 2016; Liao et al., 2013; Paulsen et al., 2015). Because TRPP3 W81 is located within the highly conserved pre-S1 domain across species (G76-T86 in human) (Fig. 2-1D) we also carried out alanine substitution in the highly conserved TRP-like domain (N561-L593) to identify a functionally important cationic residue(s). We found that only mutation K568A, but not K575A, K585A or K590A, corresponds to loss of function (Fig. 2-1E and H). Substitution of K568 by an acidic residue (D or E) also led to loss of function while substitution by cationic R retained full channel function (Fig. 2-1F and H). Sequence alignment also showed that K568 is highly conserved across different species (Fig. 2-1G). Taken together, our data suggest that TRPP3 channel function requires the presence of an interaction between the pre-S1 and TRP-like domains that is mediated by the W81-K568 pair, presumably forming cation-π interactions.

We next performed co-IP experiments and found that the TRPP3 N-terminal peptide I40- L95 (P3NP) and full-length (FL) TRPP3 are in the same complex, and that this interaction is abolished if W81 in P3NP or K568 in FL TRPP3 is changed to A (Fig. 2-1I), indicating that the W81-K568 pair mediates the interaction. We next performed in vitro pull-down assays using the recombinant and purified GST-tagged TRPP3 N-terminus M1-L95 (GST-P3N) and the His- tagged C-terminal peptide I560-K660 (His-P3CP). The two peptides directly bound each other and the binding was abolished in the presence of the W81A or K568A mutation in the respective peptide (Fig. 2-1J), confirming that the

W81-K568 pair mediates the N-C binding. The N-C interaction was further supported by whole-oocyte co-immunofluorescence assays: after cRNA injection, peptide P3NP was distributed along the oocyte surface membrane if the FL TRPP3 cRNA was co-injected (Fig. 2-1K). This attachment of P3NP to the surface membrane remained unaffected by the W81F mutation in P3NP but was not observed in the presence of the W81A mutation in P3NP or the K568A mutation in FL TRPP3, or in the absence of FL TRPP3 expression. These co-IP and immunofluorescence data together are in support of the concept that the W81-K568 pair-mediated interaction between P3NP and FL TRPP3 allows P3NP to co-localize with FL TRPP3 along the surface membrane.

We wondered whether the expressed peptide P3NP would compete with the P3NP fragment within the FL TRPP3 protein for binding with the K568 residue in the TRP-like domain of the FL TRPP3, thereby disrupting the N-C binding within FL TRPP3 and abolishing the channel function. Indeed, co-expression of P3NP or P3NP-W81F completely or substantially inhibited the FL TRPP3 channel function, while co-expression of mutant peptide P3NP-W81A had no effect (Fig. 2-1L), indicating that P3NP acts as a blocking peptide that inhibits TRPP3 function through disrupting the N-C binding in the FL channel. In summary, our data demonstrate that direct N-C binding does occur in TRPP3 and that residues W81 of the pre-S1 and K568 of the TRP-like domain, presumably through π-cation interaction, are crucial for this interaction which is required for TRPP3 channel activation.

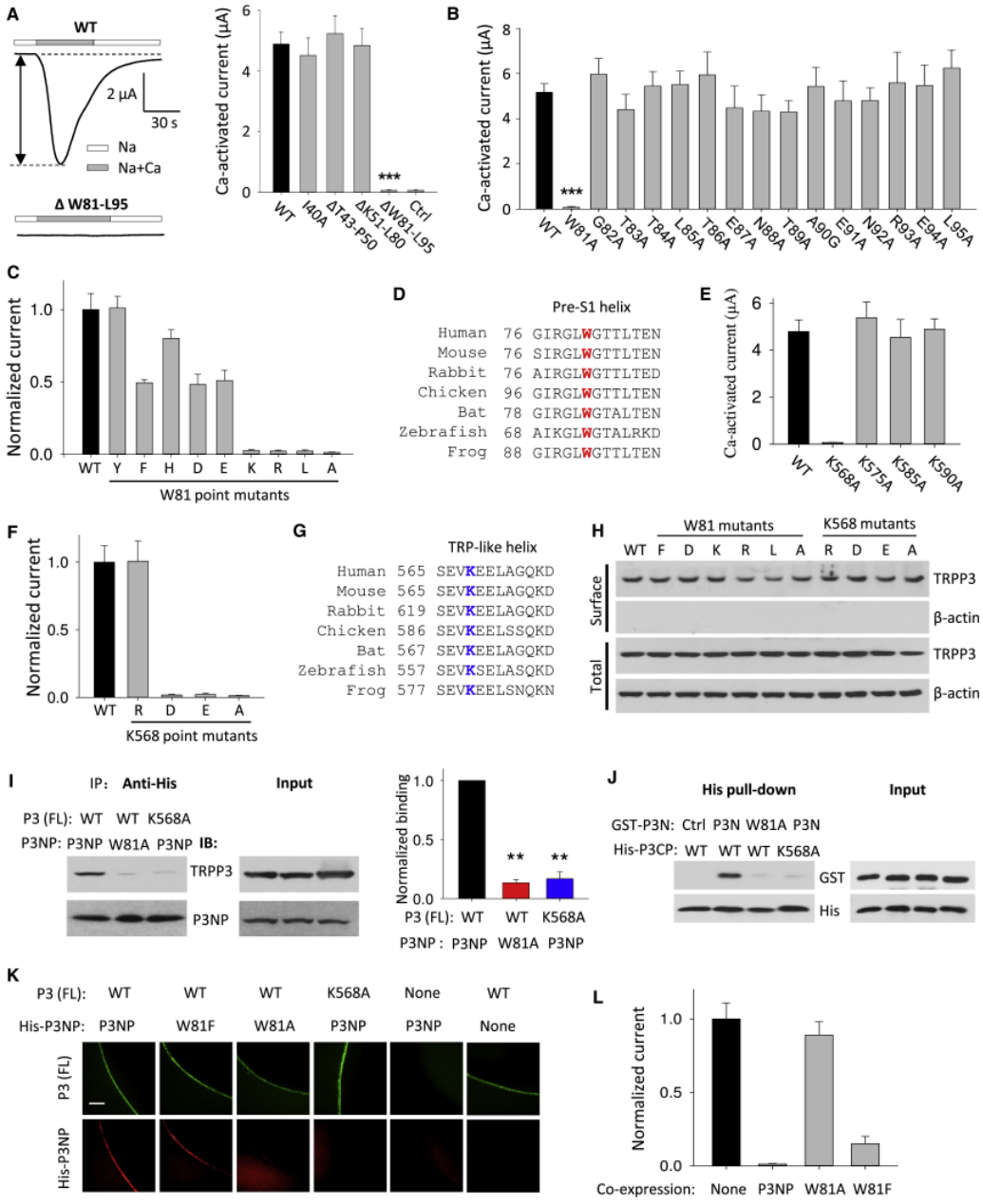

Fig. 2-1. Roles of the TRPP3 W81 (pre-S1) and K568 (TRP-like domain) residues in the N- C interaction and channel function. (**A**) *Left panel*, representative whole-cell current traces obtained from *Xenopus* oocytes expressing human TRPP3 WT or mutant ΔW81-L95 (with the W81-L95 domain deletion), using the two-electrode voltage clamp technique. Oocytes were voltage clamped at -50 mV. Currents were measured using the Na^+-containing extracellular solution (Na) (100 mM NaCl, 2 mM KCl, 1 mM $MgCl_2$, 10 mM HEPES at pH 7.5) or added with 5 mM $CaCl_2$ (Na+Ca). *Right panel*, averaged Ca^{2+}-activated

currents (ie, current at "Na+Ca" – current at "Na") obtained at -50 mV from oocytes expressing TRPP3 WT or an indicated mutant or H_2O injected oocytes (Ctrl) (mean ± SEM; n = 17 - 22). Oocytes were from three batches. ***P < 0.001 (compared with WT). (**B**) Averaged Ca^{2+}-activated currents obtained under the same condition as in panel A from oocytes expressing TRPP3 WT or an indicated point mutant. ***P < 0.001. (**C**) Averaged Ca^{2+}-activated currents under the same condition as in panel A from oocytes expressing TRPP3 WT or an indicated W81 point mutant. Currents were averaged from three independent experiments and normalized to that of WT. (**D**) Amino acid sequence alignment of the TRPP3 pre-S1 helix from indicated species, with the highlighted residue W. (**E**) Averaged Ca^{2+}- activated currents obtained from oocytes expressing TRPP3 WT or an indicated point mutant in TRP-like domain. (**F**) Averaged Ca^{2+}-activated currents from oocytes expressing TRPP3 WT or an indicated K568 point mutant. Currents were averaged from three independent experiments and normalized to that of WT. (**G**) Amino acid sequence alignment of the TRPP3 TRP-like domain from indicated species, with the highlighted residue K. (**H**) Representative immunoblots of the surface biotinylated (Surface) and whole-cell (Total) TRPP3 WT or indicated W81 or K568 point mutants. β-actin was used as a control. (**I**) Left panel, W81-K568 interaction examined with co-immunoprecipitation assays using oocytes co-expressing full-length (FL) TRPP3 and His-tagged TRPP3 N-terminal peptide (His-P3NP, I40-L95). *Right panel*, data from experiments in left panel were quantified, averaged and normalized (**P < 0.01, n = 3). (**J**) W81-K568 interaction examined with His pull-down assays using the purified GST-tagged human TRPP3 N-terminus (GST-P3N, M1-L95) and His-tagged human TRPP3 C-terminal peptide (His-CP, I560-K660) from *E. coli*. Ctrl, purified GST-human FUBP1 M1-V112 from *E. coli*. (**K**) Colocalization of P3NP with FL TRPP3 examined with co-immunofluorescence assays using oocytes co-expressing FL TRPP3 and His-P3NP. (**L**) Effects of co-expressed P3NP or its point mutants on TRPP3 Ca^{2+}-activated currents. None, no P3NP expression. Shown are normalized and averaged currents three independent experiments (n = 15 to 20).

TRPP3 shares 70% overall sequence similarity with TRPP2 encoded by PKD2 gene, in which mutations account for 15% of autosomal dominant polycystic kidney disease (ADPKD), and an even higher homology in the pre-S1, TRP-like and transmembrane domains. The corresponding aromatic and cationic residues in the pre-S1 and TRP-like

domains of human TRPP2 are W201and K688, respectively (Fig. 2-2A). The low basal channel activity of TRPP2 alone impairs reliable recording of currents in oocytes and mammalian cells. However, as the TRPP2 F604P mutation renders TRPP2 in an activated state (Arif et al., 2016) we used mutant F604P-mediated currents as a function readout and replaced W201 or K688 residue with A in the F604P mutant. No current was detectable for the W201A or K688A mutant although the overall protein expression and surface membrane targeting were not affected (Fig. 2-2B and C), indicating that residues W201 and K688 are functionally essential. As in TRPP3, the TRPP2 N-terminal peptide G161-S215 (P2NP) interacted with the FL TRPP2 and the interaction was weakened by the W201A mutation in P2NP or K688A mutation in TRPP2 (Fig. 2-2D). Consistently, P2NP, but not P2NP-W201A, acted as a blocking peptide by drastically reducing the function of TRPP2 F604P (Fig. 2-2E) without affecting its plasma membrane expression (Fig. 2-S1). Overall, our data support the hypothesis that similar to TRPP3, there exists an interaction between the N- and C-termini of TRPP2 mediated by W201 and K688 that is essential for TRPP2 channel function.

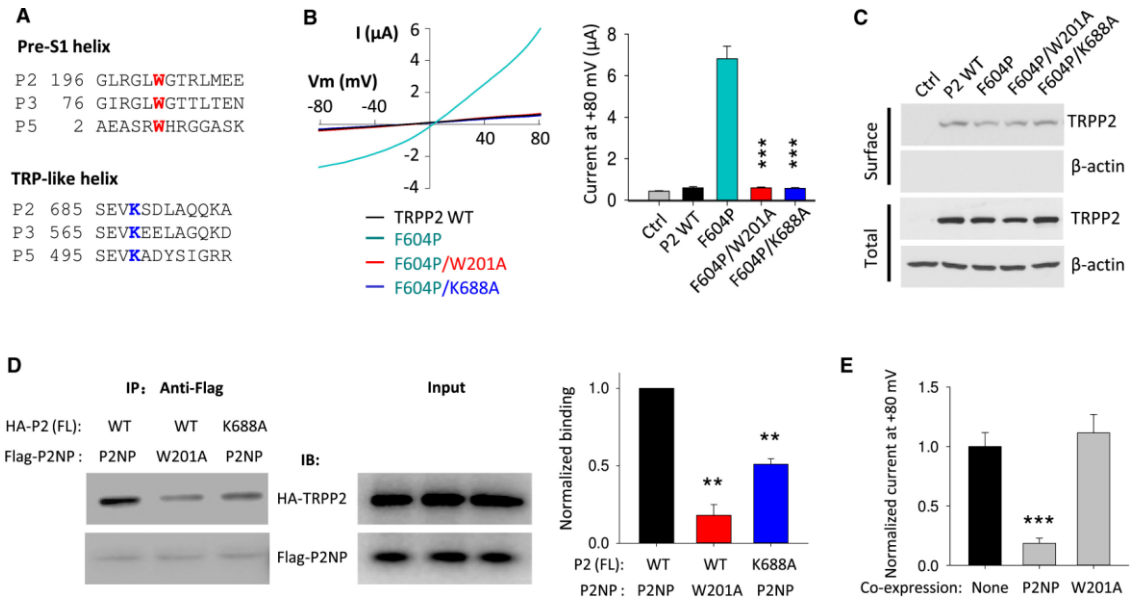

Fig. 2-2 Roles of the TRPP2 residues W201 (pre-S1) and K688 (TRP-like domain) in the channel function and N-C binding. (**A**) Sequence alignment of pre-S1 and TRP-like helices among human TRPP channels. Conserved aromatic tryptophan and cationic lysine are indicated in red and blue, respectively. (**B**) *Left panel*, representative I-V curves obtained from oocytes expressing human WT or a mutant TRPP2, as indicated, in the presence of a Na^+-containing, divalent-free solution (in mM): 100 NaCl, 2 KCl, 10 HEPES at pH 7.5. *Right panel*, averaged currents at +80 mV under the same experimental conditions as in left panel. Ctrl, H_2O-injected oocytes. Currents were averaged from 13 - 17 oocytes of three batches. ***P < 0.001. (**C**) Representative immunoblots of surface biotinylated and total proteins of TRPP2 WT and mutants. (**D**) *Left panel*, Representative co-immunoprecipitation data showing the effects of TRPP2 W201 and K688 on the N-C interaction using oocytes co-expressing human HA-tagged FL TRPP2 and Flag-tagged TRPP2 N-terminal peptide (Flag-P2NP, G161-S215). K688A or W201A mutation was introduced to FL TRPP2 or P2NP, respectively. *Right panel*, data from experiments in *left panel* were quantified, averaged and normalized (**P < 0.01, n = 3). (**E**) Blocking effects of Flag-P2NP and Flag-P2NP-W201A on channel function of FL TRPP2 mutant F604P by use of co- expression. None, no P2NP was co-expressed with FL F604P. Normalized currents at +80 mV were obtained and averaged from three independent experiments. ***P < 0.001.

We recently showed that TRPP2 co-expressed with PKD1, a large transmembrane protein mutated in 85% of ADPKD, in mammalian cells can be activated by WNT

molecules, such as WNT9B (Kim et al., 2016). Therefore, we tested the effects of W201A, K688A, ΔY684 (in- frame deletion of residue Y684), and Y684A mutations on WNT9B-activated channel activity of human TRPP2 co-transfected with human PKD1 in CHO-K1 cells. We included Y684 in the analysis because it is located within the TRP-like domain in close proximity to K688 (Fig. 2-2A). In addition, in-frame deletion of Y684 was first identified as a somatic mutation in a patient with a germline inactivating mutation in PKD2 (Watnick et al., 2000). However, its functionality has never been tested. Cell surface biotinylation experiments in HEK293T cells, which are more suited for biochemical experiments than CHO-K1 cells because of their high levels of transfectability, did not show significant differences in cell surface expression of the mutants to wild-type (WT) (Fig. 2-3A). Compared to WT TRPP2, mutant W201A or K688A showed substantially reduced WNT9B-activated peak currents (Fig. 2-3B and D). Interestingly, the two mutants also exhibited pronounced inactivation and completely reduced steady-state currents (Fig. 2-3B, C and E), suggesting that W201A or K688A mutation destabilized the channel in the open state induced by WNT9B. In comparison, mutations ΔY684 and Y684A rendered the channel completely insensitive to WNT9B (Fig. 2-3D and E). In summary, using WNT9B as an activating ligand, we showed that W201A and K688A mutations suppress channel activity via an apparently similar mechanism, at least based on current kinetics, but distinct from that of ΔY684 or Y684A mutation, which is consistent with the possible engagement of W201 and K688 in a

physical interaction during channel activation. The residual peak current in TRPP2 W201A or K688A mutant could be due to the possible contribution of PKD1 in pore formation, which is currently unexplored and beyond the scope of this study.

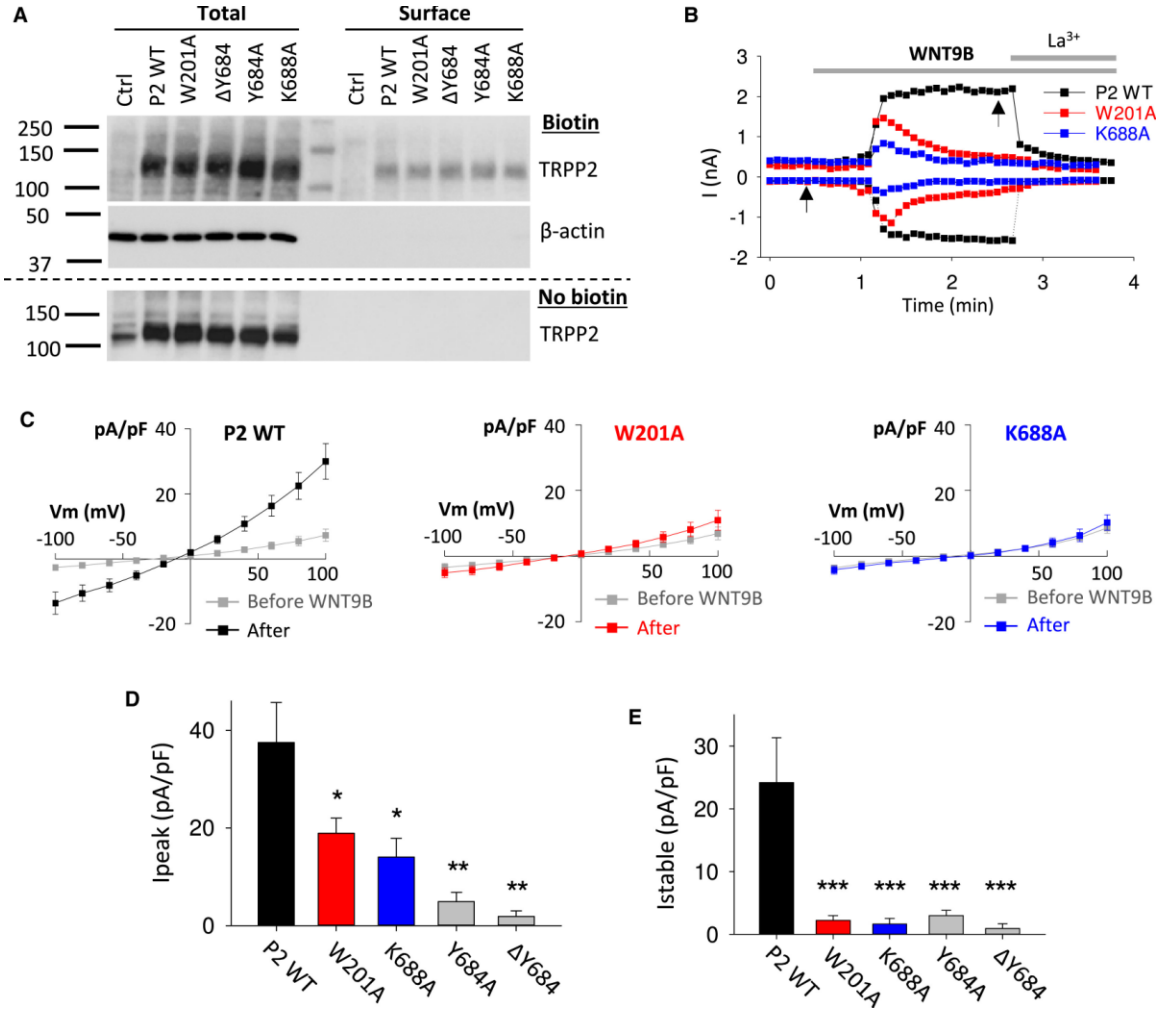

Fig. 2-3. Roles of TRPP2 residues W201 and K688 in WNT9B-induced whole-cell currents. (**A**) Cell surface expression of WT TRPP2 and mutants W201A, ΔY684, Y684A and K688A in HEK293T cells by transient co-transfection together with PKD1. Cells transfected with empty pcDNA3 plasmid serve as control (Ctrl). Cells were labeled with 1 mg/ml cell impermeant biotin (Sulfo-NHS-SS-Biotin) (upper and middle panel) or left untreated (lower panel). 20 µg of total lysates were immunoprecipitated with

Neutravidin beads. Biotinylated proteins were immunoblotted with a goat polyclonal TRPP2 (upper and lower panel) or mouse monoclonal β-actin antibody (middle panel). (**B**) Representative whole-cell current traces obtained at +100 and - 100 mV before and after extracellular addition of WNT9B (0.5 μg/ml) or La^{3+} (100 μM) in CHO-K1 cells transiently co-expressing PKD1 with WT TRPP2, the W201A or K688A mutant. The normal Na^{+}-containing Tyrode solution was used as the extracellular solution. (**C**) Same experimental conditions as in panel B. Averaged steady-state I-V curves obtained before and ~2 min after application of WNT9B, at time points indicated by arrows in panel B. WT TRPP2, n = 7 cells; W201A, n = 11 cells; K688A, n = 7 cells. **D** and **E**. Averaged peak (**D**) and steady-state (**E**) currents induced by WNT9B in CHO-K1 cells under the same experimental conditions as in panel B. WT TRPP2, n = 7 cells; W201A, n = 11 cells; ΔY684, n = 8 cells; Y682A, n = 10 cells; K688A, n = 7 cells. *P < 0.05, **P < 0.01, ***P < 0.001.

Characterization of the N-C binding in TRPM8, TRPV1 and TRPC4

Alignment of the pre-S1 and TRP domains of all members of the TRPM, TRPC and TRPV subfamilies revealed that the tryptophan and the lysine residues examined in TRPP2 and TRPP3 above are highly conserved (Fig. 2-4A, 2-S3A and 2-S4A), only with exception of TRPV4, TRPV5 and TRPV6 (Fig. 2-S3A). Rat TRPM8 channel mediated large depolarization-activated cation currents in oocytes that were completely abolished by alanine substitution at W682 or R998 (Fig. 2-4B) without affecting the plasma membrane expression (Fig. 2-S2A). At negative membrane potentials, menthol as a known agonist induced large inward cation currents in oocytes expressing wild-type TRPM8, but not in those expressing the TRPM8 mutant W682A or R998A (Fig. 2-4C). Similarly, in HEK 293 cells expressing TRPM8, Ca^{2+} entry was increased in the presence of menthol, assessed by ratiometric Fura-2 as Ca^{2+} indicator, whereas TRPM8 mutant W682A or R998A did not respond (Fig. 2-4D). In summary, our data using both oocytes

and HEK cells demonstrated that W682 in pre-S1 and R998 in the TRP domain are essential for TRPM8 channel function. As in TRPP3, these two residues are critical for the TRPM8 N-C interaction (Fig. 2-4E and F). Either the W682A mutation in the N-terminal peptide N642-K691 (M8NP) or the R998A mutation in the FL TRPM8 completely abolished the interaction of M8NP with the FL TRPM8 protein (Fig. 2-4E). In addition, the W682A mutation in FL TRPM8 or the W998A mutation in the C-terminal peptide G980-F1029 (M8CP) abolished the interaction of M8CP with FL TRPM8 (Fig. 2-4F). Therefore, as in TRPP channels, conserved W682 and R998 in TRPM8 may mediate the physical interaction between N- and C-termini, possibly through a π- cation bond.

Next, we examined the activity of TRPV1, TRPV1-W426A and TRPV1-R701A in oocytes in the presence of the agonist capsaicin and found that residues W426 and R701 are functionally important (Fig. 2-4G, H, S3D and S3E). The N-terminal peptide D383-R432 (V1NP) and the C-terminal peptide N687-D736 (V1CP) interacted with FL TRPV1 as revealed by co-IP. A single alanine substitution either in W426 or R701 was sufficient to abolish the interaction very much alike as in TRPP3, TRPP2 and TRPM8. Similar alanine substitution of the corresponding residue in mouse TRPC4, W314 (pre-S1) or R639 (TRP domain) abolished the activity of the constitutively active mutant TRPC4-G503S channel (Beck et al., 2013) (Fig. 2-S4B and C).

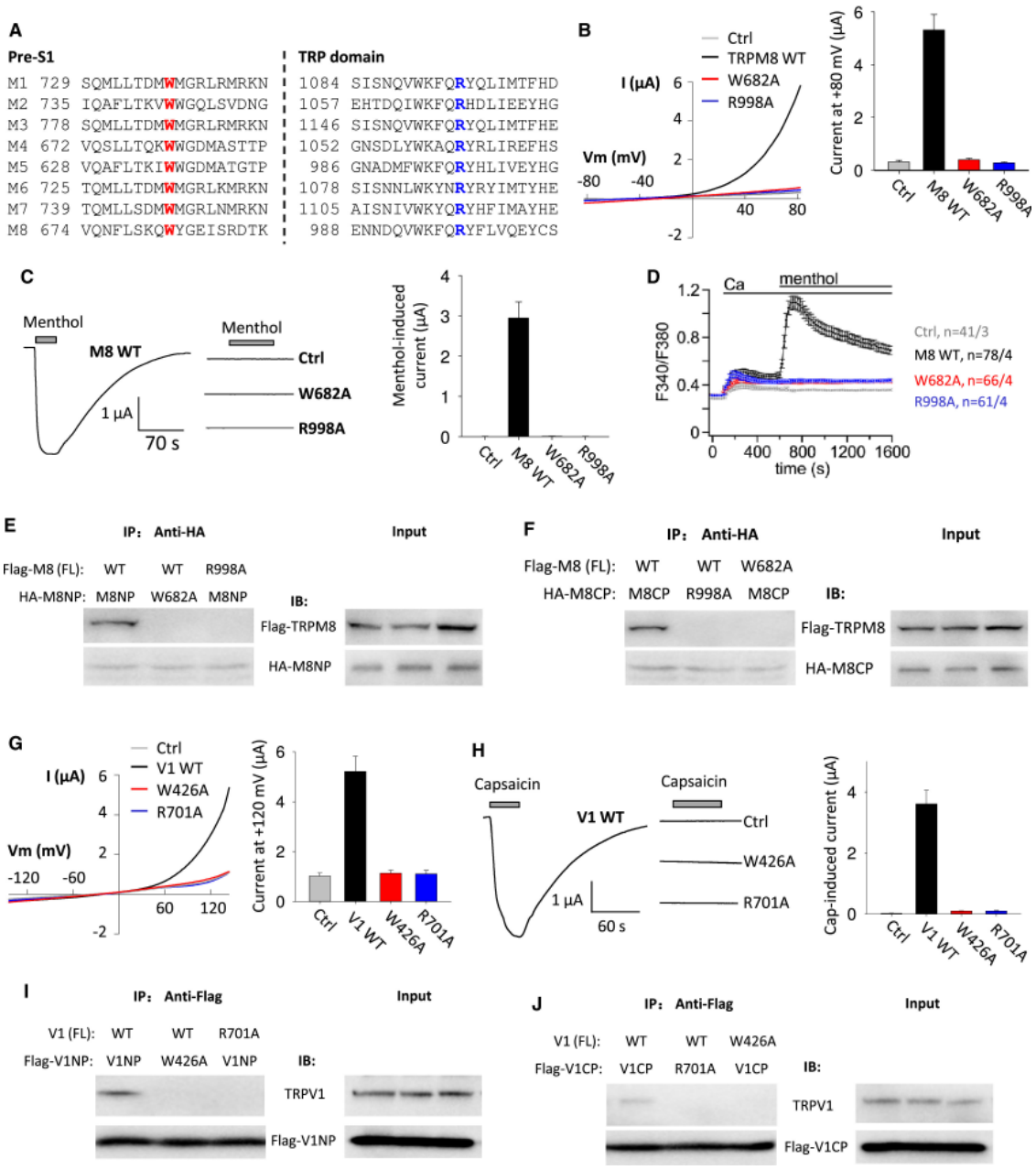

Fig. 2-4. Roles of TRPM8 and –TRPV1 aromatic and cationic residues in the pre-S1 and TRP-like domains, respectively, in the N-C binding and channel function. (**A**) Sequence alignment of human TRPMs pre-S1 and TRP-like domains. Conserved aromatic W and cationic R are indicated in red and blue, respectively. (**B**) *Left panel*, representative whole-cell I-V curves obtained from oocytes expressing rat TRPM8 WT or a mutant channel in the presence of Na^+- containing extracellular solution at RT. Ctrl, H_2O-injected oocytes. *Right panel*, averaged currents at +80 mV obtained under the same experimental conditions as in *left panel* from 12 - 18 oocytes of three batches. (**C**) *Left panel*, representative current

traces obtained at -50 mV from oocytes expressing WT or a mutant TRPM8 in the presence of the Na^+-containing solution before and after addition of 0.5 mM menthol. Ctrl, H_2O-injected oocytes. *Right panel*, averaged menthol-induced currents under the same experimental conditions as in *left panel* from 12 - 18 oocytes of three batches. (**D**) Ca^{2+}-imaging measurements showing averaged fura-2 ratios obtained before and after Ca^{2+} (2 mM) and menthol (0.5 mM) addition to Na^+-containing extracellular solution, in HEK cells transiently co-expressing GFP with rat WT or a mutant TRPM8, or none (Ctrl) at 37°C. (**E**) and (**F**) Effects of point mutations W682A and R998A in FL TRPM8, M8NP and/or M8CP on the FL TRPM8-peptide interaction. Representative co-immunoprecipitation data using oocytes expression, showing the interaction of Flag-tagged FL TRPM8 with HA-tagged TRPM8 N-terminal peptide (HA-M8NP, N642-K691) (**E**) or C-terminal peptide (HA-M8CP, G980-F1029) (**F**). (**G**) *Left panel*, representative whole-cell I-V curves obtained from oocytes expressing rat WT or a mutant TRPV1 in the presence of the Na^+-containing solution at RT. Ctrl, H_2O-injected oocytes. *Right panel*, averaged currents at +120 mV under the same experimental conditions as in left panel from 10 - 16 oocytes of three batches. (**H**) *Left panel*, similar experimental conditions as in **G**. Representative current traces obtained at -50 mV in rat WT or a mutant TRPV1 expressing oocytes before and after extracellular addition of capsaicin (15 μM). *Right panel*, averaged capsaicin-induced currents, as from experiments in left panel, from 10 - 16 oocytes of three batches. (**I**) and (**J**) Representative co-immunoprecipitation data using oocytes expression, showing the interaction of rat FL TRPV1 with Flag-tagged TRPV1 N-terminal peptide (Flag-V1NP, D383-R432) (**I**) or C-terminal peptide (Flag-V1CP, N687-D736) (**J**).

Regulation of the TRPs N-C binding by PIP2

To explore how the N-C interaction can be modulated, we examined the effect of the negatively charged, membrane anchored phosphoinositide PIP2 on the N-C interaction. We looked into PIP2 because it has been shown to modulate the function of most mammalian TRP channels except of TRPP3, TRPP5, TRPML2 and TRPML3 (Rohacs, 2014). Interestingly, the R998 residue of TRPM8 which pairs with W682 to mediate the N-C binding in TRPM8 (Fig. 2-4B-F) is part of the TRPM8's binding pocket for PIP2

(Rohacs et al., 2005). Thus, we next tested whether PIP2 can modulate TRP channel function through affecting the N-C interaction. In oocytes expressing human TRPP3, injection of diC8 PIP2, a H_2O-soluble dioctanoyl-analogue of PIP2 (Rohacs et al., 2005), significantly reduced Ca^{2+}-activated TRPP3 channel activity at -50 mV to 28 ± 4% compared to control oocytes (in the absence of PIP2, Fig. 2-5A). Reversely, by incubating oocytes for 1 hour in the presence of wortmannin, a membrane-permeable phosphatidylinositol 4-kinase inhibitor that depletes PIP2 (Zhang et al., 2003; Czirjak et al., 2001), Ca^{2+}-activated currents were increased by 1.7 ± 0.2 folds (Fig. 2-5B). To rule out the possible contribution of DAG and/or IP3, TRPP3-mediated currents were measured in the presence of the PLC inhibitor U-73122 (Lockhart and McNicol, 1999), which reduced channel activity to 23 ± 4%, suggesting that PIP2, but not DAG or IP3, inhibited TRPP3 channel function (Fig. 2-5C).

PIP2 is known to regulate channel function by interacting with cationic residues in the C- terminal TRP domain of several TRPs including TRPV1, TRPM8 and TRPM5 (Poblete et al., 2015; Rohacs et al., 2005; Nilius et al., 2008). PIP2 was also shown to bind to the TRPM4 C- terminal cationic residue-rich pleckstrin homology (PH)-like domain, located downstream of the TRP domain (Nilius et al., 2006). Sequence alignments revealed the presence of such a PH-like domain in a number of other TRPs (Nilius et al., 2008), including TRPPs (Fig. 2-5D). We thus wondered whether cationic residues in the TRPP3 C-terminal PH-like domain $_{594}$**RL**R**L**R**K**$_{599}$, called a RRRK motif,

could be involved in PIP2 binding. Given the vicinity of residues W81 and K568 to the cytoplasmic leaflet of the plasma membrane and proximity of K568 to the RRRK motif, a possible PIP2-TRPP3 interaction could disrupt the TRPP3 N-C binding (Fig. 2-1), thereby inhibiting channel function. We found that replacing one or more of the four cationic residues in TRPP3 $_{594}$**R**L**R**L**RK**$_{599}$ with glutamine (Q) significantly increases TRPP3 channel activity (Fig. 2-5E and F) without affecting the protein expression (Fig. 2-S5), suggesting that each of these substitutions might have disrupted PIP2-TRPP3 binding and thereby lifted channel inhibition by the endogenous PIP2 present in oocytes. In co-IP experiments PIP2 was in the same complex with wild-type TRPP3 (Fig. 2-5G), but not with mutant channel proteins in which the motif RRRK was deleted or the four cationic residues were substituted by Q (quadruple glutamine mutant) (Fig. 2-5G). Wortmannin treatment had little effect on the activity of the quadruple glutamine mutant channel, compared to wild-type (Fig. 2-5H). In summary these data show that the RRRK motif confers sensitivity to PIP2, most likely by forming an interaction domain with PIP2, and that the TRPP3-PIP2 interaction has a negative effect on channel activation.

In subsequent co-IP experiments we found that addition of diC8 PIP2 to the cell lysate disrupts the P3NP-TRPP3 binding in oocytes co-expressing FL TRPP3 and His-P3NP (Fig. 2-5I) but has no effect on the P3NP-TRPP3 binding when motif RRRK was mutated in FL TRPP3 (Fig. 2-5J), suggesting that binding between PIP2 and the RRRK motif is required for PIP2 to disrupt the N-C interaction. Similarly, the inhibitory

effect of PIP2 on the N-C binding was also demonstrated in TRPP2 by co-IP of P2NP and FL TRPP2 (Fig. 2-5K). Because TRPM8 R998 is part of the PIP2 binding pocket (Rohacs et al., 2005) we next tested the role of the corresponding residue K568 in TRPP3 for PIP2 binding by co-IP. As shown in Fig. 5L the K568A, but not W81A, mutation in TRPP3 disrupts the PIP2-TRPP3 binding, indicating that K568 is part of the PIP2 binding pocket in TRPP3. In summary, our data together demonstrated that PIP2 binds to TRPP3 through motif RRRK and K568. PIP2 binding to TRPP3 disrupts the W81-K568 pair- mediated N-C binding which is needed for channel activation and stabilization at the open state. Based on our data on TRPP2 (Fig. 2-5K) and the presence of a similar motif ($_{714}$**K**L**K**L**KK**$_{719}$), we propose that TRPP2 and TRPP3 share a similar mechanism of channel modulation by PIP2.

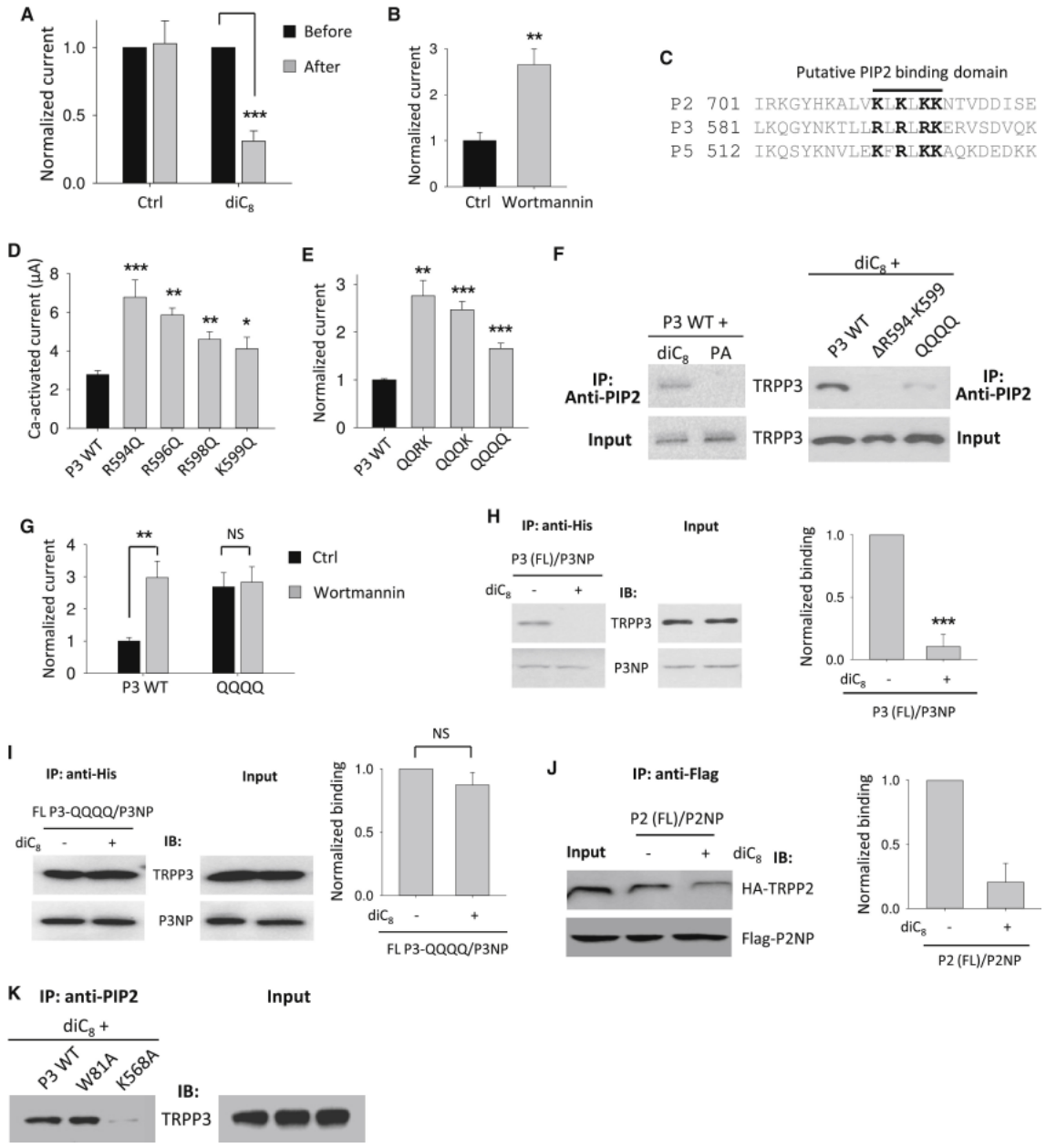

Fig. 2-5. Inhibition of the TRPP3 channel function and N-C interaction by PIP2. (**A**) Averaged Ca^{2+}-activated currents obtained from TRPP3-expressing oocytes pre-injected with 25 nl water containing diC_8 (5 mM), an analogue of PIP2, or water (Ctrl). Injection was performed 10 min prior to measurements. Currents were averaged from three independent experiments (with n = 12 - 15). ***P < 0.001. (**B**) Averaged and normalized Ca^{2+}-activated currents obtained from TRPP3-expressing oocytes pre-incubated with 10 μM wortmannin (a PIP2 inhibitor) or DMSO (Ctrl) for 1 hr before measurements. **P < 0.01. (**C**) Averaged and normalized Ca^{2+}-activated currents obtained from TRPP3-expressing oocytes pre-incubated

with 10 μM U73122 (PLC inhibitor) or DMSO (Ctrl) for 30 min. ***P < 0.001. (**D**) Alignment of the human TRPPs pleckstrin homology (PH)-like domain, putatively for binding lipids. Conserved cationic residues are highlighted. (**E**) Averaged Ca^{2+}-activated currents obtained from oocytes expressing WT or a mutant TRPP3 (n = 14 – 18). *P < 0.05, **P < 0.01 and ***P < 0.001. (**F**) Averaged and normalized Ca^{2+}-activated currents obtained under similar experimental conditions as in E. QQRK, R594Q/R596Q double mutant; QQQK, R594Q/R596Q/R598Q triple mutant; QQQQ, R594Q/R596Q/R598Q/K599Q quadruple mutant. **P < 0.01 and ***P < 0.001. (**G**) Representative co-IP data showing interaction of PIP2 with WT or a mutant TRPP3 expressed in oocytes. ΔR594-K599, TRPP3 deleted with fragment R594-K599. An anti-PIP2 antibody (sc-53412) from Santa Cruz biotechnology was used for immunoprecipitation. (**H**) Averaged and normalized Ca^{2+}-activated currents obtained from oocytes expressing WT TRPP3or the QQQQ mutant. Oocytes were treated with 10 μM wortmannin or DMSO (Ctrl) for 1 hr before measurements. **P < 0.01; NS, not significant. (**I**) *Left panel*, representative co-IP data showing the effect of diC8 on the interaction of P3NP with FL TRPP3 in oocytes. 3 μM diC8 was added in the cell lysis buffer. *Right panel*, data from three independent experiments in *left panel* were quantified, averaged and normalized. ***P < 0.001. (J) *Left panel*, representative co-IP data showing the effect of diC_8 on the interaction of P3NP with the TRPP3 QQQQ mutant under the same experimental conditions as in **I**. *Right panel*, data from three independent experiments in left panel were quantified, averaged and normalized (NS, not significant). (**K**) *Left panel*, representative co-IP data showing the effect of diC_8 on the interaction of P2NP with FL TRPP2 under the same experimental conditions as in **I**. *Right panel*, data from three independent experiments in *left panel* were quantified, averaged and normalized. (**L**) Representative co-IP data showing the interaction of PIP2 with expressed WT or a mutant TRPP3 in oocytes.

The TRPM8 and TRPV1 proteins possess a similar cationic rich motif and the additional R residue within the TRP domain that mediates binding to the N-terminal W residue. In contrast to TRPP channels, we found by co-IP assays that PIP2 enhances the binding of rat FL TRPM8 with its N-terminal peptide M8NP or C-terminal peptide M8CP (Fig. 2-6A and B). This is in agreement with the known stimulatory effect of PIP2 on the

TRPM8 channel function (Rohacs et al., 2005; Nilius et al., 2008), suggesting that the positive effect of PIP2 on TRPM8 is mediated through stabilizing the interaction between the N- and C-termini of TRPM8. Using a similar approach, we found that PIP2 promoted N-C binding in TRPV1 (Fig. 2-6C and D). This finding was also consistent with the positive regulation of TRPV1 by PIP2 direct binding (Lukacs et al., 2007; Poblete et al., 2015). Overall, our data showing a positive or negative effect of PIP2 on N- C binding among different TRP channels revealed a unifying mechanism underlying how PIP2 regulates TRP channel function.

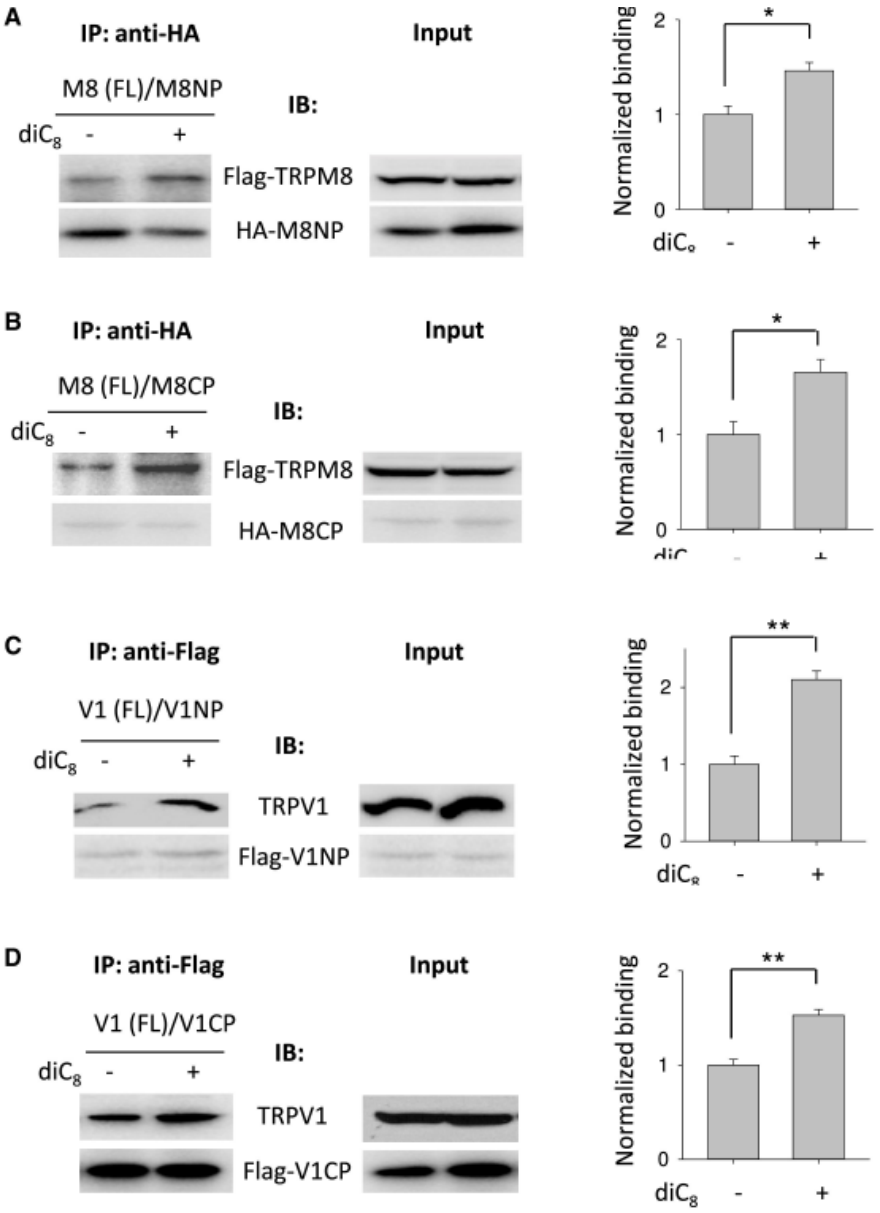

E Shared mechanism of TRPs channel activation

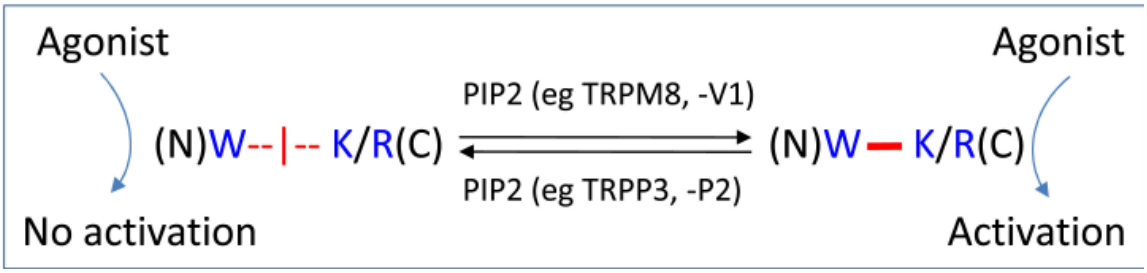

Fig. 2-6. Effects of PIP2 on the N-C interaction in TRPM8 and TRPV1. (**A**) *Left panel*, representative

co-IP data showing the effect of diC_8 on the interaction between expressed M8NP and FL TRPM8 under the same experimental conditions as in Fig. 2-4H. *Right panel*, data from three independent experiments in *left panel* were quantified, averaged and normalized (*P < 0.05). (**B**) *Left panel*, representative co-IP data showing the effect of diC_8 on the interaction between M8CP and FL TRPM8 under the same experimental conditions as in Fig. 2-4H. *Right panel*, data from three independent experiments in *left panel* were quantified, averaged and normalized (*P < 0.05). (**C**) *Left panel*, representative co-IP data showing the effect of diC_8 on the interaction between the V1NP fragment and FL TRPV1 under the same experimental conditions as in Fig. 2-4H. *Right panel*, data from three independent experiments in *left panel* were quantified, averaged and normalized (**P < 0.01). (**D**) *Left panel*, representative co-IP data showing the effect of diC_8 on the interaction of V1CP with FL TRPV1 under the same experimental conditions as in Fig. 2-4H. *Right panel*, data from three independent experiments in *left panel* were quantified, averaged and normalized (**P < 0.01). (**E**) Schematic model showing role of the PIP2-regulated, W-K/R pair- mediated N-C binding in TRP channels activation and function. In this model, the N-C binding is mediated between the conserved aromatic residue W in pre-S1 and the cationic residue K or R in the TRP(-like) domain and is either inhibited (as in TRPP3 and -P2) or enhanced (as in TRPM8 and -V1) by PIP2 through binding to the TRPs protein. The presence of the N-C binding is required for TRPs agonists to functionally activate the channel.

2.5 DISCUSSION

Although TRP channels respond to a variety of stimuli they share several common structural features including the conserved intracellular pre-S1 and TRP(-like) domains, a S6 gate motif, and S4-S5 linker. In an effort to determine whether TRP channels share common gating mechanims and how these mechanisms are further modulated, in the present study, we have investigated several TRP channels from the four major subfamilies. Our data revealed a previously unrecognized gating mechanism involving a physical intramolecular interaction between the N- and C-termini in these TRP channels. This N-C binding is mediated by an evolutionarily conserved aromatic tryptophan residue in the N-terminal pre-S1 domain and a cationic lysine/arginine residue in the C-terminal TRP/TRP-like domain of TRPs. We further showed that PIP2 can modulate TRP channel activity by directly interfering with the N-C interaction. In TRPP3 and TRPP2 this interference resulted in positive regulation, whereas in TRPM8 and TRPV1 it resulted in negative regulation. The scheme in Fig. 2-6E summarizes these findings, in which 1) the TRP N-C binding is either inhibited or enhanced by PIP2 and 2) an agonist is able to activate the channel when the N-C binding is present, whereas it is not when the N-C binding is absent or weak.

The high resolution of the TRPV1 structure first revealed an intramolecular proximity of the pre-S1 (or S4-S5 linker) and TRP domains (Liao et al., 2013; Cao et al.,

2013; Gao et al., 2016). This observation was later confirmed in the structures of TRPA1 (Paulsen et al., 2015), TRPV2 (Huynh et al., 2016; Zubcevic et al., 2016), TRPV6 (Saotome et al., 2016), TRPP2 (Wilkes et al., 2017; Grieben et al., 2016; Shen et al., 2016) and NOMPC (Jin et al., 2017), suggesting that residues in pre-S1, S4-S5 linker and TRP domains may mediate intramolecular interactions that are important for structural stability, channel gating, or allosteric modulation. In line with this suggestion, the interaction among the pre-S1 linker, pre-S1 and TRP domains was shown to be required for proper folding, assembly and trafficking of TRPV1 and TRPV4 channels (Garcia-Elias et al., 2015).

In this study, we identified residues essential for the interaction of the pre-S1 within the N-terminus and the C-terminal TRP(-like) domain (N-C interaction). This interaction underlies allosteric gating of several TRP channels representative for TRPP, TRPM, TRPV and TRPC subfamilies. Of note, the interaction between the TRPV1 W426 (pre-S1) and TRPV1 R701 (TRP domain) identified here, was not resolved in the previous TRPV1 structures (Liao et al., 2013; Cao et al., 2013; Gao et al., 2016) which instead proposed the Q423-R701 interaction. Comparing TRPV1 structures (PDB: 3J5P, 3J5R and 3J5Q) at closed and activated (capsaicin- or vanilloid agonist resiniferatoxin (RTX)/spider double-knot toxin (DkTx)-bound) states revealed that Q423 moves away from R701 during the activation (Fig. 2-S3F and G), suggesting that the Q423-R701 interaction might not be required for channel activation. In contrast, residues W426 and R701

remained close to each other during activation (Fig. 2-S3F and G), suggesting the W426-R701 binding may be required for channel function. In support of this, our functional studies revealed that mutant Q423A can still be activated by depolarization and capsaicin (Fig. 2-S3B-E) while W426A behaved as a total loss-of-function mutant (Fig. 2-4G and H). Interestingly, while the W426-R701 pair distance is minimally affected by capsaicin binding (Fig. 2-S3F), it became shorter in the combined presence of RTX and DkTx (Fig. 2-S3G), which seemed to dictate the previous observation that RTX and DkTx together induce larger pore opening than capsaicin (Cao et al., 2013).

In addition to the intramolecular N-C binding, interaction of the S4-S5 linker and TRP/TRP-like domain was also recognized and supported by the identification of several functionally important residues within the S4-S5 linker (Hofmann et al., 2017b). The leucine residue at position 596 (L596) in the S4-S5 linker of TRPV4 was reported to interact with W733 in the TRP domain, presumably via a hydrogen bond, and this interaction was proposed to act to maintain the closed state since disrupting this interaction through mutations resulted in constitutive opening (Teng et al., 2015). In TRPV6, F518 and T519 in the S4-S5 linker seems to interact with T621 located in the linker between S6 and the TRP domain and such interaction could be enhanced by substitution of G516 by S or C to result in a higher channel activity (Hofmann et al., 2017a). A similar gain-of-function mutation was also reported in TRPC4 and TRPC5 (Beck et al., 2013). It remains to be determined by future studies as to whether the pre-

S1-TRP(-like) and S4-S5 linker-TRP(-like) interactions are independent of each other.

PIP2 was reported to up- and down-regulate TRPV1 channel function under different conditions (Lukacs et al., 2007). In excised patches, PIP2 was required for TRPV1 channel function and enhanced the activation by capsaicin, while in whole-cell configuration PIP2 exhibited a net inhibitory effect which was explained by an indirect inhibitory regulation likely absent in excised patches (Lukacs et al., 2007; Chuang et al., 2001). It was speculated from these studies that PIP2 may exhibit a stimulatory effect on TRPV1 through direct binding whereas it may display a net inhibitory effect when an indirect regulator pathway is also present. In fact, this type of dual effects of PIP2 was also reported for TRPA1 and TRPC channels (Lemonnier et al., 2008; Dai et al., 2007; Hofmann et al., 1999). Our data (Fig. 2-6C and D) showed that the functional stimulation of TRPV1 by PIP2 is through an enhanced N-C binding by PIP2 despite the possibility that the indirect pathway may also be present in oocytes under our whole-cell configuration.

The role of PIP2 in TRPP3 channel function has been unknown. However, TRPP2 has been shown to be inhibited by PIP2, but by an unknown mechanism (Ma et al., 2005). Our current study revealed that PIP2 binds to TRPP3 K568 and cationic residues in the motif $_{594}$**RLRLRK**$_{599}$. In particular, PIP2 binding by K568 disrupts W81-K568 mediated N-C interaction thereby inhibiting TRPP3 channel activation. Because of the high sequence similarity, especially the conserved PIP2 binding residues (K688 and motif

$_{714}$**K**L**K**L**KK**$_{719}$ in TRPP2), TRPP2 presumably shares a similar way of regulation. Our immunoprecipitation data (Fig. 2-5K) suggest that PIP2 inhibits the TRPP2 channel function through compromising the N-C binding, supporting this regulatory mechanism.

PIP2 was reported to enhance the activation of the TRPM8 channel by its agonist menthol (Liu and Qin, 2005; Rohacs et al., 2005), which is consistent with our data (Fig. 2-S2B). Neutralization of the conserved cationic residues K995, R998 and R1008 in the TRP domain, which are likely part of the PIP2 binding pocket, significantly inhibited the channel function (Rohacs et al., 2005), suggesting that the effect of PIP2 on TRPM8 is through direct binding. PIP2 stabilizes the TRPM8 N-C interaction (Fig. 2-6A and B) that is mediated by the W682 and R998 residues, is critical for channel function (Fig. 2-4B-F) and enables menthol to induce channel activation (Fig. 2-6E).

One of the key properties shared by TRPP3 and TRPM8 is that the cationic residue in the TRP domain, K568 of TRPP3 or R998 of TRPM8, mediates both the N-C interaction and binding to PIP2. We showed that PIP2 weakens the N-C binding of TRPP3, presumably by competing for binding to the K residue in the TRP-like domain with the aromatic residue in the pre-S1. This mechanism could be shared with TRPP2. In contrast, in TRPM8, PIP2 surprisingly enhanced the N-C binding. In TRPV1, PIP2 also enhanced the N-C binding although R701 that pairs with the N-terminal W426 was reported not to be part of the PIP2 binding pocket (Poblete et al., 2015). Significant conformational changes following PIP2 binding by the Kir2.2 channel has previously

been reported (Hansen et al., 2011) and similar structural constraints, induced by PIP2, may lead to a stronger W-R interaction in TRPM8 and TRPV1.

In summary, this study identified conserved amino acid residues, a tryptophan and a lysine/arginine residue in the N-terminal pre-S1 and the C-terminal TRP(-like) domains, respectively, that underlie interaction of the two domains. This N-C binding in TRPs is critical for the channel gating and regulation by PIP2 through direct binding. This intracellular N-C binding may serve as a shared molecular switch that transduces the conformational changes induced by diverse ligands to channel pore opening and closing.

2.6 SUPPLEMENTARY INFORMATION

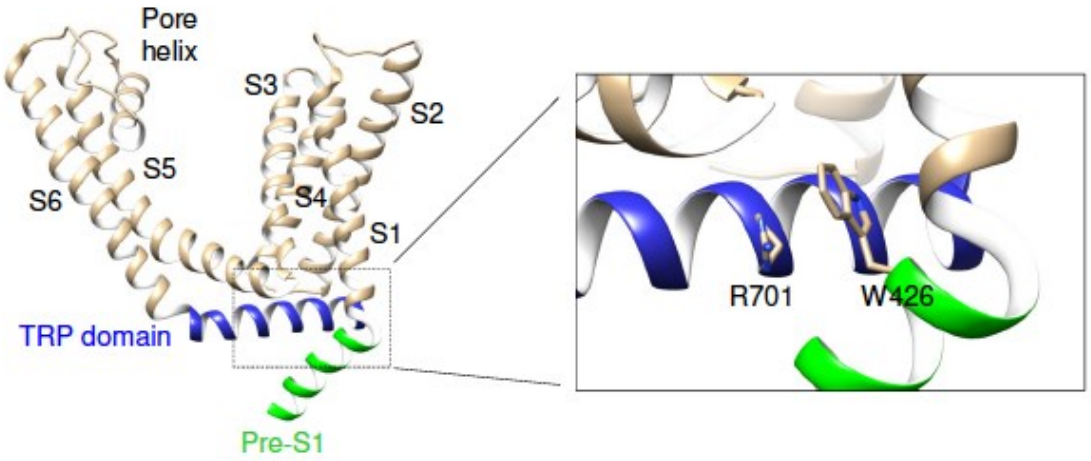

Fig. 2-S1. Physical proximity between TRPV1 pre-S1 and TRP domains, related to Fig. 2-1. Ribbon diagram of TRPV1 structure (PDB: 3J5P) showing direct contact between Nterminal pre-S1 (green) and C-terminal TRP helices (blue). The N-terminal fragment before pre-S1 and C-terminal fragment after the TRP domain are not shown. The π-cation stacking between W426 and R701 was shown.

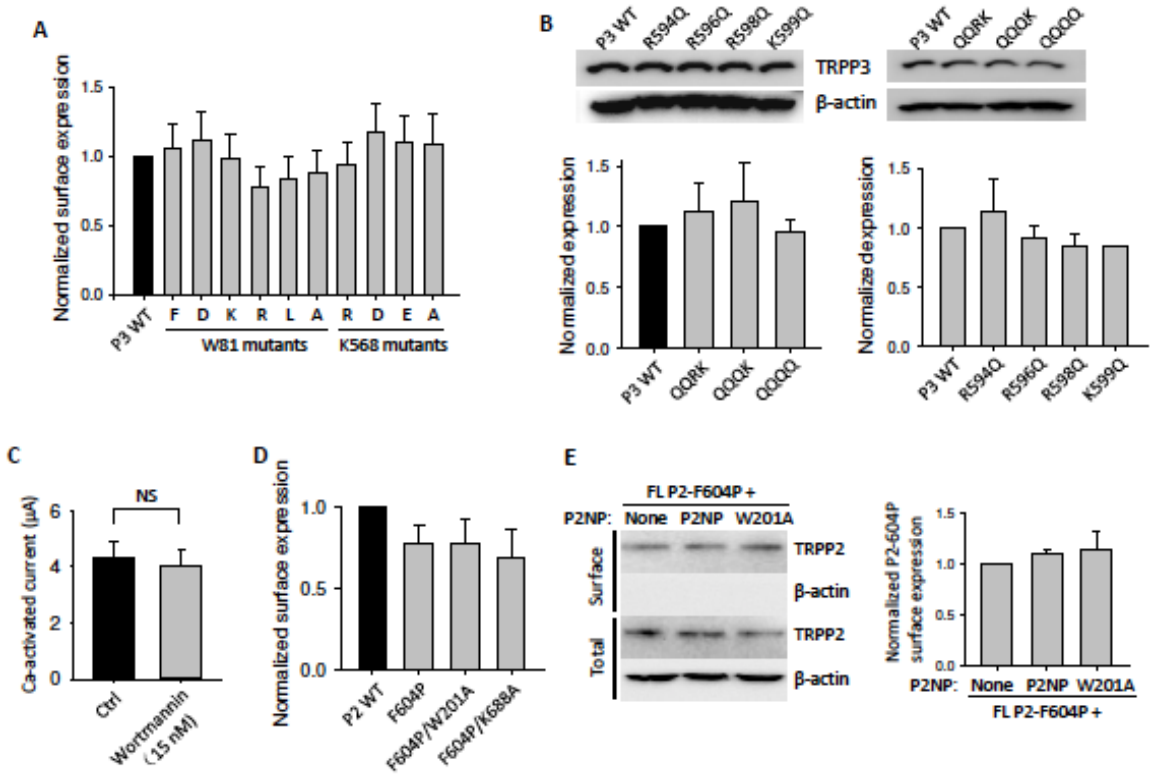

Fig. 2-S2. Effects of mutations on TRPP3 or TRPP2 surface expression and effects of 15 nM wortmannin on TRPP3 channel function, related to Fig. 2-1, 2-2 and 2-5. (**A**) Averaged and normalized surface expression of TRPP3 WT, W81 or K568 point mutants from three independent experiments. (**B**) *Upper panel*, representative immunoblots of total protein of TRPP3 WT or mutant expressed in oocytes. QQRK, R594Q/R596Q double mutant; QQQK, R594Q/R596Q/R598Q triple mutant; QQQQ, R594Q/R596Q/R598Q/K599Q quadruple mutant. *Lower panels*, data from three independent experiments in *upper panel* were quantified, averaged and normalized. (**C**) Averaged Ca^{2+}-activated currents obtained from TRPP3-expressing oocytes pre-incubated with 15 nM wortmannin or DMSO (Ctrl) for 1 hr before measurements. NS, no significance by t-test. (**D**) Averaged and normalized surface expression of TRPP2 WT or indicated mutants from three independent experiments. (**E**) *Left panel*, representative immunoblots of the surface biotinylated and total protein of the FL TRPP2 F604P mutant co-expressed with P2NP, P2NP-W201A, or none. β-actin was used as a control. *Right panel*, data from three independent experiments in *left panel* were quantified, averaged and normalized. Data are presented as mean ± SEM.

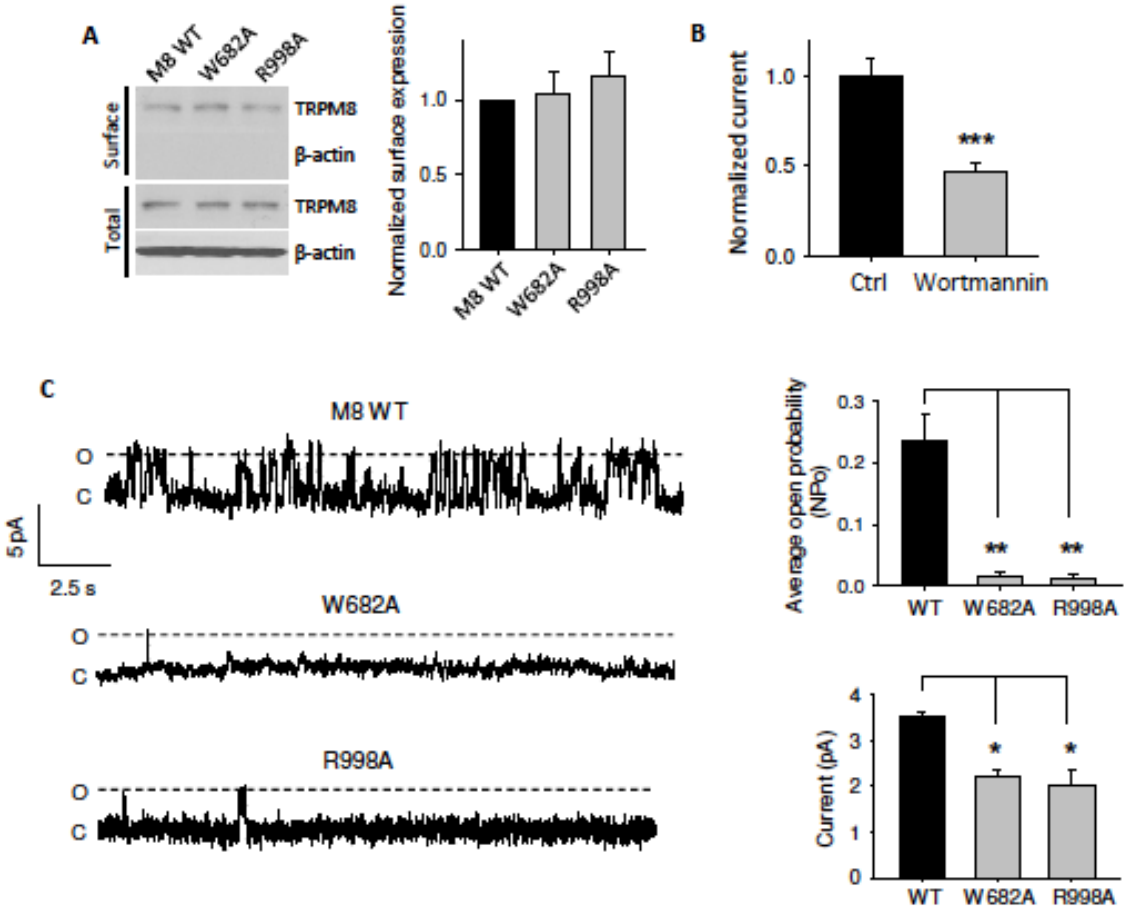

Fig. 2-S3. Surface expression and single-channel currents of WT and mutant TRPM8, related to Figure 2-4. (**A**) *Left panel*, representative immunoblots of the surface biotinylated and total protein of TRPM8 WT or indicated mutants expressed in oocytes. β-actin was used as a control. *Right panel*, data from three independent experiments in *left panel* were quantified, averaged and normalized. (**B**) Averaged and normalized 0.5 mM menthol-induced currents obtained from TRPM8-expressing oocytes pre-incubated with 10 μM wortmannin or DMSO (Ctrl) for 1 hr before measurements. (**C**) *Left panel*, representative single-channel traces recorded at +100 mV in HEK293 cells expressing TRPM8 WT (n = 5), W682A (n = 5) or R998A (n = 4) mutant under the cell-attached configuration. 'C' and 'O' indicate the closed and open states, respectively. Measurements were performed as previously (Zheng et al., 2018b). *Right panels*, averaged channel open probabilities and current amplitudes obtained from single-channel recordings each of around 20-s duration. Data are presented as mean ± SEM. Statistical analyses were performed with t-test. *p < 0.05; **p < 0.01; ***p < 0.001.

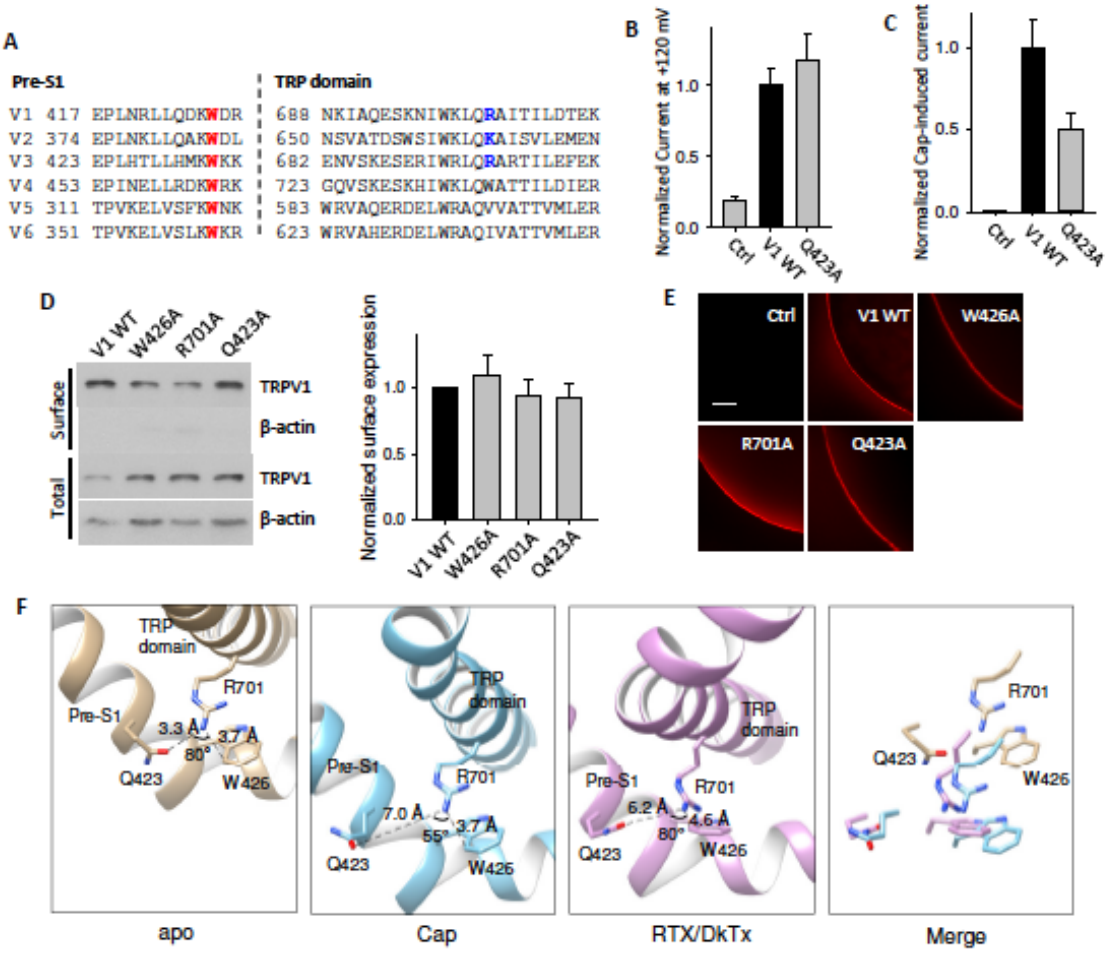

Fig. 2-S4. Effects of mutations on the expression, function and N-C interaction of TRPV1, related to Fig. 2-4. (**A**) Amino acid alignment of human TRPVs pre-S1 and TRP domains. Conserved aromatic W and cationic R/K (except TRPV4-6) are indicated in red and blue, respectively. (**B**) Averaged and normalized currents at +120 mV under the same experimental conditions as Figure 4G *left panel* from oocytes expressing TRPV1 WT or Q423A mutant. Ctrl, H_2O-injected oocytes. (**C**) Averaged and normalized capsaicin-induced currents under the same experimental conditions as Figure 4H *left panel* from oocytes expressing TRPV1 WT or Q423A mutant. Ctrl, H_2O-injected oocytes. (**D**) *Left panel*, representative immunoblots of surface biotinylated and total protein of TRPV1 WT or mutant expressed in oocytes. β-actin was used as a control. *Right panel*, data from three independent experiments in *left panel* were quantified, averaged and normalized. (**E**) Representative whole-mount immunofluorescence showing

surface expression of TRPV1 WT or mutant expressed in an oocyte. Ctrl, H_2O-injected oocyte. *Scale bar*, 50 µm. (**F**) Relative position of TRPV1 R701 to Q423 and W426 in the apo state (PDB 3J5P), the activated state in the presence of capsaicin (Cap, PDB 3J5R), and the combined presence of vanilloid agonist resiniferatoxin (RTX) and spider double-knot toxin (DkTx) (PDB 3J5Q). *Right panel*, merge of the three residues at the different states. Data are presented as mean ± SEM.

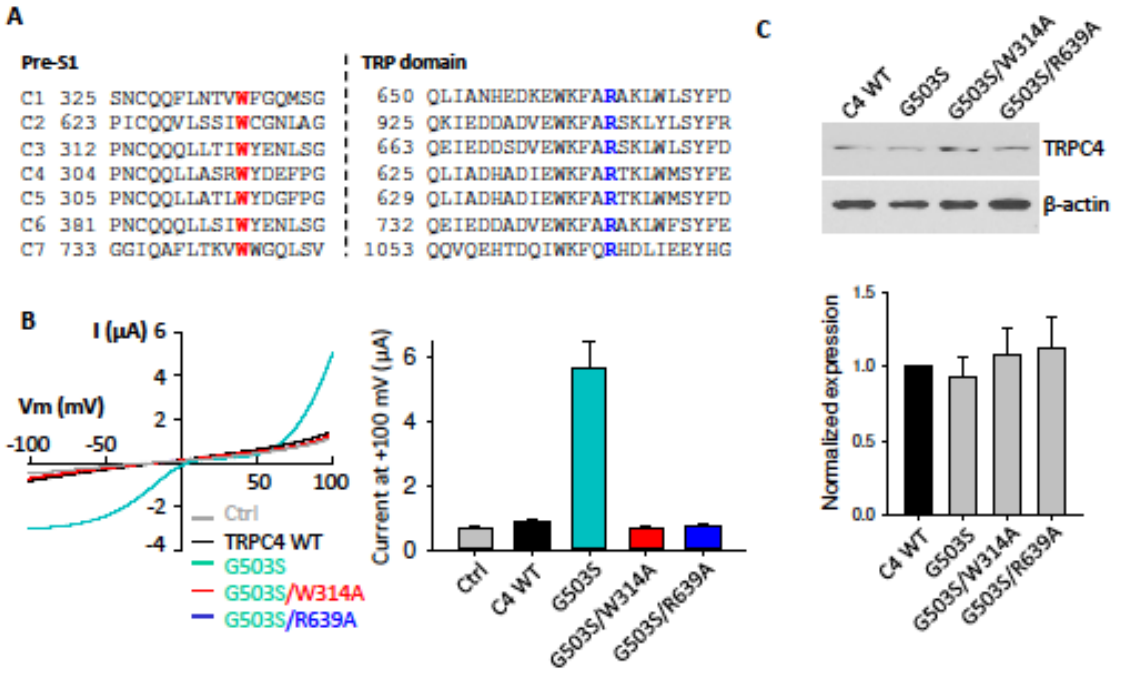

Fig. 2-S5. Roles of the mouse TRPC4 residues W314 (pre-S1) and R639 (TRP domain) in the channel function, related to Fig. 2-4. (**A**) Amino acid alignment of human TRPCs pre-S1 and TRP domains. Human TRPC2 is a pseudogene and mouse TRPC2 was used instead. Conserved aromatic W and cationic R are indicated in red and blue, respectively. (**B**) *Left panel*, representative I-V curves obtained from oocytes expressing mouse WT or a mutant TRPC4β, as indicated, in the presence of a Na^+-containing solution. Ctrl, H2O-injected oocytes. *Right panel*, averaged currents at +100 mV under the same experimental conditions as in *left panel*. (**C**) *Upper panel*, representative immunoblots of total protein of TRPC4β WT or mutant expressed in oocytes. *Lower panel*, data from three independent experiments in *upper panel* were quantified, averaged and normalized. Data are presented as mean ± SEM.

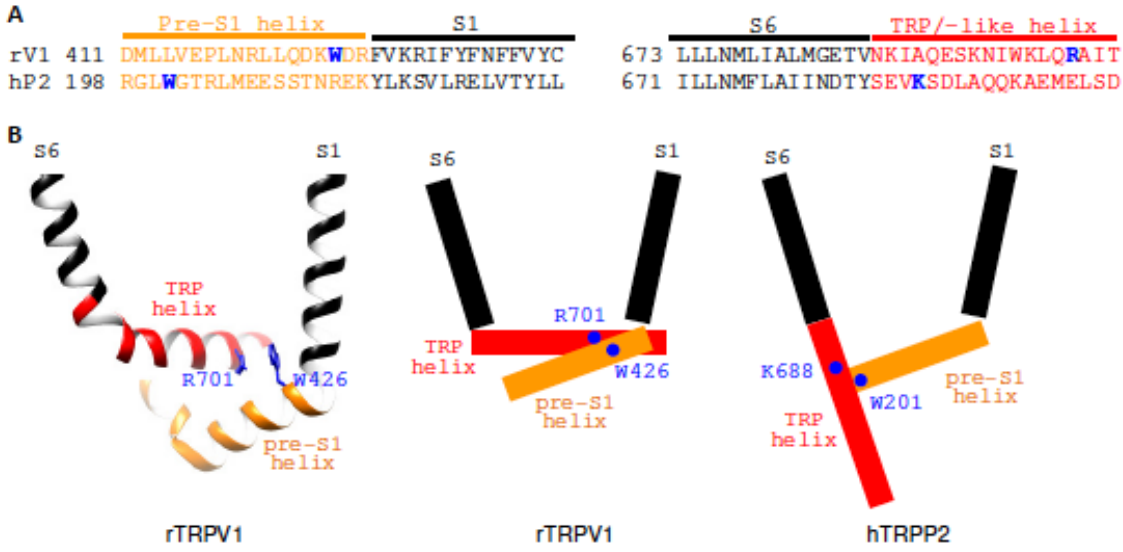

Fig. 2-S6. Comparison of the N-C interaction in TRPV1 and TRPP2, related to Fig. 2-2 and 2-4. (A) Sequence alignment of rat TRPV1 (rV1) and human TRPP2 (hP2) showing different positions of the tryptophan residue (blue) in the pre-S1 helix and the cationic residue (blue) in the TRP/TRP-like helix. (**B**) *Left panel*, ribbon diagram of TRPV1 structure (PDB: 3J5P) showing direct contact between the pre-S1 helix (orange) and TRP helix (red). W426 and R701 residues are shown. *Central panel*, schematic illustration (with a horizontal TRP helix) showing the W426-R701 interaction in TRPV1. *Right panel*, schematic illustration (with TRP-like helix parallel to S6) showing the W201-K688 interaction in TRPP2.

CHAPTER 3

RESULTS #2

Autoinhibition of TRPV6 channel and regulation by PIP2

3.1 ABSTRACT

Transient receptor potential vanilloid 6 (TRPV6), a calcium-selective channel possessing six transmembrane domains (S1-S6) and intracellular N-/C-termini, plays crucial roles in calcium absorption in epithelia and bone and is involved in human diseases including vitamin-D deficiency, osteoporosis and cancer. The TRPV6 function and regulation remain poorly understood. Here we show that the TRPV6 intramolecular S4-S5 linker to C-terminal TRP helix (L/C) and N-terminal pre-S1 helix to TRP helix (N/C) interactions, mediated by Arg470:Trp593 and Trp321:Ile597 bonding, respectively, are autoinhibitory and are required for maintaining TRPV6 at basal states. Disruption of either interaction by mutations or blocking peptides activates TRPV6. The N/C interaction depends on the L/C interaction but not reversely. Three cationic residues in S5 or C-terminus are involved in binding PIP2 to suppress both interactions thereby activating TRPV6. This study reveals 'PIP2-intramolecular interactions' regulatory mechanism of TRPV6 activation-autoinhibition, which will help elucidating the corresponding mechanisms in other TRP channels.

3.2 INTRODUCTION

Mammalian transient receptor potential (TRP) superfamily of ion channels contains 28 members divided into six subfamilies known as TRP canonical (TRPC), vanilloid (TRPV), polycystin (TRPP), melastatin (TRPM), ankyrin (TRPA) and mucolipin (TRPML) (Gees et al., 2010). TRP proteins share tetrameric assembly and membrane topology, i.e., six transmembrane domains (S1-S6) and intracellular N- and C-termini (Liao et al., 2013; Saotome et al., 2016). As a member of the TRPV subfamily TRPV6 is a cation channel highly selective to calcium (Ca) with a permeability (P) ratio PCa/PNa = 130 (Yue et al., 2001). It is expressed in several human tissues such as small intestine, kidney, placenta and testis (Peng et al., 1999). Physiologically, TRPV6 plays crucial roles in Ca^{2+} homeostasis of small intestine and kidney and in Ca^{2+}-dependent sperm maturation (Bianco et al., 2007; van Goor et al., 2017). A TRPV6 loss-of-function mutation in male mice leads to severely impaired sperm mobility and fertility (Weissgerber et al., 2012; Weissgerber et al., 2011). TRPV6 is also essential in responding to fluid shear stress during microvilli development (Miura et al., 2015). Malfunction of TRPV6 is associated with a variety of human diseases including vitamin D-deficiency rickets, kidney stone disease and osteoporosis (van Abel et al., 2003; Suzuki et al., 2008; Lieben et al., 2010). Elevated expression of or mutations in TRPV6 is found in cancer including breast, prostate, non-small cell lung, kidney and skin cancer, making

it a potential target for clinical interventions (Peters et al., 2012; Peng et al., 2000; Forbes et al., 2008, 31897233).

TRPV6 structures determined by X-ray crystallography and cryo-electron microscopy (EM) revealed proximity of the C-terminal TRP helix with the N-terminal pre-S1 and intracellular S4-S5 linker (McGoldrick et al., 2018; Saotome et al., 2016). Similar physical arrangements were also seen in other TRP members of resolved structures, while TRPP channels have a TRP-like helix (Su et al., 2018; 24305160, 31184289). However, whether and how these domains interact with each other and the functional implications of these interactions are poorly understood.

Predominantly anchored to the inner plasma membrane, phosphatidylinositol 4,5-bisphosphate (PIP2, or PI(4,5)P2) accounts for more than 99% of double-phosphorylated PIs in mammalian cells, with PI(3,4)P2 and PI(3,5)P2 accounting for the rest (Vanhaesebroeck et al., 2001). Phospholipase C dialyzes PIP2 into second messengers inositol 1,4,5-trisphosphate and diacylglycerol. PIP2 is known to modulate ion channels through electrostatic force between its negatively charged inositol head and a pocket formed by cationic residues in a channel protein. For instance, cationic residues in TRPP3, -M4, -M8 and -V1 have been identified to be part of the PIP2 binding pocket (Zheng et al., 2018a; Nilius et al., 2008). PIP2 may exert an inhibitory or stimulatory effect on a TRP channel. For example, PIP2 stimulates the function of TRPV5, -V6, -M4, -M5, -M7 and -M8 while it inhibits TRPP2 and -P3 (Zheng et al., 2018a; Ma et al., 2005,

30305626). The effect of PIP2 on TRPV1 may be stimulatory or inhibitory, depending on experiment conditions (Lukacs et al., 2007). Based on a rabbit TRPV5 cryo-EM structure resolved with the analogue diC8-PIP2 present in the nanodisc, it was suggested that PIP2 would bind to residues in the N-terminus, S4-S5 linker and TRP domain (Hughes et al., 2018).

In the present study, we characterized intramolecular interactions among the S4-S5 linker, TRP and pre-S1 helices of TRPV6 by means of co-immunoprecipitation (co-IP), in vitro pull-down and co-immunofluorescence (co-IF). We examined how they modulate the TRPV6 channel function by the two-electrode voltage clamp electrophysiology in *Xenopus* oocytes and Ca^{2+} imaging in mammalian cells. We also identified TRPV6 residues involved in these interactions or PIP2 binding and determined how PIP2 modulates TRPV6 intramolecular interactions through which it activates TRPV6.

3.3 METHODS

Plasmids, mutations, antibodies and chemical reagents

Human TRPV6 cDNA was subcloned into *Xenopus* expression vector pBSMXT-MCS. For expression in HEK293 cells, human TRPV6 cDNA was subcloned into the mammalian expression vector pMAX-GFP. QuickChange Lightning Site-Directed Mutagenesis kit (Agilent Technologies, La Jolla, CA) was used to generate mutations, which were all verified by sequencing. Antibody against TRPV6 was custom made in house, as previously described (Fecher-Trost et al., 2013). Antibodies against β-actin, GST, His, HA and Flag were purchased from Santa Cruz Biotechnology (Santa Cruz, CA). Secondary anti-mouse, -rabbit and -goat antibodies were purchased from GE Healthcare (Waukesha, WI). Wortmannin and NFA were purchased from Millipore Sigma Canada (Oakville, ON) and diC8-PIP2 from Echelon Biosciences (Salt Lake City, UT).

Xenopus oocyte expression

Capped RNAs encoding TRPV6 and peptides were synthesized by an in vitro transcription T3 or T7 mMESSAGE mMACHINE kit (Ambion, Austin, TX) and injected (25-50 ng per oocyte) into *Xenopus* oocytes prepared as described (Zheng et al., 2018b). Oocytes injected with equal volumes of water served as control. After injection, oocytes were incubated at 18℃ for 1-2 days before experiments. The present study was approved

by the Ethical Committee for Animal Experiments of the University of Alberta and was carried out in accordance with the Guidelines for Research with Experimental Animals of the University of Alberta and the Guide for the Care and Use of Laboratory Animals (NIH Guide) revised in 1996.

Two-electrode voltage clamp electrophysiology

The two-electrode voltage clamp electrophysiology experiments in *Xenopus* oocytes were performed as we described previously (Zheng et al., 2018c; Zheng et al., 2016). Briefly, the electrodes (Capillary pipettes, Warner Instruments, Hamden, CT) that impale an oocyte were filled with 3 M KCl for a tip resistance of 0.3-2 MΩ. Unless otherwise indicated, an NMDG-containing extracellular solution was used (in mM): 100 NMDG, 2 KCl, 0.2 $MgCl_2$ and 10 HEPES (pH 7.5) with or without 5 mM $CaCl_2$ with the presence of 1 mM NFA, and oocytes were clamped at -50 mV. The Na^+-containing solution was formed by replacing NMDG with Na. On-site injection of diC8-PIP2 was performed by a third electrode after the initial measurements. The second measurements were performed 10 min after the injection (Zheng et al., 2018a). Unless described otherwise, measurements were performed when an oocyte was voltage clamped and held at -50 mV. Whole-cell currents and membrane potentials were recorded at room temperature and analyzed using a Geneclamp 500B amplifier and Digidata 1322A AD/DA converter (Molecular Devices, Union City, CA) together with the pClamp 9 software (Axon

Instruments, Union City, CA). Current and voltage signals were digitized at 200 μs/sample and filtered at 2 kHz through a Bessel filter. SigmaPlot 13 (Systat Software, San Jose, CA) and GraphPad Prism 8 (GraphPad Software, San Diego, CA) were used for data plotting.

Surface protein biotinylation

After 3-time washes with ice-cold PBS solution, *Xenopus* oocytes were incubated with 0.5 mg/ml sulfo-NHS-SS-Biotin (Pierce, Rockford, IL) for 30 min at room temperature. Non-reacted biotin was quenched using 1 M NH4Cl. Oocytes were then washed with ice-cold PBS solution and harvested in ice-cold CelLytic M lysis buffer (Sigma) supplemented with proteinase inhibitor cocktail (Thermo Scientific, Waltham, MA). With gentle shaking, lysates were incubated at 4℃ overnight upon addition of 100 μl streptavidin (Pierce). The surface protein absorbed by streptavidin was resuspended in SDS loading buffer and subjected to SDS-PAGE.

Whole oocyte immunofluorescence

Immunofluorescence assays using whole *Xenopus* oocytes were performed as described (Zheng et al., 2018a). After PBS wash, 15 min fixation in 4% paraformaldehyde and 3-time washes in PBS plus 50 mM NH4Cl, oocytes were permeabilized with 0.1% Triton X-100 for 4 min. PBS plus 3% skim milk was used to

block oocytes for 30 min. Oocytes were then incubated at 4℃ overnight with indicated primary antibodies (with Flag tag for NP, CP and their mutants and HA tag for LP and its mutant), followed by incubation with secondary Alexa-488-conjugated donkey anti-rabbit or Cy3-conjugated goat anti-mouse antibodies (Jackson ImmunoResearch Laboratories, West Grove, PA) for 30 min. Oocytes were then mounted in Vectashield (Vector Labs, Burlington, ON) and examined on an AIVI spinning disc confocal microscopy (Cell Imaging Facility, Faculty of Medicine and Dentistry, University of Alberta).

Co-IP and *in vitro* pull-down

Co-IP experiments were performed as we previously described (Zheng et al., 2018a). Briefly, a group of 20-30 oocytes were washed with PBS and solubilized in ice-cold CelLytic-M lysis buffer (Sigma) supplemented with proteinase inhibitor cocktail. After centrifugation at 13,200 rpm for 15 min, supernatants were collected and precleaned for 1 hour (hr) with 50% protein G-Sepharose (GE Healthcare), followed by incubation with antibodies at 4℃ for 4 hr. The mixture upon the addition of 100 µl of 50% protein G-Sepharose was incubated at 4℃ overnight with gentle shaking. The immune complexes conjugated to protein G-Sepharose were washed five times with Nonidet P-40 lysis buffer (1% Nonidet P-40, 150 mM NaCl, 50 mM Tris, pH 7.5) and eluted by SDS loading buffer. Precipitated proteins were loaded to SDS-PAGE gel and transferred to a PVDF membrane (Bio-Rad, Hercules, CA), and then analyzed by WB.

GST- or His-tagged human TRPV6 peptides were purified from *E. coli* and incubated at the same amount (2 μg) and solubilized in the CelLytic-M lysis buffer (Sigma). The mixture was incubated at 4℃ for 4 hr with gentle shaking, followed by overnight incubation after addition of 10 μl 50% Ni-NTA agarose beads (Qiagen, Hilden, Germany). The beads were then washed three times with PBS buffer supplemented with 1% Nonidet P-40, and the remaining proteins were eluted using SDS loading buffer and resolved by SDS-PAGE and transferred to PVDF membrane (Bio-Rad). His and GST antibodies were used to immunoblot the membrane.

Ratiometric Ca^{2+} imaging

HEK293 cells plated on PLL-coated glass coverslips in the incubation medium were loaded with 5 μM Fura-2-AM in the dark and incubated at 37°C for 30 min. Cells were then washed with bath solution (in mM): 1 $MgCl_2$, 2 $CaCl_2$, 4 KCl, 140 NaCl, 10 HEPES, 10 glucose, pH adjusted to 7.2 with NaOH. $CaCl_2$ was replaced by $MgCl_2$ to form a nominal Ca^{2+}-free solution. An inverted microscope (Axiovert S100, Zeiss, Oberkochen, Germany) equipped with a monochromator (Polychrome V, TILL-Photonics Graefelfing, Germany) and a 20× Fluar objective (Zeiss) was used for all measurements. Fura-2 was alternately excited at 340 nm and 380 nm for 30 ms every 2 s and the emitted fluorescence (>510 nm) was recorded with a cooled charge-coupled device (CCD) camera (TILL Imago, TILL-Photonics). F340 and F380 pictures were used to calculate

the ratiometric images after background correction, i.e. subtraction by the fluorescence intensity in a cell-free area corresponding to 340 and 380 nm excitation, respectively. Single cells were marked as regions of interest and the F340/F380 ratio was plotted versus time. Monochromator, camera, acquisition and analysis were controlled by TILLvisION software (TILL-Photonics).

Knockdown of zebrafish Trpv5/6 by CRISPR-Cas9

Single guide RNAs (sgRNAs: CGGTGTCCTCCTGAAATCAT and CCTGAAATCATGCCACCCGC) targeting the second coding exon of zebrafish Trpv5/6 (ENSDART00000127453.3) was designed and synthesized as previously described (Zhang et al., 2019). The Cas9 protein was purchased from NEB (Ipswich, MA). Mixture of sgRNA and Cas9 was injected into one-cell stage zebrafish embryos (sgRNA 150 pg/embryo and Cas9 300 ng/embryo). The effect of injected CRISPR-Cas9 was confirmed by sequencing (Sangon, Shanghai, China) and quantitative PCR (Q-PCR) using SYBR qPCR master mix (Vazyme, Nanjing, China).

Total RNA was extracted using Trizol reagent (Invitrogen, Carlsbad, CA) according to the manufacturer's instructions and extracted with RNeasy Min Elute Clean up kit (Tiangen, Beijing, China). Reverse transcription reaction was performed using 1 μg of total RNA with cDNA synthesis kit (Vazyme). The mRNA expression level was determined by Q-PCR and Q-PCR Detection System (Applied Biosystems, Foster City,

CA). Primers used were as below: Trpv5/6-F: CCATCCTGCACCTGTTGGTTTT, Trpv5/6-R: CATCCCTTGCAGCGAGTTTGAA. β-actin-F: 5'-CTCCCCTTGTTCACAATAACCTACTAATACACAGC; β-actin-R: TTCTGTCCCATGCCAACCATCACTC. Gene expression was normalized to β-actin. Genomic DNA was isolated from an individual 2 dpf embryo, as previously described (Zhang et al., 2019). Genotyping was performed by PCR amplification of the region of interest using the primers Trpv5/6-F: CCCTTTAACCTATTGGGTTTTACAG, Trpv5/6-R: CATATTCAATCTAATAAGAACAATCAATGC. Mutations were confirmed by sequencing.

Staining protocol was performed as previously reported (Vanoevelen et al., 2011; Walker and Kimmel, 2007). Briefly, zebrafish embryos at 7 dpf were fixed in 4% formaldehyde (Sigma) with shaking at room temperature for 2 hr. Embryos were then dehydrated in 50% ethanol and stained with Alcian blue 8GX (Sigma) in 70% ethanol with 80 mM $MgCl_2$. After bleaching using 1% H_2O_2 and 1% KOH, embryos were washed in sodium tetraborate solution and digested with trypsin for 1 hr. Embryos were then stained using Alizarin red S (Sigma) in 1% KOH and stored in 70% glycerol at 4℃. Pictures were taken using Nikon SMZ18 (Tokyo, Japan). The notochord tip area was selected and the corresponding intensity quantified using ImageJ. Zebrafish experiments were carried out in compliance with the protocol specifically approved for the use of laboratory animals of the Hubei University of Technology.

Statistical analysis

All statistical data in this study are expressed as mean ± SEM (standard error of the mean) from N measurements. Statistical significance was determined by two-sided paired or unpaired Student's t-test. *, ** and *** indicate $p < 0.05$, 0.01 and 0.001, respectively; ns indicates statistically not significant.

3.4 RESULTS

Functionally critical residues in the S4-S5 linker and TRP helix of TRPV6

Pathogenic mutations have been found in the S4-S5 linker of several TRP channels such as TRPV4, -A1, -M4 and -ML1 (Dai et al., 2010; Goldin et al., 2004; Kremeyer et al., 2010; Stallmeyer et al., 2012). However, the mechanism of how the linker exercises its functional importance is largely unclear. Based on the proximity of the TRPV6 S4-S5 linker to the C-terminal TRP helix (McGoldrick et al., 2018) we examined the functional relevance of the residues that may be involved in the physical arrangement. For this we first substituted all aromatic and charged residues with alanine in this region of human TRPV6 and examined the channel function of the resulting mutants using the two-electrode voltage clamp in *Xenopus* oocytes in extracellular solutions containing 1 mM niflumic acid (NFA) to block the endogenous Ca^{2+}-activated Cl channels (Huang et al., 2012; Peng et al., 1999; Wang et al., 2019), similarly as we recently did for TRPP2 with or without co-expression of PKD1 in oocytes (Wang et al., 2019). Under this condition, steady-state currents elicited by extracellular Ca^{2+} (5 mM) relative to the solution containing impermeable N-methyl D-glucamine (NMDG) served as a TRPV6 function readout. We found that each of the mutations R470A and F478A in the S4-S5 linker (Fig. 3-S1A) substantially increases Ca^{2+}-induced steady-state currents without affecting the plasma membrane expression in expressing oocytes (Fig. 3-1A, B and S1B).

Because fragment 593-WRAQI-597 within the TRP helix is located proximal to the S4-S5 linker under cryo-EM conditions (Fig. 3-S1C), we tested the function of TRPV6 mutants W593A and R594A and found that mutant W593A, but not R594A, exhibits substantially activated channel function compared with WT TRPV6 given the unaffected surface membrane expression by these mutations (Fig. 3-1A and B). We further generated R470F, W593F and W593Y mutants and found that they have similar or reduced function compared with WT channel (Fig. 3-S1D and E), which presumably means the presence of an interaction between sites 470 (or 478) and 593, possibly of a π-π or π-cation interaction. Consistently, Na^+ currents, serving as another function readout of TRPV6, mediated by mutants R470A and W593A increased 4.3 and 3.5 folds (Fig. 3-S2). In summary, we found that residues R470 and F478 in the linker and W593 in the TRP helix are required to maintain TRPV6 channel at its basal function (i.e., prevent it from activation), suggesting their involvement in the linker/TRP helix association.

Interaction between the S4-S5 linker and TRP helix

We next examined the S4-S5 linker to TRP helix (referred to as L/C) interaction by co-IP assays using the linker-containing peptide LP (amino-acid (aa) V465-F493) and full-length (FL) TRPV6 co-expressed in oocytes. We found that LP indeed associates with TRPV6 and that the association is substantially reduced in the presence of the R470A mutation in LP or the W593A mutation in TRPV6 (Fig. 3-1C) but remains

unaffected by the F478A mutation in LP (Fig. 3-S3). These data indicate that R470 and W593 mediate the LP/TRPV6 interaction, presumably through forming a R470:W593 cation-π bond. We also documented the L/C interaction by examining colocalization of LP or C-terminal TRP helix-containing peptide CP (aa W583-V602) with FL TRPV6 using co-IF with whole oocytes. FL TRPV6, but not peptide LP or CP, was localized on the surface membrane of oocytes when expressed alone, as expected (Fig. 3-1D). Both LP and CP were localized on the surface membrane when co-expressed with WT TRPV6. LP failed to be on the surface membrane when it contains mutation R470A or when there is mutation W593A in TRPV6, but mutation F478A in LP had no effect, suggesting that TRPV6 retains LP to the surface membrane through their binding mediated by the R470:W593 pair. Interestingly, each of mutations W593A in CP and R470A in TRPV6, which is assumed to disrupt the L/C interaction, failed to affect the surface membrane targeting of CP (Fig. 3-1D, last two columns), suggesting the possibility that CP can bind with TRPV6 through another site, which will be examined in the next section.

We further documented the L/C interaction by in vitro pull-down experiments using purified (from *E. coli*) glutathione S-transferase (GST)-tagged LP and His-tagged C-terminal peptide CP1 (aa M578-L677) that contains the TRP helix, to further characterize the interaction. We found that the two peptides directly bind with each other and that the binding is significantly reduced by the R470A mutation in LP or the W593A mutation in CP1 (Fig. 3-1E). Our data together suggested that the S4-S5 linker directly

binds with the TRP helix possibly through the R470:W593 pair, which is required to maintain TRPV6 channel function at its basal levels and prevent channel activation (Fig. 3-1A and B).

We next utilized a blocking peptide strategy to further document the functional importance of the R470:W593-mediated L/C interaction. For this we co-expressed LP or CP with FL TRPV6 in oocytes and reasoned that over-expressed LP or CP would disrupt the intramolecular L/C binding within the TRPV6 protein and thus activate TRPV6. Indeed, LP and CP significantly increased TRPV6 channel function (Fig. 3-1F) without affecting its surface expression (Fig. 3-S4). Mutant peptide LP-R470A did not stimulate TRPV6 function (Fig. 3-1F) as expected because of lack of physical binding between them (Fig. 3-1C and E), whereas CP-W593A continued to activate TRPV6 channel (Fig. 3-1F), which is consistent with its co-localization with TRPV6 (Fig. 3-1D). It is noted that a blocking peptide may induce functionally important structural changes in addition to disrupting the L/C binding, which requires further investigations. Also, there might be other residues in the S4-S5 linker and TRP helix that are involved in the L/C interaction but they do not seem to be as essential as the R470-W593 pair of which the involvement has been verified by several pieces of data. In summary, our data using the blocking peptide strategy further supported the autoinhibitory role of R470:W593-mediated intramolecular L/C interaction in TRPV6.

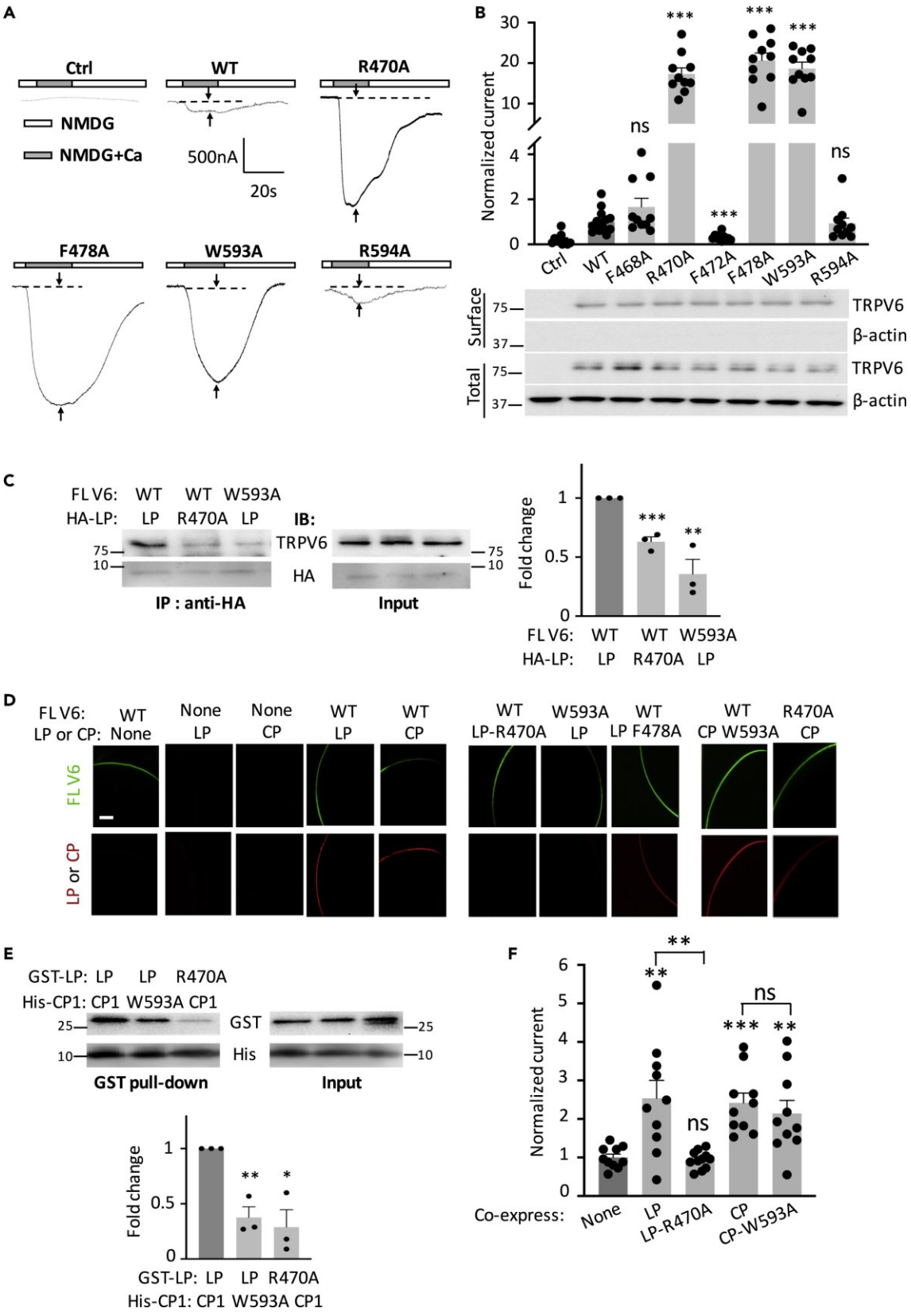
A
Ctrl
WT
R470A
NMDG
NMDG+Ca
500nA
20s
F478A
W593A
R594A
B
Normalized current
Ctrl
WT
F468A
R470A
F472A
F478A
W593A
R594A
ns
***
Surface
Total
TRPV6
β-actin
75
37
C
FLV6: WT WT W593A
HA-LP: LP R470A LP
IB:
TRPV6
HA
IP : anti-HA
Input
Fold change
D
FLV6:
LP or CP:
None
WT
LP
CP
LP-R470A
W593A
F478A
R470A
FLV6
LP or CP
E
GST-LP: LP LP R470A
His-CP1: CP1 W593A CP1
GST
His
GST pull-down
Input
F
Co-express:
None
LP
LP-R470A
CP
CP-W593A

Fig. 3-1. Roles of residues in the TRPV6 S4-S5 linker and TRP helix in the channel function, L/C interaction and L/C co-localization. (**A**) Representative whole-cell current traces obtained from *Xenopus* oocytes expressing human TRPV6 or a mutant (as indicated), measured by two-electrode voltage clamp. Oocytes were clamped at -50 mV and perfused with a NMDG-containing solution (100 mM NMDG, 2 mM KCl, 0.2 mM $MgCl_2$, 10 mM HEPES at pH 7.5) with (NMDG+Ca) or without (NMDG) 5 mM $CaCl_2$, in with the presence of 1 mM NFA throughout. Ca^{2+}-induced currents were measured as a time point indicated by arrows. Ctrl, water injected oocytes. (**B**) *Upper panel*: normalized Ca^{2+}-activated currents obtained as in panel A. Data were averaged from N = 10-14 oocytes from three batches. ***$p < 0.001$ and ns (not significant) in comparison with WT, by Student's t-test. Currents were normalized to the mean current for WT TRPV6. Statistical significance was examined using Student's t-test. *Lower panel*: representative surface and total expression of WT and mutant TRPV6 by biotinylation, with β-actin as loading controls. Protein markers (in kDa) were labeled. (**C**) *Left panel*: representative co-IP data from FL TRPV6 and HA-tagged TRPV6 LP with or without an indicated mutation. *Right panel*: data from three independent co-IP experiments were quantified, normalized and averaged. **$p < 0.01$, compared with dark grey group. (**D**) Representative images showing co-localization of LP or CP with FL TRPV6 by co-IF using oocytes expressing FL TRPV6 or a peptide, with or without a mutation. *Scale bar*, 50 μm. (**E**) *Upper panel*: representative data from a His pull-down assay showing binding between (*E. coli*) purified GST-tagged human TRPV6 S4-S5 linker peptide (GST-LP) and His-CP1 with or without an indicated mutation. *Lower panel*: data from three independent *in vitro* binding experiments were quantified, normalized and averaged. *$p < 0.05$, compared with dark grey group. (**F**) Representative Ca^{2+}-induced currents in oocytes expressing FL TRPV6 with or without indicated peptide. Data were normalized and averaged from 10-11 oocytes from three batches.

Interaction between the pre-S1 and TRP helices

Given the proximity between W321 and I597 in the intracellular pre-S1 and TRP helices, respectively, revealed by TRPV6 structures (Fig. 3-S1C) (McGoldrick et al., 2018; Saotome et al., 2016), we first tested the functional roles of W321 and I597 and found that mutants W321A and I597A both exhibit substantial channel activation (Fig. 3-2A-C).

In agreement with Ca^{2+} activation, we determined the Na^{+} currents of these two mutants (Fig. 3-S2). Both mutants showed a significantly larger Na^{+} current (3.0-4.0 folds) compared with WT. Further, we also employed human embryonic kidney (HEK) cells in combination with Fura-2 Ca^{2+} fluorimetry as a readout of the Ca^{2+} influx to examine the functional importance of residues W321 and W593. We found that expression of mutant W321A or W593A results in significantly increased intracellular Ca^{2+} levels, with or without extracellular Ca^{2+}, compared with WT TRPV6 (Fig. 3-2D-F), indicating that both are activated mutants, in agreement with our data using oocytes. The increased basal intracellular Ca^{2+} levels in cells expressing mutant W321A or W593A should presumably due, at least in significant part, to Ca^{2+} entry during incubation with Ca^{2+}-containing culture medium. Interestingly, we additionally found that expression of W321A or W593A mutant significantly induces more death both in oocytes and HEK293 cells (Fig. 3-S5), similar to a previous study on the TRPV5 gate hinge mutant (van der Wijst et al., 2017), indicative of gain-of-function nature of these mutants.

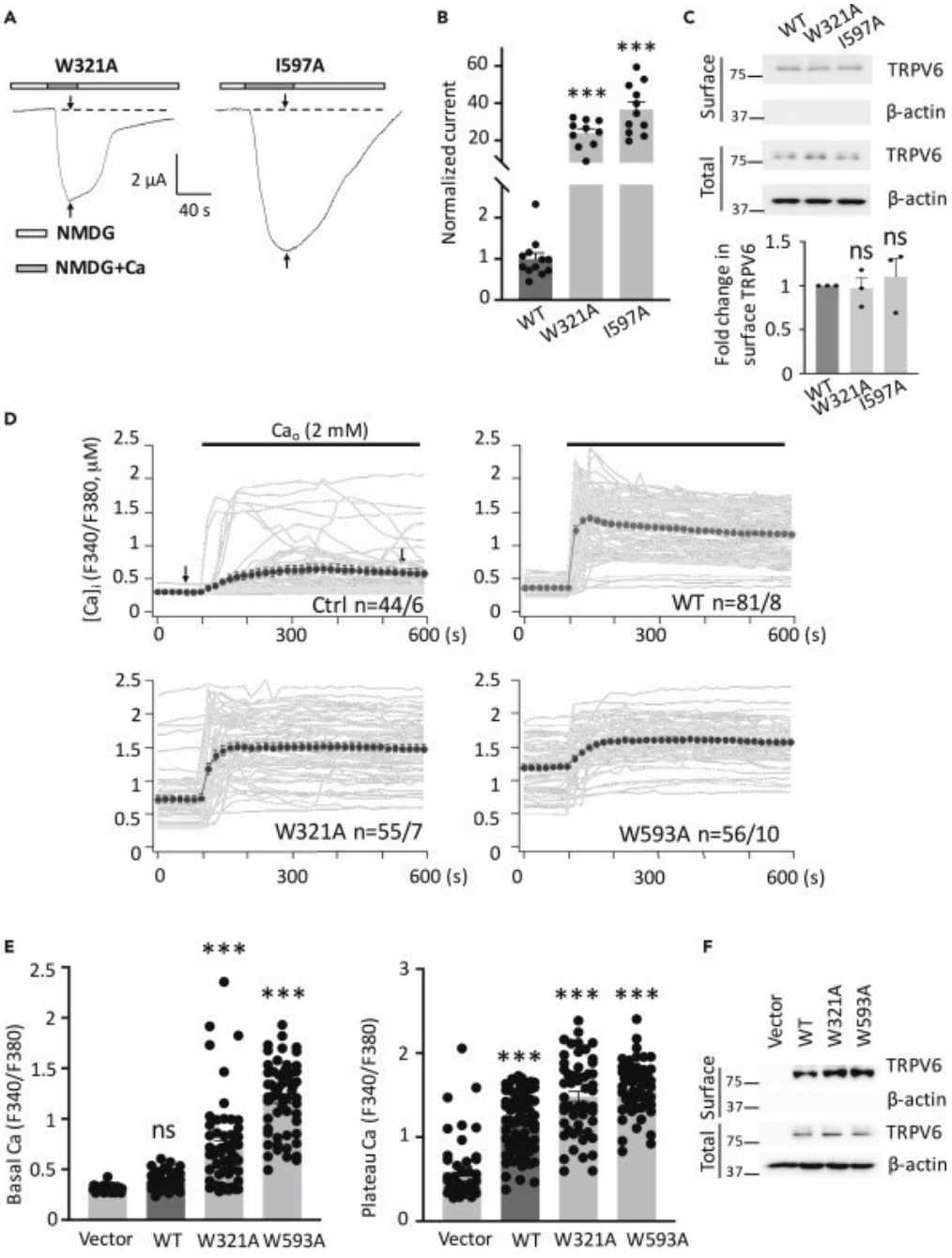

Fig. 3-2. Characterization of functional critical residues in the pre-S1 and TRP helices of TRPV6 in oocytes and HEK293 cells. (**A**) Representative Ca^{2+}-induced current traces recorded in oocytes expressing a mutant TRPV6, as indicated. (**B**) Normalized Ca^{2+}-activated currents obtained at -50 mV from WT or an indicated mutant TRPV6. Data were averaged from 10-12 oocytes from three batches. (**C**) *Upper panel*: representative data showing the surface and total expression of TRPV6 and mutants measured by

biotinylation and WB. *Lower panel*: data from three independent experiments were quantified, normalized and averaged. ns, not significant compared with WT. (**D**) Time dependence (0-600 s) of the intracellular Ca^{2+} concentration ($[Ca]_i$) traces in HEK293 cells expressing human WT or a mutant TRPV6 determined as the F340/F380 ratio by Fura-2 ratiometric Ca^{2+} imaging, before and after application of 2 mM extracellular Ca^{2+} (Ca_o). Averaged traces were obtained from 44-81 cells from 6-10 batches, as indicated. (**E**) Averages of basal Ca^{2+} levels determined from panel D at a time point between 1-100 s (indicated by an arrow) before Ca^{2+} application. Averages of steady-state Ca^{2+} levels determined at a time point between 500-600 s (indicated by an arrow) in the presence of Ca^{2+}. (**F**) Representative WB data showing surface and total expression of WT and mutant TRPV6 in HEK cells.

These data suggest the possibility that the W321:I597 pair forms a bond, plausibly by a van der Waals force, to mediate physical interaction between pre-S1 and TRP helix (referred to as N/C interaction) that is required to prevent TRPV6 channel activation. We reasoned that disrupting and re-establishing the bonding at 321:597 should result in activation and 'rescue' of function, respectively. For this we tested mutants W321I (no bonding by the I:I pair), I597W (W:W bonding) and double mutant W321I-I597W (rescued I:W bonding, vs W:I bonding in WT TRPV6) and indeed found that W321I is an activated mutant while the other two have comparable channel function than WT TRPV6 (Fig. 3-3A and B). The function 'rescue' of mutant W321I-I597W possessing the I:W bonding strongly supported the concept that the W321 directly interacts with I597 rather than indirectly affecting the bonding formed by another pair of residues in pre-S1 and TRP helices. To provide further documentations, we mutated W321 or I597 to anionic glutamic acid to break down the hypothetical bond within the pair and indeed found that

both mutants W321E (E:I) and I597E (W:E) exhibit substantial channel activation (Fig. 3-3C and D). Further, introduction of a cationic residue R to the other side of the pair in these two mutants, which generated double mutants W321E-I597R (E:R) and W321R-I597E (R:E), significantly rescued the channel function to its basal levels (Fig. 3-3C and D), possibly through forming a salt bridge. These data together strongly supported the possibility that the W321:I597 pair mediates the N/C binding that is autoinhibitory for TRPV6.

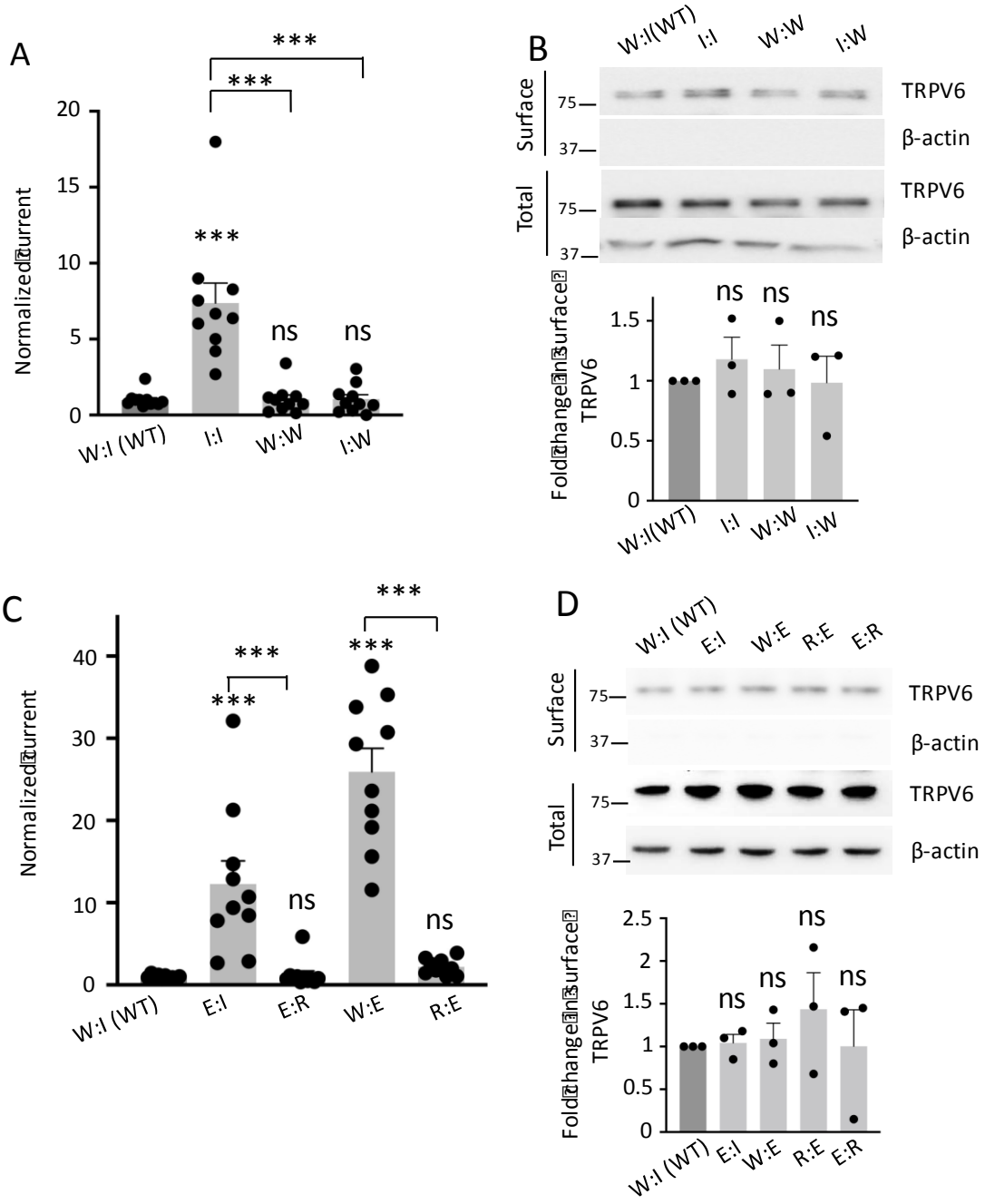

Fig. 3-3. Functional rescues by mutations at the W321:I597 pair. (**A**) Normalized Ca^{2+}-activated currents at -50 mV showing functional rescues by the WI: to I:W mutation (W321I-I597W). Data were averaged from 9-11 oocytes from three batches. (**B**) *Upper panel*: representative data from a biotinylation assay showing the surface and total expression of TRPV6 proteins in panel A. *Lower panel*: data from three

independent experiments were quantified, normalized and averaged. ns, not significant compared with WT. (**C**) Normalized Ca^{2+}-activated currents obtained from TRPV6-expressing oocytes. Data were averaged from three batches of oocytes (N = 10-11). (**D**) *Upper panel*: representative biotinylation data on TRPV6 mutants in panel C. *Lower panel*: data from three independent experiments were quantified, normalized and averaged.

We next investigated the N/C interaction by co-IP assays and found that TRPV6 N-terminal peptide NP (aa T298-P327) containing the pre-S1 helix and FL TRPV6 are in the same complex in oocytes and that the complex is disassembled by the W321A mutation in NP or the I597A mutation in TRPV6 (Fig. 3-4A), which supports the involvement of the W321:I597 pair in the interaction. By in vitro pull-down assays using purified TRPV6 N-terminal peptide NP1 (aa H228-P327) and C-terminal peptide CP1 that contains pre-S1 and TRP helix, respectively, we found that NP1 directly associates with CP1 and that the association is disrupted in the presence of mutation W321A in NP1 or I597A in CP1 (Fig. 3-4B), supporting that W321:I597 mediates direct binding between NP1 and CP1. We also used NP to precipitate the TRPV6 N-terminal truncation mutant (TRPV6-ΔN, aa Y328-I725) that lacks the N/C binding within the molecule, to further document the relationship between the N/C binding strength and channel function and found that the N/C binding strength inversely correlates with the channel activity (Fig. 3-4C and D).

We also investigated the N/C interaction by co-IF experiments using whole oocytes. Peptide NP was co-localized on the surface membrane with WT TRPV6 and this

co-localization was disrupted by mutation W321A in NP or I597A in TRPV6 (Fig. 3-4E). These data strongly supported that the W321:I597-mediated NP/TRPV6 interaction retains NP on the surface membrane. We noticed that mutation W321A in TRPV6 or I597A in CP, which presumably disrupts the TRPV6/CP, fails to dissociate CP from the surface membrane (Fig. 3-4E and 1D), probably because CP can still bind to the S4-S5 linker within TRPV6. Indeed, double mutation W593A-I597A in CP was then sufficient to bring CP down from the surface membrane. These data together thus nicely supported that the autoinhibitory N/C interaction is mediated by the W321:I597 pair.

We further documented the N/C interaction and its functional roles using our blocking peptide strategy. Similar to LP and CP, expression of NP significantly stimulated the TRPV6 channel activity without altering the surface membrane targeting (Fig. 3-4F and S4), consistent with the assumption that NP acts as a blocking peptide that weakens the intramolecular L/C binding within the TRPV6 molecule. While the W321A mutation in NP abolished its stimulating effect, only double mutation I597A-W593A in CP, but not each of the single mutations, abolished its stimulating effect (Fig. 3-1F and 4F). This is presumably because when CP only carries single mutation I597A (or W593A), it can still competitively reduce the TRPV6 intramolecular L/C (or N/C) binding to activate TRPV6 whereas when CP carries the double mutation, it can no longer bind with TRPV6 (and thus no longer has functional effect). Therefore, these data together strongly supported

that each of the N/C and L/C interactions is functionally autoinhibitory and that disruption of either interaction leads to channel activation.

We next wanted to examine whether the TRPV6 intramolecular L/C and N/C interactions are independent of each other. Because NP precipitated more mutant TRPV6-W321A than WT channel (Fig. 3-S6), likely due to the absence of the N/C interaction within the TRPV6-W321A protein, we next utilized TRPV6-W321A for assessing the NP/TRPV6 interaction. By co-IP assays we found that either mutation R470A or W593A, which removes the intramolecular L/C interaction within TRPV6-W321A, almost abolishes the NP/TRPV6 (N/C) interaction (Fig. 3-4G), indicating that the L/C interaction is required for the maintenance of the N/C interaction. Similarly, we utilized TRPV6-R470A for the assessment of the LP/TRPV6 interaction. In contrast, none of the W321A and I597A mutations, which disrupts the N/C interaction within TRPV6-R470A, affected the LP/TRPV6 (L/C) interaction (Fig. 3-4H), indicating that the N/C interaction is not required for the L/C interaction. Thus, it seems that the N/C interaction is downstream of the L/C interaction in a regulatory relay in TRPV6.

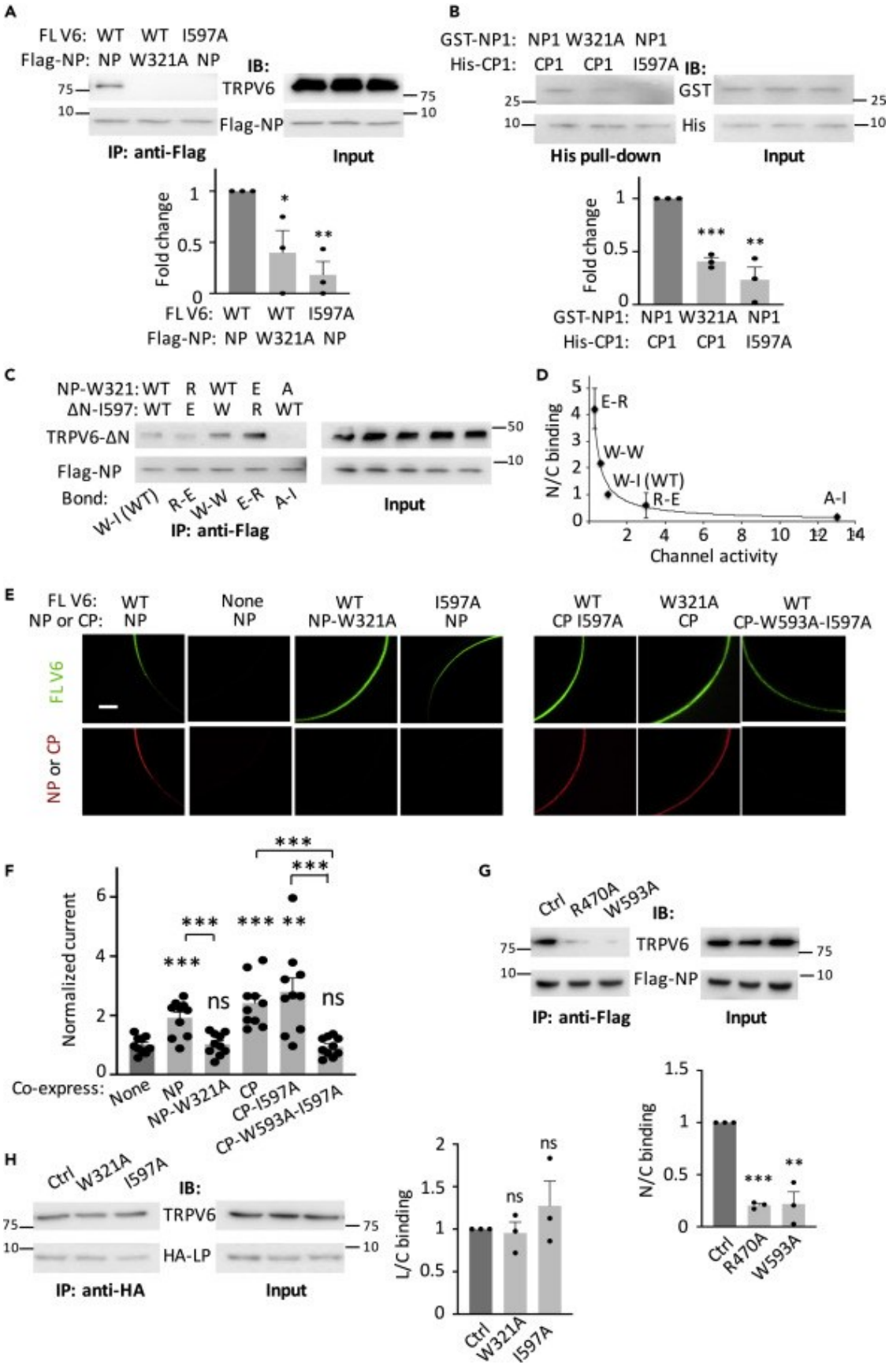
A
FLV6: WT WT I597A
Flag-NP: NP W321A NP
IB:
TRPV6
Flag-NP
IP: anti-Flag
Input
Fold change
FLV6: WT WT I597A
Flag-NP: NP W321A NP
B
GST-NP1: NP1 W321A NP1
His-CP1: CP1 CP1 I597A
IB:
GST
His
His pull-down
Input
Fold change
GST-NP1: NP1 W321A NP1
His-CP1: CP1 CP1 I597A
C
NP-W321: WT R WT E A
ΔN-I597: WT E W R WT
TRPV6-ΔN
Flag-NP
Bond: W-I (WT) R-E W-W E-R A-I
IP: anti-Flag
Input
D
N/C binding
E-R
W-W
W-I (WT)
R-E
A-I
Channel activity
E
FLV6: WT None WT I597A WT W321A WT
NP or CP: NP NP NP-W321A NP CP I597A CP CP-W593A-I597A
FLV6
NP or CP
F
Normalized current
Co-express: None NP NP-W321A CP CP-I597A CP-W593A-I597A
ns
G
Ctrl R470A W593A
IB:
TRPV6
Flag-NP
IP: anti-Flag
Input
N/C binding
H
Ctrl W321A I597A
IB:
TRPV6
HA-LP
IP: anti-HA
Input
L/C binding

Fig. 3-4. Roles of the W321:I597 pair in the N/C interaction, colocalization and channel function of TRPV6 and dependence between the N/C and L/C interaction. (**A**) *Upper panel*: representative co-IP data from oocytes co-expressing full length (FL) TRPV6 and Flag-tagged TRPV6 NP with or without a mutation, as indicated. *Lower panel*: data from three independent co-IP experiments were quantified, normalized and averaged. By Student's t-test, comparison with dark grey group. (**B**) *Upper panel*: representative data from His pull-down showing binding between purified GST-tagged human TRPV6 N-terminal peptide (GST-NP1) and His-tagged human TRPV6 C-terminal peptide (His-CP1), with or without an indicated mutation. *Lower panel*: data from three independent *in vitro* binding experiments were quantified, normalized and averaged. (**C**) Representative co-IP data obtained using Flag-NP to precipitate TRPV6-ΔN, carrying an indicated mutation at 321 and 597, respectively. (**D**) Inverse correlation between normalized binding strength (y) and normalized Ca^{2+}-induced steady-state current (x). Data from three independent experiments as in the panel C were quantified, normalized and averaged. Curve represents the best fit using the inverse function y = a/x, with a = 1.06 and correlation coefficient R = 0.97. (**E**) Representative co-IF images from oocytes expressing FL TRPV6 or a peptide, with or without mutation. *Scale bar*, 50 μm. (**F**) Representative Ca^{2+}-induced currents at -50 mV from oocytes expressing FL TRPV6 with or without indicated peptide. Data were normalized and averaged from 10-11 oocytes from three batches. **p < 0.01 and ***p < 0.001, by Student's t-test. (**G**) *Upper panel*: representative co-IP data accessing the N/C interaction obtained using oocytes expressing Flag-tagged NP and FL TRPV6-W321A (Ctrl) carrying mutation R470A or W593A, as indicated. *Lower panel*: data from three independent experiments as in the upper panel were quantified, normalized and averaged. (**H**) *Left panel*: representative co-IP data assessing the L/C interaction obtained from oocytes expressing HA-LP and FL TRPV6-R470A (Ctrl) carrying mutation W321A or I597A, as indicated. *Right panel*: data from three independent experiments as in the left panel were quantified, normalized and averaged.

Rescue of Trpv5/6 knockdown-derived defects in zebrafish by TRPV6 activated mutant

We next examined potential rescue effect of human TRPV6 activated mutant W593A in vivo in zebrafish. A zebrafish homologue Trpv5/6 loss-of-function mutant R304X was

previously found to result in loss of notochord tip ossification, a defective bone formation (Vanoevelen et al., 2011). We mimicked this condition through knocking down Trpv5/6 using CRISPR-Cas9 technique and confirmed by sequencing (Fig. 3-5A). A significant 77% reduction in Trpv5/6 mRNA expression was found in CRISPR-Cas9 injected embryos (Fig. 3-5B). Using Alizarin red S staining we found that larval fish at 7 days post-fertilization (dpf) with Trpv5/6 knockdown exhibits much increased likelihood of developing loss of ossification at the notochord tip (Fig. 3-5B). We then examined the effect of human TRPV6 activated mutant W593A on fish bone formation through mRNA co-injection into embryos. While 10 pg W593A mutant mRNA significantly rescued the bone abnormality 10 and 30 pg WT TRPV6 mRNA had no rescuing effect, respectively (Fig. 3-5C), indicating that mutant W593A acts as an activated (or gain-of-function) mutant in vivo in zebrafish.

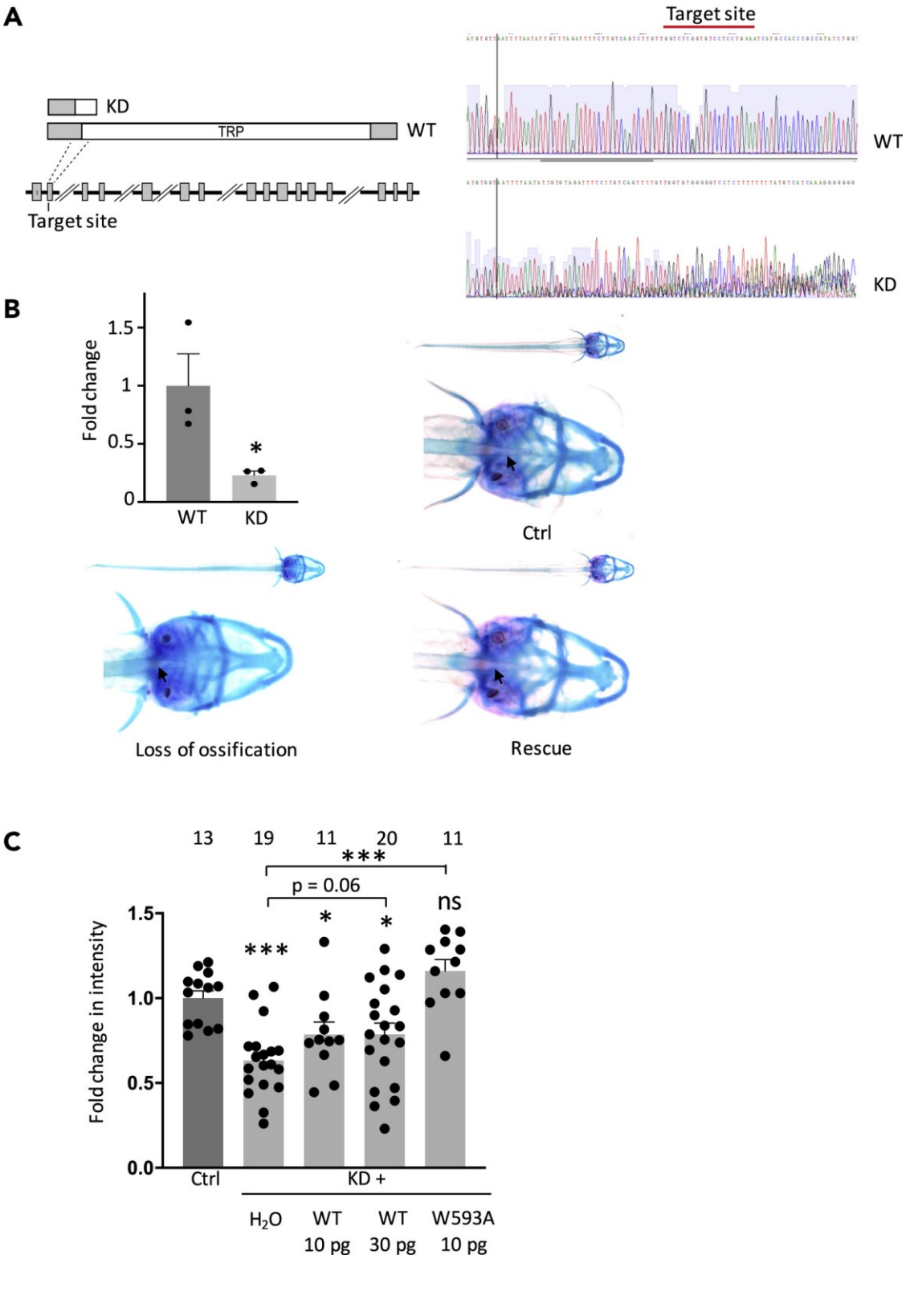

Fig. 3-5. Rescue effect of TRPV6 activated mutant W593A on Trpv5/6 knockdown-induced bone

abnormality in zebrafish. (**A**) *Left panel*: schematic representation of the Trpv5/6 gene/protein domain architecture and CRISPR target site. The gene loci are shown with coding exons (grey boxes) and introns (solid black lines), with large introns not drawn to scale. The position of the CRISPR target site sequences at the beginning of exon 2 in Trpv5/6 is indicated and the predicted truncated proteins in the mutant lines are drawn above. *Right panel*: sequencing of WT and Trpv5/6 mutant fish at 3 dpf. Red lines indicate CRISPR target sites. (**B**) *Upper left panel*: Trpv5/6 mRNA was detected by Q-PCR. The total RNA isolated from 5 dpf WT or Trpv5/6 mutant embryos (>10 embryos/sample) from three batches. Representative images of 7 dpf zebrafish embryos with cartilage (red) and bone (blue) staining. The notochord tip is indicated by an arrow. "Loss of ossification" was from an embryo injected with Trpv5/6 sgRNA and water while "rescue" was from an embryo co-injected with sgRNA and 10 pg of human TRPV6 W593A mutant mRNA. Ctrl, from a WT embryo. (**C**) Fold change in the intensity in zebrafish notochord tip from indicated groups. Data were averaged from 11-18 embryos from three independent experiments. Ctrl, control zebrafish; KD, CRISPR-Cas9 injected Trpv5/6 knockdown zebrafish.

Characterization of the PIP2/TRPV6 binding

PIP2 was previously reported to up-regulate, and is required for, TRPV6 channel function (Thyagarajan et al., 2008; Zakharian et al., 2011). However, the mechanism of regulation and the PIP2 binding sites in TRPV6 are not well understood (Hughes et al., 2018). We examined the PIP2/TRPV6 binding by lipid dot blot assays using lysates of TRPV6-expressing oocytes, *E. coli* purified GST-NP1 and His-CP1, and PIP2 antibody for detection. We found that water-soluble PIP2 analogue diC8-PIP2 binds to TRPV6 and CP1 but not NP1 (Fig. 3-6A). Because PIP2 was known to bind with cationic residues in other TRP channels (Nilius et al., 2008), we neutralized all cationic residues in the S2-S3 linker, inner S5 helix and CP1 by glutamine substitution to test their involvement in PIP2 binding. We found that K484Q, R589Q and R632Q, but not the other mutations, decrease

the channel activity compared to WT TRPV6 (Fig. 3-6B, S7 and S8). We and other groups have previously employed PIP2 monoclonal antibodies to precipitate TRP and other channels (Hamilton et al., 2014; Huang et al., 1998; Huang et al., 2013; Zheng et al., 2018a). By a similar approach we found that each of the K484Q, R589Q and R632Q mutations but not the R628Q mutation (Ctrl) abolishes the PIP2/TRPV6 interaction (Fig. 3-6C), consistent with the functional data (Fig. 3-6B). We also found that the W321A or W593A mutation has no effect on the PIP2/TRPV6 binding (Fig. 3-S9), which further indicates that the two residues are not part of the PIP2 binding pocket. Further, we found that diC8-PIP2, injected into oocytes by a third electrode, increases Ca^{2+}-induced steady-state currents by nearly 13 folds in oocytes expressing WT TRPV6 but only by 2.3-4.2 folds in those expressing one of the three mutants (Fig. 3-6D). Consistently, we found that these three mutants are more sensitive to PIP2 depletion by wortmannin than WT channel and that neutralization of all the three residues abolishes the channel function (Fig. 3-6E and F). While according to the structural data, R632 locates in distal C-terminus being away from inner cell membrane and may not directly bind to PIP2. These data together showed that K484, R589 and R632 may be involved in PIP2 binding.

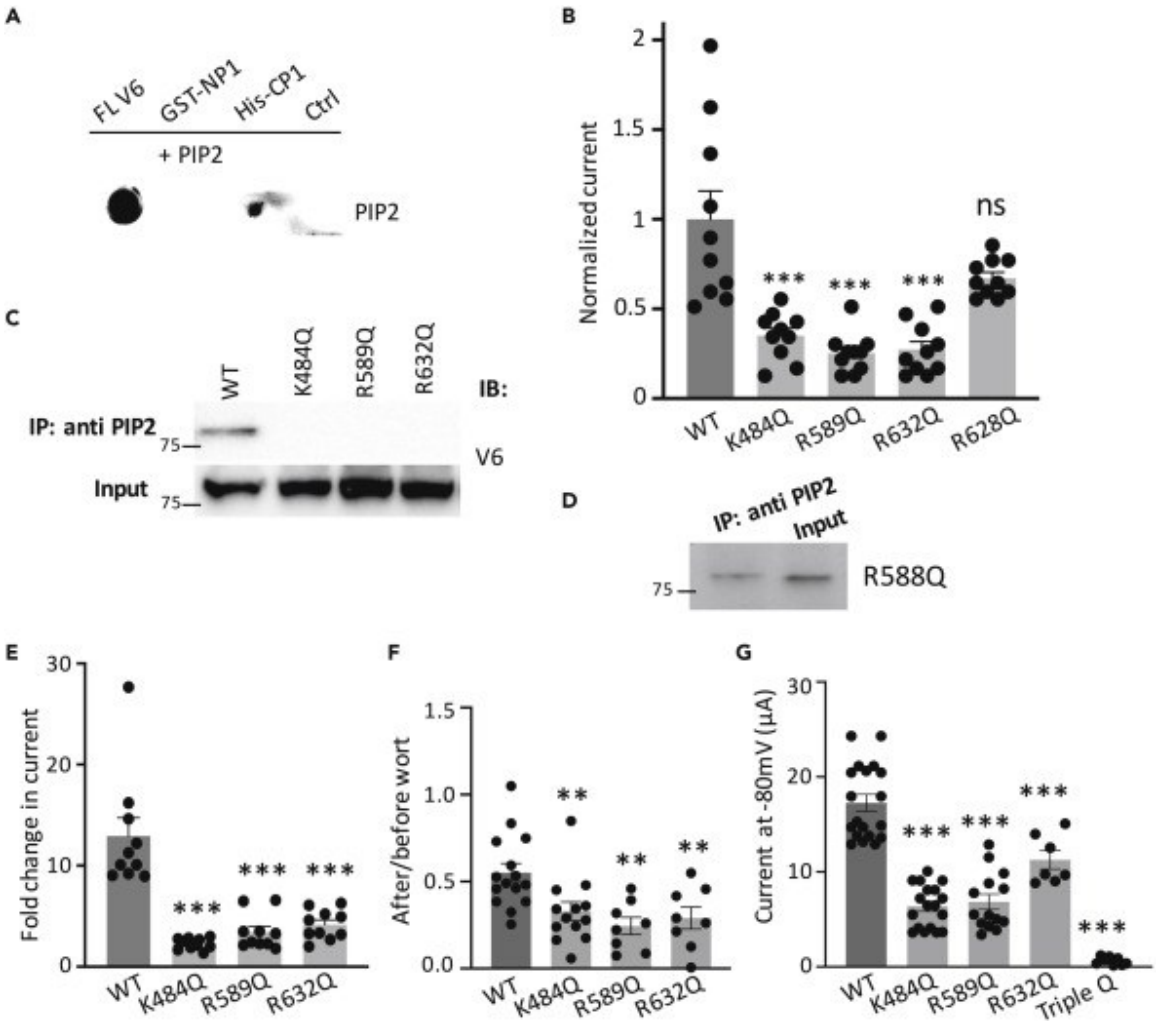

Fig. 3-6. Characterization of the physical and functional PIP2/TRPV6 interaction. (**A**) Representative dot-blot data obtained using diC_8-PIP2 with lysates of oocytes expressing FL TRPV6, GST-NP1, His-CP1 or None (Ctrl). (**B**) Normalized Ca^{2+}-induced currents obtained at -50 mV from oocytes expressing WT or a mutant TRPV6. Residues R409 and R414 are in the S2-S3 linker, K484 in the inner S5 helix and the others within CP1. Data were normalized and averaged from 10 oocytes from three batches. (**C**) Representative co-IP data obtained from expressing oocytes showing the effect of mutations on the PIP2/TRPV6 interaction. (**D**) Representative co-IP data obtained using oocytes showing the interaction between PIP2 and TRPV6 mutant R628Q. (**E**) Effects of mutations on the activation of TRPV6 by diC_8-PIP2, assessed by Ca^{2+}-activated currents obtained from expressing oocytes. Fold change was calculated before and 10 min after injection of 25 nl of diC_8-PIP2 (5 mM) by a third electrode (see Methods), for an estimated final

intracellular diC_8-PIP2 concentration of 0.25 mM. Injection of 25 nl of water was carried out as control and had no significant effect on the channel activity. Shown data were averaged from N = 10 oocytes from three batches. (**F**) Ratios of monovalent currents from oocytes expressing WT or an indicated mutant after and before wortmannin treatment. (**G**) Bar graphs of monovalent currents from oocytes expressing WT or indicated mutants.

Modulation of TRPV6 intramolecular interactions by PIP2

Although the L/C and N/C interaction sites are not part of the PIP2 binding site, we wondered whether the PIP2 regulates TRPV6 channel function through altering the L/C or N/C interaction indirectly. We found by co-IP assays that addition of diC8-PIP2, but not lipid phosphatidic acid (as control), into lysates of oocytes co-expressing TRPV6 and LP (or NP) reduces (or abolishes) the LP/TRPV6 (or NP/TRPV6) interaction (Fig. 3-7A and B). In contrast, diC8-PIP2 did not alter either interaction in the presence of triple mutation K484Q/R589Q/R632Q (referred to as TRPV6-3Q) or even single mutation K484Q and R589Q (Fig. 3-7C, D and S10). These data indicated that PIP2 disrupts the two autoinhibitory L/C and N/C interactions through binding to TRPV6 protein thereby activating the channel. We also examined whether any of the four activated mutants R470A, W593A, W321A and I597A that correspond to the four residues mediating the L/C or N/C interaction has altered sensitivity to PIP2 regulation. We utilized membrane permeable wortmannin, a PI4K inhibitor, to block PIP2 synthesis thereby depleting the endogenous PIP2 (Downing et al., 1996). Distinct from WT TRPV6, none of the four mutants was inhibitable by wortmannin (Fig. 3-7E), consistent with the conclusion that

PIP2 activates TRPV6 through disrupting the L/C or N/C interaction. As expected, when both interactions were disrupted by alanine substitution, the resulting activated double mutant W321A-W593A is no longer inactivated by PIP2 depletion (Fig. 3-7E). However, we should keep in mind that the functional change in the double mutation might also be due to other structural changes that affect interaction with PIP2.

Taken together, our study suggested that PIP2 binds to cationic residues in the inner S5 helix and C-terminus of TRPV6, which disrupts the R470:W593-mediated L/C and W321:I597-mediated N/C interactions thereby activating the channel.

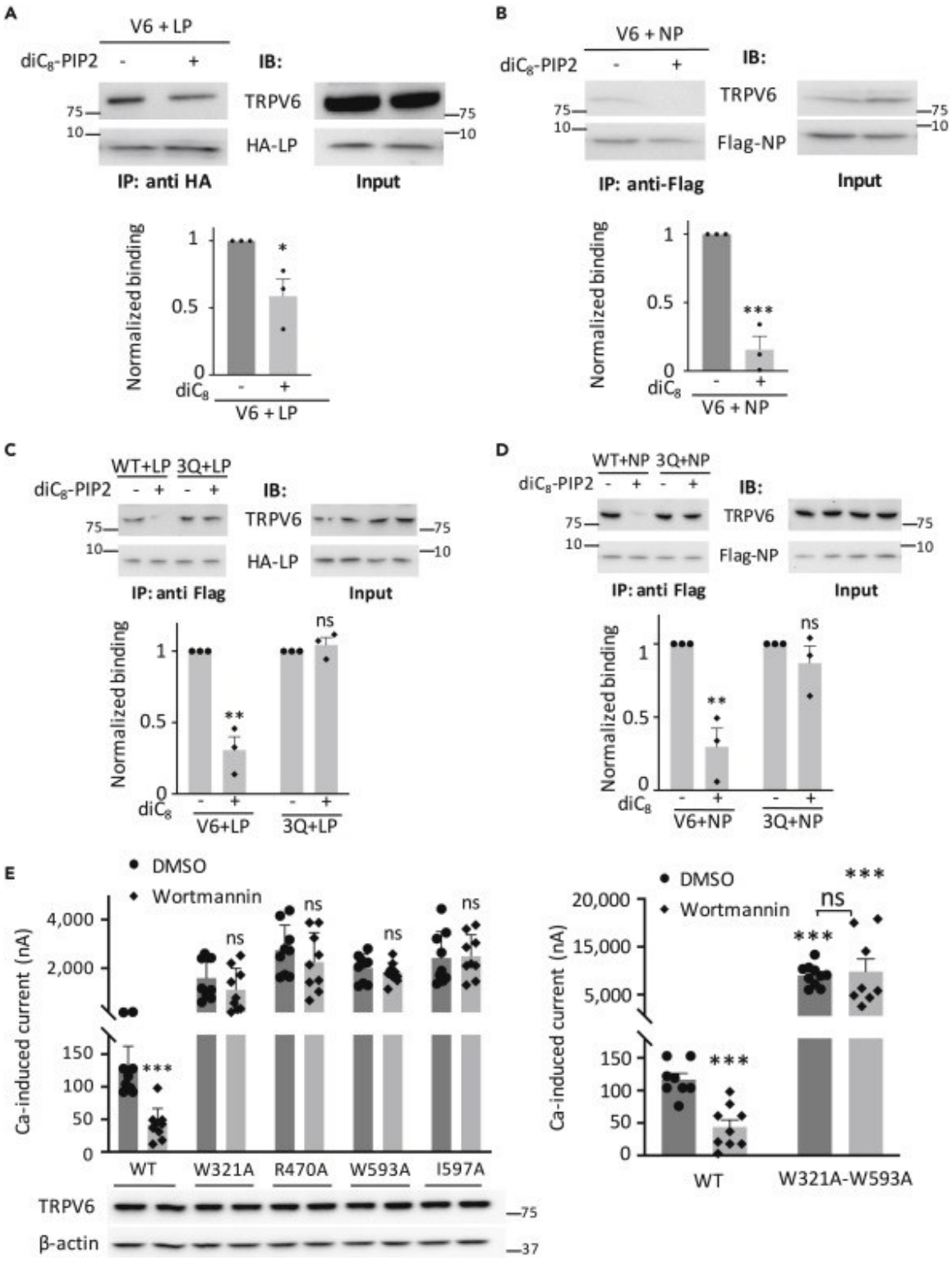

Fig. 3-7. Regulation of the TRPV6 L/C and N/C interactions by PIP2. (**A**) *Upper panel*: representative

co-IP data showing the effect of PIP2 on HA-LP/FL TRPV6 interaction. *Lower panel*: statistical data from three independent experiments as in *upper panel* after quantification and normalization. (**B**) *Upper panel*: representative co-IP data showing the effect of PIP2 on the Flag-NP/TRPV6 interaction. *Lower panel*: data from three independent experiments as in *upper panel* were quantified, normalized and averaged. (**C**) *Upper panel*: representative co-IP data showing the effect of PIP2 on the interaction of HA-LP with WT TRPV6 or triple mutant K484Q/R589Q/R632Q (3Q). *Lower panel*: statistical data from three independent experiments as in *upper panel* after quantification and normalization. (**D**) *Upper panel*: representative co-IP data showing the effect of PIP2 on the NP/TRPV6 interaction with or without 3Q mutation. *Lower panel*: data averaged from three independent experiments as in *upper panel* after quantification and normalization. (**E**) *Left upper panel*: averaged Ca^{2+}-induced currents obtained at -50 mV from expressing oocytes pre-incubated with wortmannin (10 μM) or DMSO (control) for 1 hr prior to measurements. Currents were averaged from 9-10 oocytes from three batches. *Left lower panel*: representative WB data obtained from oocytes after the wortmannin or DMSO treatment, as in the upper panel. *Right panel*: averaged Ca^{2+}-induced steady-state currents obtained from expressing oocytes. Shown representative data were averaged from 5-6 oocytes from one of the three independent experiments.

3.5 DISCUSSION

The structure of TRPV6 has recently been resolved at high resolutions by X-ray crystallography and cryo-EM, which revealed physical proximity between different domains such as S4-S5 linker/TRP helix, pre-S1/TRP helices and S4/S5 transmembrane helices (McGoldrick et al., 2018; Saotome et al., 2016). However, whether physical interaction is present between each pair and if yes, what is the underlying functional role have remained unknown. Phospholipid PIP2 activates the TRPV6 function but it is unclear to which residues it binds TRPV6 and how it affects the protein conformation (Thyagarajan et al., 2008; Zakharian et al., 2011). In the present study, we have characterized the physical interaction between the S4-S5 linker and TRP helix (L/C interaction), and between the pre-S1 and TRP helices (N/C interaction), and showed that disruption of the L/C or N/C interaction, by mutations at binding sites or blocking peptides, results in substantial activation of channel function, indicating that these intramolecular interactions present under basal conditions are autoinhibitory (Fig. 3-8). We found that the L/C and N/C interactions are not independent of each other, with the L/C binding as a requirement for the N/C binding, but not reversely. We also identified three cationic residues in TRPV6 involved in PIP2 binding and showed that the PIP2/TRPV6 binding represses the L/C and N/C association thereby suppressing the

autoinhibition and activating the channel. Taken together, our study revealed a relay 'PIP2-L/C-N/C' in TRPV6 that mediates the regulation of the channel.

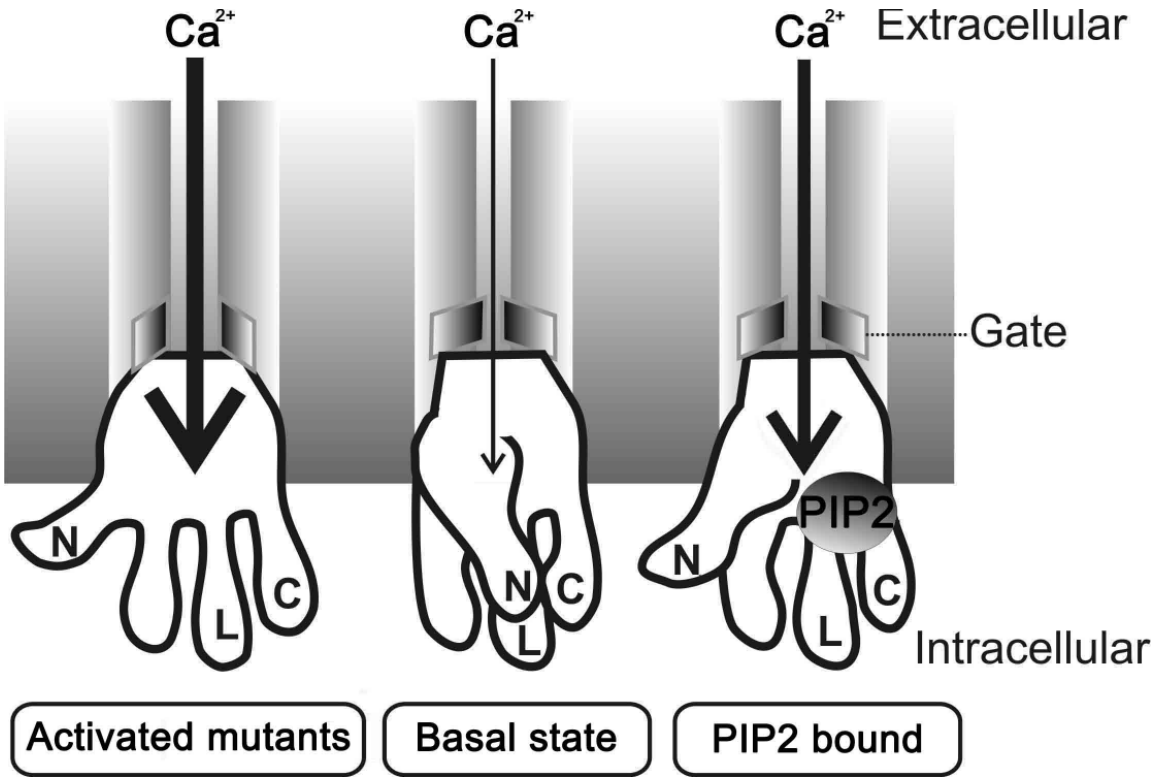

Fig. 3-8. Schematic model illustrating the mechanism of TRPV6 activation-autoinhibition. For simplicity, only the intracellular pre-S1 helix (N), S4-S5 linker (L) and TRP helix (C) of one TRPV6 monomer are shown. The gate (or lower gate) is indicated. At the basal state, the autoinhibitory interactions among N, L and C maintain the channel at basal activity and prevent channel activation while an activating mutation or PIP2 binding disrupts the interactions thereby activating the channel.

We previously reported the functional importance of a conserved glycine residue in the S4-S5 linker of TRPV6, -C4 and -C5 (Beck et al., 2013; Hofmann et al., 2017). Functional importance of linker residues L596 of TRPV4, E571 of TRPV1 and K856 of

TRPM8 have also been reported (Teng et al., 2015; Voets et al., 2007; Yang et al., 2015). Recently resolved Cryo-EM structures of TRPV2-cannabidiol complex revealed that the S4-S5 linker plays important roles in TRPV2 channel gating and activation induced by cannabidiol binding (Pumroy et al., 2019). The high-resolution cryo-EM structure of rat TRPV1, the first one in the TRP superfamily, displays close proximity of the S4-S5 linker and pre-S1 with TRP (or TRP-like) helix (Liao et al., 2013), an architectural arrangement now known to be shared by several other TRPs (Grieben et al., 2017; Paulsen et al., 2015; Saotome et al., 2016). However, it remains to be determined whether there is physical interaction between them and what are the functional consequences of breaking down the assembly. In rat TRPV1, the S4-S5 linker was suggested to interact with the TRP helix through the F559:W697 pair forming a hydrogen bonding (Liao et al., 2013). While this has yet to be verified it is noted that the TRPV1 W697 corresponds to the functionally important W593 in human TRPV6 (Fig. 3-S1A). Homology modeling proposed that hydrogen bonding mediated by the corresponding pair L596:W733 in TRPV4 maintains a closed conformation (Teng et al., 2015). Indeed, both mutants L596P and W733R were found to be activated mutants, with increased open probability. However, this L596:W733 pairing was not seen in subsequently resolved TRPV4 crystal and cryo-EM structures (Deng et al., 2018). For TRPV6, the S4-S5 linker was not resolved in the crystal structure initially (Saotome et al., 2016). Subsequent structural studies by cryo-EM resolved the linker configuration and showed that the oxygen backbone of R470

is only 2.6 Å away from the indole ring of W593 (McGoldrick et al., 2018), consistent with our current finding of the R470:W593-mediated L/C interaction. Interestingly, we found that the channel activity of mutant R470F is comparable to WT channel (Fig. 3-S1D), while R470A is an activated mutant (Fig. 3-1A and B). These data are inconsistent with the formation of hydrogen bonding at R470:W593, as suggested based on TRPV6 structure (McGoldrick et al., 2018), because of the invariable oxygen backbone in residues R, F and A, but support the presence of a F470:W593 (presumably π-π) bonding in mutant R470F and a R470:W593 (presumably cation-π) bonding in WT channel and the absence of an A470:W593 bonding. Of note, structural data suggested an alternative hypothesis that R470 interacts with lipids to stabilize the closed conformation of TRPV6 through unclear mechanisms (McGoldrick et al., 2018). We propose that lipid binding to R470 may competitively weaken the R470-W593 interaction, which opens the channel. Accordingly, the R470A mutation would mimic an extreme condition of lipid-TRPV6 binding, which couldn't be achieved physiologically, with total loss of the R470-W593 interaction, and acts as a gain-of-function mutation (Fig. 3-1B). Thus, it seems that a flexible S4-S5 linker may reflect a dynamic R470-W593 interaction (i.e., functional regulation) in response to upstream signaling such as binding of PIP2 and other ligands to TRPV6.

A salt bridge between K425 (pre-S1) and E709 (TRP helix) of rat TRPV1 was proposed based on cryo-EM structure (Liao et al., 2013). Molecular dynamics

simulations on TRPV4 suggested the presence of pre-S1 to TRP helix interaction through a salt bridge formed by the corresponding K462:E745 pair (Garcia-Elias et al., 2015). However, mutation E745A that disrupts the putative bonding only had a moderate effect on protein folding, with undetermined roles of the two residues in the channel function. Thus, whether the K:E pair in TRPV1 and -V4 actually mediates the N/C binding and what is its functional role have yet to be determined. We recently characterized the functionally critical N/C interaction in TRPP3, -P2, -M8, -V1 and -C4 that is mediated by a conserved residue W in pre-S1 and the last (cationic) residue K(R) in the W(Y)xxxK(R) (x indicates any amino acid) motif of their TRP (or TRP-like) helix, presumably by forming π-cation W:K(R) bonding (Zheng et al., 2018a), rather than a salt bridge based on a distance of 3.7 Å and 3.2 Å between the pre-S1 and TRP helices in TRPV1 and -V4, respectively, revealed from structures (Liao et al., 2013). In fact, the W residue in pre-S1 is conserved in all mammalian TRP members except TRPML (with residue F), while the K(R) residue in the W(Y)xxxK(R) motif is shared by the majority of the TRP members except TRPV4-V6, with the residue I(V) in the corresponding WxxxI(V) motif of TRPV6 and -V5. Thus, the mechanism of the W:I-mediated N/C interaction in TRPV6 discovered in the present study can be broadly interpreted as being shared by the W:K(R)-mediated N/C interaction in those other TRP channels (Zheng et al., 2018a). Reversely, it would be interesting to determine in future studies whether the TRPV6 L/C interaction is also shared by other TRP channels.

However, the TRPV6 N/C as well as L/C interaction is autoinhibitory, which is opposite to the N/C interaction of TRPP3/P2/V1/M8/C4 channels in that disruption of the N/C interaction in these channels results in loss of channel function (Zheng et al., 2018a). Also, the W321:I597 pair distance of 3.7 Å (McGoldrick et al., 2018)indicates the presence of weak van der Waals bonding, which would account for the detectable basal channel activity of WT TRPV6 (with W:I bonding), substantially activated activity with broken bonding (*e.g.*, A:I), and inhibited activity in the presence of stronger π-π bonding (W:W) or salt bridge (E:R) (Fig. 3-3). This is further supported by the fact that the channel activity was inversely correlated with the 321:597 bonding strength (Fig. 3-4C and D).

While both the L/C and N/C interactions are functionally autoinhibitory, they are not independent of each other. In fact, our co-IP experiments showed that the L/C binding is required for the N/C binding but not reversely (Fig. 3-4G and H), which infers that the likelihood of the L/C binding would be higher than that of the N/C binding but not reversely. Indeed, LP/CP1 binding band was more intense than the NP1/CP1 band (i.e., L/C binding is more likely than the N/C binding) (Fig. 3-S11). Disruption of either L/C or N/C binding in TRPV6 leads to channel activation, which is consistent with the activation of TRPV4 by mutation W733R (Teng et al., 2015), but is opposite in TRPP3/-P2/-V1/-M8/-C4 in which disrupting the N/C binding resulted in loss of function (Zheng et al., 2018a). In summary, the L/C and N/C interaction in TRPV6 play an

autoinhibitory role in the prevention from channel activation; loss of either interaction by mutations (at endogenous levels of PIP2) or increased PIP2 suppresses the autoinhibition thereby activating the channel.

PIP2 has been found to positively or negatively regulate most TRP channels. By electrophysiology with cultured cells PIP2 was shown to directly activate TRPV6 (Cao et al., 2013; Thyagarajan et al., 2009; Zakharian et al., 2011), which is consistent with our results (Fig. 3-6). Being negatively charged, PIP2 is known to bind with cationic residues in the C-terminus of several TRP channels including TRPC4, -C6, -V1, -V5, -M4, -M5 and -M8 (Nilius et al., 2008). Cationic residues involved in PIP2 binding have also been identified in the S4-S5 linker of TRPV1 (Poblete et al., 2015). In contrast, although surface plasmon resonance analysis suggested the presence of PIP2-binding cationic residues in the C-terminus of TRPM1 and -M4 so far this has not directly been shown by experimental data (Bousova et al., 2015; Jirku et al., 2015). We recently found that a C-terminal cationic residue-rich domain ($_{594}$**R**L**R**L**RK**$_{599}$) and a conserved K residue in the TRP-like helix of TRPP3 form part of the PIP2 binding cassette (Zheng et al., 2018a). The specific PIP2 binding sites in TRPV6, however, have so far not been well characterized and PIP2 even failed to fit into the human TRPV6 cryo-EM structure and surrounding lipid (McGoldrick et al., 2018). A rabbit TRPV5 structure by cryo-EM revealed the involvement of the N-terminal R302, K484 in the S5 helix and C-terminal R584 (corresponding to R302, K484 and R584 of human TRPV6) in the PIP2/TRPV5

binding (Hughes et al., 2018). None of the R302Q and K484Q mutations in TRPV5 affected the function, although they increased sensitivity to wortmannin (Hughes et al., 2018); in contrast, the K484Q mutation in TRPV6 significantly reduced currents carried by monovalent cations (Hughes et al., 2018), supporting its involvement in PIP2 binding. The involvement of K484, but not R584, in the PIP2 binding is in fact consistent with our functional data on TRPV6 (Fig. 3-6). The inconsistency on the two other residues might be due to differences in the sequences (~70% amino acid identity with TRPV5) and experimental conditions. Our current study showed that K484 in the inner S5 and R589 and R632 in the C-terminus are involved in the PIP2 binding. Of note, according to TRPV6 structural data (McGoldrick et al., 2018) residue R632 in the distal C-terminus is far away from the inner cell surface. Thus, the role of R632 in PIP2 binding may be indirect and requires further studies. Proximity of R589 to W593 and I597, and of K484 to R470 may have rendered the PIP2 being disruptive for the R470:W593-mediated L/C interaction, and thereby for the N/C interaction as well (Fig. 3-4G). This is supported by our observation that PIP2 had no effect on the L/C or N/C interaction in mutant TRPV6-3Q lacking the PIP2 binding. Thus, TRPV6 shares with other TRPs (Zheng et al., 2018a) in terms of regulation by PIP2 in that PIP2 blocks the N/C interaction through which it modulates the channel function.

TRPV6 cryo-EM structures suggested that a salt bridge between Q473 and R589 in the S4-S5 linker and TRP helix, respectively, is present in an open conformation and that

disruption of the interaction leads to channel closure (McGoldrick et al., 2018). In contrast, we found that R589 is involved in PIP2 binding and is thus critical for PIP2-induced channel activation (Fig. 3-6), whereas mutant Q473A has similar channel function as WT TRPV6 (Fig. 3-S12), which does not support the presence of a Q473:R589 salt bridge under our conditions. This discrepancy may be due to differences in the experimental condition (cryo-EM vs oocyte) and thus in the protein conformation (Shoemaker and Ando, 2018). In basal conditions where PIP2 is low, TRP helix would be in firm association with the S4-S5 linker and pre-S1 helix, rendering the adjacent S6 to be in an α-helix configuration. When cellular PIP2 is elevated, the PIP2/TRPV6 binding results in disrupted or weakened L/C and N/C interaction, presumably leading to S6 helix to undergo α- to π-helix transition to activate the channel, similar to that of TRPV3 (Zubcevic et al., 2018). In contrast, the S6 helix of TRPP2 undergoes an opposite, π- to α-helix, transition to activate the channels (Zheng et al., 2018c). However, all these TRP channels together seem to broadly share a common mechanism of channel activation, i.e., when the intramolecular N/C (and L/C) binding is suppressed in TRPV6 (or increased in other TRPs), which forces the TRP helix to be in a conformation that renders the adjacent S6 helix to be in a π-helix (or α-helix in other TRPs) configuration to allow activation.

In summary, our present study characterized the autoinhibitory TRPV6 intramolecular L/C and N/C interactions presumably mediated by cation-π and van der Waals bonding, respectively. PIP2 directly binds to cationic residues in TRPV6 and

suppresses the L/C and N/C interactions thereby activating TRPV6. Therefore, the 'PIP2-L/C-N/C' relay in TRPV6 represents a novel molecular switch that mediates the regulation of TRPV6 channel under physiological conditions.

3.6 SUPPLEMENTARY INFORMATION

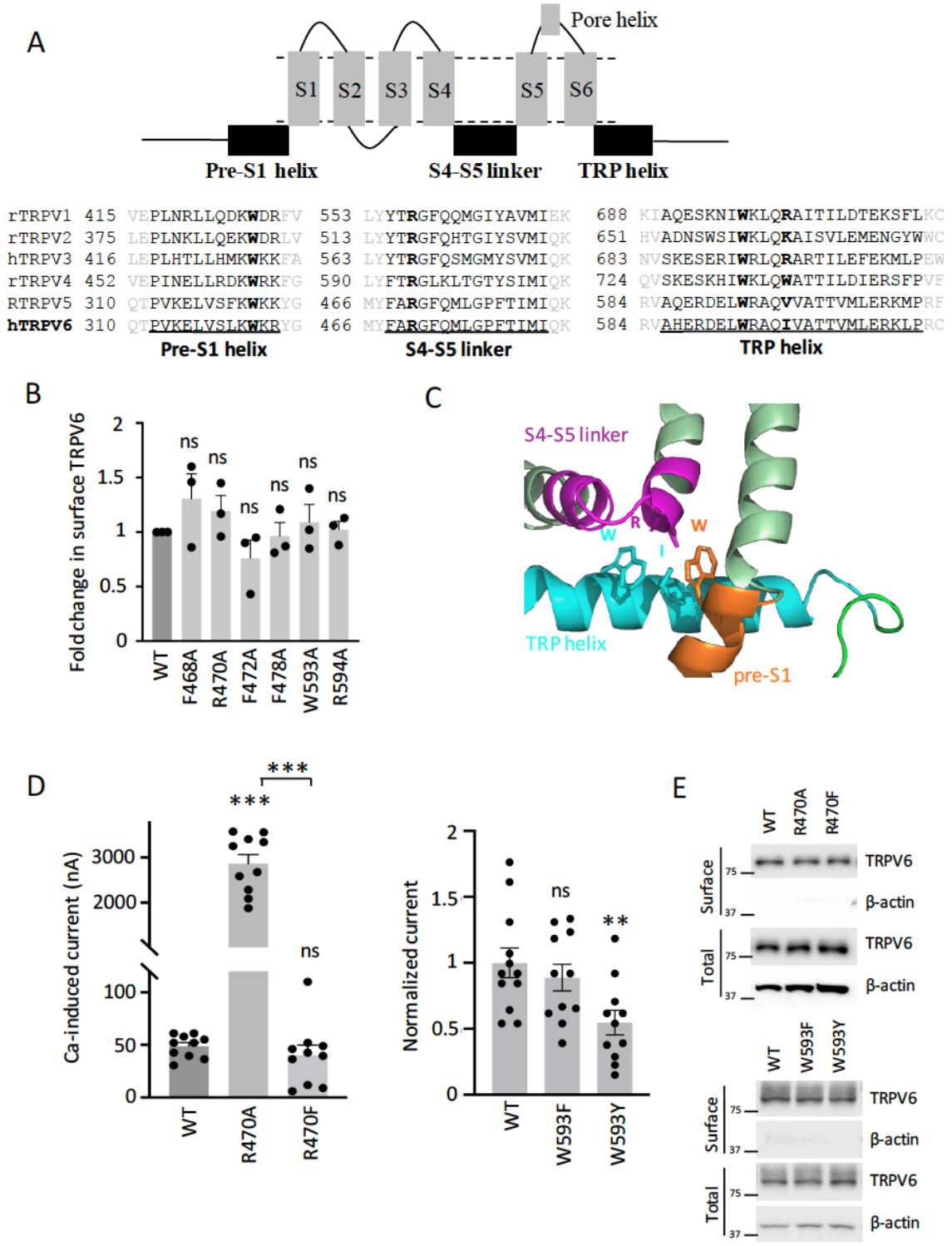

Fig. 3-S1. Membrane topology of TRPV channels, surface membrane expression and proximity between key domains of TRPV6. (**A**) *Upper panel*: membrane topology of TRPV channels with indicated key domains. Dashed lines indicate the lipid membrane. *Lower panel*: sequences of the TRPV pre-S1, S4-S5 linker and TRP helices. The four residues involved in intramolecular interactions are in bold. (**B**) Data from three independent surface biotinylation experiments were quantified, normalized and averaged. ns, not significant compared with WT. (**C**) Structural data (PDB: 6BO8) showing proximity of TRPV6 pre-S1 and S4-S5 linker to TRP helix, generated using PyMOL. The four key residues are shown. (**D**) Bar graphs showing the channel function of WT or mutant TRPV6. Normalized Ca^{2+}-induced currents obtained at -50 mV from expressing oocytes. (**E**) Representative images showing the surface and total expression of indicated proteins. Data were averages from 10-12 oocytes from three batches.

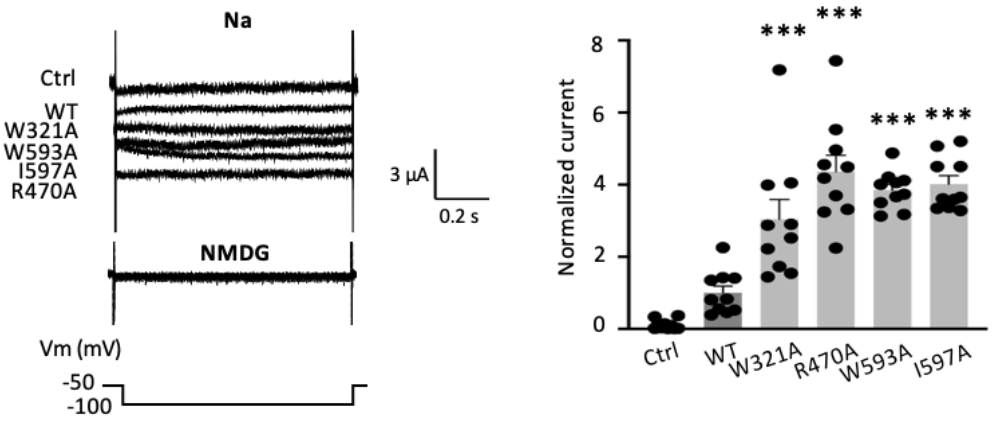

Fig. 3-S2. Na^+ currents mediated by TRPV6 gain-of-function mutants. *Left panel*, representative membrane currents obtained using a jump protocol, as indicated, in the presence of the extracellular solution Na or NMDG. Dashed lines indicate the zero current level. *Right panel*, averaged plateau current amplitudes at -100 mV obtained under the same experimental conditions as in the left panel (n = 10 from three batches). ***$p < 0.001$, by Student's t-test.

Fig. 3-S3. Effect of the F478A mutation within LP on LP/ TRPV6. Representative co-IP data showing interaction of HA-tagged LP with FL TRPV6 co-expressed in oocytes, with or without mutation F478A in LP.

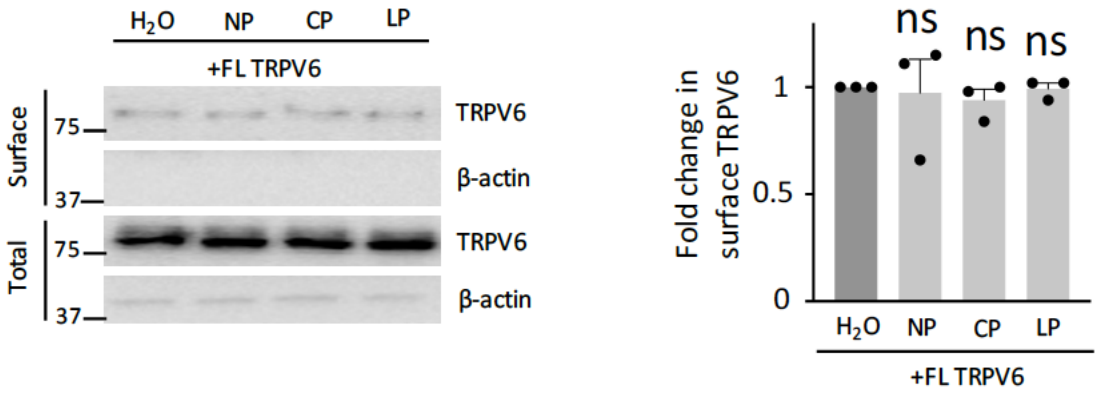

Fig. 3-S4. Effects of key domains on TRPV6 expression. *Left panel*: representative data in oocytes showing effects of peptides NP, CP, LP on the surface and total expression of WT TRPV6, revealed by biotinylation. *Right panel*: data from three independent experiments were quantified, normalized and averaged. ns, not significant compared with dark grey group.

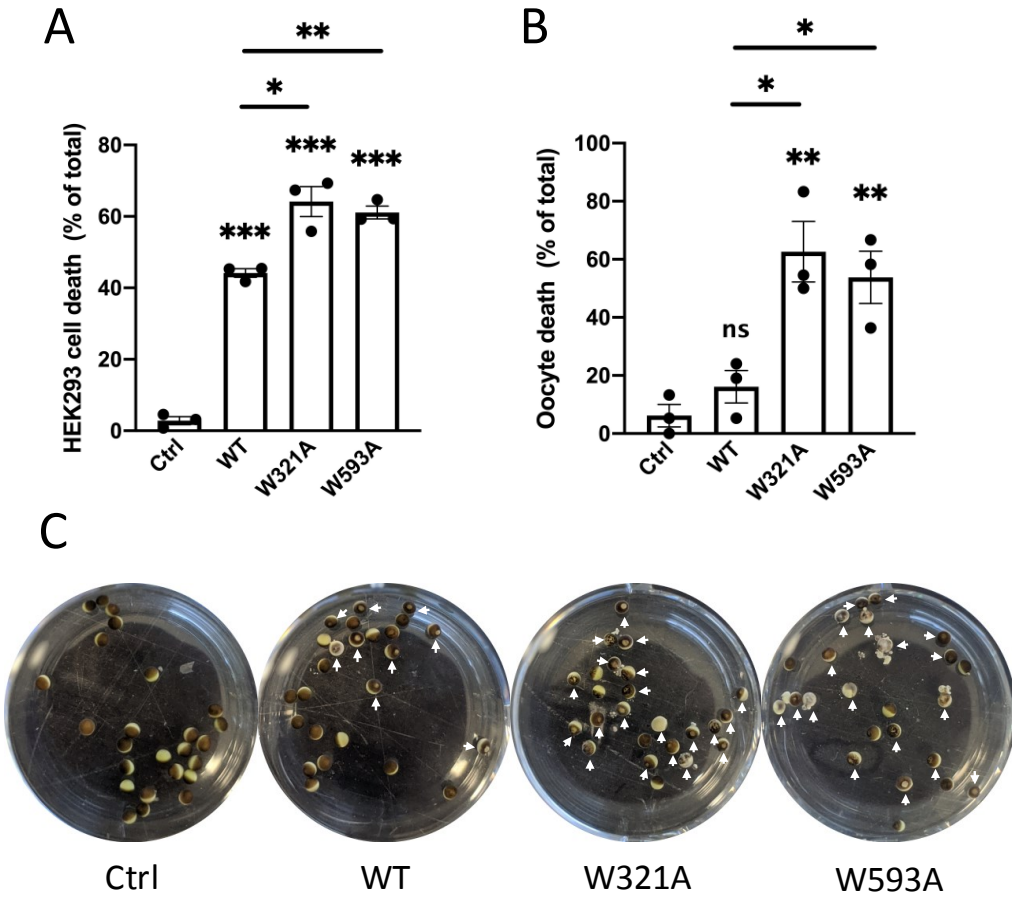

Fig. 3-S5. Cell death induced by gain-of-function mutants. Bar graphs showing death percentage in oocytes (**A**) and HEK293 cells (**B**) expressing WT or mutant channel. (**C**) Representative images showing healthy and dead (white arrows) oocytes expressing WT or a mutant channel. Experiments were performed three times from three batches of oocytes.

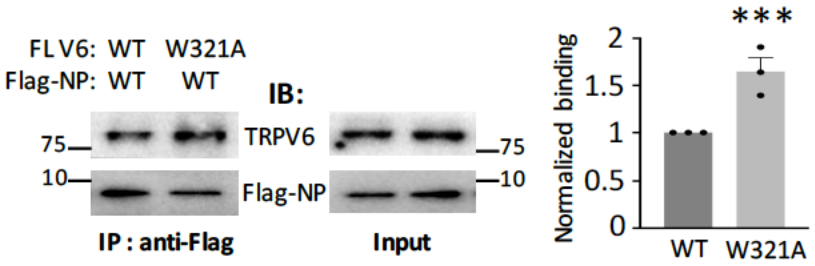

Fig. 3-S6. Effect of mutation W321A in TRPV6 on its interaction with NP. *Left panel*: Representative co-IP data showing the effect of mutation W321A within the TRPV6 pre-S1 domain on the NP/TRPV6 interaction. *Right panel*: statistical data after quantification and normalization from three independent experiments.

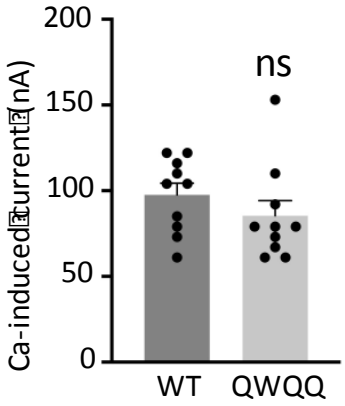

Fig. 3-S7. Effect of the K320Q/K322Q/R323Q (QWQQ) triple mutation on the TRPV6 function. Ca^{2+}-induced currents obtained from oocytes expressing WT or triple mutant QWQQ TRPV6. Currents were averaged from 10 oocytes (three batches).

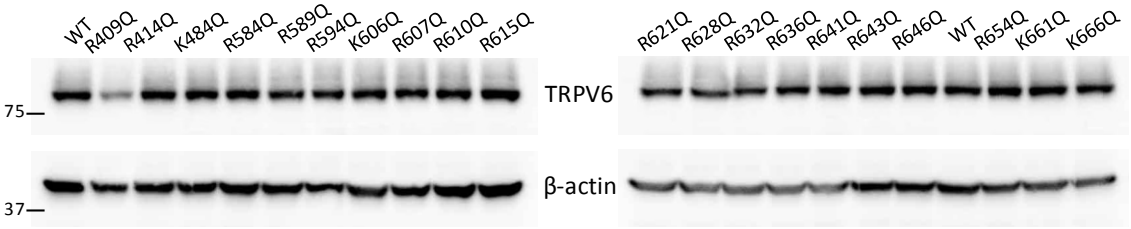

Fig. 3-S8. Expression of WT and neutralized TRPV6 mutants. Representative WB data showing the oocyte expression of WT and neutralized (glutamine substituted) mutants used for function measurements (as in Fig. 3-6B).

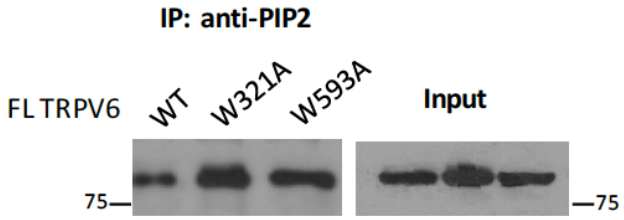

Fig. 3-S9. Importance of residues involved in the L/C or N/C binding for the PIP2/TRPV6 binding. Representative co-IP data obtained using expressing oocytes, showing the effect of mutation W321A or W593A on the PIP2/TRPV6 binding.

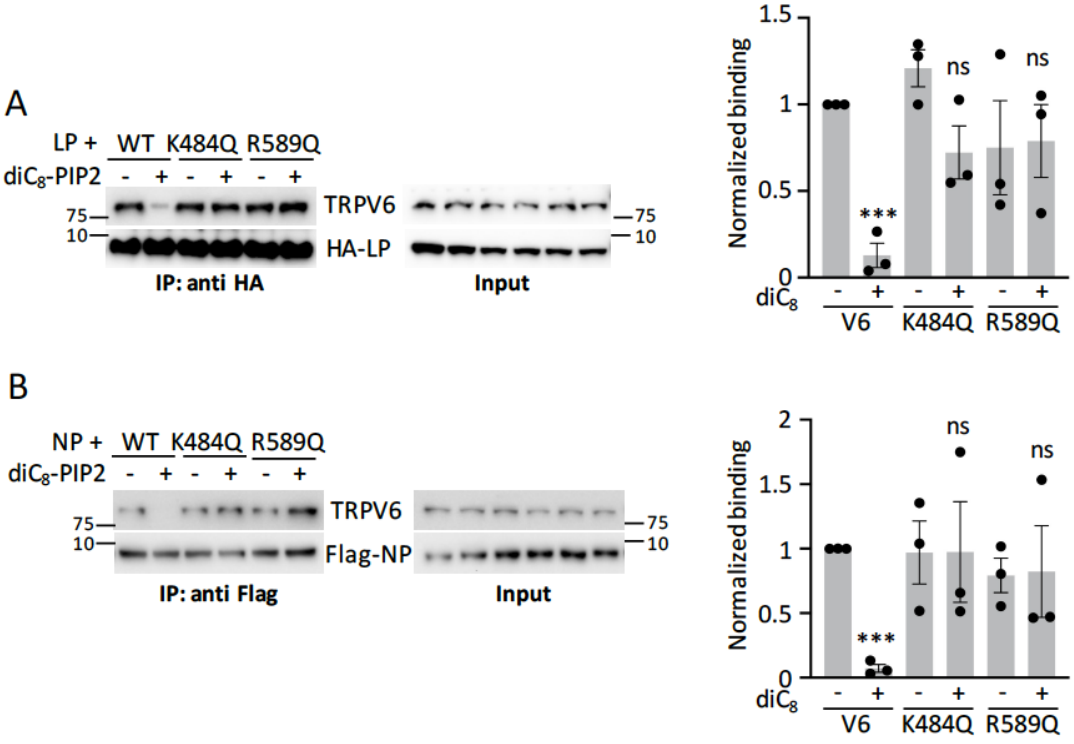

Fig. 3-S10. Regulation of the TRPV6 L/C and N/C interactions by PIP2. (**A**) *Left panel*: representative co-IP data showing the effect of PIP2 on the interaction of HA-LP with WT TRPV6 or single mutant

K484Q or R589Q. *Right panel*: statistical data from three independent experiments as in the left panel after quantification and normalization. (**B**) *Left panel*: representative co-IP data showing the effect of PIP2 on the NP/TRPV6 interaction in the presence of a Q mutation. *Right panel*: data averaged from three independent experiments as in the upper panel after quantification and normalization.

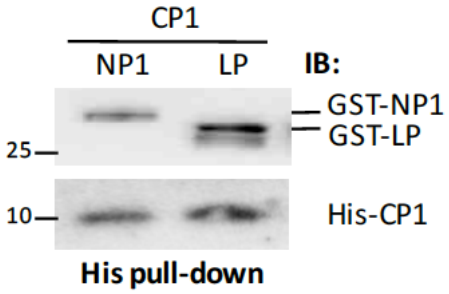

Fig. 3-S11. L/C and N/C binding assessed by pull-down assays. Representative data obtained from a His pull-down assay, showing the LP/CP1 and NP1/CP1 binding. GST-tagged pre-S1-containing human TRPV6 N-terminal peptide NP1 (GST-NP1), S4-S5 linker-containing peptide (GST-LP), and His-tagged TRPV6 C-terminal peptide CP (His-CP1) were expressed in and purified from *E. coli.*

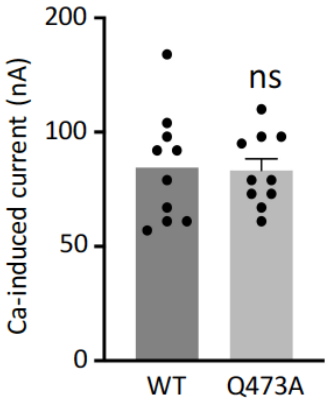

Fig. 3-S12. Effect of Q473A mutation on TRPV6 function, related to Figure 6. Ca-induced currents obtained from oocytes expressing WT or Q473A mutant TRPV6. Currents were averaged from 10 oocytes (three batches). Data are presented as mean ± SEM.

CHAPTER 4

RESULTS #3

Role of the S5/S6 helix interaction in the regulation of the TRPV6 channel function and breast cancer progression

4.1 ABSTRACT

TRPV6, as a highly Ca^{2+}-selective channel within the TRP superfamily of cation channels, is abnormally elevated in placenta, intestine, kidney and bone marrow. TRPV6 is vital to Ca^{2+} absorption and abnormal expression or function of TRPV6 is associated with human diseases including transient neonatal hyperparathyroidism, Lowe syndrome/Dent disease, renal stone, osteoporosis and importantly, breast, pancreas, colon and thyroid cancers. However, the biophysical/molecular mechanisms of TRPV6 channel function are not well understood, and how TRPV6 contributes to breast cancer remains largely unknown. Here by electrophysiology, *in vitro* pull-down and molecular simulations, we showed that a novel intramolecular S5/S6 helix interaction mediated by residues R532 and D620 is functionally autoinhibitory in TRPV6. Further, a predicted pathogenic mutant R532Q, with a disrupted S5/S6 helix interaction, was found to promote breast cancer progression through binding to the nSH2 and cSH2 domains of p85 subunit, which activates a PI3K/Akt/GSK3β pathway, up-regulates epithelial–mesenchymal transition and inhibits apoptosis. This study unveils novel mechanisms of TRPV6 regulation and its oncogenic importance in breast cancer, which contributes to further understanding of TRPV6 gating and potentially developing clinical interventions.

4.2 INTRODUCTION

The mammalian transient receptor potential (TRP) superfamily is composed of 28 members responsible for sensory processes and activated by a variety of chemical, mechanical or thermal stimuli (Gees et al., 2010). TRP Vanilloid 6 (TRPV6) together with its closest homologue TRPV5 turns out to be the most calcium-selective channel (Peng et al., 2018). Initially cloned from the rat duodenum, TRPV6 is originally proposed to mediate transcellular calcium absorption in epithelial cells of the small intestine (Peng et al., 1999). Besides its enrichment in the intestine, TRPV6 has also been detected in the kidney, pancreas, mammary gland, salivary gland, sweat gland and reproductive organs (Peng et al., 2018). Abnormal expression of or pathogenic mutations of TRPV6 is linked to male fertility, transient neonatal hyperparathyroidism (TNHP), kidney stone formation, or importantly carcinoma (Peng et al., 2018). Understanding the TRPV6 channel gating and regulation represents an important step towards clinical intervention of the related human diseases.

Recent technical advances in cryogenic electron microscopy (cryo-EM) reveal high-resolution structures of the TRPV6 channel in both the open and closed states (Vangeel and Voets, 2019). Similar to other TRP channels, TRPV6 has cytosolic N- and C-termini and six membrane-spanning domains, with an aspartate (D582) residue within its selectivity filter located between the S5 and S6 helices. Based on a closed-state

TRPV6 cryo-EM structure the pore-lining S6 helix contains a methionine residue (M618) that forms a hydrophobic energy barrier (or called a pore gate) to the ion flow (Vangeel and Voets, 2019). Different from an alpha-helical configuration of S6 helix at closed state, the S6 helix at open state adopts a π helix configuration, indicating that channel activation involves an α to π transition to open the pore gate. We recently identified autoinhibitory intramolecular S4-S5 linker/TRP and pre-S1/TRP interactions in TRPV6 and found that each interaction is mediated by a pair of conserved amino acid residues. The TRPV6 channel function substantially increased when either interaction is disrupted. The well-known PtdIns(4,5)P2 (PIP2) presumably affects these interactions thereby stimulating the TRPV6 channel function. Identification and characterization of further intramolecular interactions within TRPV6 is critical to better understanding the gating and regulation of TRPV6.

Breast cancer is the most common and fatal cancer among women globally (Akram et al., 2017). Depending on the presence or absence of estrogen receptor (ER), human epidermal growth factor receptor 2 (HER2) and progesterone receptor (PR), the breast cancer is clinically classified into luminal A ($ER^+/HER^-/PR^+$), luminal B ($ER^+/HER^+/PR^-$), HER2 positive ($ER^-/HER^+/PR^-$) and basal-like ($ER^-/HER^-/PR^-$) to guide the hormone therapy targeting the present receptor. The basal-like breast cancer, also named as triple-negative breast cancer, currently has the poorest treatment outcome and is the most deadly breast cancer. Previous studies found that both mRNA and protein expression of

TRPV6 in tumor are much increased compared with the corresponding normal breast tissue (Zhuang et al., 2002). A subsequent study further described elevated TRPV6 protein levels in the invasive regions of human breast tumor tissues (Dhennin-Duthille et al., 2011). Consistently, TRPV6 knockdown or application of TRPV6 inhibitors in TRPV6-expressing MCF-7, MDA-MB-231 and T-47D cell lines impairs their viability, migration or invasion of the cells (Dhennin-Duthille et al., 2011; Peters et al., 2012). TRPV6 has been well described as a highly Ca^{2+} selective channel, which presumably contributes to the carcinogenesis in cultured cells although there is no direct evidence. Despite all the reported relevance of TRPV6 to breast cancer progression, the mechanisms of how TRPV6 exercises its oncogenic roles in human breast cancer so far remains poorly investigated.

Cancer cells are characterized with elevated proliferation, migration, invasion and apoptotic resistance. One of the critical pathways controlling these processes is the Akt/GSK-3β pathway, which regulates the stability of the epithelia-mesenchymal transition (EMT) and expression of pro-survival markers. The class IA phosphoinositide 3-kinases (PI3K) as a heterodimer composed of a regulatory subunit named p85 and a catalytic subunit called p110 (Zhang et al., 2011) is the upstream activator of the Akt/GSK-3β pathway. The subunit p85 interacts with, stabilizes and inhibits p110. PI3K is known to be recruited to the surface membrane and then activated through competing interaction of inhibitory p85 with a colocalized receptor or adaptor molecule locating on

the cell surface (Geering et al., 2007). Upon extracellular stimuli or genetic mutations, epithelial cells may undergo EMT to attenuate cell-cell adhesion and render the cells aggressively mobile and invasive. Various ion channels including chloride, potassium, sodium, and calcium channels are found to correlate with EMT in breast, liver, lung and head/neck cancers (Azimi and Monteith, 2016). The calcium channels, such as Orai1, TRPC6, -M7 and M8 were proposed to induce EMT in breast or liver cancer cell lines (Azimi and Monteith, 2016). Nevertheless, whether TRPV6 is also involved in EMT and what would be the underlying mechanism are not known.

The present study employed two-electrode voltage clamp in *Xenopus* oocytes, molecular dynamics (MD) simulation, and cultured breast cancer cells to identify residues that mediate intramolecular interaction between S5 and S6 helices and examine the functional importance of the interaction. We also examined the roles of predicted pathogenic mutant R532Q in cell proliferation, migration, invasion and oncogenesis of MCF-7 and MDA-MB-231 breast cancer cell lines, as well as further signaling pathways involved. Our findings here proposed a new autoinhibitory interaction in the TRPV6 channel and a novel mechanism of the GOF R532Q mutant contributing to human breast cancer tumorigenesis.

4.3 METHODS

Plasmids, reagents and antibodies

Xenopus oocyte expression vector pBSMXT-MCS encoding human TRPV6 cDNA was generated previously. For mammalian cell expression, human TRPV6 cDNA was subcloned into the pCMV vector. Q5 hot start high-fidelity master mix (New England Biolabs) was used to introduce mutation(s) and mutants were verified by sequencing. TRPV6 antibody was made as described previously (Fecher-Trost et al., 2013). Commercial antibodies against β-actin, MCL-1 and p85 were from Santa Cruz Biotechnology and p-Akt, Akt, p-GSK-3β, GSK-3β, SNAI1, e-cadherin, vimentin and HA-tag were from Cell Signaling Technology. DTT and MONNA were purchased from Fisher Scientific and Tocris Bioscience. Menthol and crystal violet were bought from Sigma-Aldrich (St. Louis, MO).

Protein expression in *Xenopus laevis* oocytes

WT or mutant plasmids were linearized and then capped RNAs were *in vitro* synthesized using mMESSAGE mMACHINE T3 transcription kit (Invitrogen, Waltham, MA). Same as previously described, 25ng RNA was injected into each oocyte (Zheng et al., 2018a). Control oocytes were those injected with water. After maintaining for 2 days, injected oocytes were subjected for experiments. The present study is reviewed and approved by

Ethical Committee for Animal Experiments of the University of Alberta, and carried out in accordance with the Guidelines for Research with Experimental Animals of the University of Alberta and the Guide for the Care and Use of Laboratory Animals (NIH Guide) revised in 1996.

Two-microelectrode voltage clamp in oocytes

Microelectrodes made from capillary pipettes were cut with resistance ranging from 0.3-2 MΩ and then filled with KCl (3 M). The oocyte was penetrated and the whole-oocyte currents were measured with perfusion of extracellular solutions indicated. At 200 μs/sample and Bessel filtered at 2 kHz, the currents and voltages were obtained, with a Geneclamp 500B amplifier and Digidata 1322 A AD/DA converter (Molecular Devices, Union City, CA). The files were analyzed with pClamp 9 (Molecular Devices, Union City, CA) and data were plotted with Prism 8 (GraphPad Software, San Diego, CA).

Immunoprecipitation and TEV cleavage

Oocytes expressing TRPV6-TEV mutant with R532C, D620C or R532C/D620C mutation were lysed and incubated with TRPV6 antibody plus 50% protein G slurry overnight at 4 °C. 0.6 mM glutathione/0.4 mM oxidized glutathione or 1 mM DTT along with AcTEV protease (Invitrogen) was added to the mixtures respectively (Klint et al., 2013). The proteins were eluted with SDS loading buffer and analyzed by Western blot.

Immunofluorescence on oocytes and mammalian cells

The oocytes or mammalian cells were washed with ice-cooled PBS and fixed with 4% paraformaldehyde, followed by permeabilization with Triton. After blocking with 3% skim milk or BSA, oocytes or cells were incubated with specific antibodies overnight at 4 °C and then with Alexa fluor 488 anti-rabbit IgG (Invitrogen) at RT for 1 hr. Fisher chemica permount mounting medium (Fisher Scientific) was used to mount the oocytes, while ProLong Gold Antifade Mountant (Molecular Probes, Life Technologies) was used to mount mammalian cells. Fluorescence was examined with Olympus IX-81 spinning confocal microscope (Cell Imaging Centre, Faculty of Medicine and Dentistry, University of Alberta).

***In vitro* pull down**

The full N-terminus, S5 and S6 fragments of TRPV6 channel were amplified and subcloned into pET-28a, pGEX-5X vectors and a vector with MBP and His tags gifted by Dr. Joanne Lemieux (University of Alberta) (Arutyunova et al., 2012). *E coli.* expression plasmids encoding nSH2, SH3 and BH of p85 were gifts from Dr. Lewis Cantley (Cornell University), and cSH2 was from Dr. Sharona E. Gordon (University of Washington). Peptides with His or GST tag produced from *E. coli.* were purified with corresponding GST (GE Healthcare) or Ni-NTA beads (Qiagen, Hilden, Germany). Purified peptides

were incubated together as indicated overnight at 4 °C and supplemented with 50% beads. After extensively wash with 1% NP-40, beads conjugated with peptides were denatured subjected to Western blot analysis.

Molecular dynamic stimulation

The initial simulation system was set up based on the cryo-EM structure of human TRPV6 (PDB: 6D7T) (Singh et al., 2018b). Only the pore region of TRPV6 (amino acids 511-640) was used for simulation. This region contains the transmembrane helix 5 (TM5), pore helix, TM6, and TRP helix. Then, the TRPV6 pore structure was modeled in a 1-palmitoyl-2-oleoyl-sn-glycero-3-phosphocholine (POPC) lipid bilayer using CHARMM-GUI membrane builder (Jo et al., 2009) (Fig. S3A and B). The system was hydrated with a total of 12,950 TIP3P water molecules on both sides of the bilayer. The approximate dimensions of the resultant simulation box were 87 Å x 87 Å x 99 Å along the x, y, and z axes, respectively. Na^+ and Cl^- ions were added to the system to neutralize it and maintain a 150 mM NaCl concentration. The two Ca^{2+} ions in the PDB structure were retained in the simulation system. The input parameters for protein, ions, water molecules, and lipids were generated by CHARMM-GUI Input Generator (Lee et al., 2016). To investigate the effect of R532Q mutation on the structural and dynamic changes of TRPV6, the residues R532 in the four subunits of TRPV6 were mutated to Q532 using the mutagenesis function of PyMOL. The two systems are noted as TRPV6

WT and TRPV6 R532Q, respectively.

Molecular dynamics simulations were carried out using the AMBER18 simulation package. The simulation protocol is similar to our previous studies (Wang et al., 2019). Totally, 400 ns simulations were performed (Fig. S3C). Before data analysis, the root mean square deviation (RMSD) for the Cα atoms of TRPV6 was calculated to assess the equilibration of the simulations. The RMSD results show that the two simulations got equilibrated after 200 ns, thus the trajectories of the last 200 ns simulations were used for data analyses. All the simulation analyses were performed using the CPPTRAJ program of AMBER18. The VMD software was used for structure visualization (Humphrey et al., 1996).

Cell culture and ratiometric Ca^{2+} imaging

MCF-7 and MDA-MB-231 cells were gifts from Dr. Zhixiang Wang (University of Alberta) and cultured in RPMI1640 or DMEM supplied with 10% FBS (Gibco) and 1% penicillin streptomycin. Stable expression of TRPV6 WT and R532Q in both cell lines were made through transfection with Fugene HD (Promega, WI) and selected with G418 (Gibco). 300 ug/ml G418 was added for maintenance of stable cell lines.

Cell proliferation assay

5×10^3 stably transfected cells were seeded in the 96-well plate with triplicate for each

group. Cell counting kit-8 (Sigma-Aldrich) was used according to manufacture's instruction. After incubation for 4 hr, OD values were measured with a microplate reader.

Wound healing assay

After cells formed the monolayer, scratches were made with a sterilized fine tip at 0 hr. Images were taken by a digital camera with C-Mount on randomly selected areas for each group. 24 hr for MCF-7 cell and 16 hr for MDA-MB-231 cell later, images of the same selected areas were taken.

Invasion assay

Invasion assay was performed using costar transwell with 8.0 μm pore polycarbonate inserts, with the use of growth factor reduced Corning Matrigel invasion chamber (Bedford, MA). 5×10^3 stably transfected MDA-MB-231 cells were seeded on the upper chamber with a starvation medium without FBS overnight. 20% FBS added medium was added to the lower chamber. 12 hr later, the assay was stopped and cells remained in the upper chamber were swapped with cotton tipped applicators. The inserts were fixed with menthol and stained with crystal violet.

Soft agar colony formation assay

2500 stably transfected cells were mixed with 0.35% agarose, low gelling temperature

(Sigma-Aldrich) and added to the 0.7% base soft agar in the 24-well plate. Cells were fed twice per week. Three weeks later, cells were imaged and the number of colonies formed was counted and analyzed.

Co-immunoprecipitation

Cells with stable expression of TRPV6 or mutant were lysed and incubated with TRPV6 antibody plus 50% protein G sepharose (GE Healthcare) overnight at 4 °C. Beads were washed and denatured with SDS loading buffer for Western blotting.

Correlation of TRPV6 expression with breast cancer patient survival

The relevance of TRPV6 expression with survival rates in BC patients was manually examined against published databases available through the Kaplan-Meier plotter (Gyorffy et al., 2010). The curves of overall survival and relapse-free survival, with the logrank P value and hazard ratio with 95% confidence intervals, were generated by segregating patients with high or low expression of *TRPV6* gene (206827_s_at).

Statistical analysis

Data presented here were all as mean ± SEM (standard error of the mean). *, ** and ***, were respectively assigned when P values, calculated by Student's t-test, were less than 0.05, 0.01 and 0.001. Statistically not significant was abbreviated as 'ns'.

4.4 RESULTS

Conserved R532 in S5 helix was functionally important

We recently characterized intramolecular interactions of the pre-S1/TRP domain with the S4-S5 linker and TRP domain in TRPV6 and their functional importance for the channel (Chapter 3). The S5 helix has been found to be in close proximity to the pore-forming S6 helix, as revealed by multiple TRPV6 swapping structures (McGoldrick et al., 2018). There are conserved lysine (K524) and arginine (R510, R532) residues within the S4-S5 linker and S5 helix. Among them, R510 is known to mediate the S4-S5 linker/TRP domain binding and K524 is involved in binding with PIP2, a TRPV6 activator, as shown by functional studies (Chapter 3) and revealed by structural studies (Hughes et al., 2018). However, the functional importance of S5 helix and R532 remains elusive. Based on a cancer database, Catalogue Of Somatic Mutations In Cancer (COSMIC), R510Q and R532Q were predicted to be pathogenic mutations (Tate et al., 2019). Here by the two-electrode voltage clamp in *Xenopus* oocytes we found that, compared with WT TRPV6, R532Q mutant is of substantial GOF, with a 50-fold increase in the current induced by 5 mM Ca^{2+} in the presence of chloride channel blocker 2-[(4-methoxynaphthalen-2-yl)amino]-5-nitrobenzoic acid (MONNA) (Fig. 4-1). To further dissect the underlying role of R532 we systematically mutated R532 to aromatic or charged amino acids and found that, similar to the R532Q mutation, substitutions of

R532 with aromatic or negatively charged amino acids strongly increase Ca^{2+}-induced currents (Fig. 4-1A and B). In contrast, cationic substitution (R532K) had no significant effect, indicating the importance of a positive charge on the side chain of the residue at 532 side chain to maintain the TRPV6 channel function. Of note, membrane targeting and total expressions of WT and these mutants were comparable (Fig. 4-1C). Together, these functional data suggest that R532 may interact with a negatively charged amino acid, which together form an energetically favorable salt bridge to maintain the basal (WT) channel function.

R532:D620 mediated the S5/S6 helix interaction

Based on proximity between proximal S5 and distal S6 suggested by available TRPV6 structures, we identified a highly conserved aspartic acid (D620) in the distal fragment of the S6 helix as a candidate residue involved in salt bridge formation with R532 (Fig. 4-S1). Indeed, removal of the negative charge (D620A or D620R) induced substantial GOF, similar to R532Q, possibly due to disruption of a bonding of site 620 with R532 (Fig. 4-1D and E). Further, substitution of D620 with aromatic tryptophan (W) or phenylalanine (F) or anionic glutamic acid (E) did not much alter the channel function, possibly because they maintained a bonding (cation-π or salt bridge) with (Fig. 4-1D and E). To verify whether the gain-of-funtion (GOF) is due to non-specific conformational changes or specifically disruption of the 532:620 bonding, we tested double mutations

(R532W/D620R, R532W/D620W and R532F/D620W), in which single mutation of R532W/F or D620R would disrupt the putative bonding while two simultaneous mutations would re-establish the bonding disrupted by the first mutation. Indeed, all the double mutants R532W/D620R, R532W/D620W and R532F/D620W rescued the channel function from substantial GOF of single mutants and exhibited activities comparable to that of the WT channel (Fig. 4-1D and E). Furthermore, we swapped the R532 and D620 and generated double mutantR532D/D620R supposedly re-forming a salt bridge between them. Indeed, different from GOF of single mutants R532D and D620R, the channel activity of double mutant R532D/D620R was similar to that of WT TRPV6 (Fig. 4-1A, B, D-F). These data together strong supported the presence of a bonding between R532 and D620 of which disruption results in GOF.

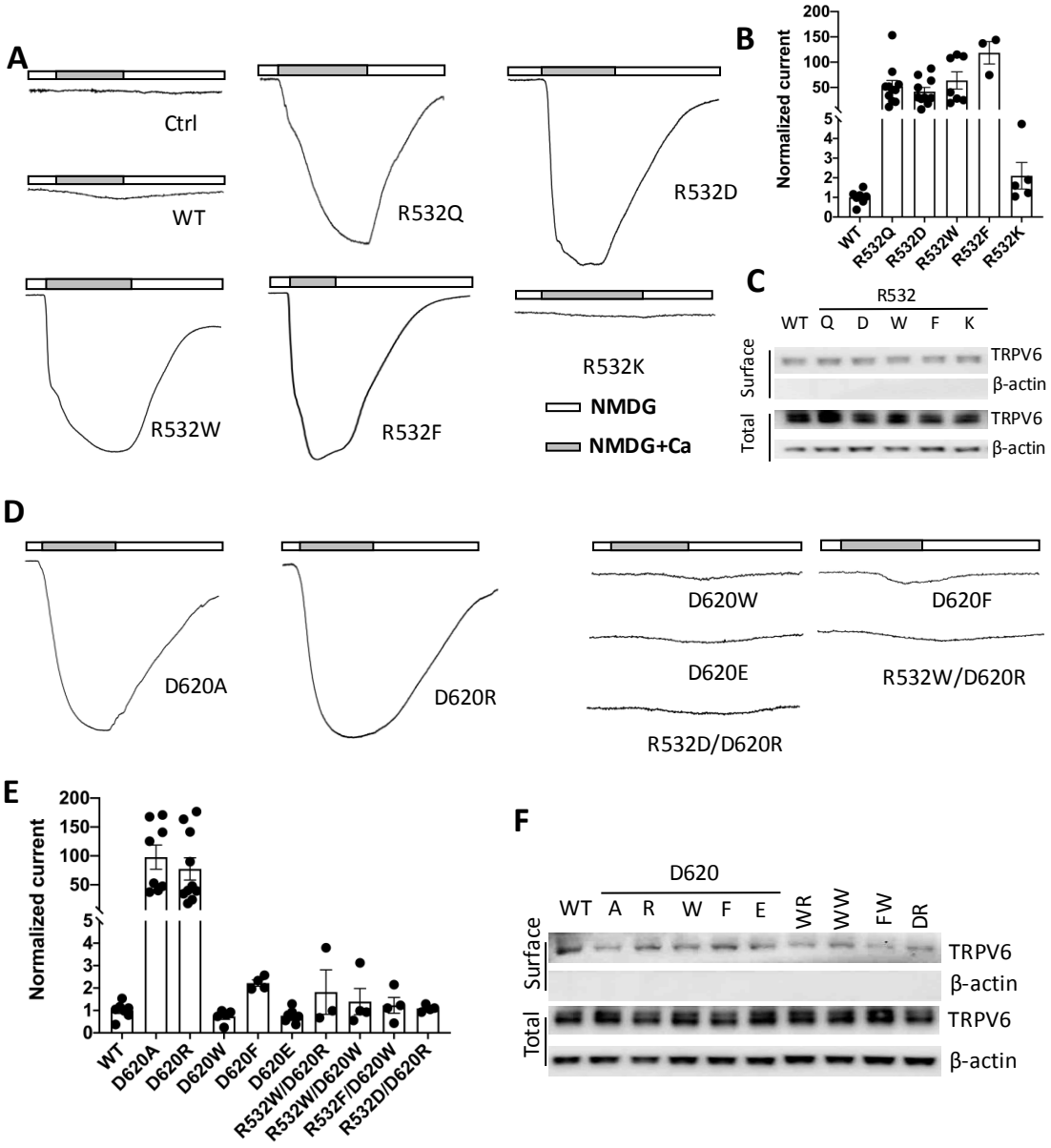

Fig. 4-1. R532 and D620 residues formed a functional pair in the TRPV6 channel. (**A**) Representative current traces from water-injected (ctrl) oocytes or oocytes expressing TRPV6 WT, indicated R532 mutants. (**B**) Averaged and normalized current values of TRPV6 WT or indicated R532 mutant expressed in oocytes. *** $p < 0.001$; ns, not significant. (**C**) Total and surface expression of TRPV6 WT, R532 mutants and β-actin. (**D**) Representative current traces from oocytes expressing mutants indicated. (**E**) Averaged and normalized current values of TRPV6 WT or indicated mutants. (**F**) Total and surface expression of TRPV6 WT, mutants indicated and β-actin.

To provide further documentations on the R532:D620 bonding, we next introduced cysteine (C) residue to replace R532 and D620 and found that double mutant R532C/D620C exhibits smaller currents compared with those mediated by WT TRPV6 (Fig. 4-2A), which is consistent with the formation of a covalent disulfide bond between sites 532 and 620 that is stronger than an electrostatic salt bridge found in WT TRPV6. Further, upon incubation with reducing reagent dithiothreitol (DTT) to disrupt the disulfide bond, the channel activity of R532C/D620C was significantly increased while WT channel had no response to the treatment (Fig. 4-2A). These data together suggested an inverse correlation between the 532:620 bonding strength and channel activity.

Next, we inserted a tobacco etch virus (TEV) protease cleavage sequence right after E559 in the extracellular S5/S6 loop of the double mutant R532C/D620C and termed the resulting mutant R532C/D620C$_{TEV}$ which may split into two fragments (around 63 and 24 kD) upon TEV cleavage and disruption of the disulfide bond. Indeed, a band of about 24kD was detected only upon treatment with both DTT and TEV protease (Fig. 4-2B), further supporting the formation of a disulfide bond at 532:620. To test whether the S5/S6 helix directly interacts with each other, we purified the fragments containing S5 (G511-V540, called GST-S5) and S6 helices (A603-L632, called His-MBP-S6) and found that GST-S5 binds to His-MBP-S6, while the presence of either the R532Q or D620A mutation broke the physical interaction (Fig. 4-2C and D). Taken together, these data showed that the S5/S6 helix direct interaction is mediated by bonding between R532 and

D620 that is essential for the maintenance of the TRPV6 basal channel function, and that disruption of the interaction leads to GOF function of TRPV6. Thus, the intramolecular S5/S6 helix interaction is autoinhibitory for the TRPV6 channel function.

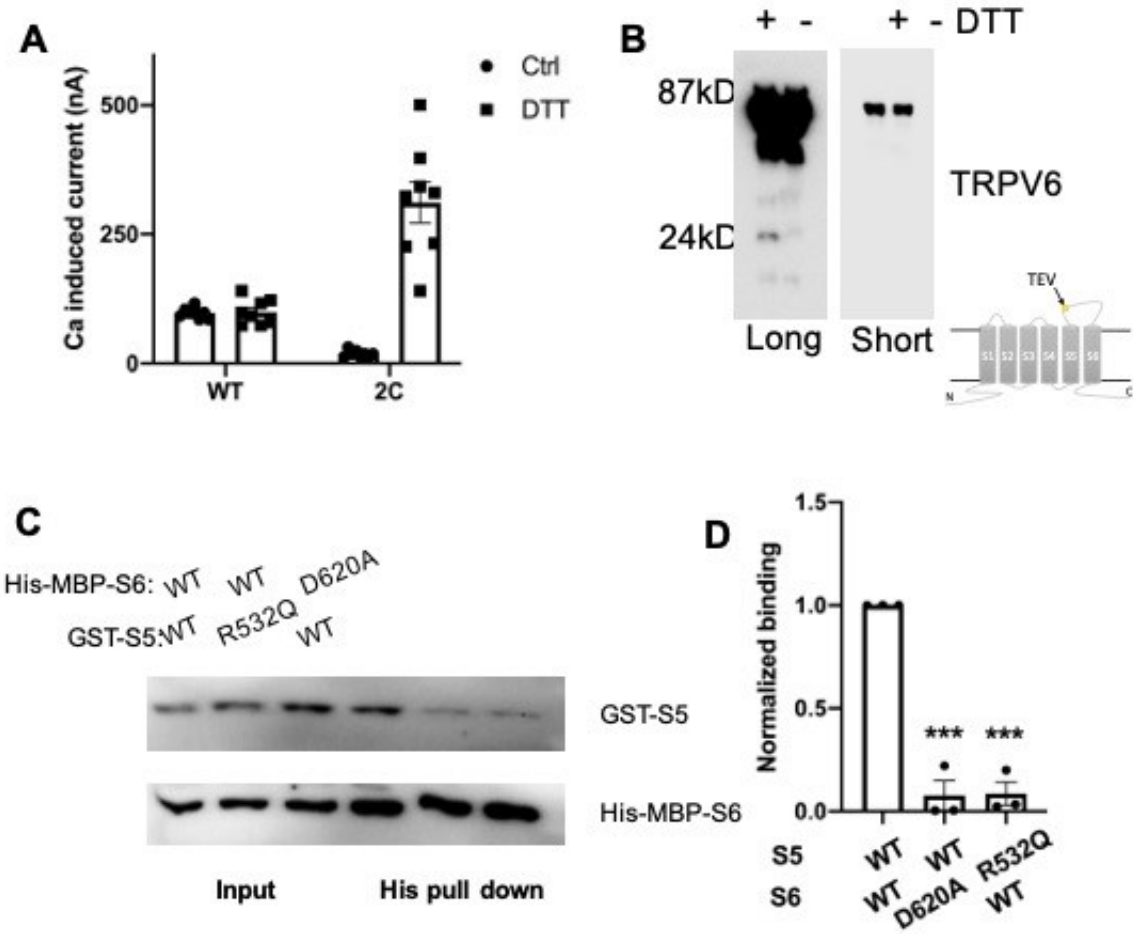

Fig. 4-2. R532 interacted with D620 in the TRPV6 channel. (**A**) Statistical analysis of currents from oocytes expressing TRPV6 WT or R532C/D620C, with or without 5 μM DTT. (**B**) Representative Western blotting images with long exposure (long) or short exposure (short) showing DTT effect on R532C/D620C$_{TEV}$ mutant. Picture illustrates the position of TEV cleavage site inserted. (**C**) Representative images of interaction between purified S5, S6 peptides without or with indicated mutation. (**D**) Averaged

and normalized S5/S6 helix binding. ***, $p < 0.001$.

R532Q mutant examined by molecular dynamic simulations

In the initial molecular dynamic (MD) simulation model, there is no hydrogen bond formed between R532 and D620 (Fig. 4-3A). To test whether the hydrogen bond could be form during the simulations, the hydrogen bond between a residue at 532 (R532 or Q532) and D620 was calculated and our results showed that the hydrogen bond was formed between R532 and D620 within one monomer of TRPV6 WT during the simulation, while there is no hydrogen bond formed in the TRPV6 R532Q mutant (Fig. 4-3A). This finding is consistent with the experimental proposition that the two residues can form a hydrogen bond. The final structures showed that residue D620 underwent larger position changes in the TRPV6 R532Q mutant compared with D620 in WT TRPV6 (Fig. 4-3B).

Since D620 is only two residues apart from M618 in S6, structural and dynamic changes of D620 may affect the dynamics of M618. To test this proposition, the helix structure occupancy and root mean square fluctuation (RMSF) for WT and R532Q mutant TRPV6 were calculated (Fig. 4-3C and D). Compared to WT TRPV6, the helix occupancy for D620 in TRPV6 R532Q was significantly decreased while the RMSF was significantly increased (Fig. 4-3C and D), indicating the R532Q mutation reduced the structural and dynamic stability of D620. Detailed analyses also showed that the R532Q mutation altered the secondary structure and dynamic stability of a region around D620 (M618-W623) in a similar way.

To further test whether the R532Q mutation could cause dynamic changes of M618 in the lower gate, the distance between the two diagonal M618 between two monomers was calculated (Fig. 4-3E). Simulation results demonstrated that the mutation causes a significant increase in the distance (9.53 ± 0.43 Å in WT vs. 13.11 ± 0.44 Å in R532Q). Compared to the initial model (12.46 Å in Figure 3B), the distance was significantly decreased in TRPV6 WT while it was not significantly altered in R532Q, indicating that the lower gate is stabilized in WT TRPV6. In addition, we found that the TRP helix in TRPV6 R532Q undergoes dramatic conformational changes compared with the WT channel (Fig. 4-3E). To provide further details on the changes we calculated the density of the TRP helix which indicates the TRP helix position along the Z-axis (Fig. 4-3F). It showed that the TRP helix in WT TRPV6 is located near the surface membrane while in mutant R532Q it is located away from the surface membrane (Fig. 4-3F).

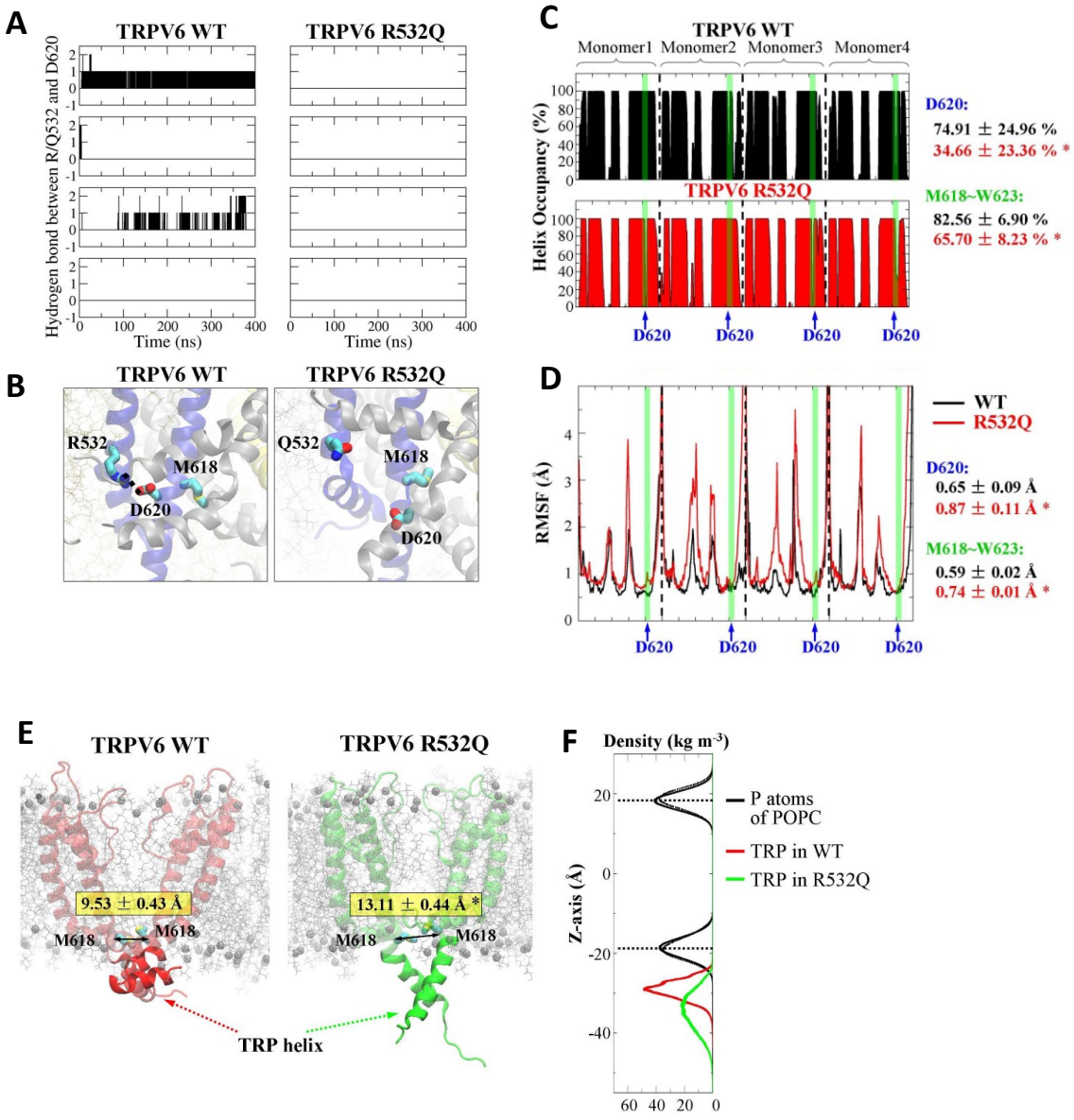

Fig. 4-3. S5/S6 helix interaction mediated by R532 and D620 revealed by MD stimulations. (**A**) Hydrogen bond between residue 532 (R532 or Q532) and D620 as a function of time. (**B**) Comparison of the conformation of D620. Structural (**C**) and dynamic (**D**) changes of D620 and the region around D620 (M618~W623). Higher occupancy value means the secondary structure is more stable, while larger value of root mean square fluctuation (RMSF) indicates the residue is more dynamically flexible. (**E**) Comparison of the distance between the two diagonal residues of M618. (**F**) Mass density for phosphate (P) atoms of POPC lipids (black lines) and TRP helix of TRPV6 (red and green lines). Dotted lines show the density

peaks of P atoms, indicating the surface of membrane. Note: The density values of P atoms of POPC are reduced 10 times to shown them in the same scale of TRP helix.

In summary, the formation of a salt bridge between R532 and D620 was observed in TRPV6 WT by MD simulations. This hydrogen bond stabilized the structure and dynamics of D620 and the region around D620 including M618 in the lower gate. These changes resulted in a decreased distance between the M618 from two diagonal monomers and a stabilized structure of the lower gate. However, the R532Q mutation not only disrupted the structural and dynamic stability of the lower gate but also caused large conformational changes of the TRP helix, which would affect the activity of TRPV6.

R532Q mutant promotes breast cancer cell progression

We established stable MCF-7 and MDA-MB-231 cells expressing WT or R532Q mutant TRPV6 to examine the effect of TRPV6 on breast cancer cells by means of Ca^{2+} imaging. We found that the WT-expressing cells have significantly higher cytosolic Ca^{2+} levels before and after Ca^{2+} application, compared with vector transfected MCF-7 and MDA-MB-231 cells (Fig. 4-4A and B). Cells expressing R532Q had much increased cytosolic Ca^{2+} levels compared to WT-expressing or control MCF-7 and MDA-MB-231 cells (Fig. 4-4A and B), indicating that the R532Q mutant expressed in both breast cancer cell lines is GOF, consistent with our functional data (Fig. 4-1). Malignant cancer cells are characterized with enhanced viability, migration, invasion as well as the ability to

form colonies from single cells (Hanahan and Weinberg, 2011). The viability of either cell line was moderately increased by expression of WT TRPV6 and largely increased by expression of mutant R532Q (Fig. 4-4C and D). Using wound healing assays we found that R532Q mutant stably expressed in MCF-7 and MDA-MB-231 cells, dramatically increases the wound closure percentage, while stably expressed WT channel only results in a moderate but significant increase (Fig. 4-4D). As MDA-MB-231, but not MCF-7, cells are invasive we also tested the effect of TRPV6 on the cell invasion using matrigel and found that cells expressing R532Q are more invasive than those expression WT channel which are more invasive than control cells (Fig. 4-4E). Further, the oncogenicity of MCF-7 and MDA-MB-231 cells was determined by colony formation and soft agar assays. We found that the colony number of the WT group has a mild and significant increase while that of the R532Q group showed a substantial increase (Fig. 4-4F and G). These data together showed that WT and R532Q mutant expressed in MCF-7 and MDA-MB-231 cells promote the cell viability, migration, invasion and anchorage-dependent or -independent colony formation and that mutant R532Q has much stronger effects than WT TRPV6, consistent with the GOF nature of R532Q.

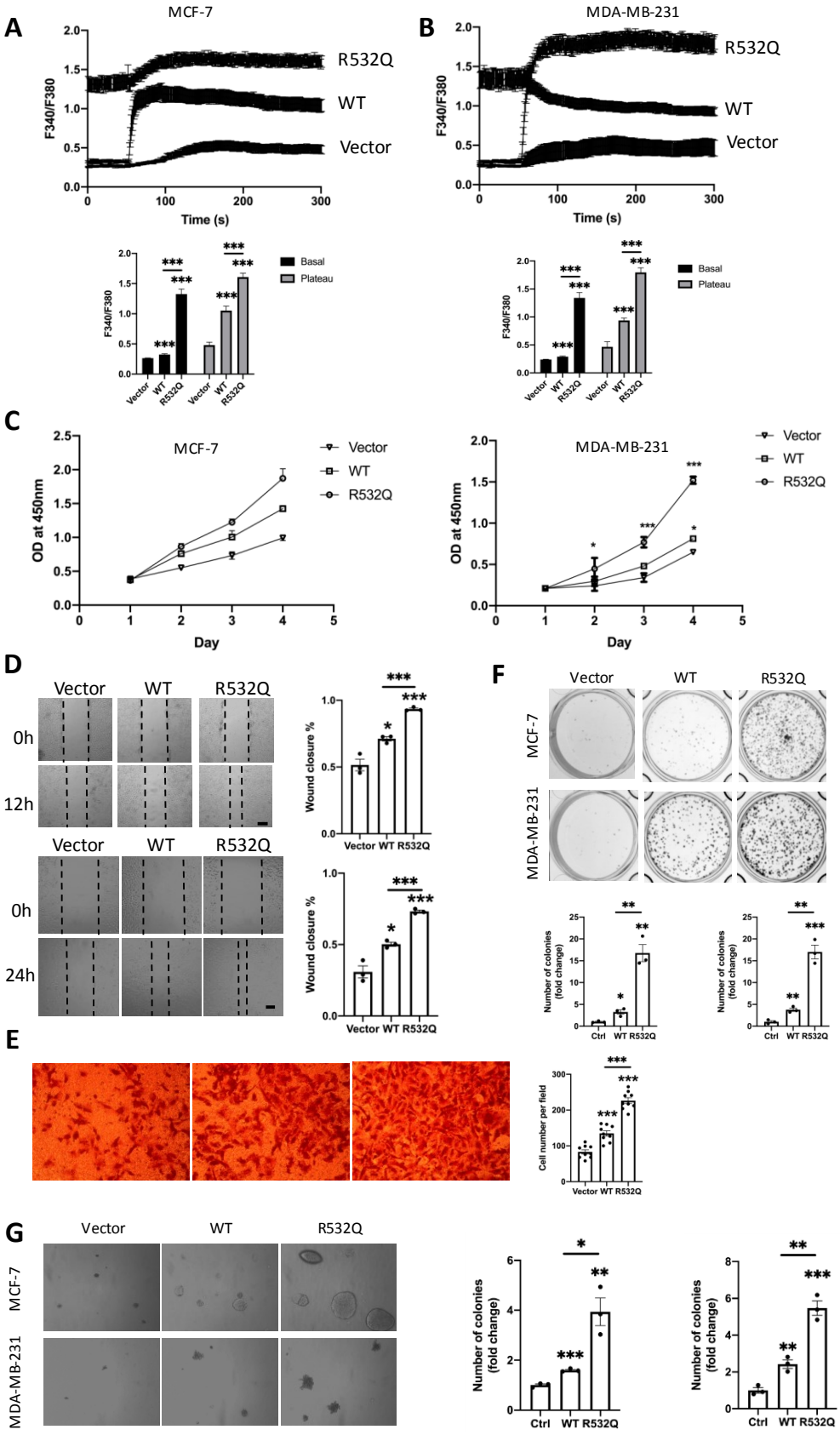
A
MCF-7
R532Q
WT
Vector
F340/F380
Time (s)
Basal
Plateau
B
MDA-MB-231
C
OD at 450nm
Day
D
Vector
WT
R532Q
0h
12h
24h
Wound closure %
E
F
Number of colonies (fold change)
Ctrl
G
Cell number per field

Fig. 4-4. TRPV6 and R532Q mutant promoted the breast cancer progression. *Upper panel*: cytosolic Ca^{2+} measured by Fura-2 AM based Ca^{2+} imaging on MCF-7 (**A**) or MDA-MB-231 (**B**) cells expressing indicated plasmids before and after application of 2 mM Ca^{2+}. Traces are averaged and obtained from 15-19 measurements of 3 independent experiments. *Lower panel*: statistical analysis of averaged basal Ca^{2+} (0 - 50 s) and plateau Ca^{2+} (250 - 300 s) from MCF-7 (**A**) or MDA-MB-231 (**B**) cells measured above. ***, $p < 0.001$. (**C**) Cell proliferation assay on MCF-7 (left) or MDA-MB-231 (right) cells expressing indicated plasmids. *, $p < 0.05$, ***, $p < 0.001$. (**D**) Representative images showing the migration of MCF-7 (upper) or MDA-MB-231 (lower) cells expressing indicated plasmids and statistical analysis on the wound closure. *, $p < 0.05$, ***, $p < 0.001$. *Scale bar* 40 um. (**E**) Representative images showing colony formation of MCF-7 (upper) or MDA-MB-231 (lower) cells expressing indicated plasmids and statistical analysis on the number of colonies formed. (**F**) Representative images showing invasion of MDA-MB-231 cells expressing indicated plasmids and statistical analysis on the number of cells invaded. (**G**) Representative images showing anchorage-independent colony formation of MCF-7 (upper) or MDA-MB-231 (lower) cells expressing indicated plasmids and statistical analysis on the number of colonies formed in soft agar. *, $p < 0.05$; **, $p < 0.01$; ***, $p < 0.001$.

R532Q mutant promoted breast cancer cell EMT and inhibited apoptosis through Ca^{2+} and the PI3K/Akt/GSK3β pathway

The expression of WT and R532Q mutant was detected in transfected xx and xx cells with no detectable TRPV6 in the control cells (Fig. 4-5A). We investigated possible involvement of the central/governing PI3K/Akt/GSK-3β pathway in the regulation of cancer cell progression by TRPV6. The activated (or phosphorylated) Akt (p-Akt) level and its phosphorylated downstream factor p-GSK-3β were higher in R532Q-expressing cells than those in cells expressing WT TRPV6, which were higher than that in control cells (Fig. 4-5A-C). p-GSK-3β is known to inhibit EMT marker SNAI1, a transcription

factor, that inhibits E-cadherin and stimulates the vimentin (Beurel et al., 2015). Consistently, we observed more increased SNAI1 and vimentin and more decreased E-cadherin by R532Q than by WT TRPV6 (Fig. 4-5A-C). Also consistently, increased p-GSK-3β attenuated the degradation of anti-apoptotic marker MCL1 (Fig. 4-5A-C), a factor important for cell viability. To summarize, the TRPV6 expression up-regulated EMT and cell viability through a PI3K/Akt/GSK-3β pathway and GOF mutant R532Q exhibited stronger effects than WT TRPV6, suggesting that the TRPV6 channel function plays a central role in the regulation.

As TRPV6 and its mutant R532Q are Ca^{2+}-selective, we next examined the role of Ca^{2+} in the regulation. We found that Ca^{2+} chelator BAPTA-AM completely inhibited the regulation by WT TRPV6 in MCF-7 and MDA-MB-231 cells and also showed partial inhibition in those expressing mutant R532Q (Fig. 4-5D). The inhibitor LY294003 of PI3K, a central regulator of the Akt activity, was able to abolish all the signaling changes induced by expression R532Q (Fig. 4-5D), suggesting that TRPV6 regulates the signaling pathway through PI3K.

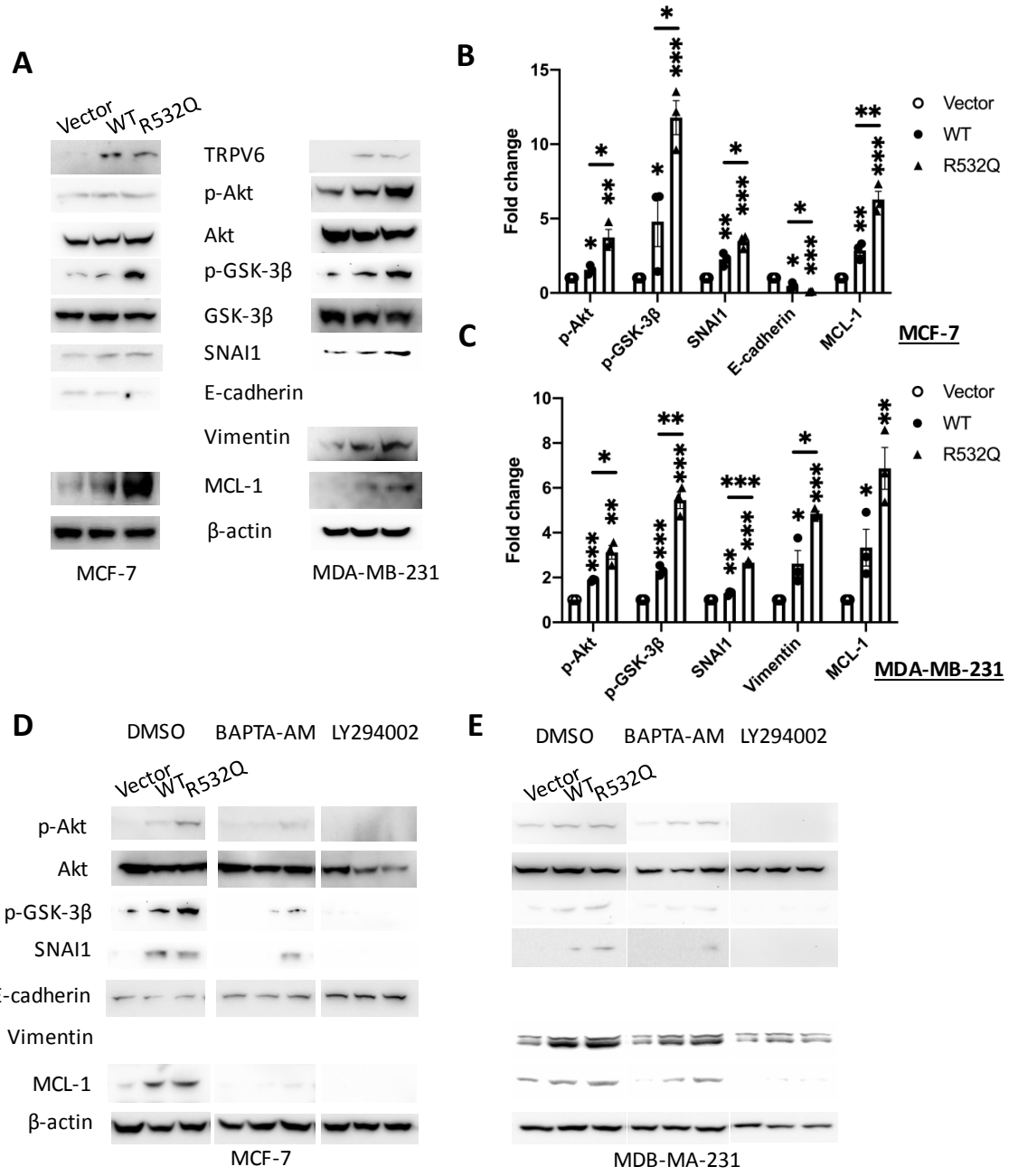

Fig. 4-5. The TRPV6 and R532Q mutant up-regulated the PI3K/Akt/GSK-3β pathway in breast cancer cells, dependent on the cytosolic Ca^{2+} and PI3K activity. (**A**) Representative Western blotting images for EMT and anti-apoptotic markers from MCF-7 (left) and MDA-MB-231 (right) cells expressing indicated plasmids. Statistical analysis of expression of indicated markers from MCF-7 (**B**) and MDA-MB-231 (**C**) cells expressing indicated plasmids. Representative images of indicated markers from

MCF-7 (**D**) and MDA-MB-231 (**E**) cells expressing indicated plasmids, treated with DMSO, BAPTA-AM or LY294002.

WT and R532Q mutant interacted with p85

PI3K is composed a catalytic p110 and an inhibitory p85. P85 is known to interact with various membrane proteins, be recruited to the membrane by interacting receptors or adaptors, and in turn activate p110 leading to activated PI3K (Yu et al., 1998). Stably expressed TRPV6 in MDA-MB-231 cells interacted with the native p85 in a Ca^{2+}-dependent manner and the R532Q mutation enhanced the interaction (Fig. 4-6A and B). Consistently, the expression of the membrane-recruited p85 was positively correlated with the channel activity of TRPV6, using cells expressing WT or mutant R532Q or control cells (Fig. 4-6C). To dissect the p85 domain responsible for the TRPV6-p85 interaction, we generated four p85 truncation mutants and a TRPV6 mutant. By co-IP we found the nSH2 and cSH2 domains as part of the TRPV6-binding cassettes in p85 and the TRPV6 N-terminus (TRPV6-N) to be involved in p85-binding (Fig. 4-6D and E). Purified fragments of p85 nSH2 and cSH2 and TRPV6-N were used for *in vitro* binding and we found confirmed the presence of the TRPV6-N-nSH2 and TRPV6-N-cSH2 interaction (Fig. 4-6F). To test the role of TRPV6-p85 interaction in the regulation of the signaling we utilized domain nSH2 as a blocking peptide to competitively disrupt the TRPV6-p85 binding. The expression of the EMT markers and anti-apoptotic MCL-1 were significantly reversed by nSH2 in WT- and R532Q-expressing cells (Fig. 4-6G).

These results together supported the concept that TRPV6 up-regulates EMT and inhibits apoptosis through physical interaction with domains nSH2 and cSH2 of p85, by which it recruits p85 to the surface membrane thereby activating PI3K.

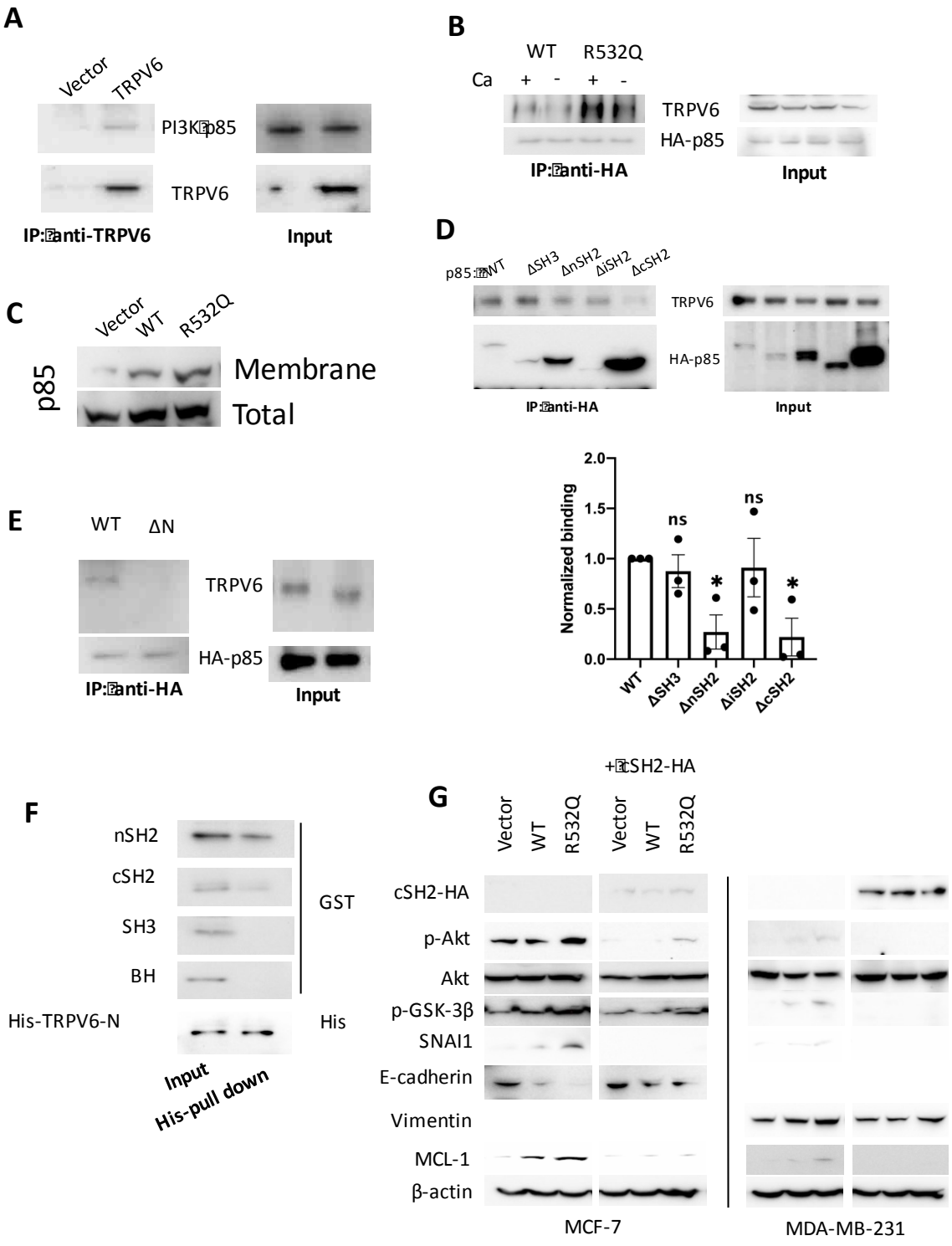

Fig. 4-6. TRPV6 and R532Q recruited p85 to activate the PI3K/Akt/GSK-3β pathway in breast cancer cells. (**A**) Representative images showing TRPV6 interacts with endogenous p85 by co-IP in

MDA-MB-231 cells. (**B**) Representative co-IP images of TRPV6 or R532Q mutant binding to p85-HA without (1 mM EGTA) or with (0.1 mM Ca^{2+}) Ca^{2+} in MDA-MB-231. (**C**) Total and membrane bound p85 in MDA-MB-231 cells transfected with indicated plasmids. (**D**) *Left panel*: representative data showing TRPV6 interacts with full-length or indicated truncations of p85 in MDA-MB-231 cells. *Right panel*: three independent experiments in above panel were quantified and analyzed. (**E**) Representative co-IP data of TRPV6 WT or ΔN interaction with p85 in MDA-MB-231 cells. (**F**) Representative *in-vitro* binding data of purified His-TRPV6-N binding to the indicated peptide. (**G**) Representative Western blotting data showing the effect of c-SH2-HA in the MCF-7 (left) and MDA-MB-231 (right) cells.

Expression of *TRPV6* was inversely correlated with the survival of breast cancer patients

The *TRPV6* mRNA expression and survival rates of breast cancer patients were examined by analyzing published breast cancer patient databases (Gyorffy et al., 2010) to further explore the clinical relevance of our present study. For all breast cancer types, the analysis showed a significant correlation between high *TRPV6* expression and poor overall survival (HR = 1.58, 1.25 - 1.99; p = 8.8e-05) and relapse-free survival (HR = 1.45, 1.29 - 1.63; p = 6.9e-10) with a 95% confidence interval (Fig. 4-7A). Specifically, a previous study suggested that patients with ER^- breast cancer have higher expression of *TRPV6* than that in patients with ER^+ breast cancer (Peters et al., 2012). Here, we also analyzed the expression of *TRPV6* in ER^- breast cancer patients and found that high *TRPV6* is significantly correlated with poor overall survival (HR = 1.92, 1.25 - 3.04; p = 0.0042) and relapse-free survival (HR = 1.31, 1.04 - 1.64; p = 0.019) with a 95% confidence interval (Fig. 4-7B). These significant clinical correlations between the

TRPV6 expression and survival found in all types and ER^- subtype of breast cancer patients are consistent with our functional data obtained using electrophysiology in cell models.

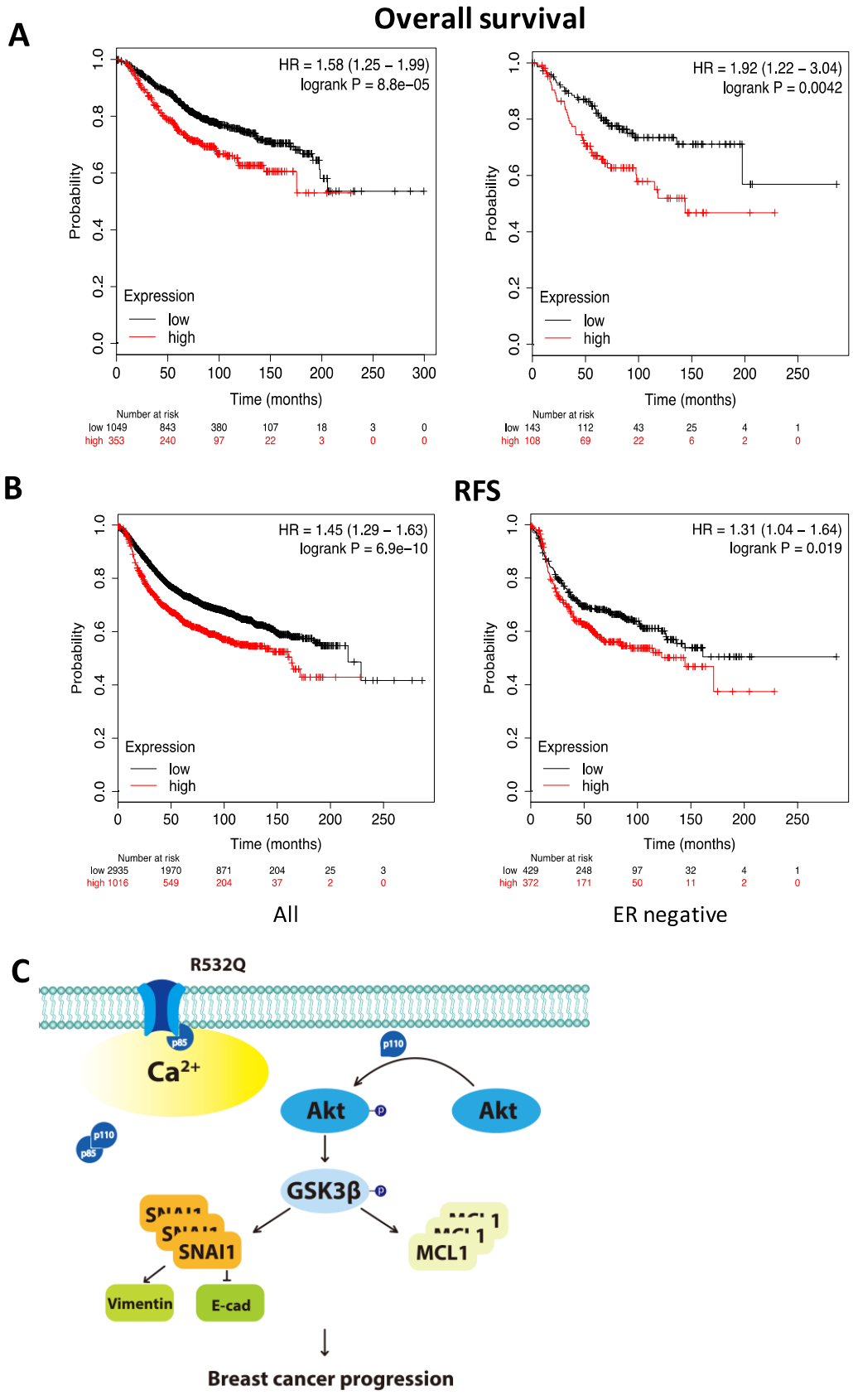
A
Overall survival
HR = 1.58 (1.25 – 1.99)
logrank P = 8.8e–05
Probability
Expression
low
high
Time (months)
Number at risk
low 1049 843 380 107 18 3 0
high 353 240 97 22 3 0 0
HR = 1.92 (1.22 – 3.04)
logrank P = 0.0042
Number at risk
low 143 112 43 25 4 1
high 108 69 22 6 2 0
B
RFS
HR = 1.45 (1.29 – 1.63)
logrank P = 6.9e–10
Number at risk
low 2935 1970 871 204 25 3
high 1016 549 204 37 2 0
All
HR = 1.31 (1.04 – 1.64)
logrank P = 0.019
Number at risk
low 429 248 97 32 4 1
high 372 171 50 11 2 0
ER negative
C
R532Q
p85
p110
Ca2+
Akt
GSK3β
SNAI1
MCL1
Vimentin
E-cad
Breast cancer progression

Fig. 4-7. *TRPV6* gene expression correlated with survival in breast cancer patients. Overall survival (**A**) or relapse-free survival (**B**) of all types of (left) or ER- (right) breast cancer patients analyzed by Kaplan–Meier plots. Hazard ratios (HR) and p values are indicated. (**C**) Schematic diagram of the proposed mechanism on R532Q GOF. (**D**) The diagram showing hypothetical mechanism of R532Q contribution to breast cancer progression.

4.5 DISCUSSION

As one of the two most Ca^{2+}-selective channels in the TRP channel superfamily, TRPV6 has been known for its physiological importance for transcellular Ca^{2+} absorption in multiple tissues. Malfunction due to mutations or altered expression of TRPV6 has been clinically linked to human breast cancer and many other diseases. Despite of the vital physiological and pathological roles TRPV6 plays, the mechanisms underlying its channel gating and oncogenic effects have not been well understood. Here we set out to characterize a novel autoinhibitory S5/S6 interaction mediated by residue R532 within proximal S5 paired with D620 within distal S6, by means of electrophysiology, protein-protein interaction and MD simulations. Further, using MDA-MB-231 and MCF-7 human breast cancer cell lines, we identified the oncogenicity of TRPV6 and GOF mutant R532Q that was predicted by be pathogenic. Specifically, we found that the TRPV6 function promotes cell viability, migration and invasion via increased cytosolic Ca^{2+} and interaction with p85 to activate the PI3K/Akt/GSK-3β pathway thereby mediating the regulation of EMT and anti-apoptotic markers. These novel findings are important mechanistic understanding of the TRPV6 channel gating and its oncogenicity in human breast cancer.

All TRP channels adopt tetrameric structures and show a domain swapping arrangement in which S5 and S6 helices of a subunit together stay close to the S1-S4

helices from an adjacent subunit, an arrangement shared by voltage-gated channels (Cao, 2020). Based on close proximity between S5 and S6 helices, a structural study previously proposed that a hydrogen bond could be formed between D529 in S5 helix and T621 in S6 helix of human TRPV6 (McGoldrick et al., 2018), and found that alanine substitution at T621 (T621A) leads to LOF (Hofmann et al., 2017). Thus, the D529-T621 interaction, which was however not observed in the closed state structure of TRPV6 (McGoldrick et al., 2018), was thought to maintain its open state in the absence of functional evidence. Distinct from this interaction, the S5/S6 helix interaction mediated by R532-D620 that we revealed was autoinhibitory for the TRPV6 channel function. The R532:D620 distance revealed by structures of TRPV6 showed that $D_{open} > D_{closed} > D_{2\text{-}ABP\ inhibited}$ (D, distance; Fig. S2), which is consistent with our proposed S5/S6 helix interaction model. Comparisons of potential S5/S6 helix interactions in available TRPV1, -V2 and -V3 structures under apo or ligand binding (open/activated) states show a similar correlation between the distance and channel activity, ie, $D_{open/agonist} > D_{closed/apo}$ (Fig. S2). Of note, the S5/S6 helix interaction was not observed in the TRPV6 structures, since the distance between R532 and D620 is 4.2 Å, longer than the distance 4 Å required to form a salt bridge. However, as TRPV6 structures are snapshots of a static channel embedded in non-living cell conditions, they may not be able to thoroughly reflect the dynamics of TRPV6 channel during physiological gating cycles on the living cell membrane. Our data obtained using systematical mutagenesis and electrophysiology indicated that a

functionally critical S5/S6 helix interaction mediated by the R532 and D620 pair should be present under living cell conditions (Fig. 4-1 and 4-2). The physical interaction between S5 and S6 helices was also proved by two independent methods (Fig. 4-1 and 4-2), in which both R532 and D620 were required for the physical interaction. Furthermore, the presence of a salt bridge between R532 and D620 in WT, but not mutant R532Q, TRPV6 was nicely supported by MD simulations (Fig. 2). Together we would like to propose that the S5/S6 helix interaction acts as an autoinhibitory switch which is critical to maintain the low levels of the TRPV6 channel function under basal physiological conditions.

From the sequence alignment, the R532 in S5 helix and D620 in S6 helix are highly conserved across species and within the TRPV subfamily (Fig. S1), which indicates the potential importance of these two residues in evolution for all TRPV members. Although the amino acid sequences of TRP channel varies a lot among the 28 members, we also found corresponding conserved candidate residues in the proximal part fo S5 helix and distal part of S6 helix in all the TRPA, -P, -M, -C and -ML subfamilies (Fig. S1). But whether these residues actually play roles in channel gating require future studies. Thus far, TRPV6 is the first channel in the TRP superfamily to be known of possessing an autoinhibitory S5/S6 helix interaction. Similar S5/S6 helix interaction has not been commonly reported for other ion channels, except for voltage-gated potassium channel EXP2 that was known to be functionally regulated by residues G421 in S5 helix and

C480 in S6 helix; the substitution with bulky amino acids (Trp, Tyr and Phe) resulted in constitutive opening of the channel in *Xenopus* oocytes (Espinosa et al., 2001).

According to the cancer database COSMIC, there are 565 coding mutations identified in the *TRPV6* gene distributed in tissues including but not limited to breast, intestine, liver, lung, skin, stomach, and urinary tract by massive genomic sequencing, while more mutations may be revealed by future studies (Tate et al., 2019). Nonetheless, the importance of the identified mutations has not yet been determined. The GOF mutant R532Q characterized here was previously predicted to be pathogenic and found in the endometrium and skin, however without any investigation. HEK293 cells transiently transfected with the D620V mutant were previously found to have significantly higher cytosolic Ca^{2+} concentrations as determined by ratiometric Ca^{2+}-imaging (Hofmann et al., 2017), but no further experiment was performed and the underlying mechanism was not examined. The results here validate that the predicted-pathogenic R532Q mutant potentially promotes breast cancer progression and that D620V possibly disrupts the R532:D620 salt bridge thereby breaking down the S5/S6 helix interaction leading to GOF of the channel. Mutations found in TRPV6 channel have also been clinically linked to another human disease, with impaired maternal-fetal Ca^{2+} transport in placenta named TNHP. The TRPV6 proteins harboring these mutations become unstable, located in S2 helix, S3 helix and cytosolic S2-S3 loop and N-termini of TRPV6 channel (Suzuki et al., 2018). Besides, the TRPV6 channel function contributes to dietary Ca^{2+} absorption in the

intestine and stone formation in the kidney. Genomic sequencing on the *TRPV6* gene in patients with kidney stone showed that the occurrence of a triple mutation, C157R/M378V/M681T, is significantly higher than that in people without kidney stone (Suzuki et al., 2008). Calcium uptake analysis on the mutant expressing *Xenopus* oocytes suggested that it is a GOF mutant with unclear mechanism.

After the cloning of TRPV6 channel, higher mRNA expression of it was first found in biopsy samples from prostate cancer patients compared to normal tissues by in situ hybridization and quantitative PCR (Peng et al., 2001; Wissenbach et al., 2001). Subsequent studies gradually found that in addition to prostate cancer, TRPV6 was also found to be overexpressed in breast, colon, ovary, thyroid cancers. The mechanism of how TRPV6 contributes to prostate cancer has been well described, namely, through an NFAT or Orai1/Annexin/S100A11 pathway to regulate the expression of TRPV6 protein. The up-regulated TRPV6 therefore promote prostate cancer (Lehen'kyi et al., 2007; Raphael et al., 2014). In contrast, the underlying details on how TRPV6 promotes breast cancer are poorly documented, except for the potential importance of cytosolic Ca^{2+} increase due to the TRPV6 channel (Peters et al., 2012). In a TRPV6 highly expressed breast cancer cell line T47D, treatment of ER antagonist tamoxifen was found to inhibit TRPV6 channel function and impair the cell viability via a TRPV6 dependent way (Bolanz et al., 2008), which was later reported to be ER independent using MCF-7 and MDA-MB231 cells transfected with TRPV6 (Bolanz et al., 2009). The presence of

TRPV6 indeed is also a prerequisite for the migration and invasion of MDA-MB-231 cells (Jiang et al., 2016). Besides the confirmation of the importance of Ca^{2+} as previously described, our data here for the first time provide strong mechanistic evidence that TRPV6 binds to p85 and activates the PI3K/Akt/GSK-3β pathway, which results in EMT and apoptotic resistance, thereby leading to breast cancer cell progression. Of note, for the colon cancer, the up-regulated TRPV6 expression is not always oncogenic, since the individuals with abundant calcium uptake from the diet have lower risk. Meanwhile, the vitamin D3 was found to up-regulate TRPV6 which contributes to chemoprevention against colon cancer (Lehen'kyi et al., 2012). These observations require further mechanism studies.

4.6 SUPPLEMENTARY INFORMATION

Fig. 4-S1. Sequence alignment of indicated domains across TRP channels with uniprot accession numbers.

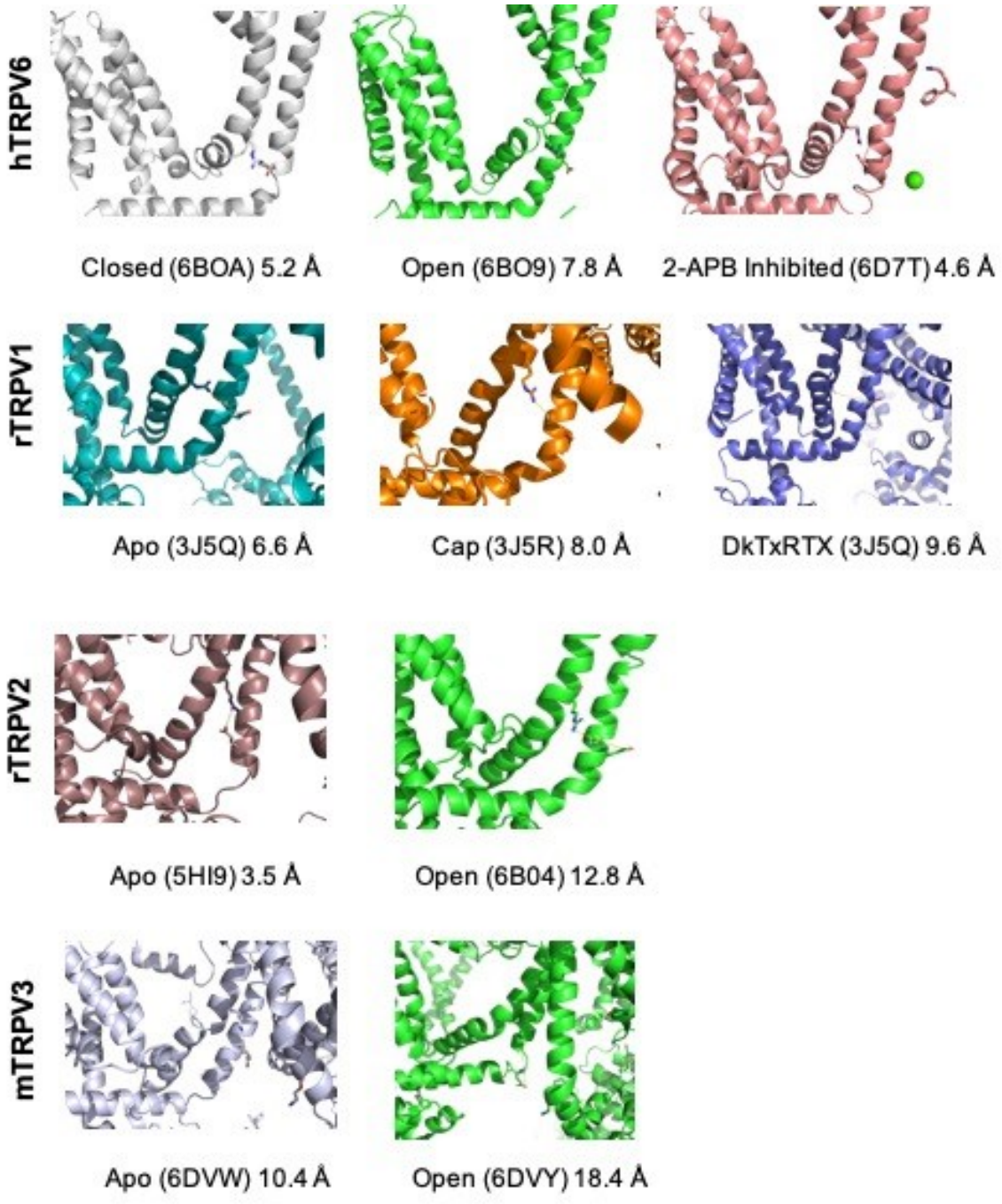

Fig. 4-S2. Structure data of TRPV channels in indicated states showing the distance between R532 and D620 in TRPV6 and corresponding residues in other TRPV channels.

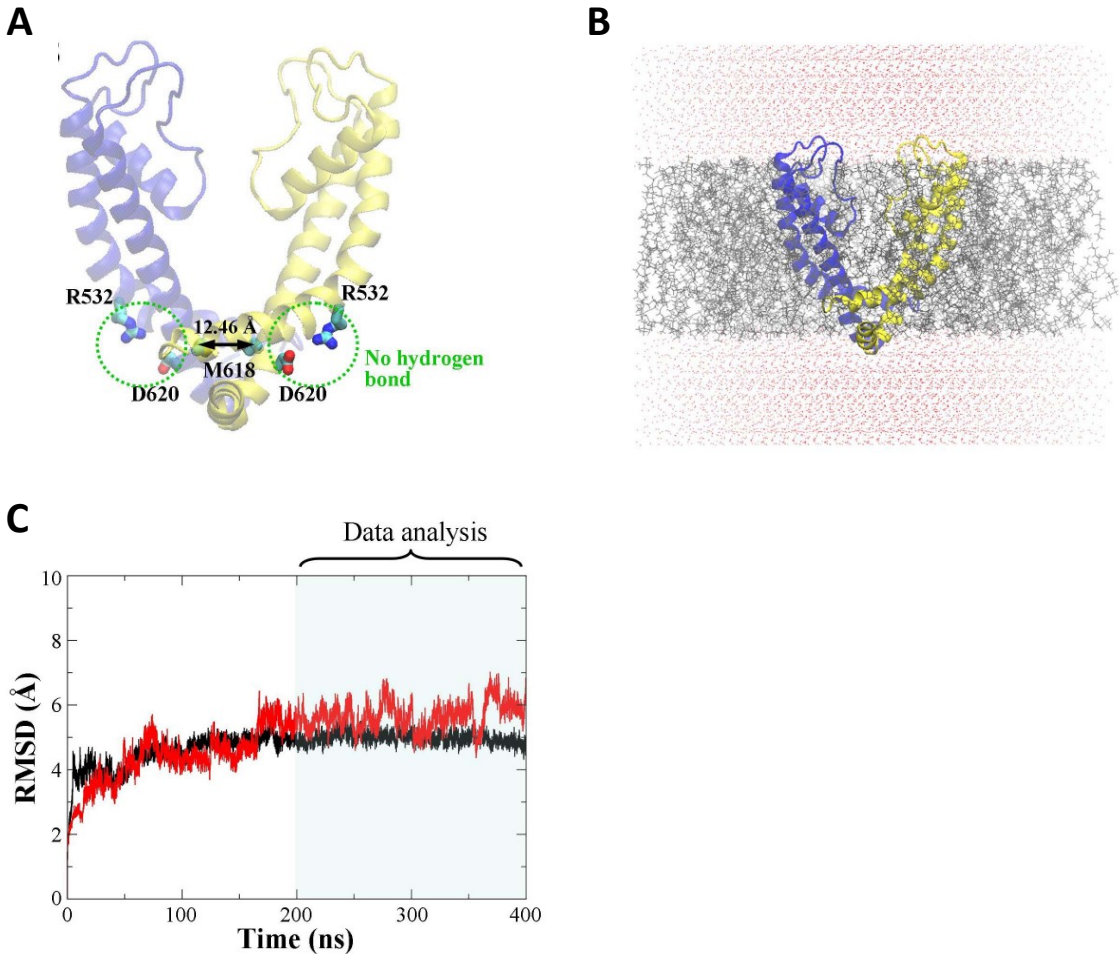

Fig. 4-S3. Initial simulation model and root mean square deviation (RMSD) for the Cα atoms of TRPV6 as a function of time. (**A**) The pore region of TRPV6 (amino acids 511~640) is embedded in a POPC lipid bilayer. For clarity, only the two diagonal monomers are shown. (**B**) In the initial model, the distance between the two diagonal Met618 is 12.46 Å and there is no hydrogen bond between R532 and D620. (**C**) RMSD results show that the simulations got equilibrated after 200 ns, and thus the last 200 ns trajectories are used for data analysis.

CHAPTER 5

RESULTS #4

Hydrophobic gates and proton binding in proton-activated chloride channel

5.1 ABSTRACT

Proton-activated chloride channel (PAC) was recently identified as an evolutionarily conserved chloride channel composed of two transmembrane helices (S1 and S2) and intracellularly localized N- and C-termini. While the PAC has no homology to any known ion channel, it was proposed to be involved in lysosome function, hypoxia adaption, stroke and carcinogenesis. Extracellular protons activate PAC with outward rectification. Given minimal understanding of the function and lack of structural information, the gate and activation mechanisms of PAC remained unknown. By means of two-electrode voltage clamp electrophysiology in *Xenopus* oocytes and based on the hydrophobic gate theory, we here found that at low/high extracellular proton concentrations, hydrophilic substitutions at W304/I307 substantially increase the channel activity. The (lower) pore gate of PAC at the closed state was formed by hydrophobic residue W304 within S2, presumably pointing to the pore center. Upon channel activation by acidification the gate was defined by smaller hydrophobic residue I307, suggesting the presence of S2 twist so that I307 points to the pore center and forms a larger pore. We also identified four conserved protonatable residues located in the extracellular loop critical for proton binding/sensing. Our study depicted a scheme in which proton binding induces conformational changes within PAC, leading to S2 twist thereby enlarging (opening) the pore.

5.2 INTRODUCTION

As the most prevalent extracellular anion, chloride passes biological membranes via chloride transporters or channels, previously classified into six families without apparent sequence homology to each other: anoctamins, bestrophins, ligand-gated anion channels, cAMP-activated chloride channels, volume-regulated anion channels and voltage-gated ClC channels (Duran et al., 2010; Terry, 1994). Chloride channels play key roles in the cell volume regulation, electrical excitability, transepithelial transport and ion homeostasis. Thus, abnormal function of chloride channels may result in channelopathies that include hyperekplexia, epilepsy, osteopetrosis, lysosome storage disorder, neurodegeneration and cystic fibrosis (Planells-Cases and Jentsch, 2009). A chloride channel with acid-induced outward rectification and with characteristics distinct from the known chloride channels remains to be molecularly identified although several previous studies described it in cultured human embryonic kidney cells, sertoli cells, umbilical vein endothelia, hippocampal and cardiac myocytes (Auzanneau et al., 2003; Capurro et al., 2015; Lambert and Oberwinkler, 2005; Ma et al., 2008; Yamamoto and Ehara, 2006). Recently, a proton activated chloride channel (PAC), previously called TMEM206, was identified as a novel anion channel through RNA interference screen (Ullrich et al., 2019; Yang et al., 2019). Enriched expression of PAC in human tissues has been found in cerebral cortex, lymph node, bone marrow, spleen, kidney, lung and bladder via RNA sequencing (Yang et al., 2019). PAC is activated by low extracellular pH, inducing cell

death along with Cl- influx (Yang et al., 2019). Temperature is known to enhance the sensitivity of PAC to protons, with an unclear mechanism (Sato-Numata et al., 2014). Under pathological conditions such as stroke and ischemia reperfusion and acidic environments, PAC may be involved in neuronal cell death. PAC knockout in mice protects brain ischemia-reperfusion caused neuronal death (Yang et al., 2019). As for cell microenvironment, pericellular acidic pH promotes cancer cell migration and invasion, while acidosis impairs immunological functions and is associated with immunodeficiency (Lardner, 2001). Of note, genomic sequencing in both Tibetans and Tibetan swines revealed that PAC genomic region exhibits one of the strongest increases in the allele frequencies, suggesting a underlying role of PAC in adaption to hypoxia (Dong et al., 2014; Yi et al., 2010).

PAC is predicted to contain two hydrophobic membrane-spanning segments (S1 and S2), a large extracellular loop as well as the cytosolic N- and C-termini (Ullrich et al., 2019). Using cysteine mutation scanning, the second transmembrane helix S2 (N302-F318 in human PAC) was suggested as a pore-forming domain (Ullrich et al., 2019; Yang et al., 2019). Given no sequence similarity to the known channels and lack of structural information, the gate(s) of PAC has yet to be investigated. We recently documented a hydrophobic gate mechanism in seven members within the transient receptor potential (TRP) superfamily of cation channels that adopt a single- or double-consecutive-residue gate (Zheng et al., 2018b; Zheng et al., 2018c) in the

pore-lining S6 helix. According to the hydrophobic gate theory, a pore composed of an hydrophobic amino acid(s) forms an energetic barrier that allows effective control of ion permeation (Aryal et al., 2015), which have been validated in numerous channels by structural, electrophysiological or molecular dynamic studies (Aryal et al., 2015). It thus remains to be determined as to what forms a PAC pore gate.

Proton-induced PAC activation has been linked to acidosis-related cell death in the brain or heart during stroke or ischemic damage, and extensively described before its molecular identification. The half maximum activation is around pH 5.0 with a best-fit Hill coefficient of 3.6, suggesting that more than one proton ion cooperatively binds to activate PAC (Lambert and Oberwinkler, 2005). The newly discovered PAC protein sequence allows examination of the proton binding sites. Insensitivity of the PAC outward rectifying current to intracellular pH buffering suggests that the residues involved in proton sensing or binding are located in the extracellular loop.

In the present study we examined the PAC gate residue(s) and those involved in proton binding using the two-electrode voltage clamp in *Xenopus* oocytes, mutagenesis and immunofluorescence. We also examined by flow cytometry the effect of a gain-of-function mutant PAC on the death of human embryonic kidney (HEK) 293 and a widely used neuronal cell model human SH-SYSY cells. Characterization of the PAC gate residues and proton binding sites would be of great importance for understanding the

mechanism underlying the channel function as well as its physiological and pathological roles.

5.3 METHODS

Plasmids, mutagenesis, antibodies and cell lines

Plasmid encoding mouse PAC (NM_025864) with Flag and Myc tags in the pCMV vector was purchased from OriGene (Rockville, MD). Mutations were introduced using Q5 site-directed mutagenesis kit (New England Biolabs, Ipswich, MA) and confirmed by sequencing. Flag, Myc and β-actin antibodies were from Cell Signaling Technology (Danvers, MA) or Santa Cruz Biotechnology (Dallas, TX). Anti-rabbit and anti-mouse secondary antibodies were from GE Healthcare (Waukesha, WI). Human neuroblastoma cell line SH-SY5Y was a gift from Dr. Thomas Simmen (University of Alberta).

Expression in *Xenopus* oocytes

mMESSAGE mMACHINE T7 transcription kit (Invitrogen, Waltham, MA) was used to generate capped RNAs encoding WT and mutant PAC. 25 ng cRNA was injected into each oocyte as previously described (Wang et al., 2018). Water-injected oocytes were served as control. Injected oocytes were cultured at 18℃ for 2-3 days until experiments. The present study was approved by the Ethical Committee for Animal Experiments of the University of Alberta and carried out in accordance with the Guidelines for Research with Experimental Animals of the University of Alberta and the Guide for the Care and Use of Laboratory Animals (NIH) revised in 1996.

Two-electrode voltage clamp electrophysiology

Two capillary pipettes (Warner Instruments, Hamden, CT) with a tip resistance of 0.3-2 MΩ and filled with 3 M KCl were used to penetrate an oocyte. Oocyte whole-cell currents were recorded at RT and perfused with extracellular solutions described in figure legends. Currents and voltages were digitized at 200 μs/sample and Bessel filtered at 2 kHz, with a Geneclamp 500B Amplifer and Digidata 1322A AD/DA converter (Molecular Devices, Union City, CA). I-V curves were obtained by application of a ramp protocol with voltages from -100 mV to + 100 mV during 1 s. Oocytes were bathed in a pH 7.5 (or 4.5) solution composed of (in mM) 100 NaCl, 2 KCl, 1 $MgCl_2$ and 10 HEPES with pH adjusted by NaOH (or 5 Na3-citrate with pH adjusted by citrate acid). Resulting data were analyzed with pClamp 9 (Axon Instruments, Union City, CA) and plotted with GraphPad Prism 8 (GraphPad Software, San Diego, CA).

Immunostaining

Whole mount oocytes were washed with PBS and fixed with 4% paraformaldehyde at RT for 15 min. After permealization with 0.1% Triton for 5 min, oocytes were incubated with 3% skim milk for 30 min. Diluted Flag antibody was used to incubate oocytes at 4°C overnight, which were next incubated with secondary anti-mouse IgG Fab2 Alexa Fluor 555 (Cell Signalling Technology) for 1 hr at RT. Oocytes were mounted

with Fisher Chemica Permount mounting medium (Fisher Scientific) and examined under Olympus IX-81 spinning confocal microscope (Cell Imaging Centre, Faculty of Medicine and Dentistry, University of Alberta). Mammalian cells for immunostaining underwent a similar procedure but were mounted with ProLong Gold Antifade Mountant (Molecular Probes, Life Technologies).

Cell culture and transfection

HEK293 and SH-SY5Y cells were maintained in Dulbecco's modified Eagle's medium with 1% penicillin/streptomycin and 10% FBS (Gibco) in an incubator with 5% CO2. Transient expression of WT aor mutant PAC channel was performed following the FUGENE HD Transfection Reagent manual (Promega, WI).

Acid-induced cell death and flow cytometry

Transfected HEK293 or SH-SY5Y cells were incubated with an acidic or neutral buffer, composed of (in mM) 145 NaCl, 2 KCl, 2 $MgCl_2$, 1.5 $CaCl_2$, 10 glucose and 10 HEPES (for the neutral buffer at pH 7.5, adjusted with NaOH) or 5 Na3-citrate (for the acidic buffer at pH 4.5, adjusted with citric acid) for 2 hr at 37°C. Cells were collected for flow cytometry analysis with eBioscience Annexin V-FITC Apoptosis Detection Kit (ThermoFisher Scientific, Waltham, MA), using Attune NxT cytometer in the Flow Cytometry Facility (Faculty of Medicine and Dentistry, University of Alberta). Cell death

percentage equals to [1- $\frac{n\,(Annexin\,V-FITC^{-}/PI^{-}\,cells)}{n\,(total\,cell)}$] × 100. Dead (non-viable) cells included Annexin V-FITC^{-}/PI^{+}, Annexin V-FITC^{+}/PI^{-} and Annexin V-FITC^{+}/PI^{+} cells.

Immunoblotting and biotinylation

For the total protein expression, oocytes or mammalian cells were lysed using CelLytic MT Cell Lysis Reagent (Sigma, Oakville, ON). Lysates were subjected to SDS-PAGE and immunoblotted using the corresponding antibodies. For the surface expression, oocytes or mammalian cells were bathed with pre-cooled PBS solution and then treated with EZ-Link Sulfo-NHS-SS-Biotin (Pierce, Rockford, IL) at RT. After quenching the extra biotin and washing cells were lysed for Western blot examination.

Data analysis

All data were presented as mean ± SEM (standard error of the mean). P values less than 0.05, 0.01 and 0.001, were assigned with *, ** and ***, respectively and were calculated by Student's t-test. Statistically not significant was abbreviated as 'ns'.

5.4 RESULTS

Identification of hydrophobic gate residue(s)

PAC is closed at neutral extracellular pH and is fully activated when pH decreases to around 4.5 (Yang et al., 2019). Based on the concept of hydrophobic gate, a hydrophobic gate residue from each PAC subunit would together form an energy barrier that allows to control the flow of hydrated ions (Aryal et al., 2015). Replacing hydrophobic gate residue with a hydrophilic or less hydrophobic residue should abolish the hydrophobic barrier and constitutively open the pore at neutral extracellular pH (Aryal et al., 2015). We here examined which hydrophobic residue(s) in helix S2 of PAC (Fig. 5-1A) would result in the channel opening upon hydrophilic substitutions. For this each of the eleven hydrophobic residues was individually mutated to hydrophilic asparagine (N) first and the function of the resulting mutant channels studied using *Xenopus* oocyte expression together with the two-electrode voltage clamp. Eight out of eleven hydrophobic residues are highly conserved across different species (Fig. 5-1A). By biotinylation, Western blotting and immunofluorescence we found that the surface expression of these mutants is similar to that of wild-type (WT) channel (Fig. 5-S1). Mutant W304N but not the wild-type (WT) or any other mutant channels exhibited constitutively open channel activity at extracellular pH 7.5 (Fig. 5-1B and C). Interestingly, unlike WT PAC, the activity of mutant W304N only slightly increased when pH dropped from 7.5 to 4.5 (Fig.

5-1D). In particular, at +80 mV, the W304N mutant activity remained unchanged between pH 7.5 and 4.5 (Fig. 5-1E). These data suggest that highly conserved hydrophobic residue W304 acts as a gate, preventing hydrated Cl- permeation at neutral extracellular pH.

We next examined the channel activity (proton induced chloride current) of the 11 mutants at extracellular pH 4.5 and found that mutant I307N exhibits much higher channel activity than that of WT PAC while the other 10 mutants have similar activity as WT channel (Fig. 5-1F). These data indicate that at the activated state in the presence of pH 4.5 the highly conserved hydrophobic residue I307 acts as the "open gate", which is in contrast to W304 acting as the "closed gate" (at neutral pH), suggesting the presence of S2 twist upon channel activation so that the gate residue changes from W304 to I307.

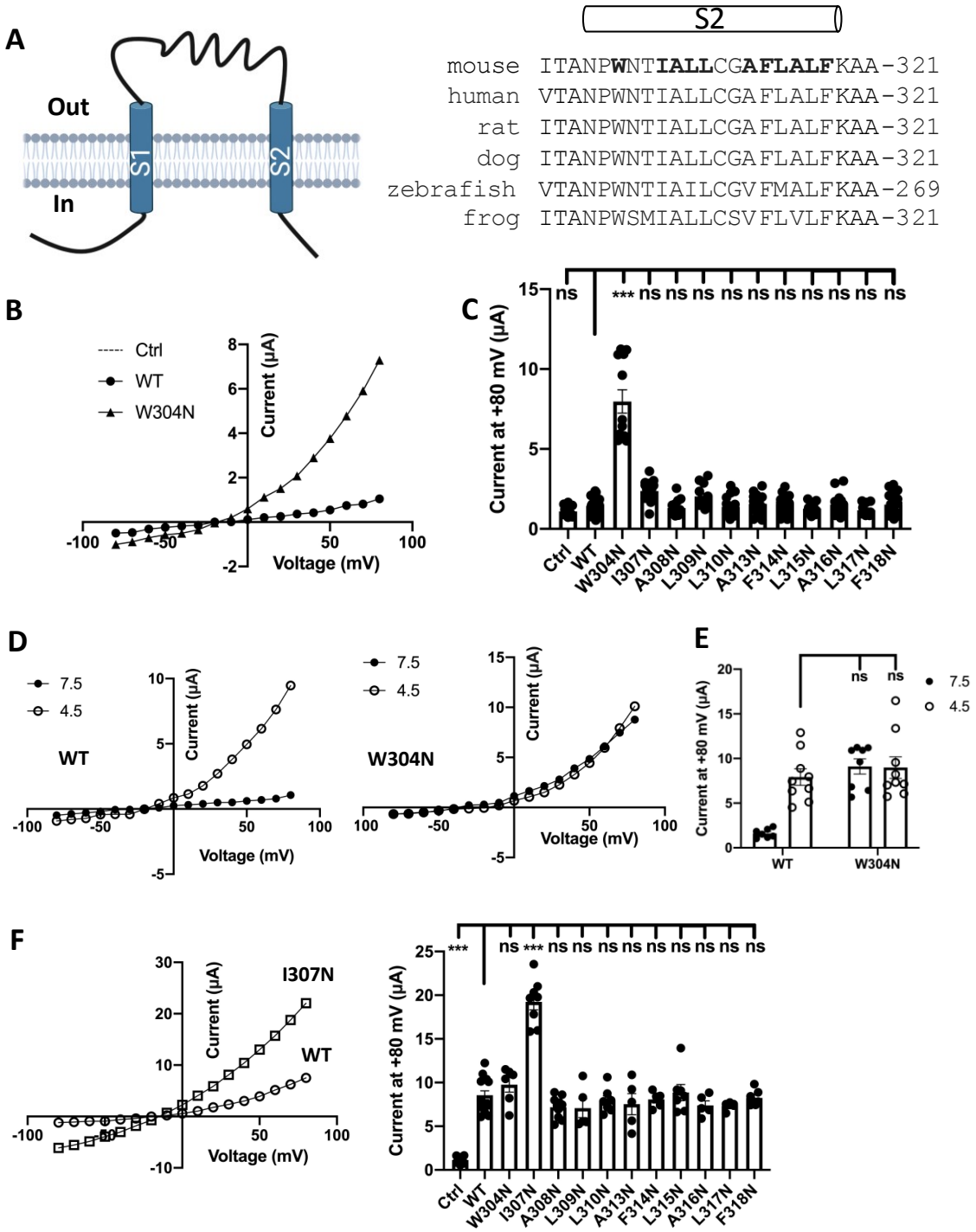

Fig. 5-1. Effects of hydrophobic residues within helix S2 on the PAC function. (**A**) Left panel: topology of the PAC. Right panel: sequence alignment of the PAC S2 helix across species. (**B**) Representative I-V curves obtained from oocytes expressing WT PAC, mutant W304N or from water-injected oocytes (Ctrl)

bathed with the pH 7.5 solution (see Methods). (**C**) Bar charts of averaged currents at +80 mV from oocytes expressing WT or mutant PAC, as indicated. ***, $p < 0.001$; ns, not significant compared with WT PAC. (**D**) Representative I-V curves obtained from oocytes expressing WT PAC (left) or mutant W304N (right) at pH 7.5 (filled circle) or pH 4.5 (open circle). (**E**) Averaged currents obtained from WT PAC or W304N expressing-oocytes at pH 7.5 or 4.5. (**F**) Left panel: representative I-V curves corresponding to WT channel (open circle) or I307N (open square) at pH 4.5. Right panel: averaged currents for water-injected, WT PAC or an indicated mutant at pH 4.5.

Correlation between hydrophobicity of the gate residue and the channel function

To further understand the importance of gate hydrophobicity for the channel function we replaced W304 or I307 with different hydrophobic or hydrophilic residues. For the closed gate W304, mutation to hydrophilic Q, N, S, T or less hydrophobic G or A constitutively opened the channel at high pH (pH 7.5), while mutation to other hydrophobic residues did not open the channel, after considering (normalizing by) their surface membrane expression determined with biotinylation (Fig. 5-2A-C). Thus, the PAC activity at high pH (7.5) inversely correlated with the hydrophobicity of the closed gate (site 304 in S2) (Fig. 5-2B). Similarly, the PAC activity at low pH (4.5) inversely correlated with the hydrophobicity of the open gate (site 307 in S2) (Fig. 5-2D-F).

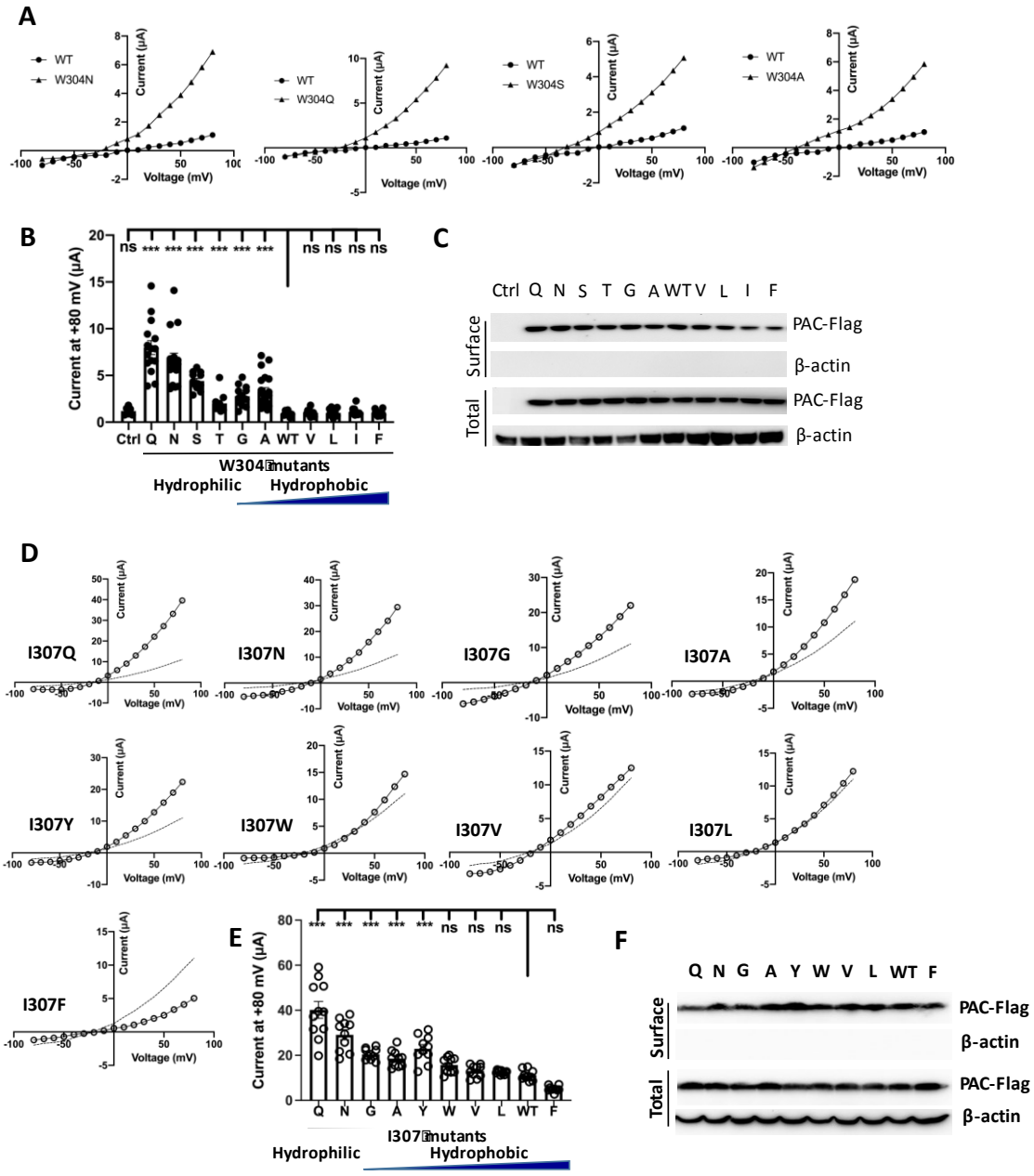

Fig. 5-2. Effects of the hydrophobicity at sites 304 and 307 on the PAC function. (**A**) Representative I-V curves obtained from oocytes expressing a W304 mutant at pH 7.5, in comparison with WT PAC. (**B**) Averaged currents at +80 mV obtained from oocytes expressing WT PAC or a W304 mutant or water-injected oocytes at pH 7.5. ***, $p < 0.001$; ns, not significant compared with WT PAC. (**C**) Total and surface expression of PAC-Flag or β-actin in oocytes similarly prepared as in panel B. (**D**) Representative I-V curves from oocytes expressing a I307 mutant at pH 4.5, in comparison with WT channel in dashed

lines. (**E**) Averaged currents at +80 mV obtained from oocytes expressing WT or a I307 mutant at pH 4.5. (**F**) Total and surface expression of PAC-Flag or β-actin in oocytes similarly prepared as in panel E.

We next investigated the relation between the two gate residues. Hydrophilic mutation to Q or N was introduced at both W304 and I307. Different from single mutants at 304 or 307, double mutants W304Q/I307Q and W304N/I307N exhibited both the constitutive open channel activity at pH 7.5 and significant activity increase upon extracellular acidification, ie, they possess an 'additive effect' of the single mutants (Fig. 5-3). Together, these data supported that W304 and I307 as closed and open gates, respectively, can independently exercise their roles at their respective pH.

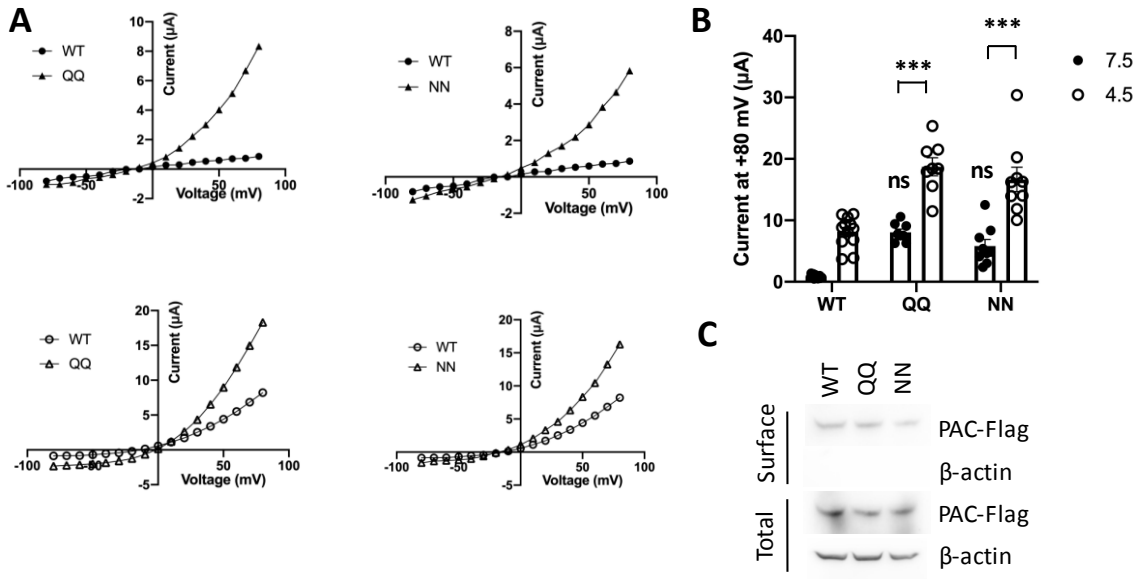

Fig. 5-3. Functional effects of double hydrophilic mutations at W304 and I307. (**A**) Representative I-V curves obtained from oocytes expressing WT, W304Q/I307Q or W304N/I307N at pH 7.5 (filled) or 4.5 (open). (**B**) Averaged currents at +80 mV obtained from oocytes expressing WT or a double mutant at pH

7.5 or 4.5. ***, $p < 0.001$; ns, not significant compared with the WT current at pH 4.5. (**C**) Total and surface expression of PAC-Flag or β-actin in oocytes similarly prepared as in panel B.

Determination of putative proton sensing/binding sites

We reasoned that an amino-acid residue involved in proton sensing or binding would be protonatable in an acidic environment and thus would be either histidine (H), aspartic acid or glutamic acid (Smith et al., 2007). As no known protein shares sequence homology to PAC (Yang et al., 2019), we performed sequence alignment across species and found 17 conserved protonatable residues located in the extracellular or cytosolic domain (Fig. 5-S2). We obtained 17 point mutants by neutralizing each of the 17 residues (H to A, E to Q, and D to N, the latter of which, respectively, is not protonatable at pH 4.5 while retain the size of the reside side chain) and found that mutants H131A, E224Q, D289N and D297N, but not the other mutants, have significantly smaller proton-activated channel activity compared with WT channel (Fig. 5-4A-D), indicating the importance of the four residues for proton-induced PAC activation. Our finding is in fact consistent with previous studies on acid-sensing ion channels (ASICs) showing that a mutant with neutralized proton binding residue requires more acidic pH to be activated (Jasti et al., 2007; Smith et al., 2007).

We next generated a quadruple mutant with all the four residues neutralized (H131A/E224Q/D289N/D297N, briefed as AQNN) to examine the correlation between channel gate and proton activation. Indeed, no significant channel activity of mutant

AQNN was found at pH 4.5 (Fig. 5-4E and F), indicating the loss of proton-induced activation for the mutant. Interestingly, hydrophilic substitution at the closed gate (W304N) of mutant AQNN still constitutively opened the channel. This result indicates that while proton-induced PAC activation requires proton binding and the ensuing conformation changes, constitutive activation/opening through hydrophilic substitutions at the closed gate site (*e.g.*, mutation W304N) does not require proton binding or the associated conformational changes.

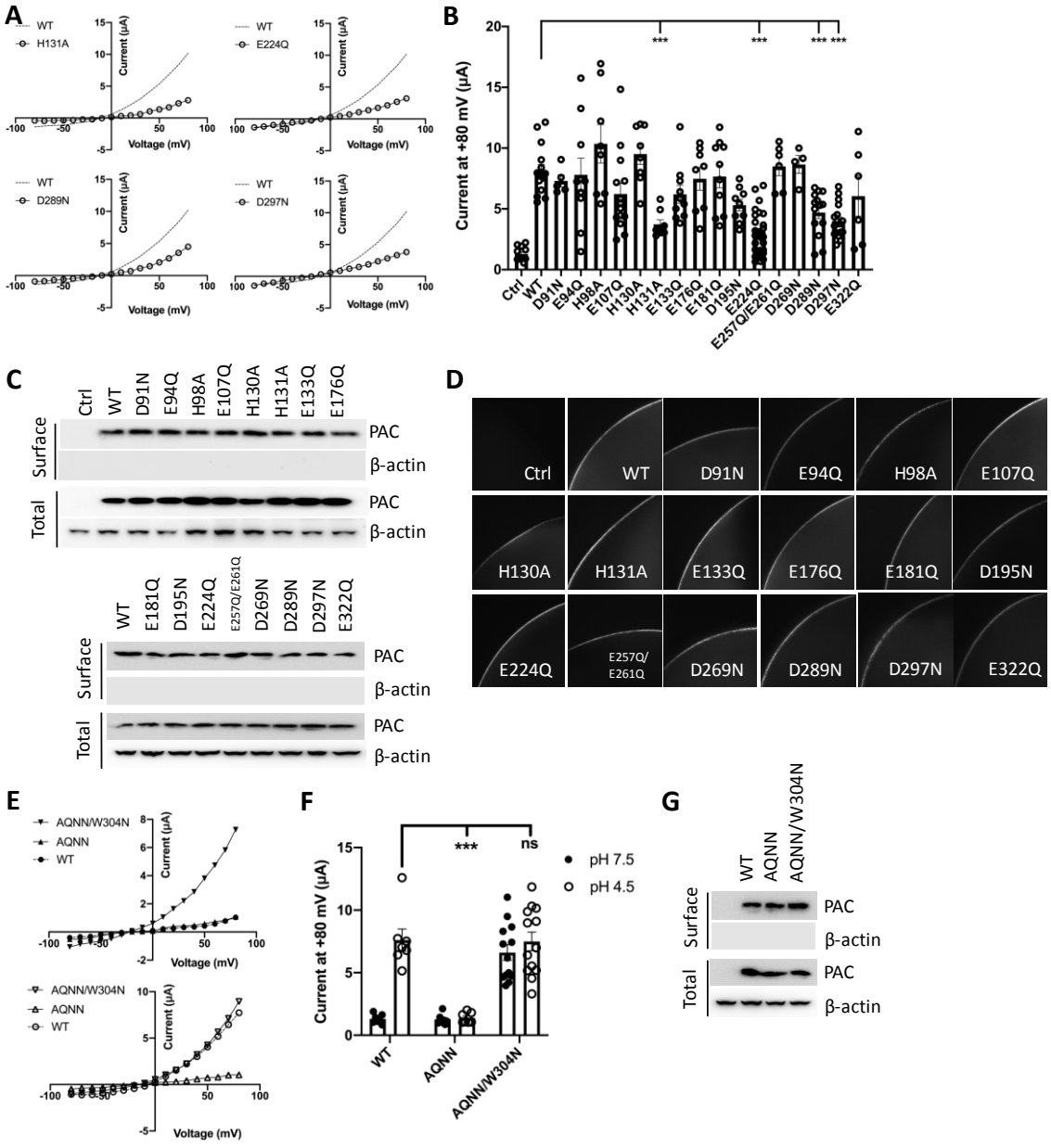

Fig. 5-4. Functional effects of protonatable residues within the extracellular loop of the PAC. (**A**) Representative I-V curves obtained from oocytes expressing WT or mutant PAC at pH 4.5. (**B**) Bar charts showing averaged currents for neutralized mutants, as indicated. ***, $p < 0.001$ by Student's t-test, in comparison with WT channel. (**C**) Total and surface expression of PAC-Flag or β-actin in oocytes similarly prepared as in panel B. (**D**) Representative immunofluorescence images showing the surface expression of WT or mutant PAC. (**E**) Representative I-V curves obtained from oocytes expressing WT, mutant

H131A/E224Q/D289N/D297N (AQNN) or W304N/AQNN at pH 7.5 (filled) or 4.5 (open). (**F**) Averaged currents at +80 mV for indicated mutants. (**G**) Total and surface expression of PAC-Flag or β-actin in oocytes similarly prepared as in panel F.

Constitutive activation of gate mutant W304N demonstrated by its effect on cell death

To further document the constitutive gain-of-function nature of gate mutant W304N, we decided to examine the effect of the mutant on the acid-induced death of cultured HEK and neuronal SHSY-5Y cells. The extracellular acidification was known to cause death of cortical neuron and various cultured cells expressing PAC (Capurro et al., 2015; Ullrich et al., 2019; Yang et al., 2019). Incubation of HEK293 cells at 37°C for 2 hours resulted in similar cell death at pH 7.5 and 4.5 when mutant W304N was expressed while similar extent of cell death was seen at pH 4.5 only (ie, not at pH 7.5) when WT PAC was expressed and no effect of pH was found in control cells (Fig. 5-5A-C). A similar toxic effect of mutant W304N at neutral pH was also observed in SHSY-5Y cells, a widely used *in vitro* neuronal cell model (Cai et al., 2015; Kovalevich and Langford, 2013) (Fig. 5-5D-F). These data were in good support of our biophysical study demonstrating the constitutive channel activation of mutant W304N.

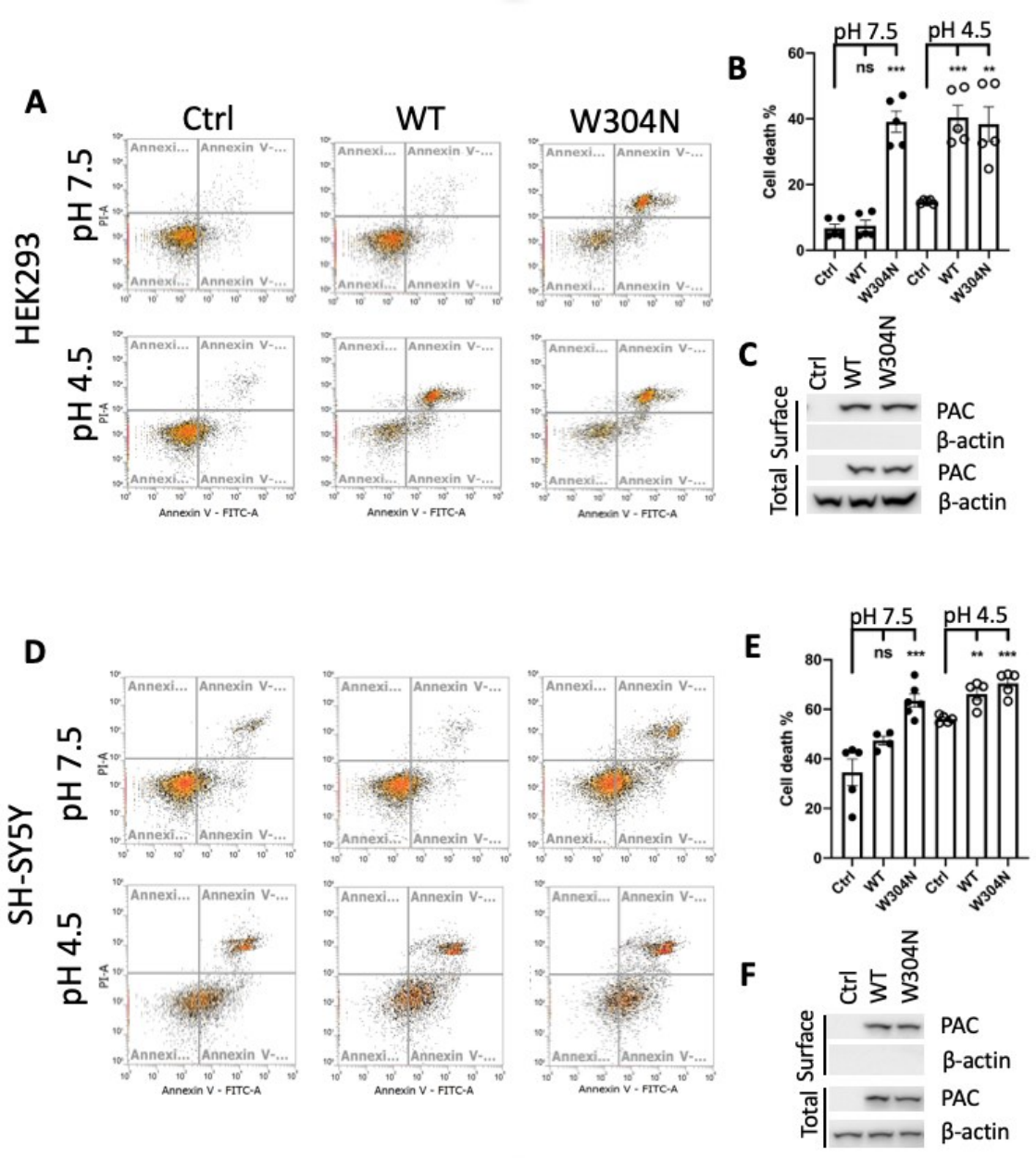

Fig. 5-5. Effect of mutant W304N on the death of HEK293 and SH-SY5Y cells at pH 7.5. (**A**) Representative flow cytometry charts showing the FITC-Annexin/PI distribution of HEK293 cells transfected with plasmids encoding empty vector (Ctrl), WT PAC or mutant W304N at pH 7.5 (upper) or 4.5 (lower). (**B**) Averaged percentages of HEK293 cell death. ns, not significant; ***, $p < 0.001$; **, $p < 0.01$. (**C**) Representative Western blot images showing the total or surface expression of PAC-Flag or β-actin in HEK293 cells. (**D**) Representative flow cytometry charts showing the FITC-Annexin/PI

distribution of SH-SY5Y cells transfected with plasmids encoding empty vector (Ctrl), WT PAC or mutant W304N at pH 7.5 (upper) or 4.5 (lower). (**E**) Averaged percentages of SH-SY5Y cell death. ns, not significant; ***, $p < 0.001$; **, $p < 0.01$ (F) Representative Western blot images showing the total or surface expression of PAC-Flag or β-actin in SH-SY5Y cells. Data were summarized from three independent experiments.

5.5 DISCUSSION

The gate of an ion channel may be defined by a single or multiple amino-acid residue (Rao et al., 2018; Zheng et al., 2018c). The gate composition and activation mechanism of the recently cloned PAC has remained largely unknown. By means of *Xenopus* oocyte expression and the two-electrode electrophysiology and based on the hydrophobic gate theory the present study has identified and characterized the gate residues (W304 and I307) and those implicated in proton-induced PAC activation. The gain-of-function nature of PAC mutant W304N has been verified in HEK293 and neuroblastoma SH-SY5Y cells by examining its toxic effect on acid-induced cell death in comparison with WT channel. The identified residues involved in the proton-induced channel activation were H131, E224, D289 and D297 that are protonatable within acidic to neutral physiological conditions.

A gate residue should be one that allows opening the channel pore when it is replaced by a more hydrophilic or smaller residue. For a ligand-gated channel this should still hold true in the absence of an agonist, which indeed was verified in the cases of TRPM8 and TRPV4 (Zheng et al., 2018b). W304 acted as the closed gate because it was the only hydrophobic residue in the putative pore-forming S2 helix that allowed constitutive channel opening upon hydrophilic substitutions at pH 7.5 (low proton concentration). In contrast to smaller hydrophobic residues, tryptophan does not typically act as a gate

residue. Among over 200 ion channels with known structures only the influenza virus M2 proton channel adopts W as its gate residue (Tang et al., 2002). The channel activity of mutant W304N at pH 7.5 was similar to the activated (at pH 4.5) WT channel activity and did not further increase by acidification, a phenomenon similarly seen in the (closed) gate mutant of TRPM8, TRPV4 and chloride channel bestrophin (Vaisey et al., 2016; Zheng et al., 2018b) with respect to their agonist. Constitutive channel opening by hydrophilic substitutions at W304 at high pH indicates that channel opening is direct, ie, it does not involve binding of protons and the ensuing conformational changes seen during proton-induced PAC activation, which is supported by our observation that when all the four protonatable residues were changed to N, constitutive opening at high pH persisted.

The fact that W304N can no longer increase its activity by acidification would suggest that the channel pore may have been fully opened. However, our finding of W304 as a gate residue apparently contradicts with the conclusion drawn based on a previous study using cysteine accessibility scanning, which identified I307 as the gate residue at acidic extracellular conditions, ie, when PAC is activated. Furthermore, at pH 4.5, we found that I307, but not any other hydrophobic residues in S2, further increases the channel activity upon hydrophilic substitutions. This indicates that I307 defines the open gate and that W304N did not fully open the channel pore. Further, mutation W304N did not increase the channel activity of I307N at low pH (W304N/I307N, NN) and reciprocally, mutation I307N did not increase the W304N activity at neutral pH (NN)

(Fig. 5-2 and 3). Substitutions with Q produced similar results (Fig. 5-2 and 3). Thus, W304 defines/controls the closed pore (at high extracellular pH) while I307, which is located nearly one helical turn downstream of W304 in S2, defines/controls the open pore (at low pH), suggesting the presence of S2 helix twisting upon acidification so that W304 points away from the pore centre while I307 points towards it (Fig. 5-6). This mechanism of 'alternate gate' in which the closed gate is defined by a residue that is different/independent from one defining the open gate may be shared by other ion channels. For example, TRPV6 structures reveal that the closed gate is defined by M618 while the open gate by I615 (McGoldrick et al., 2018), also three amino acids apart, though we should bear in mind that structural and functional data may lead to identification of different gate residues (McGoldrick et al., 2018; Zheng et al., 2018b). It remains to be determined as to whether this mechanism of 'alternate gate' is shared by other ion channels such as TRPM8 and TRPV4.

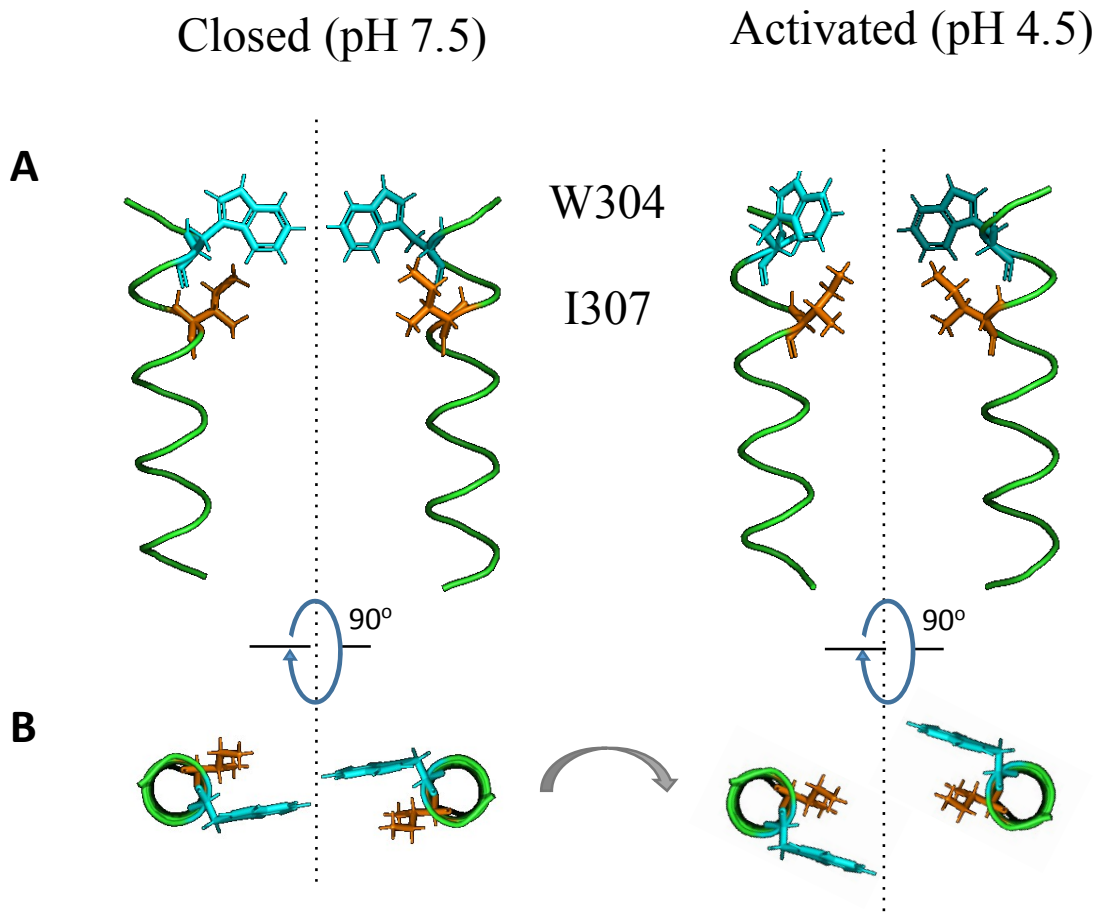

Fig. 5-6. 'Alternate gate' model for PAC showing helix S2 twist upon activation. Side (A) and top (B) views of two S2 helices showing residues W304 (blue) and I307 (orange) at closed (pH 7.5) and activated (pH 4.5) states. The pore gate is defined by W304 and I307 at closed and activated states, respectively, with transition between the two states that can be accomplished through S2 helix twisting.

The hydrophobic gate theory was originally proposed based on the observation of hydrating-dewetting transition in nanopore or nanotube by molecular dynamics (MD) simulations (Aryal et al., 2015). Subsequent investigations extensively validated the theory in various ion channels, including but not limited to chloride channels,

mechanically activated channels, TRP channels, and potassium channels by electrophysiology, MD stimulation and structural studies (Aryal et al., 2015; Zheng et al., 2019). PAC activity strongly correlated with the hydrophobicity, but not the residue size, at site 304 (high pH) or 307 (low pH). This is well supported by data obtained using hydrophilic and also hydrophobic substitutions (Fig. 5-2). For hydrophobic substitutions at W304, consistent with the fact that V, L, F and I are much smaller than W but have similar or higher hydrophobicity than W, mutants W304V/-L/-F/-I did not exhibit higher activity than WT at pH 7.5 (Fig. 5-2B). Similarly for I307 mutants at pH 4.5, substitution with larger but less hydrophobic Y increased the activity while replacement with residues of similar hydrophobicity and various sizes (V, W, F and L) did not significantly alter the function (Fig. 5-2E). In summary, the hydrophobicity, but not the size, of a gate residue, plays a predominant role in regulating the PAC function, which seems to be shared by Ca^{2+}-activated chloride channel bestrophin (Vaisey et al., 2016) but differs from TRPP2 channel in which both the hydrophobicity and size of the gate residue L677 are important for the function (Zheng et al., 2018c).

Activated PAC was previously predicted to bind three to four protons based on the Hill coefficient of 3.6 (Lambert and Oberwinkler, 2005). Neutralization of residues involved in the proton binding attenuates the proton dependence of PAC, which is similar to what happened in ASICs (Jasti et al., 2007; Ramaswamy et al., 2013). The pH50 value of PAC was reported to be around 5.0 at room temperature (RT), which seems to be

consistent with our current finding of four residues composed of H, D(x2) and E implicated in the proton binding and pH50 of 5.0 would presumably be achieved by a microenvironment cooperatively by these protonatable residues with their pKa value of 6.10, 3.86 and 4.07, respectively. While normal physiological conditions correspond to a pH range of 7.2 to 7.4 extracellular pH can be as low as 5.5 in inflammatory reactions, 5.7 outside tumors and 6.5 during stroke (Rehncrona, 1985; Tong et al., 2011). Further, as the pH50 value at 37°C may rise to around 6.0 (Yang et al., 2019), it is possible that PAC plays roles in inflammation, carcinogenesis or ischemia reperfusion injury. Our identification and characterization of the gain-of-function gate mutants and acid-insensitive mutants would help understanding physiological roles of PAC, for example, through the use of mutant knock-in animals.

5.6 SUPPLEMENTARY INFORMATION

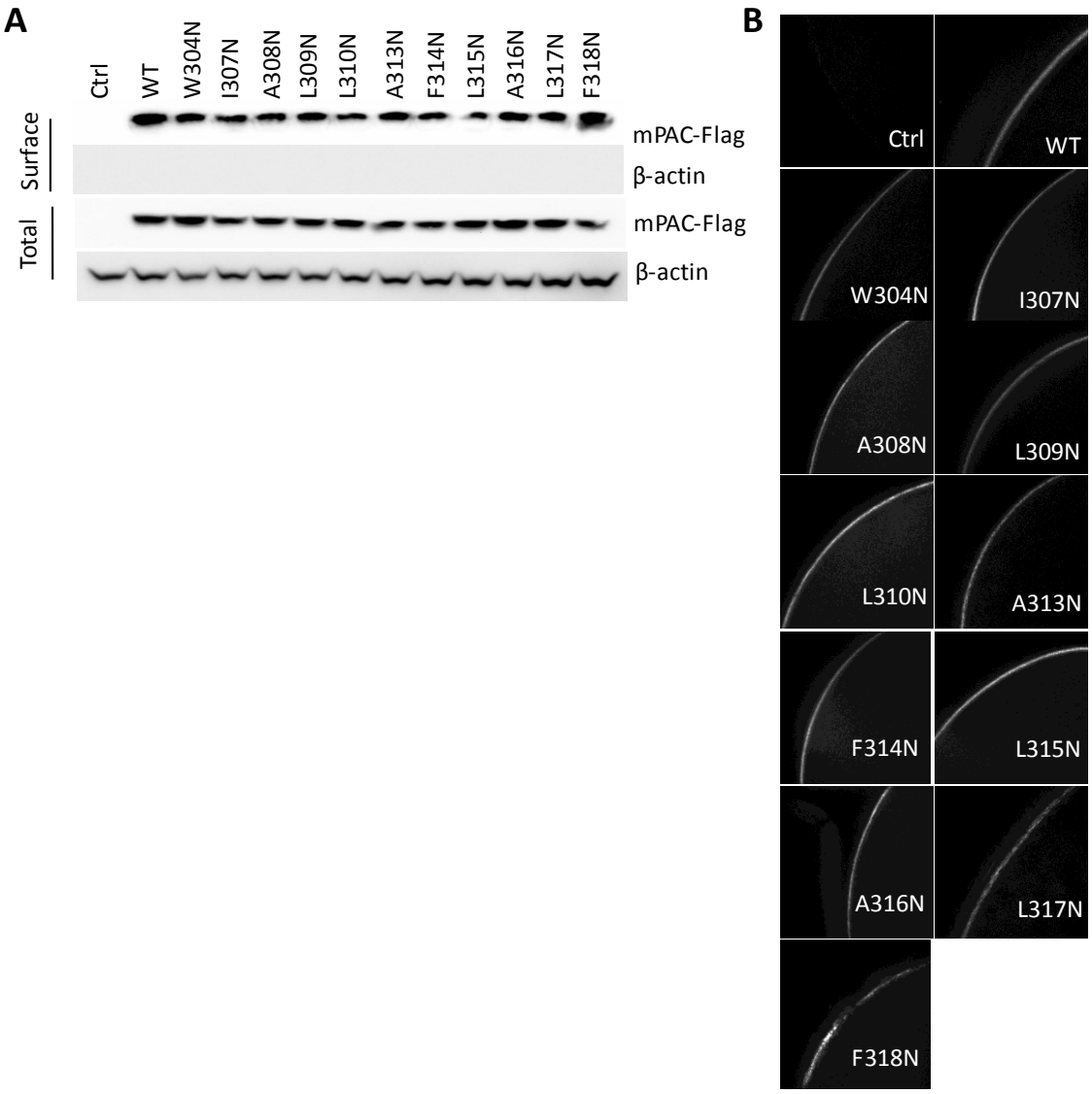

Fig. 5-S1. Expression of WT and mutant PAC in oocytes. (**A**) Representative biotinylation and Western blotting data showing the total and surface expression of WT and mutant PAC, as indicated. (**B**) Representative immunofluorescence images showing the surface expression of WT and mutant PAC.

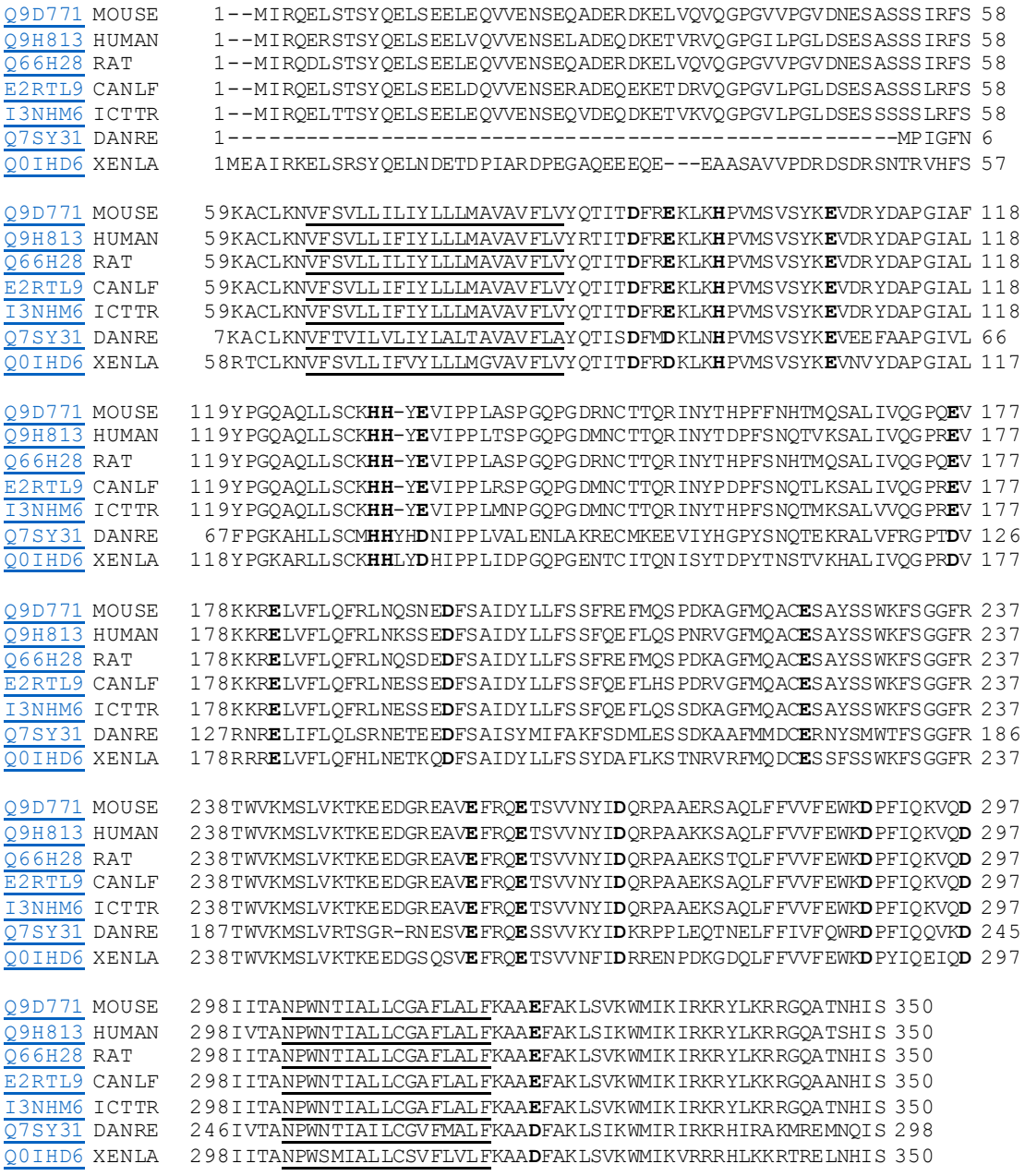

Fig. 5-S2. Sequence alignment of the PAC from species. UniProt accession numbers are indicated and conserved candidate residues for protons binding are in bold. Sequences for the putative S1 and S2 helices are underlined.

CHAPTER 6

GENERAL DISCUSSION

6.1 Intramolecular interactions in TRP and other ion channels

The mammalian TRP channel superfamily includes 28 members divided into 6 subfamilies, among which there is mild sequence homology. The large amount of TRP channel structures, representing those from at least two members from each subfamily, at atomic resolution provide structural insights that more shared structural similarities exist, besides previously recognized overall architectures including tetrameric assembly shared by all TRP channels. First of all, close proximity between cytosolic pre-S1 and TRP (or TRP-like) domains is found in different TRP subfamilies. Although TRPM8 structure doesn't contain a typical S4-S5 linker, the TRP (or TRP-like) domain also stays closely with the S4-S5 linker in other TRP members. However, similar structural arrangements in fact have distinct functional implications. As we showed in Chapter 2, in TRPP3, -P2, -V1, -C4 and -M8 channels, the interaction between the pre-S1 and TRP (or TRP-like) domains, termed 'the N/C interaction', is required for channel opening; disruption of the N/C interaction resulted in loss-of-function. In contrast, the N/C interaction was autoinhibitory for TRPV6 channel and, when disrupted, the channel became gain-of-function. Interestingly, putting these six TRP channels together, their N/C interactions, though differently affecting the channel function, are mediated by energetically favorable π-cation bonding or van der Waals force. Of note, the van del Waals force, which is a relatively weaker bonding compared with π-π, π-cation or salt bridge bonding characterized in the TRPV6 N/C interaction might explain why TRPV6

channel is mildly open under resting (physiological) conditions. This notion is supported by data showing an inverse relationship between bonding strength and channel function (Fig. 3-4 C and D). In TRPV6 channel, we also characterized an inhibitory S4-S5 linker/TRP domain interaction, termed 'the L/C interaction', which is reminiscent of an interaction proposed in the same domains of TRPV4 channel to stabilize its closed state (Teng et al., 2016). In addition, there is possibility that the autoinhibitory interactions identified in TRPV6 could be the same case in TRPV5, which shares the highest homology to TRPV6 and was speculated as gene duplication of *TRPV6* during evolution from reptiles to mammals (Peng, 2011). Furthermore, the two intramolecular interactions are not independent of each other as we found that that the L/C interaction is required for the N/C interaction in TRPV6. It remains unclear why disruption of the N/C interaction activates TRPV6 while inhibits TRPP, -C4, -V1 and -M8 channels. I would suggest that ligands binding to TRP channels modulate the L/C and/or N/C interactions to induce subsequent conformational changes leading to channel opening or closure.

All physiologically relevant structures of TRP channels share a feature called domain swapping, ie, the S1-S4 helices together in one subunit (monomer) are close to the S5-S6 helices of a neighbor subunit. Importantly, a non-swapping TRPV6 crystal structure was found to be non-physiological (Saotome et al., 2016). Therefore, this domain-swapping arrangement is physiologically relevant, but with an unclear underlying reason. We here showed that in TRPV6 the S5 helix interacts with S6 helix through a salt bridge formed

by R532:D620, which, like N/C and L/C bindings, is inhibitory. Importantly, both R532 and D620 are highly conserved across different TRP subfamilies and species, indicating the possible functional importance of this interaction in other TRP channel members. With currently available structures for several TRP channels, proximity between the corresponding residues in other TRP channels have been discussed in Chapter 4. It is noted that structural data are not fully consistent with our proposed L/C, N/C or S5/S6 helix interactions: some of our discovered residue pairs may be found (by structural data) to be far away from each other or to have their interacting side chains oriented in directions that are unfavorable for binding. This discrepancy may be due, at least in part, to differences between cryo-EM or X-ray crystallography conditions and living cells used in our study. We may expect to depend on more advanced microscopy techniques in the future to obtain structures under more physiological conditions.

6.2 PIP2 regulation on TRP and other ion channels

PIP2 regulates most, if not all, TRP members. PIP2 inhibits TRPPs, -C4, -V3 and -ML1 but stimulates TRPMs, -V2, -V4, -V5 and -V6 (Rohacs, 2014). The effect of PIP2 on TRPC5, -C6, -C7 and -V1 is more arguable based on studies from different groups under different experimental conditions (Nilius et al., 2008). PIP2 was found by several groups to activate TRPV1 in excised patches, indicating an activation by direct binding (Rohacs,

2014). For PIP2 direct effects, PIP2-binding cationic residues such as those in TRPM4, -M5 and -M8 were searched while for indirect effects the involvement of a PLC pathway has been studied (Nilius et al., 2008). Here, we propose that PIP2 binds to positively charged residues and modulates the N/C and/or L/C interactions of TRP channels to induce allosteric conformational changes on pore helices thereby opening or closing the channel. While disruption of the intramolecular N/C interaction causes loss-of-function in TRPPs, -V1, -M8, PIP2 exhibits distinct effects on the N/C binding of these channels. In fact, PIP2 breaks down the N/C binding in TRPPs, consistent with its inhibitory effect on the function, but strengthens the N/C binding in TRPV1 and -M8, consistent with its stimulatory effect on the function. On the other hand, the N/C and L/C bindings in TRPV6 are functionally inhibitory, and accordingly, PIP2 activates the channel through disrupting the N/C and L/C bindings. Importantly, PIP2 binding to a TRP channel is a prerequisite to modulate the N/C and L/C interactions, and consequently, when the putative PIP2 binding residues are neutralized, PIP2 can't no longer effectively regulate the TRP channel. These data together provide novel underlying mechanisms on how PIP2 regulates TRP channels. It remains to be determined whether this mechanism would be applicable to other TRP channels.

6.3 TRPV6 and cancer

Cancer is still the most severely lethal threat to human health. It has been proposed that TRPV6, a ubiquitously expressed protein, is oncogenic and is implicated in a number of cancer types, including breast, ovary, colon, thyroid, cervix, prostate, lung and pancreas carcinomas (Stewart, 2020). Among these, TRPV6 is recognized as a promising prognostic marker for subtypes of breast, prostate, cervical and pancreas cancer. Elevated expression of TRPV6 is detected in the majority of cancer types, indicating its oncogenic effects, with exception of the early stage cervical squamous cell carcinoma (Stewart, 2020), which suggests potentially different roles that TRPV6 could play on progressions of a specific cancer type. Several mechanisms have been proposed on the increased calcium influx mediated by TRPV6 as it's one of the most calcium selective members among TRP channels and calcium has been underscored as a critical factor affecting cancer development. A study using prostate cancer cells LNCaP showed that calcium entry through TRPV6 channel initiates a calcium/nuclear factor of activated T-cells (NFAT) pathway to promote cell proliferation and to escape from apoptosis (Lehen'kyi et al., 2007). A subsequent study from the same group attributed the increased surface expression of TRPV6 to being controlled by an Orai1-mediated Ca^{2+}/Annexin I/S100A11 pathway in LNCaP cells (Raphael et al., 2014). In prostate and breast cancer cells, a tumor suppressor called NUMB forms a complex with TRPV6 to inhibit the TRPV6 function and expression (Kim et al., 2014; Kim et al., 2013). However, this observation

was challenged by a subsequent study using pancreatic Capan-2 cells, which showed that knockdown of NUMB does not affect the TRPV6 expression (Song et al., 2018). The presently accepted mechanism on the TRPV6 involvement in progression of breast cancer cells MCF-7 and MDA-MB-231 suggests that gain-of-function mutant TRPV6 R532Q binds to the inhibitory subunit p85 of PI3K through which it activates the PI3K/Akt pathway, resulting in EMT. Besides, novel findings also propose a mechanism on how up-regulated TRPV6 contributes to breast cancer development. This similar mechanism might be applicable to other cancers in which the R532Q mutation may be present or the TRPV6 expression may be up-regulated.

6.4 Gate and regulation of PAC

Recent reports on the molecular identity of PAC provide basis for understanding the gate and functional regulation of the channel. Although the assembly of PAC is still unknown, the S2 helix is proposed to be the pore-lining helix based on studies using substituted cysteine scanning (Yang et al., 2019). We here identified two independent gate residues W304 and I307 controlling the ion permeation in closed and open states, respectively. The open gate formed by residue I307 has been suggested previously using cysteine scanning. Our current study (Chapter 5) found that when the channel is closed, the gate is formed by W304, a residue located nearly one helical turn upstream of the

open state gate residue I307. Assuming a α-helical structure in this S2 region, the angle between W304 and I307 would be roughly 60 degree. This suggests the presence of S2 helix twist of about 60 degree during proton-induced channel activation. Our data showed that PAC adopts hydrophobic gates similar to other chloride, TRP, potassium and mechano-sensitive channels (Zheng et al., 2018c). The hydrophobic gate theory may thus turn out to be an important mechanism on how ion channel pore gates are formed.

The PAC gate residues W304 and I307 are close to the extracellular end of the S2 helix, a phenomenon also seen in several other chloride channels such as volume-regulated anion channel SWELL1 (Kefauver et al., 2018), bestrophin (Miller et al., 2019) and CLC-1 channel (Park and MacKinnon, 2018). Interestingly, cation channels such as voltage-gated and TRP channels often have their gate residue(s) located near the inner end of the pore-lining helix (Zheng et al., 2018b). This sounds reasonable because under the same membrane voltage this would facilitate anions and cations to flow at the opposite directions. Besides, it remains to be investigated how the proton sensing is linked to the gating process in PAC.

6.5 Future directions

The intramolecular interactions we described in the thesis are presumably mediated by conserved amino acids across TRP channels. It would be highly attractive to examine

the corresponding residues in other TRP channels not yet tested. Since TRP channels are implicated in diverse human diseases, frequently caused by malfunction, it is thus possible to take advantage of the characterized intramolecular interactions to efficiently modulate the abnormality in the channel function through precise gene editing techniques. For example, in Chapter 3, we have showed that a gain-of-function TRPV6 mutant could effectively alleviate the loss-of-calcification in zebrafish. Considering the uncertainty of gene editing in human, chemicals or peptide drugs specifically target and modulate the functionally critical intramolecular interactions could be designed and screened. As for human disease like transient neonatal hyperparathyroidism, where the fetal-maternal calcium absorption is substantially impaired, we might restore the channel function by application of the chemicals efficiently modulate. For several TRP channels with unclear physiological relevance we can generate intramolecular interaction-modified mutant channels to elucidate their physiological function.

In Chapter 4, the predicted-to-be pathogenic mutant R532Q is characterized as a gain-of-function mutant in oocytes and cancer cell lines. It promotes proliferation, EMT and apoptotic resistance in breast cancer cell lines. Further *in vivo* Xenograft experiments are of high importance to validate the suggested oncogenic potential of R532Q. Additional genetically modified mouse models with R532Q knocked-in would also be valuable to understand whether TRPV6 plays oncogenic roles in mammals. Specifically, it would be interesting and important to verify whether the tissue-specific (for example

mammary gland) knocked-in mice would develop malignant cancer with the presence of R532Q mutation. With the in depth mechanism studies we presented in Chapter 4, we should recognize the patients harboring TRPV6 R532Q mutant could be highly pathogenic. Therefore, we could also aim to design specific drugs bring the disrupted S5/S6 helix back together. Recently, a small peptide called Soricidin is reported to inhibit TRPV6 and it could be worthwhile to examine whether Soricidin could inhibit the R532Q mutant. In addition, the calcium homeostasis, including the serum calcium, hormones regulating the TRPV6, trancellular calcium absorption in small intestine, in the R532Q knock-in mice should be examined and systematically compared with the existing TRPV6 knock-out mice, which would provide unforeseen insights into the physiological role of TRPV6.

The novel PAC channel was molecularly identified in 2019. More physiological and mechanistic studies are required. *PAC* knockout (loss-of-function) mice were found without any defective phenotype (Yang et al., 2019). With the gain-of-function gate mutants we characterized in Chapter 5, we think that knockin of gain-of-function in mice may provide unique tools to reveal physiological roles of PAC. Future availability of structural information on PAC under different conformations would provide more details and verify our finding of alternate gates for the closed and open states and the presence of S2 twist during channel activation. The previously reported thermo-regulation of PAC showed that temperature increase from 25 to 37 °C shifts its pH sensitivity to higher pH

(Sato-Numata et al., 2014) but the the domain responsible for the thermo sensation remains to be determined. Further, the identity and role of the PAC selectivity filter remain unknown. In bestrophin, the selectivity filter is composed of a valine residue close to the cytosol side, which is also distinct from the close-to-extracellular selectivity filter found in cationic TRP and potassium channels.

7. REFERENCES

Akram, M., Iqbal, M., Daniyal, M., and Khan, A.U. (2017). Awareness and current knowledge of breast cancer. Biol Res *50*, 33.

Altier, C., Dubel, S.J., Barrere, C., Jarvis, S.E., Stotz, S.C., Scott, J.D., Nargeot, J., Zamponi, G.W., and Bourinet, E. (2012). AKAP79 modulation of L-type channels involves disruption of intramolecular interactions in the CaV1.2 subunit. Channels (Austin) *6*, 157-165.

Anishkin, A., and Sukharev, S. (2004). Water dynamics and dewetting transitions in the small mechanosensitive channel MscS. Biophys J *86*, 2883-2895.

Arif Pavel, M., Lv, C., Ng, C., Yang, L., Kashyap, P., Lam, C., Valentino, V., Fung, H.Y., Campbell, T., Møller, S.G., et al. (2016). Function and regulation of TRPP2 ion channel revealed by a gain-of-function mutant. Proc. Natl. Acad. Sci. USA *113*, E2363–E2372.

Arutyunova, E., Brooks, C.L., Beddek, A., Mak, M.W., Schryvers, A.B., and Lemieux, M.J. (2012). Crystal structure of the N-lobe of lactoferrin binding protein B from Moraxella bovis. Biochem Cell Biol *90*, 351-361.

Aryal, P., Sansom, M.S., and Tucker, S.J. (2015). Hydrophobic gating in ion channels. J Mol Biol *427*, 121-130.

Auzanneau, C., Thoreau, V., Kitzis, A., and Becq, F. (2003). A Novel voltage-dependent chloride current activated by extracellular acidic pH in cultured rat Sertoli cells. J Biol Chem *278*, 19230-19236.

Azimi, I., and Monteith, G.R. (2016). Plasma membrane ion channels and epithelial to mesenchymal transition in cancer cells. Endocr Relat Cancer *23*, R517-R525.

Azimi, I., Roberts-Thomson, S.J., and Monteith, G.R. (2014). Calcium influx pathways in breast cancer: opportunities for pharmacological intervention. Br J Pharmacol *171*, 945-960.

Beck, A., Speicher, T., Stoerger, C., Sell, T., Dettmer, V., Jusoh, S.A., Abdul- mughni, A., Cavalie, A., Philipp, S.E., Zhu, M.X., et al. (2013). Conserved gating elements in TRPC4 and TRPC5 channels. J. Biol. Chem. *288*, 19471–19483.

Becker, S. (2015). A historic and scientific review of breast cancer: The next global healthcare challenge. Int J Gynaecol Obstet *131 Suppl 1*, S36-39.

Benn, B.S., Ajibade, D., Porta, A., Dhawan, P., Hediger, M., Peng, J.B., Jiang, Y., Oh, G.T., Jeung, E.B., Lieben, L.*, et al.* (2008). Active intestinal calcium transport in the absence of transient receptor potential vanilloid type 6 and calbindin-D9k. Endocrinology *149*, 3196-3205.

Beurel, E., Grieco, S.F., and Jope, R.S. (2015). Glycogen synthase kinase-3 (GSK3): regulation, actions, and diseases. Pharmacol Ther *148*, 114-131.

Bianco, S.D., Peng, J.B., Takanaga, H., Suzuki, Y., Crescenzi, A., Kos, C.H., Zhuang, L., Freeman, M.R., Gouveia, C.H., Wu, J., et al. (2007). Marked disturbance of calcium homeostasis in mice with targeted disruption of the Trpv6 calcium channel gene. J.Bone Miner.Res. *22*, 274-285.

Bolanz, K.A., Hediger, M.A., and Landowski, C.P. (2008). The role of TRPV6 in breast carcinogenesis. Mol Cancer Ther *7*, 271-279.

Bolanz, K.A., Kovacs, G.G., Landowski, C.P., and Hediger, M.A. (2009). Tamoxifen inhibits TRPV6 activity via estrogen receptor-independent pathways in TRPV6-expressing MCF-7 breast cancer cells. Mol Cancer Res *7*, 2000-2010.

Bousova, K., Jirku, M., Bumba, L., Bednarova, L., Sulc, M., Franek, M., Vyk- licky, L., Vondrasek, J., and Teisinger, J. (2015). PIP2 and PIP3 interact with N-terminus region of TRPM4 channel. Biophys. Chem. *205*, 24–32.

Bray, F., Ferlay, J., Soerjomataram, I., Siegel, R.L., Torre, L.A., and Jemal, A. (2018). Global cancer statistics 2018: GLOBOCAN estimates of incidence and mortality worldwide for 36 cancers in 185 countries. CA Cancer J Clin *68*, 394-424.

Britschgi, A., Bill, A., Brinkhaus, H., Rothwell, C., Clay, I., Duss, S., Rebhan, M., Raman, P., Guy, C.T., Wetzel, K.*, et al.* (2013). Calcium-activated chloride channel ANO1 promotes breast cancer progression by activating EGFR and CAMK signaling. Proc Natl Acad Sci U S A *110*, E1026-1034.

Busch, T., Kottgen, M., and Hofherr, A. (2017). TRPP2 ion channels: Critical regulators of organ morphogenesis in health and disease. Cell Calcium *66*, 25-32.

Bustin, S.A., Li, S.R., and Dorudi, S. (2001). Expression of the Ca^{2+}-activated chloride channel genes CLCA1 and CLCA2 is downregulated in human colorectal cancer. DNA Cell Biol *20*, 331-338.

Cai, R., Xue, W., Liu, S., Petersen, R.B., Huang, K., and Zheng, L. (2015). Overexpression of glyceraldehyde 3-phosphate dehydrogenase prevents neurovascular degeneration after retinal injury. FASEB J *29*, 2749-2758.

Cao, C., Zakharian, E., Borbiro, I., and Rohacs, T. (2013). Interplay between calmodulin and phosphatidylinositol 4,5-bisphosphate in Ca^{2+}-induced inactivation of transient

receptor potential vanilloid 6 channels. J.Biol.Chem. *288*, 5278-5290.

Cao, E. (2020). Structural mechanisms of transient receptor potential ion channels. J Gen Physiol *152*.

Cao, E., Liao, M., Cheng, Y., and Julius, D. (2013). TRPV1 structures in distinct conformations reveal activation mechanisms. Nature *504*, 113–118.

Capurro, V., Gianotti, A., Caci, E., Ravazzolo, R., Galietta, L.J., and Zegarra-Moran, O. (2015). Functional analysis of acid-activated Cl(-) channels: properties and mechanisms of regulation. Biochim Biophys Acta *1848*, 105-114.

Chen, X.Z., Vassilev, P.M., Basora, N., Peng, J.B., Nomura, H., Segal, Y., Brown, E.M., Reeders, S.T., Hediger, M.A., and Zhou, J. (1999). Polycystin-L is a calcium-regulated cation channel permeable to calcium ions. Nature *401*, 383-386.

Chow, J., Norng, M., Zhang, J., and Chai, J. (2007). TRPV6 mediates capsaicin-induced apoptosis in gastric cancer cells--Mechanisms behind a possible new "hot" cancer treatment. Biochim Biophys Acta *1773*, 565-576.

Clapham, D.E. (2003). TRP channels as cellular sensors. Nature *426*, 517-524.

Clapham, D.E. (2007). Calcium signaling. Cell *131*, 1047-1058.

Clapham, D.E., Runnels, L.W., and Stru€bing, C. (2001). The TRP ion channel family. Nat. Rev. Neurosci. *2*, 387–396.

Cosens, D.J., and Manning, A. (1969). Abnormal electroretinogram from a Drosophila mutant. Nature *224*, 285-287.

Czirjak, G., Petheo, G.L., Spat, A., and Enyedi, P. (2001). Inhibition of TASK-1 potassium channel by phospholipase C. Am. J. Physiol. Cell Physiol. 281, C700–C708.

Dai, J., Cho, T.J., Unger, S., Lausch, E., Nishimura, G., Kim, O.H., Superti-Furga, A., and Ikegawa, S. (2010). TRPV4-pathy, a novel channelopathy affecting diverse systems. J.Hum.Genet. *55*, 400-402.

Dai, X.Q., Ramji, A., Liu, Y., Li, Q., Karpinski, E., and Chen, X.Z. (2007). Inhibition of TRPP3 channel by amiloride and analogs. Mol Pharmacol *72*, 1576-1585.

De Clercq, K., and Vriens, J. (2018). Establishing life is a calcium-dependent TRiP: Transient receptor potential channels in reproduction. Biochim Biophys Acta Mol Cell Res *1865*, 1815-1829.

Deng, Z., Paknejad, N., Maksaev, G., Sala-Rabanal, M., Nichols, C.G., Hite, R.K., and Yuan, P. (2018). Cryo-EM and X-ray structures of TRPV4 reveal insight into ion permeation and gating mechanisms. Nat.Struct.Mol.Biol. *25*, 252-260.

Desai, B.N., and Clapham, D.E. (2005). TRP channels and mice deficient in TRP channels. Pflugers Arch *451*, 11-18.

Dhani, S.U., and Bear, C.E. (2006). Role of intramolecular and intermolecular interactions in ClC channel and transporter function. Pflugers Arch *451*, 708-715.

Dhennin-Duthille, I., Gautier, M., Faouzi, M., Guilbert, A., Brevet, M., Vaudry, D., Ahidouch, A., Sevestre, H., and Ouadid-Ahidouch, H. (2011). High expression of transient receptor potential channels in human breast cancer epithelial cells and tissues: correlation with pathological parameters. Cell Physiol Biochem *28*, 813-822.

Dong, K., Yao, N., Pu, Y., He, X., Zhao, Q., Luan, Y., Guan, W., Rao, S., and Ma, Y.

(2014). Genomic scan reveals loci under altitude adaptation in Tibetan and Dahe pigs. PLoS One *9*, e110520.

Downing, G.J., Kim, S., Nakanishi, S., Catt, K.J., and Balla, T. (1996). Characterization of a soluble adrenal phosphatidylinositol 4-kinase reveals wortmannin sensitivity of type III phosphatidylinositol kinases. Biochemistry *35*, 3587-3594.

Du, J., Fu, J., Xia, X.M., and Shen, B. (2016). The functions of TRPP2 in the vascular system. Acta Pharmacol Sin *37*, 13-18.

Duran, C., Thompson, C.H., Xiao, Q., and Hartzell, H.C. (2010). Chloride channels: often enigmatic, rarely predictable. Annu Rev Physiol *72*, 95-121.
Earley, S., and Brayden, J.E. (2015). Transient receptor potential channels in the vasculature. Physiol Rev *95*, 645-690.

Espinosa, F., Fleischhauer, R., McMahon, A., and Joho, R.H. (2001). Dynamic interaction of S5 and S6 during voltage-controlled gating in a potassium channel. J Gen Physiol *118*, 157-170.

Fan, C., Sukomon, N., Flood, E., Rheinberger, J., Allen, T.W., and Nimigean, C.M. (2020). Ball-and-chain inactivation in a calcium-gated potassium channel. Nature *580*, 288-293.

Fecher-Trost, C., Weissgerber, P., and Wissenbach, U. (2014). TRPV6 channels. Handb Exp Pharmacol *222*, 359-384.

Fecher-Trost, C., Wissenbach, U., Beck, A., Schalkowsky, P., Stoerger, C., Doerr, J., Dembek, A., Simon-Thomas, M., Weber, A., Wollenberg, P.*, et al.* (2013). The in vivo TRPV6 protein starts at a non-AUG triplet, decoded as methionine, upstream of canonical initiation at AUG. J Biol Chem *288*, 16629-16644.

Fixemer, T., Wissenbach, U., Flockerzi, V., and Bonkhoff, H. (2003). Expression of the Ca^{2+}-selective cation channel TRPV6 in human prostate cancer: a novel prognostic marker for tumor progression. Oncogene *22*, 7858-7861.

Forbes, S.A., Bhamra, G., Bamford, S., Dawson, E., Kok, C., Clements, J., Menzies, A., Teague, J.W., Futreal, P.A., and Stratton, M.R. (2008). The Catalogue of Somatic Mutations in Cancer (COSMIC). Curr.Protoc.Hum.Genet. *Chapter 10*, Unit.

Gao, Y., Cao, E., Julius, D., and Cheng, Y. (2016). TRPV1 structures in nano- discs reveal mechanisms of ligand and lipid action. Nature *534*, 347–351.

Garcia-Elias, A., Berna-Erro, A., Rubio-Moscardo, F., Pardo-Pastor, C., Mrkonjic, S., Sepu´lveda, R.V., Vicente, R., Gonza´lez-Nilo, F., and Valverde, M.A. (2015). Interaction between the linker, pre-S1, and TRP domains determines folding, assembly, and trafficking of TRPV channels. Structure *23*, 1404–1413.

Geering, B., Cutillas, P.R., and Vanhaesebroeck, B. (2007). Regulation of class IA PI3Ks: is there a role for monomeric PI3K subunits? Biochem Soc Trans *35*, 199-203.

Gees, M., Colsoul, B., and Nilius, B. (2010). The role of transient receptor potential cation channels in Ca^{2+} signaling. Cold Spring Harb Perspect Biol *2*, a003962.

Goldin, E., Stahl, S., Cooney, A.M., Kaneski, C.R., Gupta, S., Brady, R.O., Ellis, J.R., and Schiffmann, R. (2004). Transfer of a mitochondrial DNA fragment to MCOLN1 causes an inherited case of mucolipidosis IV. Hum.Mutat. *24*, 460-465.

Grieben, M., Pike, A.C., Shintre, C.A., Venturi, E., El-Ajouz, S., Tessitore, A., Shrestha, L., Mukhopadhyay, S., Mahajan, P., Chalk, R., et al. (2017). Structure of the polycystic kidney disease TRP channel Polycystin-2 (PC2). Nat. Struct. Mol. Biol. *24*, 114–122.

Gyorffy, B., Lanczky, A., Eklund, A.C., Denkert, C., Budczies, J., Li, Q., and Szallasi, Z. (2010). An online survival analysis tool to rapidly assess the effect of 22,277 genes on breast cancer prognosis using microarray data of 1,809 patients. Breast Cancer Res Treat *123*, 725-731.

Hamilton, P.J., Belovich, A.N., Khelashvili, G., Saunders, C., Erreger, K., Javitch, J.A., Sitte, H.H., Weinstein, H., Matthies, H.J.G., and Galli, A. (2014). PIP2 regulates psychostimulant behaviors through its interaction with a membrane protein. Nat.Chem.Biol. *10*, 582-589.

Hanahan, D., and Weinberg, R.A. (2011). Hallmarks of cancer: the next generation. Cell *144*, 646-674.

Hansen, S.B., Tao, X., and MacKinnon, R. (2011). Structural basis of PIP2 acti- vation of the classical inward rectifier K^+ channel Kir2.2. Nature *477*, 495–498.

Hardie, R.C. (2001). Phototransduction in Drosophila melanogaster. J Exp Biol *204*, 3403-3409.

Hardie, R.C., and Minke, B. (1992). The trp gene is essential for a light-activated Ca^{2+} channel in Drosophila photoreceptors. Neuron *8*, 643-651.

Himmel, N.J., Gray, T.R., and Cox, D.N. (2020). Phylogenetics Identifies Two Eumetazoan TRPM Clades and an Eighth TRP Family, TRP Soromelastatin (TRPS). Mol Biol Evol *37*, 2034-2044.

Hoenderop, J.G.J., Nilius, B., and Bindels, R.J.M. (2005). Calcium absorption across epithelia. Physiol Rev 85, 373-422.

Hofmann, L., Wang, H., Beck, A., Wissenbach, U., and Flockerzi, V. (2017). A conserved gating element in TRPV6 channels. Cell Calcium *63*, 24-28.

Holendova, B., Grycova, L., Jirku, M., and Teisinger, J. (2012). PtdIns(4,5)P2 interacts with CaM binding domains on TRPM3 N-terminus. Channels (Austin) *6*, 479–482.

Holzer, P. (2011). TRP channels in the digestive system. Curr Pharm Biotechnol *12*, 24-34.

Horio, N., Yoshida, R., Yasumatsu, K., Yanagawa, Y., Ishimaru, Y., Matsunami, H., and Ninomiya, Y. (2011). Sour taste responses in mice lacking PKD channels. PLoS One *6*, e20007.

Huang, C.L., Feng, S., and Hilgemann, D.W. (1998). Direct activation of inward rectifier potassium channels by PIP2 and its stabilization by Gbetagamma. Nature *391*, 803-806.

Huang, F., Wong, X., and Jan, L.Y. (2012). International Union of Basic and Clinical Pharmacology. LXXXV: calcium-activated chloride channels. Pharmacol.Rev. *64*, 1-15.

Huang, X., Pan, Q., Sun, D., Chen, W., Shen, A., Huang, M., Ding, J., and Geng, M. (2013). O-GlcNAcylation of cofilin promotes breast cancer cell invasion. J.Biol.Chem. *288*, 36418-36425.

Huber, S.M. (2013). Oncochannels. Cell Calcium *53*, 241-255.

Hughes, T.E.T., Pumroy, R.A., Yazici, A.T., Kasimova, M.A., Fluck, E.C., Huynh, K.W., Samanta, A., Molugu, S.K., Zhou, Z.H., Carnevale, V*., et al.* (2018). Structural insights on TRPV5 gating by endogenous modulators. Nat Commun *9*, 4198.

Hummer, G., Rasaiah, J.C., and Noworyta, J.P. (2001). Water conduction through the

hydrophobic channel of a carbon nanotube. Nature *414*, 188-190.

Humphrey, W., Dalke, A., and Schulten, K. (1996). VMD: visual molecular dynamics. J Mol Graph *14*, 33-38, 27-38.

Hussein, S., Zheng, W., Dyte, C., Wang, Q., Yang, J., Zhang, F., Tang, J., Cao, Y., and Chen, X.Z. (2015). Acid-induced off-response of PKD2L1 channel in Xenopus oocytes and its regulation by Ca(2.). Sci Rep *5*, 15752.

Huynh, K.W., Cohen, M.R., Jiang, J., Samanta, A., Lodowski, D.T., Zhou, Z.H., and Moiseenkova-Bell, V.Y. (2016). Structure of the full-length TRPV2 channel by cryo-EM. Nat. Commun. *7*, 11130.

Jiang, Y., Gou, H., Zhu, J., Tian, S., and Yu, L. (2016). Lidocaine inhibits the invasion and migration of TRPV6-expressing cancer cells by TRPV6 downregulation. Oncol Lett *12*, 1164-1170.

Jin, P., Bulkley, D., Guo, Y., Zhang, W., Guo, Z., Huynh, W., Wu, S., Meltzer, S., Cheng, T., Jan, L.Y., et al. (2017). Electron cryo-microscopy structure of the mechanotransduction channel NOMPC. Nature *547*, 118–122.

Jirku, M., Bumba, L., Bednarova, L., Kubala, M., Sulc, M., Franek, M., Vyklicky, L., Vondrasek, J., Teisinger, J., and Bousova, K. (2015). Characterization of the part of N-terminal PIP2 binding site of the TRPM1 channel. Biophys.Chem. *207*, 135-142.

Jo, S., Lim, J.B., Klauda, J.B., and Im, W. (2009). CHARMM-GUI Membrane Builder for mixed bilayers and its application to yeast membranes. Biophys J *97*, 50-58.

Kaneko, Y., and Szallasi, A. (2014). Transient receptor potential (TRP) channels: a

clinical perspective. Br J Pharmacol *171*, 2474-2507.

Karlin, A., and Akabas, M.H. (1998). Substituted-cysteine accessibility method. Methods Enzymol *293*, 123-145.

Kaufhold, S., and Bonavida, B. (2014). Central role of Snail1 in the regulation of EMT and resistance in cancer: a target for therapeutic intervention. J Exp Clin Cancer Res *33*, 62.

Kefauver, J.M., Saotome, K., Dubin, A.E., Pallesen, J., Cottrell, C.A., Cahalan, S.M., Qiu, Z., Hong, G., Crowley, C.S., Whitwam, T.*, et al.* (2018). Structure of the human volume regulated anion channel. Elife *7*.

Kim, K.M., Wijerathne, T., Hur, J.H., Kang, U.J., Kim, I.H., Kweon, Y.C., Lee, A.R., Jeong, S.J., Lee, S.K., Lee, Y.Y.*, et al.* (2018). Distinct gating mechanism of SOC channel involving STIM-Orai coupling and an intramolecular interaction of Orai in Caenorhabditis elegans. Proc Natl Acad Sci U S A *115*, E4623-E4632.

Kim, S., Nie, H., Nesin, V., Tran, U., Outeda, P., Bai, C.X., Keeling, J., Maskey, D., Watnick, T., Wessely, O.*, et al.* (2016). The polycystin complex mediates Wnt/Ca(2+) signalling. Nat Cell Biol *18*, 752-764.

Kim, S.Y., Hong, C., Wie, J., Kim, E., Kim, B.J., Ha, K., Cho, N.H., Kim, I.G., Jeon, J.H., and So, I. (2014). Reciprocal positive regulation between TRPV6 and NUMB in PTEN-deficient prostate cancer cells. Biochem Biophys Res Commun *447*, 192-196.

Kim, S.Y., Yang, D., Myeong, J., Ha, K., Kim, S.H., Park, E.J., Kim, I.G., Cho, N.H., Lee, K.P., Jeon, J.H.*, et al.* (2013). Regulation of calcium influx and signaling pathway in cancer cells via TRPV6-Numb1 interaction. Cell Calcium *53*, 102-111.

Klint, J.K., Senff, S., Saez, N.J., Seshadri, R., Lau, H.Y., Bende, N.S., Undheim, E.A., Rash, L.D., Mobli, M., and King, G.F. (2013). Production of recombinant disulfide-rich venom peptides for structural and functional analysis via expression in the periplasm of E. coli. PLoS One *8*, e63865.

Kovalevich, J., and Langford, D. (2013). Considerations for the use of SH-SY5Y neuroblastoma cells in neurobiology. Methods Mol Biol *1078*, 9-21.

Kremeyer, B., Lopera, F., Cox, J.J., Momin, A., Rugiero, F., Marsh, S., Woods, C.G., Jones, N.G., Paterson, K.J., Fricker, F.R., et al. (2010). A gain-of-function mutation in TRPA1 causes familial episodic pain syndrome. Neuron *66*, 671-680.

Lee, J., Cheng, X., Swails, J.M., Yeom, M.S., Eastman, P.K., Lemkul, J.A., Wei, S., Buckner, J., Jeong, J.C., Qi, Y.*, et al.* (2016). CHARMM-GUI Input Generator for NAMD, GROMACS, AMBER, OpenMM, and CHARMM/OpenMM Simulations Using the CHARMM36 Additive Force Field. J Chem Theory Comput *12*, 405-413.

Lehen'kyi, V., Flourakis, M., Skryma, R., and Prevarskaya, N. (2007). TRPV6 channel controls prostate cancer cell proliferation via Ca(2+)/NFAT-dependent pathways. Oncogene *26*, 7380-7385.

Lehen'kyi, V., Raphael, M., and Prevarskaya, N. (2012). The role of the TRPV6 channel in cancer. J Physiol *590*, 1369-1376.

Liao, M., Cao, E., Julius, D., and Cheng, Y. (2013). Structure of the TRPV1 ion channel determined by electron cryo-microscopy. Nature *504*, 107-112.

Lieben, L., Benn, B.S., Ajibade, D., Stockmans, I., Moermans, K., Hediger, M.A., Peng, J.B., Christakos, S., Bouillon, R., and Carmeliet, G. (2010). Trpv6 mediates intestinal calcium absorption during calcium restriction and contributes to bone homeostasis. Bone

47, 301-308.

Liu, B., and Qin, F. (2005). Functional control of cold- and menthol-sensitive TRPM8 ion channels by phosphatidylinositol 4,5-bisphosphate. J. Neurosci. *25*, 1674–1681.

Lopez-Romero, A.E., Hernandez-Araiza, I., Torres-Quiroz, F., Tovar, Y.R.L.B., Islas, L.D., and Rosenbaum, T. (2019). TRP ion channels: Proteins with conformational flexibility. Channels *13*, 207-226.

Lukacs, V., Thyagarajan, B., Varnai, P., Balla, A., Balla, T., and Rohacs, T. (2007). Dual regulation of TRPV1 by phosphoinositides. J.Neurosci. *27*, 7070-7080.

Ma, R., Li, W.P., Rundle, D., Kong, J., Akbarali, H.I., and Tsiokas, L. (2005). PKD2 functions as an epidermal growth factor-activated plasma membrane channel. Mol Cell Biol *25*, 8285-8298.

McGoldrick, L.L., Singh, A.K., Saotome, K., Yelshanskaya, M.V., Twomey, E.C., Grassucci, R.A., and Sobolevsky, A.I. (2018). Opening of the human epithelial calcium channel TRPV6. Nature *553*, 233-237.

McLaughlin, S., Wang, J., Gambhir, A., and Murray, D. (2002). PIP(2) and pro- teins: interactions, organization, and information flow. Annu. Rev. Biophys. Biomol. Struct. *31*, 151–175.

McNamara, C.R., and Degterev, A. (2011). Small-molecule inhibitors of the PI3K signaling network. Future Med. Chem. *3*, 549–565.

Miller, A.N., Vaisey, G., and Long, S.B. (2019). Molecular mechanisms of gating in the calcium-activated chloride channel bestrophin. Elife *8*.

Minke, B., and Cook, B. (2002). TRP channel proteins and signal transduction. Physiol Rev *82*, 429-472.

Miura, S., Sato, K., Kato-Negishi, M., Teshima, T., and Takeuchi, S. (2015). Fluid shear triggers microvilli formation via mechanosensitive activation of TRPV6. Nat.Commun. *6*, 8871.

Montell, C. (2005). The TRP superfamily of cation channels. Sci. STKE *2005*, re3.

Montell, C., and Rubin, G.M. (1989). Molecular characterization of the Drosophila trp locus: a putative integral membrane protein required for phototransduction. Neuron *2*, 1313-1323.

Moran, M.M., Xu, H., and Clapham, D.E. (2004). TRP ion channels in the nervous system. Curr Opin Neurobiol *14*, 362-369.

Ng, L.C.T., Vien, T.N., Yarov-Yarovoy, V., and DeCaen, P.G. (2019). Opening TRPP2 (PKD2L1) requires the transfer of gating charges. Proc Natl Acad Sci U S A *116*, 15540-15549.

Niemeyer, B.A. (2005). Structure-function analysis of TRPV channels. Naunyn Schmiedebergs Arch Pharmacol *371*, 285-294.

Niemeyer, B.A., Bergs, C., Wissenbach, U., Flockerzi, V., and Trost, C. (2001). Competitive regulation of CaT-like-mediated Ca^{2+} entry by protein kinase C and calmodulin. Proc Natl Acad Sci U S A *98*, 3600-3605.

Nilius, B. (2007). TRP channels in disease. Biochim Biophys Acta *1772*, 805-812.

Nilius, B., and Owsianik, G. (2011). The transient receptor potential family of ion

channels. Genome Biol *12*, 218.

Nilius, B., Mahieu, F., Prenen, J., Janssens, A., Owsianik, G., Vennekens, R., and Voets, T. (2006). The Ca^{2+}-activated cation channel TRPM4 is regulated by phosphatidylinositol 4,5-biphosphate. EMBO J. *25*, 467–478.

Nilius, B., Owsianik, G., and Voets, T. (2008). Transient receptor potential channels meet phosphoinositides. EMBO J *27*, 2809-2816.

Otsuguro, K., Tang, J., Tang, Y., Xiao, R., Freichel, M., Tsvilovskyy, V., Ito, S., Flockerzi, V., Zhu, M.X., and Zholos, A.V. (2008). Isoform-specific inhibition of TRPC4 channel by phosphatidylinositol 4,5-bisphosphate. J. Biol. Chem. *283*, 10026–10036.

Park, E., and MacKinnon, R. (2018). Structure of the CLC-1 chloride channel from Homo sapiens. Elife *7*.

Paulsen, C.E., Armache, J.P., Gao, Y., Cheng, Y., and Julius, D. (2015). Structure of the TRPA1 ion channel suggests regulatory mechanisms. Nature *520*, 511-517.

Peng, J.B. (2011). TRPV5 and TRPV6 in transcellular Ca(2+) transport: regulation, gene duplication, and polymorphisms in African populations. Adv Exp Med Biol *704*, 239-275.

Peng, J.B., Chen, X.Z., Berger, U.V., Vassilev, P.M., Tsukaguchi, H., Brown, E.M., and Hediger, M.A. (1999). Molecular cloning and characterization of a channel-like transporter mediating intestinal calcium absorption. J Biol Chem *274*, 22739-22746.

Peng, J.B., Chen, X.Z., Berger, U.V., Weremowicz, S., Morton, C.C., Vassilev, P.M., Brown, E.M., and Hediger, M.A. (2000). Human calcium transport protein CaT1. Biochem.Biophys.Res.Commun. *278*, 326-332.

Peng, J.B., Suzuki, Y., Gyimesi, G., and Hediger, M.A. (2018). TRPV5 and TRPV6 Calcium-Selective Channels. In Calcium Entry Channels in Non-Excitable Cells, J.A. Kozak, and J.W. Putney, Jr., eds. (Boca Raton (FL)), pp. 241-274.

Peng, J.B., Zhuang, L., Berger, U.V., Adam, R.M., Williams, B.J., Brown, E.M., Hediger, M.A., and Freeman, M.R. (2001). CaT1 expression correlates with tumor grade in prostate cancer. Biochem Biophys Res Commun *282*, 729-734.

Peretti, M., Angelini, M., Savalli, N., Florio, T., Yuspa, S.H., and Mazzanti, M. (2015). Chloride channels in cancer: Focus on chloride intracellular channel 1 and 4 (CLIC1 AND CLIC4) proteins in tumor development and as novel therapeutic targets. Biochim Biophys Acta *1848*, 2523-2531.

Peters, A.A., Simpson, P.T., Bassett, J.J., Lee, J.M., Da Silva, L., Reid, L.E., Song, S., Parat, M.O., Lakhani, S.R., Kenny, P.A.*, et al.* (2012). Calcium channel TRPV6 as a potential therapeutic target in estrogen receptor-negative breast cancer. Mol Cancer Ther *11*, 2158-2168.

Poblete, H., Oyarzun, I., Olivero, P., Comer, J., Zuniga, M., Sepulveda, R.V., Baez-Nieto, D., Gonzalez, L.C., Gonzalez-Nilo, F., and Latorre, R. (2015). Molecular determinants of phosphatidylinositol 4,5-bisphosphate (PI(4,5)P2) binding to transient receptor potential V1 (TRPV1) channels. J.Biol.Chem. *290*, 2086-2098.

Prevarskaya, N., Skryma, R., and Shuba, Y. (2018). Ion Channels in Cancer: Are Cancer Hallmarks Oncochannelopathies? Physiol Rev *98*, 559-621.

Pumroy, R.A., Samanta, A., Liu, Y., Hughes, T.E., Zhao, S., Yudin, Y., Rohacs, T., Han, S., and Moiseenkova-Bell, V.Y. (2019). Molecular mechanism of TRPV2 channel modulation by cannabidiol. Elife. *8*.

Ramsey, I.S., Delling, M., and Clapham, D.E. (2006). An introduction to TRP channels. Annu Rev Physiol *68*, 619-647.

Rao, S., Klesse, G., Stansfeld, P.J., Tucker, S.J., and Sansom, M.S.P. (2019). A heuristic derived from analysis of the ion channel structural proteome permits the rapid identification of hydrophobic gates. Proc Natl Acad Sci U S A *116*, 13989-13995.

Raphael, M., Lehen'kyi, V., Vandenberghe, M., Beck, B., Khalimonchyk, S., Vanden Abeele, F., Farsetti, L., Germain, E., Bokhobza, A., Mihalache, A.*, et al.* (2014). TRPV6 calcium channel translocates to the plasma membrane via Orai1-mediated mechanism and controls cancer cell survival. Proc Natl Acad Sci U S A *111*, E3870-3879.

Rohacs, T. (2014). Phosphoinositide regulation of TRP channels. Handb Exp Pharmacol *223*, 1143-1176.

Rohacs, T., Lopes, C.M., Michailidis, I., and Logothetis, D.E. (2005). PI(4,5)P2 regulates the activation and desensitization of TRPM8 channels through the TRP domain. Nat. Neurosci. *8*, 626–634.

Rohacs, T., Thyagarajan, B., and Lukacs, V. (2008). Phospholipase C mediated modulation of TRPV1 channels. Mol. Neurobiol. *37*, 153–163.

Samanta, A., Hughes, T.E.T., and Moiseenkova-Bell, V.Y. (2018). Transient Receptor Potential (TRP) Channels. Subcell Biochem *87*, 141-165.

Saotome, K., Singh, A.K., Yelshanskaya, M.V., and Sobolevsky, A.I. (2016). Crystal structure of the epithelial calcium channel TRPV6. Nature *534*, 506-511.

Sato-Numata, K., Numata, T., Inoue, R., Sabirov, R.Z., and Okada, Y. (2017). Distinct

contributions of LRRC8A and its paralogs to the VSOR anion channel from those of the ASOR anion channel. Channels (Austin) *11*, 167-172.

Sato-Numata, K., Numata, T., Okada, T., and Okada, Y. (2013). Acid-sensitive outwardly rectifying (ASOR) anion channels in human epithelial cells are highly sensitive to temperature and independent of ClC-3. Pflugers Arch *465*, 1535-1543.

Sato-Numata, K., Numata, T., and Okada, Y. (2014). Temperature sensitivity of acid-sensitive outwardly rectifying (ASOR) anion channels in cortical neurons is involved in hypothermic neuroprotection against acidotoxic necrosis. Channels (Austin) *8*, 278-283.

Sharmin, N., and Gallin, W.J. (2017). Intramolecular interactions that control voltage sensitivity in the jShak1 potassium channel from Polyorchis penicillatus. J Exp Biol *220*, 469-477.

Shen, P.S., Yang, X., DeCaen, P.G., Liu, X., Bulkley, D., Clapham, D.E., and Cao, E. (2016). The structure of the polycystic kidney disease channel PKD2 in lipid nanodiscs. Cell *167*, 763–773.e11.

Shimizu, T., Janssens, A., Voets, T., and Nilius, B. (2009). Regulation of the murine TRPP3 channel by voltage, pH, and changes in cell volume. Pflugers Arch *457*, 795-807.

Shoemaker, S.C., and Ando, N. (2018). X-rays in the Cryo-Electron Microscopy Era: Structural Biology's Dynamic Future. Biochemistry *57*, 277-285.

Singh, A.K., McGoldrick, L.L., Twomey, E.C., and Sobolevsky, A.I. (2018a). Mechanism of calmodulin inactivation of the calcium-selective TRP channel TRPV6. Sci Adv *4*, eaau6088.

Singh, A.K., Saotome, K., McGoldrick, L.L., and Sobolevsky, A.I. (2018b). Structural bases of TRP channel TRPV6 allosteric modulation by 2-APB. Nat Commun *9*, 2465.

Song, H., Dong, M., Zhou, J., Sheng, W., Li, X., and Gao, W. (2018). Expression and prognostic significance of TRPV6 in the development and progression of pancreatic cancer. Oncol Rep *39*, 1432-1440.

Stallmeyer, B., Zumhagen, S., Denjoy, I., Duthoit, G., Hebert, J.L., Ferrer, X., Maugenre, S., Schmitz, W., Kirchhefer, U., Schulze-Bahr, E., et al. (2012). Mutational spectrum in the Ca(2+)--activated cation channel gene TRPM4 in patients with cardiac conductance disturbances. Hum.Mutat. *33*, 109-117.

Steinberg, X., Lespay-Rebolledo, C., and Brauchi, S. (2014). A structural view of ligand-dependent activation in thermoTRP channels. Front. Physiol. *5*, 171.

Sternberg, J.R., Prendergast, A.E., Brosse, L., Cantaut-Belarif, Y., Thouvenin, O., Orts-Del'Immagine, A., Castillo, L., Djenoune, L., Kurisu, S., McDearmid, J.R.*, et al.* (2018). Pkd2l1 is required for mechanoception in cerebrospinal fluid-contacting neurons and maintenance of spine curvature. Nat Commun *9*, 3804.

Stewart, J.M. (2020). TRPV6 as A Target for Cancer Therapy. J Cancer *11*, 374-387.

Su, Q., Hu, F., Liu, Y., Ge, X., Mei, C., Yu, S., Shen, A., Zhou, Q., Yan, C., Lei, J.*, et al.* (2018). Cryo-EM structure of the polycystic kidney disease-like channel PKD2L1. Nat Commun *9*, 1192.

Suh, B.C., and Hille, B. (2008). PIP2 is a necessary cofactor for ion channel function: how and why? Annu Rev Biophys *37*, 175-195.

Suh, K.S., Crutchley, J.M., Koochek, A., Ryscavage, A., Bhat, K., Tanaka, T., Oshima, A.,

Fitzgerald, P., and Yuspa, S.H. (2007). Reciprocal modifications of CLIC4 in tumor epithelium and stroma mark malignant progression of multiple human cancers. Clin Cancer Res *13*, 121-131.

Sun, Y.S., Zhao, Z., Yang, Z.N., Xu, F., Lu, H.J., Zhu, Z.Y., Shi, W., Jiang, J., Yao, P.P., and Zhu, H.P. (2017). Risk Factors and Preventions of Breast Cancer. Int J Biol Sci *13*, 1387-1397.

Suzuki, Y., Chitayat, D., Sawada, H., Deardorff, M.A., McLaughlin, H.M., Begtrup, A., Millar, K., Harrington, J., Chong, K., Roifman, M.*, et al.* (2018). TRPV6 Variants Interfere with Maternal-Fetal Calcium Transport through the Placenta and Cause Transient Neonatal Hyperparathyroidism. Am J Hum Genet *102*, 1104-1114.

Suzuki, Y., Pasch, A., Bonny, O., Mohaupt, M.G., Hediger, M.A., and Frey, F.J. (2008). Gain-of-function haplotype in the epithelial calcium channel TRPV6 is a risk factor for renal calcium stone formation. Hum Mol Genet *17*, 1613-1618.

Tate, J.G., Bamford, S., Jubb, H.C., Sondka, Z., Beare, D.M., Bindal, N., Boutselakis, H., Cole, C.G., Creatore, C., Dawson, E.*, et al.* (2019). COSMIC: the Catalogue Of Somatic Mutations In Cancer. Nucleic Acids Res *47*, D941-D947.

Teng, J., Loukin, S.H., Anishkin, A., and Kung, C. (2015). L596-W733 bond between the start of the S4-S5 linker and the TRP box stabilizes the closed state of TRPV4 channel. Proc.Natl.Acad.Sci.U.S.A *112*, 3386-3391.

Teng, J., Loukin, S.H., Anishkin, A., and Kung, C. (2016). A competing hydrophobic tug on L596 to the membrane core unlatches S4-S5 linker elbow from TRP helix and allows TRPV4 channel to open. Proc Natl Acad Sci U S A *113*, 11847-11852.

Thyagarajan, B., Benn, B.S., Christakos, S., and Rohacs, T. (2009). Phospholipase

C-mediated regulation of transient receptor potential vanilloid 6 channels: implications in active intestinal Ca^{2+} transport. Mol.Pharmacol. *75*, 608-616.

Thyagarajan, B., Lukacs, V., and Rohacs, T. (2008). Hydrolysis of phosphatidylinositol 4,5-bisphosphate mediates calcium-induced inactivation of TRPV6 channels. J Biol Chem *283*, 14980-14987.

Tong, C.W.S., Wu, M., Cho, W.C.S., and To, K.K.W. (2018). Recent Advances in the Treatment of Breast Cancer. Front Oncol *8*, 227.

Tsagareli, M.G., and Nozadze, I. (2019). An overview on transient receptor potential channels superfamily. Behav Pharmacol.

Ullrich, F., Blin, S., Lazarow, K., Daubitz, T., von Kries, J.P., and Jentsch, T.J. (2019). Identification of TMEM206 proteins as pore of PAORAC/ASOR acid-sensitive chloride channels. Elife *8*.

Urrego, D., Tomczak, A.P., Zahed, F., Stuhmer, W., and Pardo, L.A. (2014). Potassium channels in cell cycle and cell proliferation. Philos Trans R Soc Lond B Biol Sci *369*, 20130094.

Valente, P., Fernandez-Carvajal, A., Camprubı-Robles, M., Gomis, A., Quirce, S., Viana, F., Fernandez-Ballester, G., Gonzalez-Ros, J.M., Belmonte, C., Planells-Cases, R., and Ferrer-Montiel, A. (2011). Membrane-tethered peptides patterned after the TRP domain (TRPducins) selectively inhibit TRPV1 channel activity. FASEB J. *25*, 1628–1640.

van, A.M., Hoenderop, J.G., van der Kemp, A.W., van Leeuwen, J.P., and Bindels, R.J. (2003). Regulation of the epithelial Ca^{2+} channels in small intestine as studied by quantitative mRNA detection. Am.J.Physiol Gastrointest.Liver Physiol *285*, G78-G85.

van der Wijst, J., Leunissen, E.H., Blanchard, M.G., Venselaar, H., Verkaart, S., Paulsen, C.E., Bindels, R.J., and Hoenderop, J.G. (2017). A Gate Hinge Controls the Epithelial Calcium Channel TRPV5. Scientific reports *7*, 45489.

van Goor, M.K.C., Hoenderop, J.G.J., and van der Wijst, J. (2017). TRP channels in calcium homeostasis: from hormonal control to structure-function relationship of TRPV5 and TRPV6. Biochim.Biophys.Acta Mol.Cell Res. *1864*, 883-893.

Vandewauw, I., De Clercq, K., Mulier, M., Held, K., Pinto, S., Van Ranst, N., Segal, A., Voet, T., Vennekens, R., Zimmermann, K.*, et al.* (2018). Publisher Correction: A TRP channel trio mediates acute noxious heat sensing. Nature *559*, E7.

Vangeel, L., and Voets, T. (2019). Transient Receptor Potential Channels and Calcium Signaling. Cold Spring Harb Perspect Biol *11*.

Vanhaesebroeck, B., Leevers, S.J., Ahmadi, K., Timms, J., Katso, R., Driscoll, P.C., Woscholski, R., Parker, P.J., and Waterfield, M.D. (2001). Synthesis and function of 3-phosphorylated inositol lipids. Annu.Rev.Biochem. *70*, 535-602.

Vanoevelen, J., Janssens, A., Huitema, L.F., Hammond, C.L., Metz, J.R., Flik, G., Voets, T., and Schulte-Merker, S. (2011). Trpv5/6 is vital for epithelial calcium uptake and bone formation. FASEB J *25*, 3197-3207.

Velisetty, P., Borbiro, I., Kasimova, M.A., Liu, L., Badheka, D., Carnevale, V., and Rohacs, T. (2016). A molecular determinant of phosphoinositide affinity in mammalian TRPV channels. Sci Rep *6*, 27652.

Venkatachalam, K., and Montell, C. (2007). TRP channels. Annu. Rev. Bio- chem. *76*, 387–417.

Vien, T.N., Wang, J., Ng, L.C.T., Cao, E., and DeCaen, P.G. (2020). Molecular dysregulation of ciliary polycystin-2 channels caused by variants in the TOP domain. Proc Natl Acad Sci U S A *117*, 10329-10338.

Voets, T., Droogmans, G., Wissenbach, U., Janssens, A., Flockerzi, V., and Nilius, B. (2004). The principle of temperature-dependent gating in cold- and heat-sensitive TRP channels. Nature *430*, 748-754.

Voets, T., Owsianik, G., Janssens, A., Talavera, K., and Nilius, B. (2007). TRPM8 voltage sensor mutants reveal a mechanism for integrating thermal and chemical stimuli. Nat.Chem.Biol. *3*, 174-182.

Voets, T., Prenen, J., Fleig, A., Vennekens, R., Watanabe, H., Hoenderop, J.G., Bindels, R.J., Droogmans, G., Penner, R., and Nilius, B. (2001). CaT1 and the calcium release-activated calcium channel manifest distinct pore properties. J Biol Chem *276*, 47767-47770.

Waks, A.G., and Winer, E.P. (2019). Breast Cancer Treatment: A Review. JAMA *321*, 288-300.

Walker, M.B., and Kimmel, C.B. (2007). A two-color acid-free cartilage and bone stain for zebrafish larvae. Biotech.Histochem. *82*, 23-28.

Wang, L., Holmes, R.P., and Peng, J.B. (2019). Modeling the structural and dynamical changes of the epithelial calcium channel TRPV5 caused by the A563T variation based on the structure of TRPV6. J Biomol Struct Dyn *37*, 3506-3512.

Wang, Q., Dai, X.Q., Li, Q., Wang, Z., Cantero Mdel, R., Li, S., Shen, J., Tu, J.C., Cantiello, H., and Chen, X.Z. (2012). Structural interaction and functional regulation of polycystin-2 by filamin. PLoS One *7*, e40448.

Wang, Q., Zheng, W., Wang, Z., Yang, J., Hussein, S., Tang, J., and Chen, X.Z. (2015). Filamin-a increases the stability and plasma membrane expression of polycystin-2. PLoS One *10*, e0123018.

Wang, Z., Ng, C., Liu, X., Wang, Y., Li, B., Kashyap, P., Chaudhry, H.A., Castro, A., Kalontar, E.M., Ilyayev, L., et al. (2019). The ion channel function of polycystin-1 in the polycystin-1/polycystin-2 complex. EMBO Rep., e48336.

Watnick, T., He, N., Wang, K., Liang, Y., Parfrey, P., Hefferton, D., St George- Hyslop, P., Germino, G., and Pei, Y. (2000). Mutations of PKD1 in ADPKD2 cysts suggest a pathogenic effect of trans-heterozygous mutations. Nat. Genet. *25*, 143–144.

Weissgerber, P., Kriebs, U., Tsvilovskyy, V., Olausson, J., Kretz, O., Stoerger, C., Mannebach, S., Wissenbach, U., Vennekens, R., Middendorff, R.*, et al.* (2012). Excision of Trpv6 gene leads to severe defects in epididymal Ca^{2+} absorption and male fertility much like single D541A pore mutation. J Biol Chem *287*, 17930-17941.

Weissgerber, P., Kriebs, U., Tsvilovskyy, V., Olausson, J., Kretz, O., Stoerger, C., Vennekens, R., Wissenbach, U., Middendorff, R., Flockerzi, V., et al. (2011). Male fertility depends on Ca(2)+ absorption by TRPV6 in epididymal epithelia. Sci.Signal. *4*, ra27.

Wissenbach, U., Niemeyer, B.A., Fixemer, T., Schneidewind, A., Trost, C., Cavalie, A., Reus, K., Meese, E., Bonkhoff, H., and Flockerzi, V. (2001). Expression of CaT-like, a novel calcium-selective channel, correlates with the malignancy of prostate cancer. J Biol Chem *276*, 19461-19468.

Wilkes, M., Madej, M.G., Kreuter, L., Rhinow, D., Heinz, V., De Sanctis, S., Ruppel, S., Richter, R.M., Joos, F., Grieben, M., et al. (2017). Molecular in- sights into lipid-assisted

Ca^{2+} regulation of the TRP channel Polycystin-2. Nat. Struct. Mol. Biol. *24*, 123–130.

Wissenbach, U., Niemeyer, B.A., Fixemer, T., Schneidewind, A., Trost, C., Cavalie, A., Reus, K., Meese, E., Bonkhoff, H., and Flockerzi, V. (2001). Expression of CaT-like, a novel calcium-selective channel, correlates with the malignancy of prostate cancer. J Biol Chem *276*, 19461-19468.

Xiao, R., and Xu, X.Z. (2009). Function and regulation of TRP family channels in C. elegans. Pflugers Arch *458*, 851-860.

Yang, F., Xiao, X., Cheng, W., Yang, W., Yu, P., Song, Z., Yarov-Yarovoy, V., and Zheng, J. (2015). Structural mechanism underlying capsaicin binding and activation of the TRPV1 ion channel. Nat.Chem.Biol. *11*, 518-524.

Yang, J., Chen, J., Del Carmen Vitery, M., Osei-Owusu, J., Chu, J., Yu, H., Sun, S., and Qiu, Z. (2019). PAC, an evolutionarily conserved membrane protein, is a proton-activated chloride channel. Science *364*, 395-399.

Yang, J., Wang, Q., Zheng, W., Tuli, J., Li, Q., Wu, Y., Hussein, S., Dai, X.Q., Shafiei, S., Li, X.G.*, et al.* (2012). Receptor for activated C kinase 1 (RACK1) inhibits function of transient receptor potential (TRP)-type channel Pkd2L1 through physical interaction. J Biol Chem *287*, 6551-6561.

Yang, J., Zheng, W., Wang, Q., Lara, C., Hussein, S., and Chen, X.Z. (2013). Translational up-regulation of polycystic kidney disease protein PKD2 by endoplasmic reticulum stress. FASEB J *27*, 4998-5009.

Yelshanskaya, M.V., Nadezhdin, K.D., Kurnikova, M.G., and Sobolevsky, A.I. (2020). Structure and function of the calcium-selective TRP channel TRPV6. J Physiol.

Yi, X., Liang, Y., Huerta-Sanchez, E., Jin, X., Cuo, Z.X., Pool, J.E., Xu, X., Jiang, H., Vinckenbosch, N., Korneliussen, T.S.*, et al.* (2010). Sequencing of 50 human exomes reveals adaptation to high altitude. Science *329*, 75-78.

Yin, Y., Wu, M., Zubcevic, L., Borschel, W.F., Lander, G.C., and Lee, S.Y. (2018). Structure of the cold- and menthol-sensing ion channel TRPM8. Sci- ence 359, 237–241.

Yu, J., Zhang, Y., McIlroy, J., Rordorf-Nikolic, T., Orr, G.A., and Backer, J.M. (1998). Regulation of the p85/p110 phosphatidylinositol 3'-kinase: stabilization and inhibition of the p110alpha catalytic subunit by the p85 regulatory subunit. Mol Cell Biol *18*, 1379-1387.

Yu, Y., Ulbrich, M.H., Li, M.H., Dobbins, S., Zhang, W.K., Tong, L., Isacoff, E.Y., and Yang, J. (2012). Molecular mechanism of the assembly of an acid-sensing receptor ion channel complex. Nat Commun *3*, 1252.

Yue, L., Peng, J.B., Hediger, M.A., and Clapham, D.E. (2001). CaT1 manifests the pore properties of the calcium-release-activated calcium channel. Nature *410*, 705-709.

Yue, Z., Xie, J., Yu, A.S., Stock, J., Du, J., and Yue, L. (2015). Role of TRP channels in the cardiovascular system. Am J Physiol Heart Circ Physiol *308*, H157-182.

Zakharian, E., Cao, C., and Rohacs, T. (2011). Intracellular ATP supports TRPV6 activity via lipid kinases and the generation of PtdIns(4,5) P(2). FASEB J *25*, 3915-3928.

Zandany, N., Lewin, L., Nirenberg, V., Orr, I., and Yifrach, O. (2015). Entropic clocks in the service of electrical signaling: 'Ball and chain' mechanisms for ion channel inactivation and clustering. FEBS Lett *589*, 2441-2447.

Zhang, H., Craciun, L.C., Mirshahi, T., Roha´ cs, T., Lopes, C.M., Jin, T., and Logothetis,

D.E. (2003). PIP(2) activates KCNQ channels, and its hydrolysis underlies receptor-mediated inhibition of M currents. Neuron *37*, 963–975.

Zhang, J.T., Jiang, X.H., Xie, C., Cheng, H., Da Dong, J., Wang, Y., Fok, K.L., Zhang, X.H., Sun, T.T., Tsang, L.L.*, et al.* (2013). Downregulation of CFTR promotes epithelial-to-mesenchymal transition and is associated with poor prognosis of breast cancer. Biochim Biophys Acta *1833*, 2961-2969.

Zhang, R., Varela, M., Vallentgoed, W., Forn-Cuni, G., van, d., V, and Meijer, A.H. (2019). The selective autophagy receptors Optineurin and p62 are both required for zebrafish host resistance to mycobacterial infection. PLoS.Pathog. *15*, e1007329.

Zhang, X., Vadas, O., Perisic, O., Anderson, K.E., Clark, J., Hawkins, P.T., Stephens, L.R., and Williams, R.L. (2011). Structure of lipid kinase p110beta/p85beta elucidates an unusual SH2-domain-mediated inhibitory mechanism. Mol Cell *41*, 567-578.

Zheng, W., Cai, R., Hofmann, L., Nesin, V., Hu, Q., Long, W., Fatehi, M., Liu, X., Hussein, S., Kong, T.*, et al.* (2018a). Direct Binding between Pre-S1 and TRP-like Domains in TRPP Channels Mediates Gating and Functional Regulation by PIP2. Cell Rep *22*, 1560-1573.

Zheng, W., Hu, R., Cai, R., Hofmann, L., Hu, Q., Fatehi, M., Long, W., Kong, T., Tang, J., Light, P.*, et al.* (2018b). Identification and characterization of hydrophobic gate residues in TRP channels. FASEB J *32*, 639-653.

Zheng, W., Shen, F., Hu, R., Roy, B., Yang, J., Wang, Q., Zhang, F., King, J.C., Sergi, C., Liu, S.M.*, et al.* (2016a). Far Upstream Element-Binding Protein 1 Binds the 3' Untranslated Region of PKD2 and Suppresses Its Translation. J Am Soc Nephrol *27*, 2645-2657.

Zheng, W., Yang, J., Beauchamp, E., Cai, R., Hussein, S., Hofmann, L., Li, Q., Flockerzi, V., Berthiaume, L.G., Tang, J.*, et al.* (2016b). Regulation of TRPP3 Channel Function by N-terminal Domain Palmitoylation and Phosphorylation. J Biol Chem *291*, 25678-25691.

Zheng, W., Yang, X., Hu, R., Cai, R., Hofmann, L., Wang, Z., Hu, Q., Liu, X., Bulkley, D., Yu, Y.*, et al.* (2018c). Hydrophobic pore gates regulate ion permeation in polycystic kidney disease 2 and 2L1 channels. Nat Commun *9*, 2302.

Zheng, W., Yang, X., Hu, R., Cai, R., Hofmann, L., Wang, Z., Hu, Q., Liu, X., Bulkley, D., Yu, Y.*, et al.* (2019). Author Correction: Hydrophobic pore gates regulate ion permeation in polycystic kidney disease 2 and 2L1 channels. Nat Commun *10*, 1452.

Zhou, B.P., Deng, J., Xia, W., Xu, J., Li, Y.M., Gunduz, M., and Hung, M.C. (2004). Dual regulation of Snail by GSK-3beta-mediated phosphorylation in control of epithelial-mesenchymal transition. Nat Cell Biol *6*, 931-940.

Zhou, F.M., Huang, Y.Y., Tian, T., Li, X.Y., and Tang, Y.B. (2018). Knockdown of Chloride Channel-3 Inhibits Breast Cancer Growth In Vitro and In Vivo. J Breast Cancer *21*, 103-111.

Zhuang, L., Peng, J.B., Tou, L., Takanaga, H., Adam, R.M., Hediger, M.A., and Freeman, M.R. (2002). Calcium-selective ion channel, CaT1, is apically localized in gastrointestinal tract epithelia and is aberrantly expressed in human malignancies. Lab Invest *82*, 1755-1764.

Zubcevic, L., Herzik, M.A., Jr., Chung, B.C., Liu, Z., Lander, G.C., and Lee, S.Y. (2016). Cryo-electron microscopy structure of the TRPV2 ion channel. Nat. Struct. Mol. Biol. *23*, 180–186.